Data Archive Users' Guide

for the

Descent Imager and Spectral Radiometer (DISR)

on the

Huygens Probe

By: The DISR Team

17 May 2016

Version 3.0

Index

Preface...

The Descent Imager and Spectral Radiometer data are in NASA's Planetary Data System Archive on the Planetary Atmospheres Data Node located in the Astronomy building of New Mexico State University in Las Cruces, NM. The data volume was placed in the archive beginning in October 2006, and first released in May 2007.

The link to the DISR page is:
http://atmos.nmsu.edu/data_and_services/atmospheres_data/Huygens/DISR.html

The direct link to the DISR data is: http://atmos.nmsu.edu/PDS/data/hpdisr_0001/

Throughout this document "hpdisr_0001" refers to the initial data volume released as: "HP-SSA-DISR-2/3-EDR/RDR-V1.0", created 2007-05-17T10:05:23.688Z.

Since this was a joint US/European mission the Archive is also available on the European Space Agency's Planetary Space Archive:
http://www.rssd.esa.int/index.php?project=PSA&page=huygens

Although the DISR Archive contains documentation for every type of data contained in the archive, the Data Archive Users Guide was commissioned to make access to the data easier for those who are not intimately familiar with the instrument or the mission. At the core of the Users' Guide are examples of how to access and use the DISR data, with supporting background information and references to related publications.

In this Guide "Dataset" is used to designate the data from one observation or collection period (e.g. a Sun sensor dataset), and DISR data or data volume designates the broader collection of data.

1.0 Introduction & Science Objectives

On January 14, 2005, the Huygens Probe, part of the joint NASA/ESA Cassini-Huygens mission to Saturn, entered the atmosphere of Titan, descended for 2.5 hours under a parachute and eventually landed softly on the surface of Titan. Six experiments collected data during the descent and on ground. This guide provides information and insight to assist the user in accessing the archive of one of those instruments, the Huygens Descent Imager and Spectral Radiometer (DISR).

The Huygens probe collected the only existing in-situ data of Titan's lower atmosphere. The DISR instrument obtained images of Titan's surface, measured the upward and downward sunlight scattered intensity (from about 350 to 1700 nm), collected sky intensity strips (6º wide x 50º high) in the red (935 nm) and blue (500 nm) for two polarization states (solar aureole), and recorded the Sun's intensity attenuation (939 nm) from about 143 km altitude to the surface.

The instrument was designed to achieve science objectives in four major areas:
1) The thermal balance and dynamics of Titan's atmosphere,
2) The distribution and properties of aerosol and cloud particles,
3) The nature of Titan's surface, and
4) The composition of the atmosphere.

The details of how the science goals were to be achieved is presented in the archived document, "The Descent Imager/Spectral Radiometer (DISR) Aboard Huygens" (Ref 1), and summarized below:

The solar flux was measured at 38 altitude levels during the Titan Descent. The profile of the net flux (down-up) gives the atmospheric absorption at each level. The measured opacity and temperature profile is used to determine the radiative cooling profile. The sky intensity strips via the solar aureole camera were measured at 69 altitude levels and from Titan's surface. Radiative transfer models of the atmosphere were constructed using the opacity structure, sky polarization, particle scattering properties (optical depth, single-scattering albedo and phase function), and temperature profile to determine aerosol size, shape and distribution, which leads to constraints on the composition of the atmosphere. The growth of methane absorption bands in the spectra obtained at different altitudes gives the methane mixing profile.

Three hundred and seventy five images were transmitted during the descent, and another 240 from Titan's surface. These are used to study the wind profile, and surface geology, topography, propensity of liquid, erosion morphology, etc.

2.0 Instrument Description

The DISR consists of 14 sub-instruments; Three panchromatic imagers (side looking, downward looking medium resolution, and downward looking high resolution), four solar aureole cameras, two spectrometers covering the visible spectrum, two spectrometers in the near infrared, two violet photometers, and a Sun sensor.

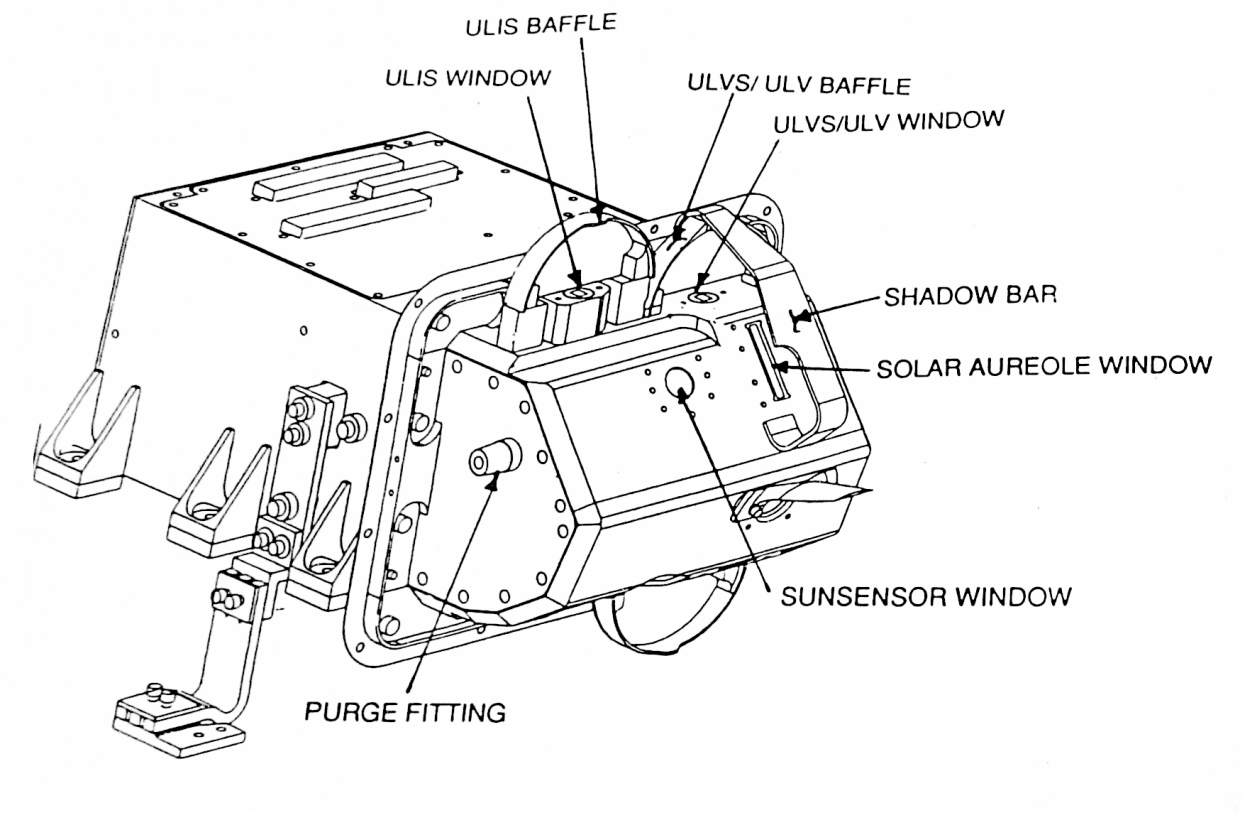

Figure 2-1: View of the top of the DISR sensor head showing its upward looking instruments.

ULIS = Upward Looking Infrared Spectrometer
ULVS = Upward Looking Visible Spectrometer
ULV = Upward Looking Violet Photometer

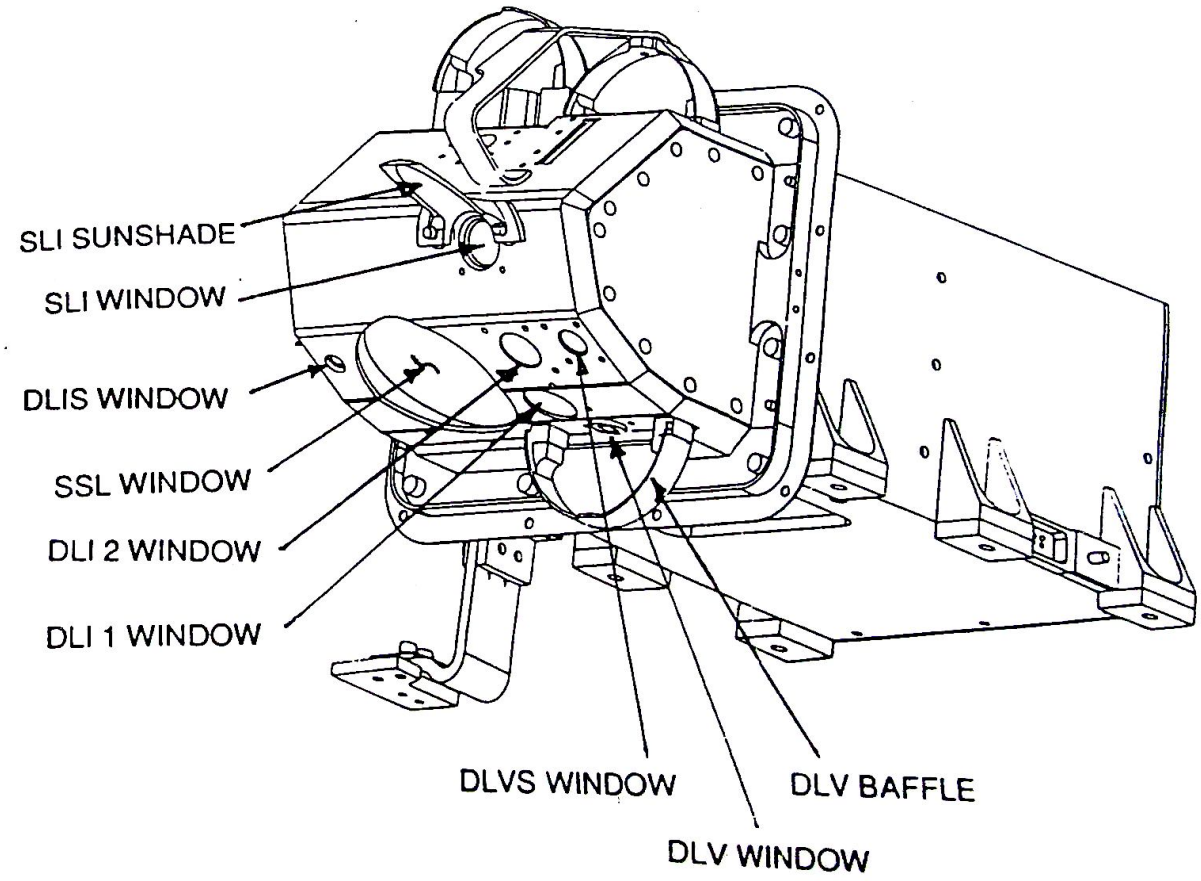

Figure 2-2: View of the bottom of the DISR sensor head showing its downward looking instruments.

DLI 1 = Downward Looking Imager 1 (aka High Resolution Imager, HRI)
DLI 2 = Downward Looking Imager 2 (aka Medium Resolution Imager, MRI)
DLIS = Downward Looking Infrared Spectrometer
DLVS = Downward Looking Visible Spectrometer
DLV = Downward Looking Violet Photometer
SLI = Side Looking Imager
SSL = Surface Science Lamp

The DISR Sensor Head (SH) protruded from the side of the Huygens probe. As the probe rotated below the parachute the SH captured observations looking both upward and downward at pre-planed azimuths relative to the predicted Sun. (However, problems with the Sun sensor caused azimuthal variations as described in section 3.0.)

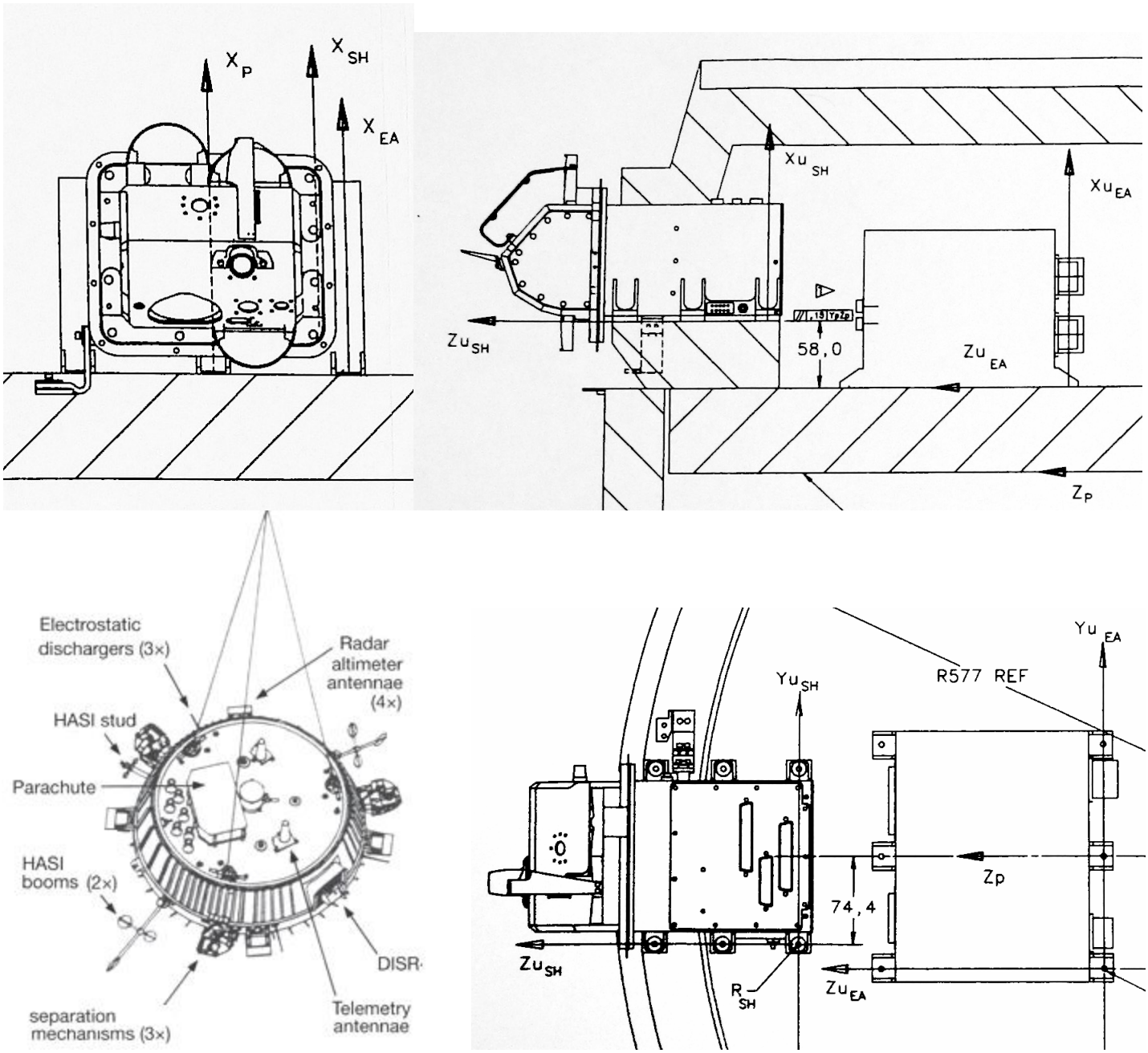

Figure 2.3 - Location of the DISR Sensor Head (SH) and Electronics Assembly (EA) in Huygens probe.

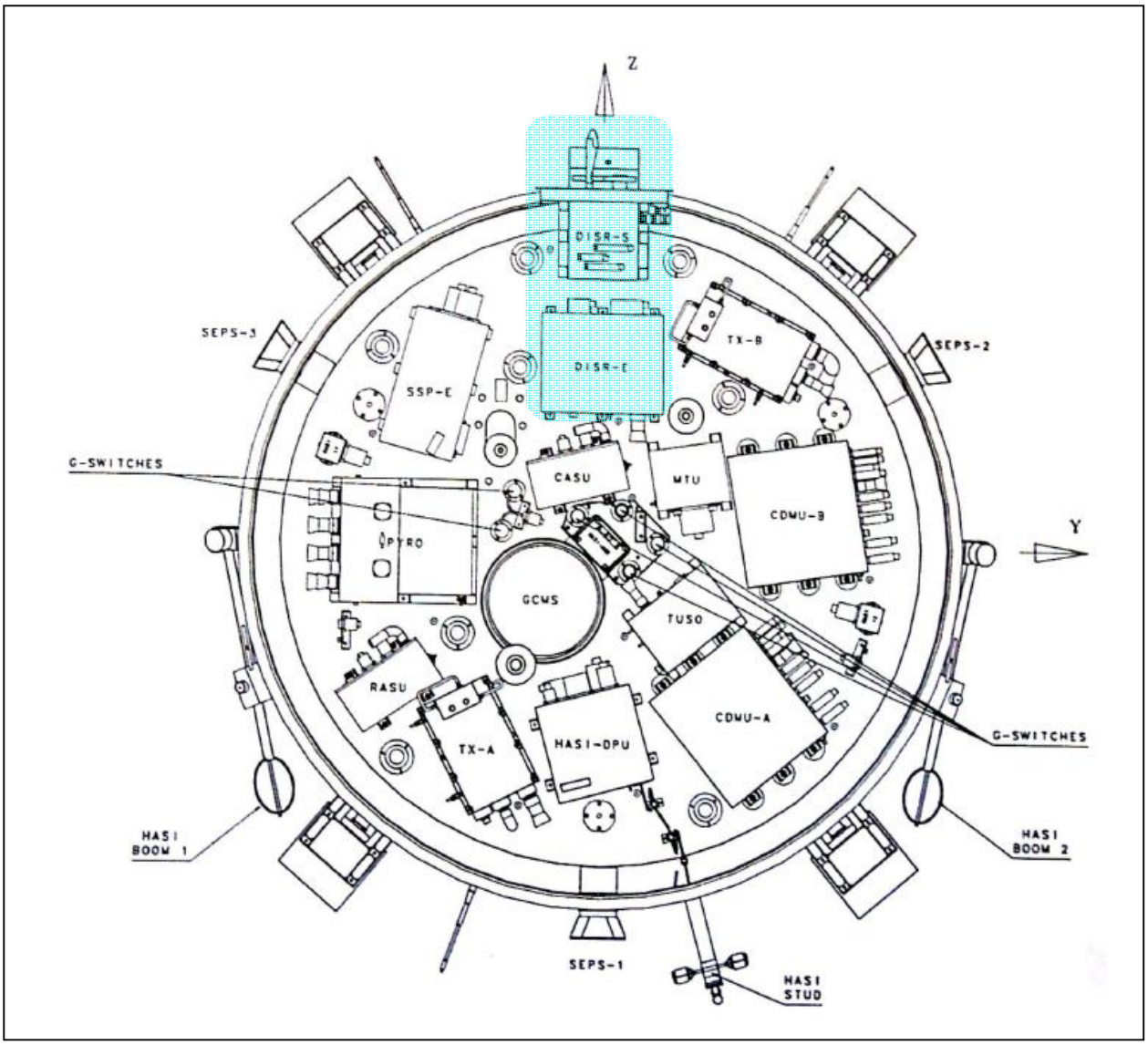

Figure 2-4: Location of Instruments on Huygens probe.

The data were taken from an altitude of approximately 143km down to Titan's surface. The data acquisition strategy was optimized by altitude and spin rate to meet the science objectives, and organized into groups of measurements called cycles.

The performance of the instrument during the descent was good, but not entirely perfect. A discussion of the off nominal behavior is presented in section 3.

The DISR data are presented in the PDS archive as described in section 4. Details of the individual instruments and their calibration are presented in section 5. Much more detailed discussion of the DISR instrument can be found in the archive under:

hpdisr_0001/CATALOG/DISRINST.CAT,
hpdisr_0001/DOCUMENT/DISR_SUPPORTING_DOCUMENTS/SPACE_SCIENCE_REVIEW,
hpdisr_0001/DOCUMENT/DISR_SUPPORTING_DOCUMENTS/ESA_SP_1177, and

hpdisr_0001/DOCUMENT/DISR_SUPPORTING_DOCUMENTS/EXPERIMENT_USERS_MANUAL.

The following tables summarize the characteristics of the Upward and Downward looking DISR sub-instruments:

Upward Looking DISR Sub-instruments Summary

Upward–Looking Instrument	Azimuth Range	Zenith Range	Spectral Range (nm)	Spectral Scale (per pixel)	Spatial Scale (per pixel)	Pixel Format
Violet Photometer (ULV)	170°	5°–88°	350–480	–	–	1
Visible Spectrometer (ULVS)	170°	5°–88°	480–960	2.4 nm	–	8 x 200
Infrared Spectrometer (ULIS)	170°	5°–88°	870–1700	6.3 nm	–	132
Solar Aureole (SA 1) Vertical Polarization	6°	25°–75°	500±25	–	1°	6 x 50
Solar Aureole (SA 2) Horizontal Polarization	6°	25°–75°	500±25	–	1°	6 x 50
Solar Aureole (SA 3) Vertical Polarization	6°	25°–75°	935±35	–	1°	6 x 50
Solar Aureole (SA 4) Horizontal Polarization	6°	25°–75°	935±35	–	1°	6 x 50
Sun Sensor (SS) (64° cone FOV)	64° cone	25°–75°	939±6	–	–	1

Downward-Looking DISR Sub-Instruments Summary

Downward–Looking Instrument	Azimuth Range	Nadir Range	Spectral Range (nm)	Spectral Scale (per pixel)	Spatial Scale (per pixel)	Pixel Format
Violet Photometer (DLV)	170°	5°–88°	350–480	–	–	1
Visible Spectrometer (DLVS)	4°	10°–50°	480–960	2.4 nm	2°	20 x 200
Infrared Spectrometer (DLIS)	6°	15.5°–24.5°	870–1700	6.3 nm	–	132
High–Resolution Imager (HRI)	9.6°	6.4°–21.6°	660–1000	–	0.06°	160 x 254
Medium–Resolution Imager (MRI)	21.1°	15.75°–46.25°	660–1000	–	0.12°	176 x 254
Side–Looking Imager (SLI)	25.6°	45.2°–96°	660–1000	–	0.20°	128 x 254

The figure below shows the relative fields of view of the various DISR sub-instruments on one of the primary calibration devices, the 24 inch integrating sphere (described in greater detail in DOCUMENT/DISR_CALIBRATION_DOCUMENTS/CALIBRATION_STANDARD/INTEGRATING_SPHERE_HOMOGENEITY).

Below is presented the view from the bottom of the integrating sphere, looking upward. The DISR is inserted from the bottom of the figure. The source and detectors are inserted at either the 4 or 8 o'clock positions, depending on the calibration mode. The FOV's for the downward looking instruments are shown on the bottom of the sphere (HRI, MRI, SLI, DLVS & DLIS), and the approximate position of the Surface Science Lamp (SSL) beam. Note the SLI extends about 6 degrees above the horizon, and the DLV covers most of the lower quarter sphere (the light green line).

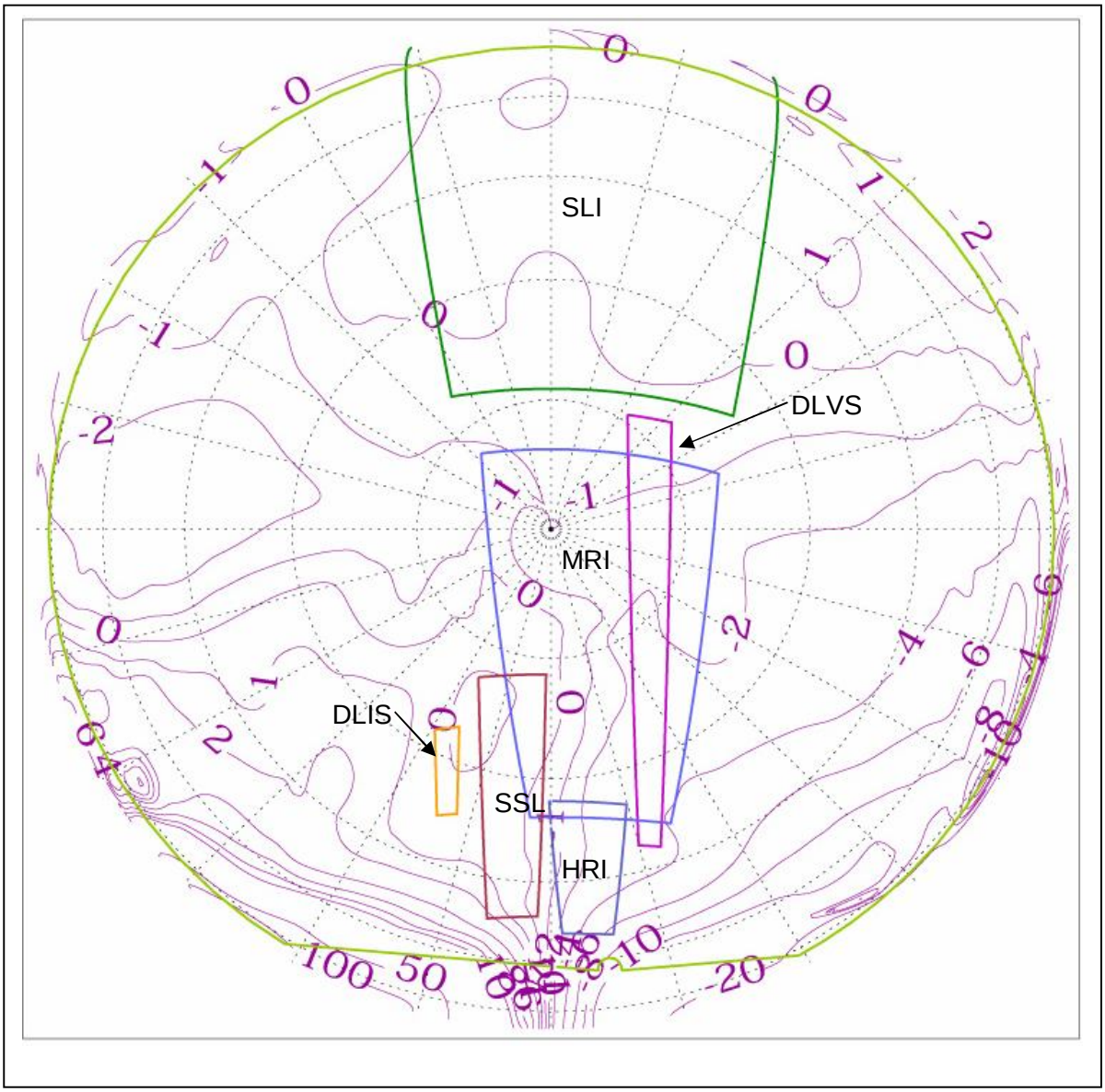

Figure 2-5: Worm's Eye view of the sub-instrument footprints on the 18 inch integrating sphere showing the relative spatial coverage. Some parallax exists since not all optics are at the center of the sphere. The contour lines show sphere intensity variation in percent.

Below is the companion figure, showing the FOV's of the upward looking DISR sub-instruments on the top of the 18 inch calibration integrating sphere. Note the SLI FOV wrapping from below (the green line toward top), and the FOV of the ULV, ULVS & ULIS cover most of the upper quarter sphere (the yellow & dark blue lines).

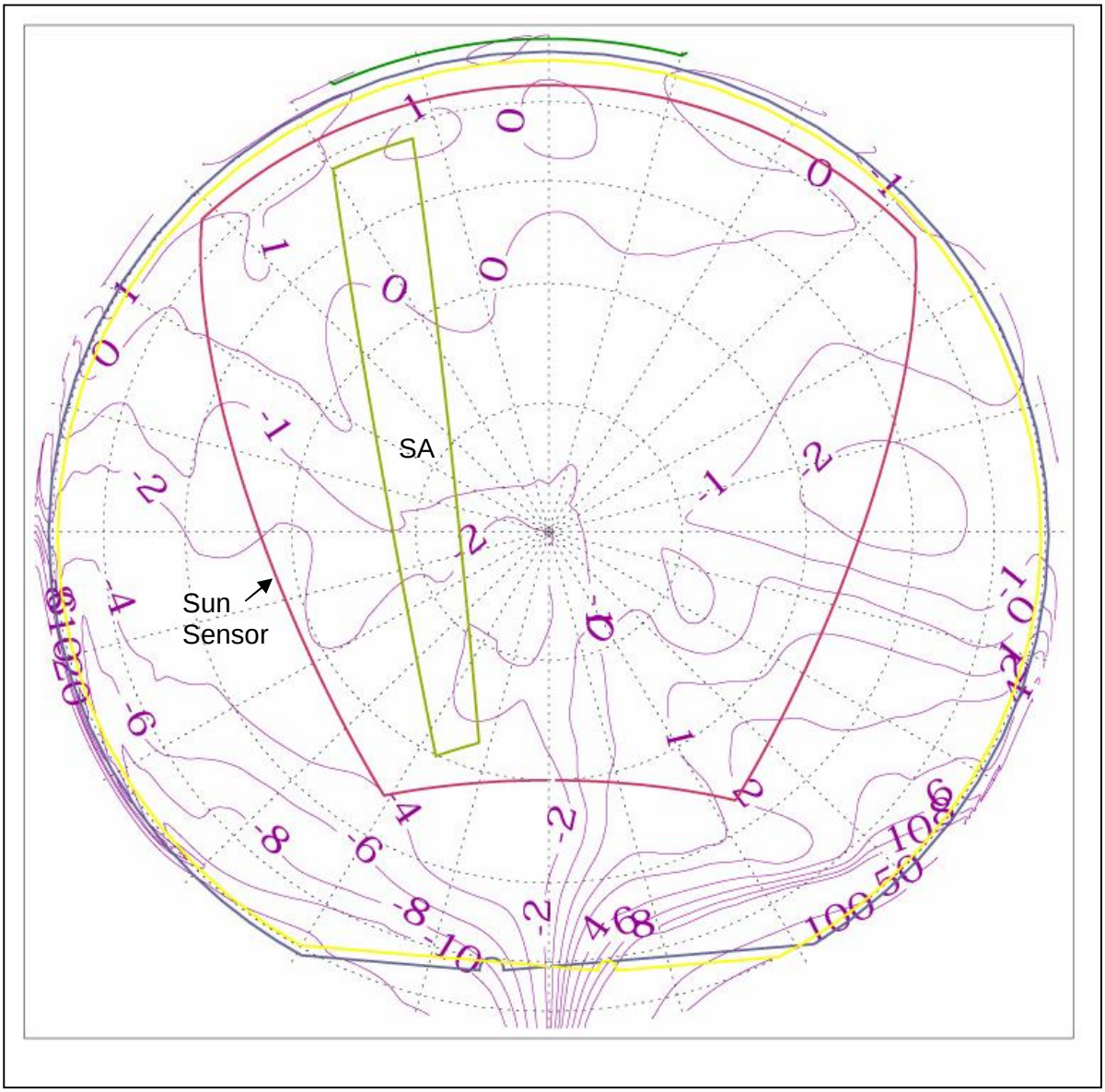

Figure 2-6: Bird's Eye view of the sub-instrument footprints on the 18 inch integrating sphere showing the relative spatial coverage. The contour lines show sphere intensity variation in percent.

3.0 Titan Descent Sequence & Divergences

A description of the intended descent sequence is presented in section 2 of this document, and in much greater detain in Reference 1, which exists in the PSS archive as:

hpdisr_0001/DOCUMENT/DISR_SUPPORTING_DOCUMENTS/ESA_SP_1177

In summary, the instrument protrudes from the side of the Huygens probe and is activated after parachute deployment at ~143 km altitude. As the probe rotates the instrument is designed to take observations at pre-determined azimuths, relative to the Sun as detected by the DISR Sun sensor. The instrument groups observations in Descent Cycles which balance desired observations with telemetry buffer space and altitude. High in the atmosphere the instrument takes plentiful images and spectra to assure the telemetry poling opportunities are optimized. At 20 km altitude the buffer is drained to secure the data taken, and lower in the atmosphere the buffer is kept only as full as necessary to avoid missed poling opportunities. At two altitudes (10 & 5 km) rapid spectral maps of the surface are to be obtained.

A good, although not entirely complete set of data was collected during the Titan descent. Most notably, only half of the DISR images taken were transmitted back to the Earth due to loss of one telemetry channel. As a result fewer overlapping images of Titan's surface were obtained and the number of stereographic images possible was significantly fewer than planned. However, even with this loss it has been possible to create a continuous view of the Titan descent, with no 'holes' in the construction. These assembled datasets are available in the EXTRAS directory of the archive as mosaics and movies of the descent as a visual aid in understanding the scope and sequencing of the data.

Just over a third (99 of 268) of the IR datasets collected were not transmitted to Cassini due to loss of the Channel A data. All of the IR data taken above 18 km, and between 18 and 4 km were sent redundantly (on both channels), however in hopes of collecting higher sampled data of Titan's surface the spectrophotometric maps taken at 18 km and 4 km, as well as all data below 4 km were split between the telemetry channels. Although the science was slightly impacted, there was still significant diversity in the data to allow generation of useful radiative transfer models of the atmosphere, and capture of a good sampling of surface spectra. A plot showing when during the descent the IR data was lost is presented in Appendix 13.

No incomplete or corrupted datasets were received from the instrument during the descent. These would be removed by the error checking in the data link. Some datasets were lost after an extended time on Titan's surface as the link margin degraded, but in general the link and probe telecommunications worked amazingly well, resulting in a useful data volume.

High-quality spectral data was collected from the near IR to the Violet, with matching spectral overlap and good spatial coverage. From this data, coupled with the Solar Aureole measurements, it has been possible to derive the atmosphere's optical depth, model Titan's aerosols, determine methane absorption coefficients, and calculate the solar heating rates. Images of features on Titan's surface made it possible to calculate the wind profile (Reference 5) and measure the reflectance spectra of the various terrains that make up Titan's surface (Reference 15).

Besides the data link problem mentioned above, there were other unexpected limitations:

a) The probe swing rates underneath the parachute were about 3 times faster, and with greater amplitude than expected, especially high in the atmosphere. The result is that the DISR Sun sensor was not able to maintain Sun lock throughout the descent, and consequently not all data were taken at the planned azimuths relative to the Sun.

Radiation exposure during the journey to Titan reduced the sensitivity of the Sun sensor. Below 30 km the optical depth of the aerosols exceeded 3 at its sensitive wavelength. This, coupled with the decreasing temperature did not allow the Sun sensor to operate below this point.

A compensating windfall was the realization that variations in the Huygens receiver AGC signal cause by the probe's rotation could be used to deduce the instantaneous azimuth of the probe, significantly aiding reconstruction of the image and spectral fields.

A post flight reconstruction of the azimuth history is presented in Appendix 5, and the deduced six degree of freedom pointing is presented in Appendix 3 at each image epoch.

c) A reversal in spin direction of the probe also caused unforeseen difficulties with the placement of measurements, particularly the IR spectra and the Solar Aureole (SA) Camera Measurements. We obtained no SA data with the Sun behind the shadow-baffle, and actually very little SA data near the Sun at low altitudes. DISR's header azimuths are defined as degrees west of north (counter-clockwise as viewed from above) relative to the Sun vector's projection on Titan's surface, in keeping with the original intended rotation sense of the probe.

d) An anomaly of the radar altimeter had two significant impacts on the DISR data ensemble. The first being that the highest Spectrophotometric map occurred at almost twice the distance from the surface as desired (18 km vs. 10). This was good and bad in that while the resolution was degraded, the coverage was extended to cover some very interesting terrain. The second impact was the loss of our coldest (lowest) calibration cycle, which was decidedly bad.

To understand this occurrence requires some insight into the DISR-Huygens data collection scheme. The altitude reported to the instruments (via the DDB) was generated by the Time-Altitude Table (TAT) until the table reached 25 km (an actual probe altitude of 26.9 km), at which time the DDB switched to using the reported altitude from the radar altimeter which was 14.8 km. This apparent instantaneous drop of ~10 km caused problems for the DISR data collection scheduling software.

The philosophy of the DISR software was to keep the data buffer as full as possible when the altitude was above 20 km to assure always having data available when polled by the probe. Below 20 km the strategy shifted to avoiding additional data (above a small polling margin) in the buffer so as not to loose valuable low altitude data upon impact. To make this transition a special data cycle executed when the DDB altitude reached 20 km, designed to deplete the buffer (called the Drain cycle). In order to avoid getting stuck in a non-data producing mode the Drain cycle was limited to 6 minutes in length.

Since the Drain cycle occurred immediately following a maximum data producing cycle (an Image cycle), the Drain cycle ran the entire 6 minutes. By this time the reported altitude was too low for the Calibration cycle to be scheduled. The radar altimeter continued to report low until it read below 10 km, which triggered the execution of the spectrophotometric map (at 18.3 km actual altitude). Shortly thereafter the radar altimeter began to function more correctly, however the maximum mission time for scheduling a calibration cycle had passed. Consequently the fourth, and coldest, Calibration cycle was missed. The effect is that for the lowest data the instrument performance must be extrapolated over a fairly wide temperature range. Fortunately there were significant data taken over temperature in the laboratory to overcome this loss.

The consequence of an early spectrophotometric map is that the resolution is degraded by nearly a factor of 2, and the signal to noise is also reduced. On the positive side more of Titan's surface is measured, and the variations between bright and dark terrain can be more fully explored (Ref 3).

The probe's altitude history has been painstakingly reconstructed by the Descent Trajectory Working Group (DTWG), and details of their work are presented in the DTWG archive. A comparison of the altitude reported during the descent via the Descent Data Broadcast (DDB), an earlier, reconstructed altitude used in the DISR headers, and the DTWG profile are presented in Appendix 7.

By combining information from the Probe receiver, DISR Sun sensor, imagers and upward looking instruments it was possible to reconstruct the sub-sampled, low frequency swing of the probe under the parachute. Those data are presented in Appendices 4 and 5 and in the PDS archive under:

/EXTRAS/PROBE_ATTITUDE/HUYGENS_DESCENT_PARAMETERS/HUYGENS_DESCENT_PARAMETERS.TXT and

/EXTRAS/PROBE_ATTITUDE/DATA_AT_SOLAR_CROSSING/AZIMUTH_MODEL_29AUG05.TXT

The Titan descent lasted almost 2.5 hours, which was about 15 minutes longer than expected. The probe survived impact and significant data was returned from Titan's surface. The following figure shows the acceleration profile upon probe impact on Titan's surface, and the corresponding mission time relative to parachute deployment (T0) from Reference 17. Recent analysis shows that the was likely some probe movement for about 10 seconds after impact (Reference 19)

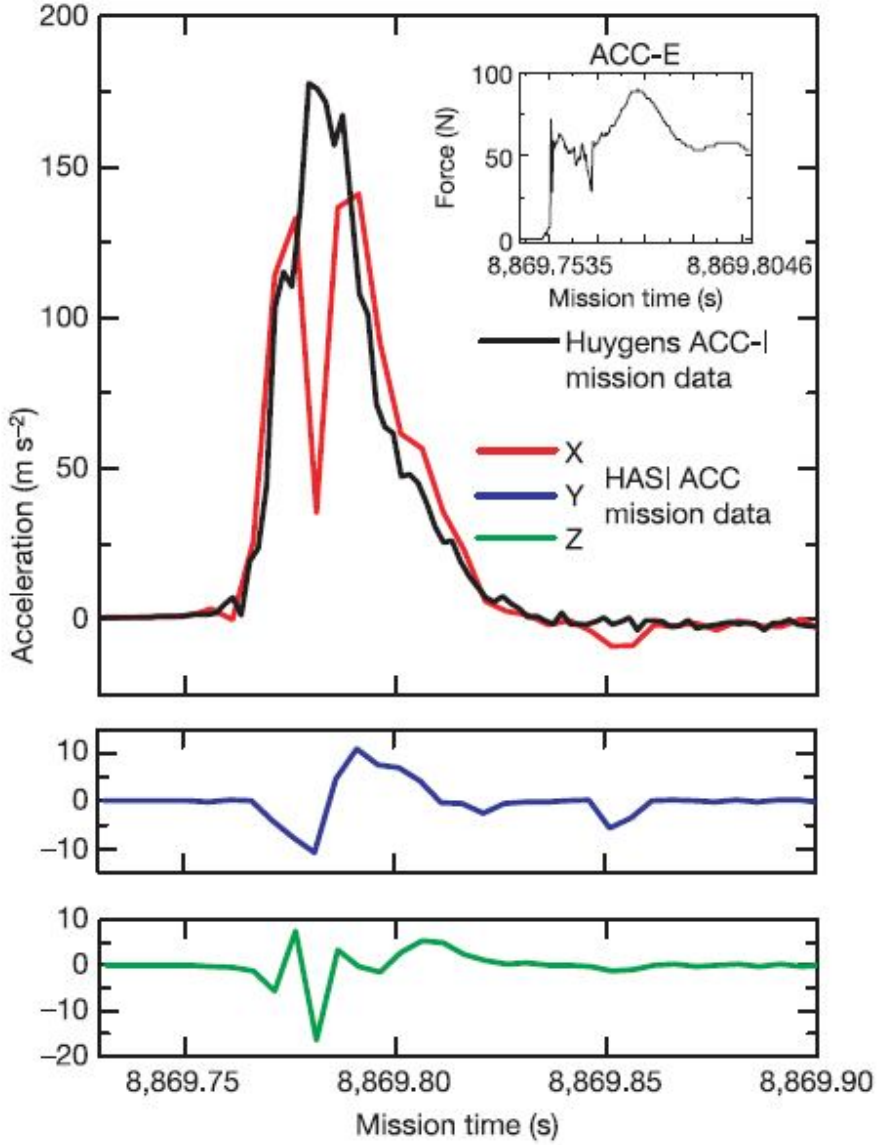

Figure 3-1- Comparison of Huygens Probe impact deceleration profiles. Surface Science Project (SSP) ACC-I in black, Huygens Atmospheric Structure Instrument (HASI) X, Y, Z in red, blue, & green respectively. The insert shows the SSP penetrometer profile. The impact time adopted for most DISR analyses is 8869.77 seconds after T0.

4.0 Archive Description

The DISR data and documentation are preserved in the National Aeronautics and Space Administration's (NASA) Planetary Data System (PDS) archive, and the European Space Agency's (ESA) Planetary Science Archive (PSA). The data can be found on the following websites:

ftp://psa.esac.esa.int/pub/mirror/CASSINI-HUYGENS/DISR/ and,

http://atmos.nmsu.edu/pdsd/archive/data/hp-ssa-disr-2-3-edr-rdr-v10/hpdisr_0001/

The most current version of the DISR archive is HP-SSA-DISR-2/3-EDR/RDR-V1.0 which first posted on 29 May 2007, and last modified on 22 October 2007 (hpdisr_0001). There will be a significant revision released in 2013 which will address:

- Corrections to calibration documents
- Inclusion of more accurate image files
- Add temperatures to label files
- Update altitude profiles to be consistent with newer DTWG data

Below is a summary of the archive's contents, however a more complete description can be found in the Experimenter to Archive Interface Control Document (EAICD) located in the DISR archive under:

hpdisr_0001/DOCUMENT/DISR_SUPPORTING_DOCUMENTS/EAICD

While reading this document, and working with the data from the archive it is important to note the conventions listed in section 9 of this document. There is additional information in the LABEL file for each dataset including a summary of the dataset's header information (altitudes, azimuth, etc) as it was known to the DISR flight software.

4.1 HP-SSA-DISR.../BROWSE/

This may be the most popular directory in the DISR archive. It contains the raw panchromatic images transmitted by DISR during the Titan Descent in 8 bit PNG format. The images are photometrically stretched from zero (black) to 2 times the mean data number (white). This produces the best result since the on-board software aims to expose the image to half of full well (half of the 4096 DN available). This stretch avoids the problem of eliminating cosmic ray hits. The images are also 'rebinned' to be twice their original pixel dimensions using bilinear interpolation smoothing. Less processed images are available in the /DATA/IMAGE directory. Higher processed images are available in the /EXTRAS directory, and in the /DATA/HIGHER_LEVEL_DATA/POSTERS directory in mosaic form.

4.2 HP-SSA-DISR.../CATALOG/

The Catalog directory contains a compendium of documents which provide an overview of the Huygens mission, DISR instrument, archive data volume, DISR personnel, and publication references. Although some of the information is dated (circa 2007) it provides a valuable top level summary of the mission.

4.3 HP-SSA-DISR.../DATA/

The DATA directory contains all the data collected by DISR during the Titan descent arranged by detector system. Although the original XDR format data are manipulated using a variant of IDL (Interactive Data Language, a product of Exelis Visual Information Solutions.), the data are here presented in tabular or ASCII form for easy accessibility. In general the individual datasets are stored in files with names in the format:
"SETID_SEQENCE#_HoursMinutesSeconds_DecimalSeconds" (i.e. VIOLET_0077_002330_2148 is Violet Photometer dataset number 77, taken 23 minutes and 30.2148 seconds after parachute deployment, T0), making it easy to find data if the set id or measurement epoch are known. See the EAICD (hpdisr_0001/DOCUMENT/DISR_SUPPORTING_DOCUMENTS/EAICD) for more details.

Each dataset has an associated Label file (.LBL). There are certain keywords in the Label files which are important for using the DISR data:

Keyword	**Importance**
RECORD_BYTES	Used to discriminate between data configurations (summed vs. un-summed etc,)
FILE_NAME	To find the associated data file
EXPOSURE_DURATION	The exposure time for the observation.
SPACECRAFT_ALTITUDE	The probe altitude at the start of the observation
AZIMUTH	The azimuth of the observation relative to the Sun (degrees to the DISR's left)
HUYGENS:EW_TILT_ANGLE	Spin axis tilt relative to Zenith, eastward positive.
INSTRUMENT_TEMPERATURE	The temperature at various points within the DISR.
INSTRUMENT_TEMPERATURE_POINT	Identification of thermistor locations.
LAMP_STATE	Which DISR lamps are activated (0 = off, 1 = on)
NATIVE_START_TIME	Probe DDB (system) time at start of the observation.
NATIVE_STOP_TIME	DDB time at end of the observation

The DARK datasets are the readout from covered columns of the CCD detector. Their values indicate the dark current being generated by the chip during the other measurements.

The DESCENT datasets record key parameters at the beginning of each cycle of optimized data taking including the altitude and cycle type. There were about 110 Descent Cycles during the descent, and another 50 or so on Titan's surface.

The HKEEPING (Housekeeping) datasets record DISR temperatures, voltages, and software indices.

The IMAGE directory contains tables of the detector readout values for each pixel, after the image has been decompressed (lossy hardware compression).

The IR datasets contain the per pixel (wavelength) readout from each Infrared spectrometer measurement. These readings have been summed into regions, relative to the azimuth of the Sun, to allow for accurate determination of the light intensity in the directions of interest by the onboard software. A summary of the IR data transmitted during the encounter is presented in Appendix 2.

LAMP datasets record when the calibration lamps and surface science lamp are powered, their applied voltage and current draw.

The SOLAR directory contains the measurements of the light intensity field in the upward direction. The intent is to measure the aureole around the Sun. The data are presented as tables of pixel values.

The STRIP datasets are two columns of summed rows on each side of the side looking imager, used to determine the brightness of the atmosphere toward the horizon as well as the tip of the probe.

The SUN sensor records the time when the Sun passes in front of the DISR instrument. It has a double V aperture slit, which allows determination of the tip in the direction of the Sun, by virtue of the crossing times. The Sun sensor information is used to 'time' the taking of all other data relative to the Sun (clocking to the Sun azimuth). Its amplitude is an independent measurement of the solar absorption at its pass band (938nm). The data are presented as a table of the times (relative to DDB T0) that the Sun passes in front of each of the 3 slits, as well as the detector reading in DN.

The TIME datasets record the DISR internal clock time, and DDB time, at each Broadcast Pulse.

The VIOLET datasets contain the reading (amplitude) of the violet photometer.

The VISIBLE directory contains the data from the Upward Looking and Downward Looking Visible spectrometers as a table of values. The rows of the tables are the wavelength dimension, and the columns are spatial. In some cases the columns (spatial dimension) are summed to reduce noise and data volume.

The VISIBLE_EXT datasets record the values of the column of pixels on each side of the corresponding visible spectrometer. This information is used to compensate for light bleeding through (scattered light) from the adjacent CCD instruments (imagers and solar aureole camera).

4.4 HP-SSA-DISR.../DERIVED_DATA_PRODUCTS

This directory contains the results of data reductions done by the DISR team on the spectral data. In general it presents tables of the Spectral Radiance looking upward and downward from 350 nm (i.e. the violet photometer) through 1.6 micron (i.e. the IR spectrometers). More specifically it contains the following files:

ULV_NET_DN & DLV_NET_DN - The upward and downward looking data numbers from the violet photometer (350 to 480 nm) after the appropriate dark bias has been removed.

ULV_DDP & DLV_DDP - The mean spectral radiance over the field of view of the violet photometers at each altitude where a measurement was taken. The calculations assume a quadratic intensity profile across the photometers' spectral band, which is generally correct to around 1% error.

ULVS_DDP & DLVS_DDP - The upward & downward looking spectral radiance (in watts/(m^2*μ*sr)) for each visible spectrometer wavelength, covering the range from 477.3 to 978.6 nm. The values represent the mean value across the field of view.

ULIS_AV_DDP & DLIS_AV_DDP - The spectral radiance (in watts/(m^2*μ*sr)) averaged over all azimuthal regions and over the field of view of the IR spectrometer for that descent cycle. This information can be used to calculate the energy absorbed in an altitude layer, but has no azimuth dependence information.

ULIS_AZ_DDP & DLIS_AZ_DDP - A table of the spectral radiance (in watts/(m^2*μ*sr)) for the quick exposure, 'snapshot mode' observations taken on and near Titan's surface. Again, the values are the mean over the field of view.

ULIS_I_DDP & DLIS_I_DDP - The average spectral radiance for each azimuthal region (4 for the ULIS or 8 for the DLIS) at each descent cycle altitude for the 136 IR spectrometer wavelengths (covering 822.7 to 1717.6 nm).

More information about how these data products were developed can be found in sections 6.0 & 5.0 of this document and in the corresponding calibration documents (see section 4.5).

4.5 HP-SSA-DISR.../DOCUMENT

The DOCUMENT directory contains the documents which describe how the DISR was calibrated, and how to convert the data into physical measurements. It also contains information about the equipment used during calibration and the method for compensating for the detectors' dark current offsets. The supporting documentation contains information about the instrument design and science objectives.

The DISR instrument calibration reports contain complete descriptions of each instrument detector system, the calibration data, methods, and algorithms for converting the instrument data numbers into physical units and intensities into data numbers.

Reduced mean intensities over the field of view (FOV) are provided for the spectrometers. However for the broad band instruments (imagers, SA camera) the mean intensity over the FOV is not a useful number since the spectral variation is important, and the bandpass changes significantly during the descent. It is felt that the best scientific approach is to create models which reproduce data numbers rather than mean intensities.

Although some lines of code exist as examples in the calibration reports, no generic calibration software is available. Interpretation of the DISR data is dependent on selection of the model parameters (i.e. atmospheric composition, intensity spectrum, surface reflectance, variation over the field of view) and key in deciphering the data. This is often best done using radiative transfer models. The scientist is encouraged to develop their own software to explore the physical interpretations of the DISR data. Section 5 of this Guide presents examples of how the data can be interpreted.

The CATALOG directory contains general information about the data set, such as involved personnel, instrument description, references, etc.

5.0 Data Calibration

5.1 General Information

All of the DISR detector systems were calibrated prior to launch at the Kuiper Lunar and Planetary Laboratory (LPL) on the University of Arizona's main campus in Tucson Arizona. Calibration reports, describing the each sub-instrument and its calibration are contained in the DISR Archive in the "hpdisr_0001/DOCUMENT/DISR_CALIBRATION_DOCUMENTS" directory. Since this was a limited duration, one time data collection a classic calibration pipeline does not exist, instead the data must be hand calibrated for the specific intended science goal. This document, as well as the calibration documents mentioned above, are intended to aid the user in that effort.

An important aspect of DISR data calibration is tracking instrument performance changes over the 7 year period from laboratory calibration to Titan encounter. Significant environmental exposures were experienced by both probe and instrument including launch, orbit insertion, atmospheric entry and surface impact along with an enhanced space radiation environment due to on-board radioscopic heaters and power plants. This tracking is made possible by a calibration lamp system within the DISR sensor head which channels light (using fiber optics) from 3 incandescent lamps to the detector systems. This system was activated several times during the flight period, and was intended to function 4 times during the descent, however one Calibration cycle was lost (as explained in section 3).

Beyond the laboratory calibration, in-transit changes, and descent calibration data one needs information on the encounter itself to make good use of the DISR data. This document contains information regarding the solar flux at Titan, Sun position, probe dynamics and descent event information for the Huygens-Titan encounter.

It is always a good idea to determine if there is updated information regarding the Titan entry parameters (i.e. time history for: altitude, tip-tilt, spin, azimuth, temperatures, etc) before proceeding with data analysis. Contact information can be found in the archive in hpdisr_0001/CATALOG/PERSON.CAT or at the end of this Guide.

The following graph presents the solar spectral irradiance used in the DISR data reduction calculations. This is the assumed intensity at 1 AU, convolved to the DISR pixels' wavelengths and extended in the blue by Erich Karkoschka, and in the red by Bruno Bezard. In calculating the solar spectral radiance, F at Titan (in watts/(m^2*micron*steradian)) these values must be divided by Pi and the distance from Titan to the Sun squared at the time of encounter which is 9.053^2 (or 81.96). The data is presented in tabular form in Appendix 1.

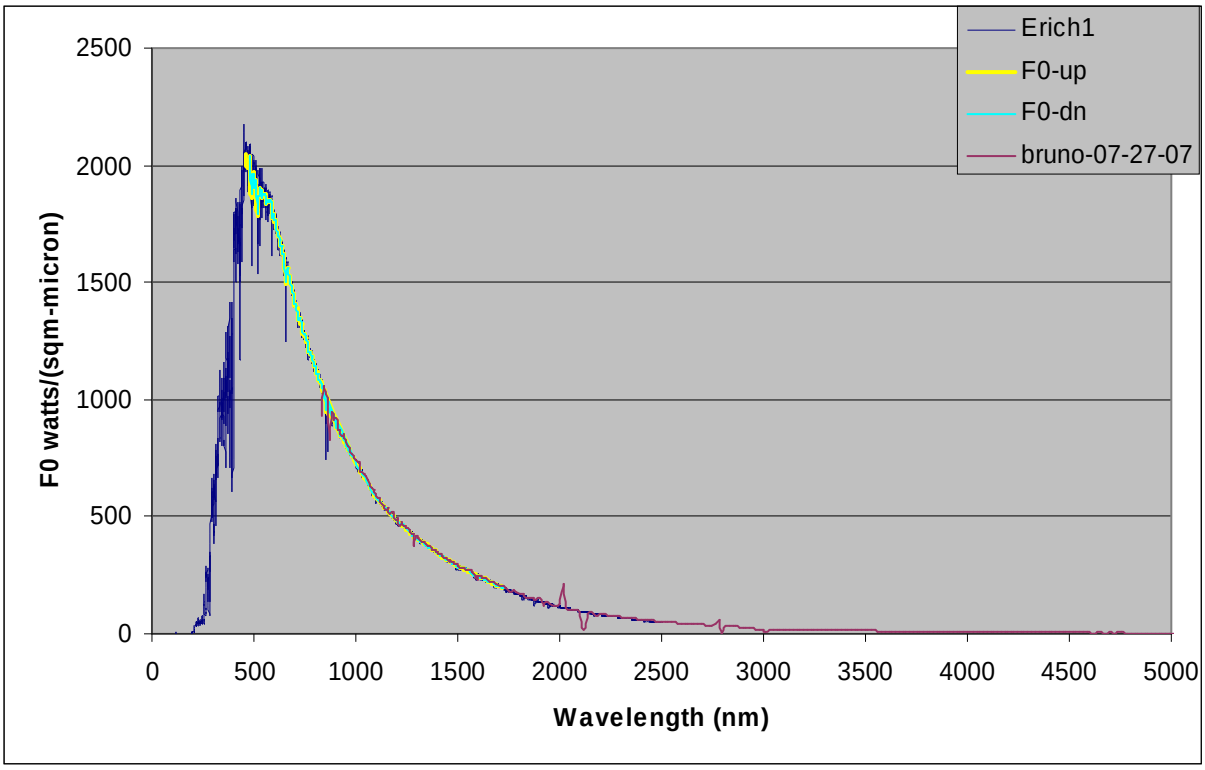

Figure 5-1: Solar Flux Spectrum (at 1 AU) used in DISR data reduction. The dark blue line is the spectrum provided by Erich Karkoschka, and the dark red is provided by Bruno Bezard, DISR team members. The yellow line is the spectrum convolved to the pixel width of the upward looking DISR spectrometers, and the light blue line is the spectrum convolved to the pixel width of the downward looking spectrometers.

5.2 Descent Cycles

The Descent Cycles datasets relay information about the data collecting schedule that was determined by the on-board software. The datasets contain the type of collection cycle, the mission time at the start of the cycle, and the DDB reported parameters of altitude and spin rate. A summary of the descent cycles experience during the encounter is presented in Appendix 6.

The following is an explanation of the text fields in the Descent Cycles datasets:

filename_pre: is the directory path on the computer that the test-log was generated on.

filename: is the name of the original file on the computer the test-log was generated on.

date_taken: is the date and time in the format *year-month-dayThour:minute:second* GMT.

set_name: designates the type of cycle (typically Descent or Calibration).

gse_ver: is the Ground Support Equipment (GSE) software version used to decode the data.

test_log: is the location and name of the target data-stream that was decoded.

seq_num: is the sequence number of the dataset which begins at 1, is the same as the sequence number in the filename (i.e DESCENT_0001_...), and should always agree with the cycle number.

m_time: is the mission time reported in seconds after T0 (parachute deploy command).

cycle_num: is an index count of the cycle being reported. For the Titan descent it is the same as the seq_num. For some calibration and in-flight test logs they may differ due to restarting of the sequence.

cycle_type: is cycle type number and corresponding designation (Image, Non-Image, etc) as described in the table below:

cycle_type	Cycle Name		cycle_type	Cycle Name
1	Standard non-image		11	High near surface
2	Standard image		12	Medium near surface
3	Flat Field		13	Low near surface
4	Cal Cycle A		14	Very low near surface
5	Cal Cycle B		15	Surface A
6	Cal Cycle C		16	Surface B
8	Dark current only		17	Surface C
9	Spectrophotometric		18	Surface D
10	Drain cycle			

scen_step: is the scenario step and represents the number in the cycle criteria table which defines why this particular type of cycle was selected based on mission time and altitude.

spm_flag: designates if the cycle is a spectrophotometric cycle (1) or not (0).

az_cycle_start: is the azimuth reported by the on-board software (in degrees, counter-clockwise from the Sun) for the beginning of the cycle (usually in considerable error due to rotation reversal and Sun sensor drop-outs). The actual azimuth history via Karkoschka is available in Appendix 5 (& Ref 5).

altitude: is the altitude reported in meters and kilometers, and the spin rate in RPM at the beginning of the cycle. Again, a more accurate determination of the probe altitude as a function of time is presented in Appendix 7.

spin: is the probe spin rate as reported by the on-board software in revolutions per minute (RPM). A better source for the actual spin rate is from the azimuth time history in Appendix 5.

5.3 Lamp Datasets

The Lamp datasets contain information about the 3 small on-board calibration lamps (~0.5 W each), as well as the 20 watt Surface Science Lamp (SSL) which is designed to illuminate Titan's surface once the probe gets close enough (nominally coming on at 700 m altitude).

When any of the DISR lamps are powered, Lamp datasets are generated which report the commanded lamp state (which lamps are commanded on) and the voltage & current being drawn by all 4 lamps. Since the calibration lamps are only commanded on for a short time, during each of the four calibration cycles, most of the Lamp datasets were generated when Huygens was on Titan's surface.

The archive label file and the data file both report the lamp command state using 4 binary numbers as follows: 1110, where the first three bits refer to the three calibration lamps (A, B & C), and the fourth bit references the SSL lamp state. In all cases 0 means off, and 1 means the lamp is commanded on.

The data file also reports the altitude at the time of the reporting, and the voltage and current for each lamp in volts and amps.

More details of the DISR lamp performance can be found in the Engineering Appendix to the User's Guide (Reference 19).

5.4 Housekeeping Data

Housekeeping datasets are generated at the beginning of each descent cycle (the descent cycles are summarized in Appendix 6). The Housekeeping datasets contain all DISR temperatures (see Appendix 23 for locations), except the IR chip temperatures, which are only reported during IR spectrometer measurements (and are offset hot by about 10C). Note the temperature field INSTRUMENT_TEMPERATURE(1) = "REF_T2" is a spare field and has no value assigned to it in any of the DISR datasets.

The Housekeeping data also contains internal instrument voltages including the Auxiliary electronics board (nominally 12 volt DC) supply which powers the IR shutter, the 5 volt CPU board voltage, which powers the on-board integrated circuits, and Analogue to Digital Converter (ADC) voltages, as well as information about the size of the software queues.

The time reported in both the label and data files is the start of the Descent cycle in seconds after T0 (parachute deployment command).

The temperatures are reported in both the label (as the INSTRUMENT_TEMPERATURE array) and data files in degrees Kelvin.

The altitude at the beginning of the Descent cycle is reported in the Housekeeping data in kilometers.

The temperature sensor supply current (t_sensor_curr) is reported in the data file in amps.

The Auxiliary Board voltage, CPU supply voltage and ADC offset are all reported in volts.

The maximum size of each system queue (Dispatcher, Alarm, Telemetry, Science Processing & Stack) is reported. Unlike the other housekeeping parameters, the queue sizes are the maximum since the last Housekeeping dataset and therefore reflect the maximum over the previous descent cycle. There is no Housekeeping dataset at the beginning of the first cycle, however the Housekeeping dataset at the beginning of the second cycle reports the queue sizes for the first cycle.

5.5 Sun Sensor Observations

The DISR instrument is equipped with a masked photodiode sensor whose primary purpose is to track the location of the Sun in Titan's sky to allow for proper azimuth angle timing of the DISR's observations. However this device is also valuable for measuring the extinction of the solar beam during the descent. The device is designed to view the Sun through one of the spectral windows (943 nm) in Titans atmosphere.

The Sun Sensor provides 3 pulses per probe revolution. The flight software is designed to use this information to determine the probes azimuth relative to the Sun. To avoid false detections a reasonably elaborate filtering algorithm is used to determine if the pulses measured by the Sun sensor are valid or not. Only when five Huygens rotations of 'valid' Sun sensor pulses are observed (Sun sensor lock) is the azimuth information from the Sun sensor used , otherwise DISR relies on the Descent Data Broadcast information for timing observations.

Unfortunately three disruptive conditions occurred during the descent which limited the usefulness of the Sun sensor data to time observations. The first is that Sun sensor was not equipped to tell the direction of rotation of the probe, so when it began to spin backwards, the software produced unexpected results. Secondly, there were greater probe swing dynamics than expected, beyond the filtering capability of the DISR flight software, so often pulses were considered 'in-valid' and Sun sensor 'lock' was lost. The third problem was that radiation exposure during the cruise from Earth to Titan cause a significant loss of sensitivity of the photodetector, and low in the atmosphere there was not enough signal left to reliably retain Sun sensor lock (see section on "Sun Sensor Performance" (7.1) of the "DISR Engineering Data Companion Document" in the archive for the details). The result was that only 45 of the 360 or so Sun crossings were measured.

The DISR Sun Sensor is a photodiode located behind a narrow band filter (943 nm) and a 3 slit mask:

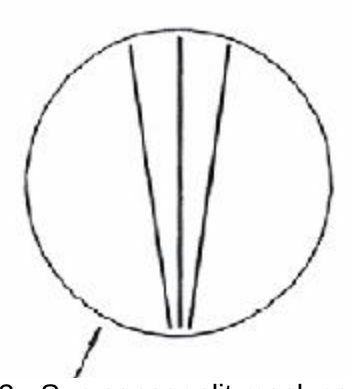

Figure 5.5-2 - Sun sensor slit mask configuration.

The Sun Sensor datasets contain the amplitude of the peak photodiode signal (in DN) and the mission time when the Sun passes in front of each slit (3 pulses per revolution) and thus gives information about the azimuth, rotation rate and tip of the probe.

Details of the Sun Sensor calibration are in the DISR Archive under: DOCUMENT/DISR_CALIBRATION_DOCUMENTS/SUN_SENSOR (see Reference 9).

A summary of the Sun sensor data is presented in Appendix 28.

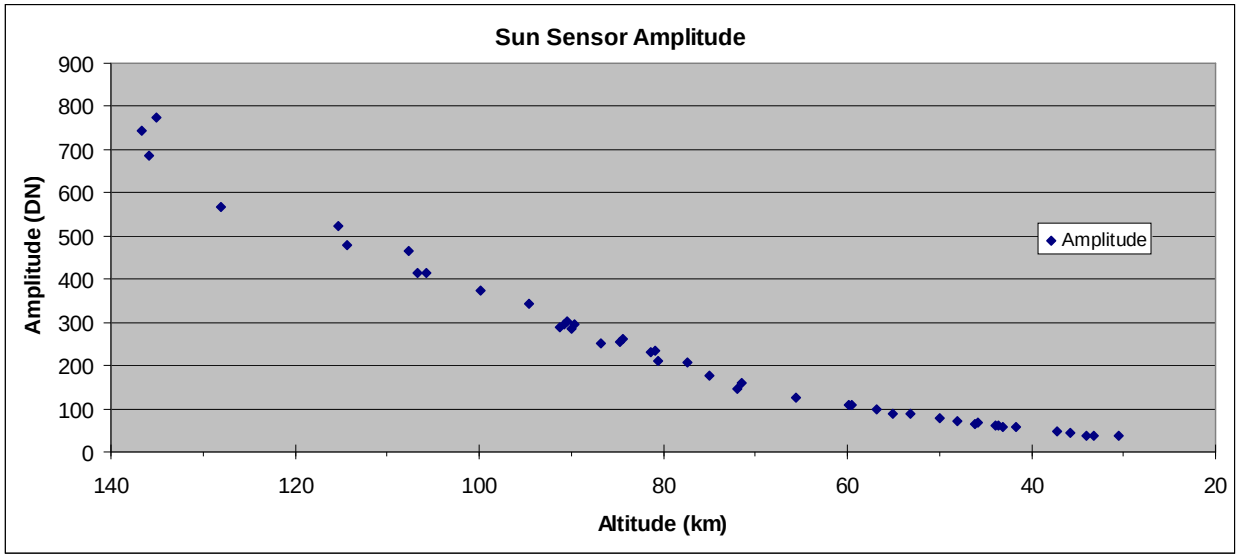

Figure 5.5-3 – DISR Sun sensor amplitude history, raw data numbers (DN)

The solar direct flux at 943 nm is related to the Sun sensor amplitude (equation 6 of Reference 9) by:

$$\text{Flux}(943\text{ nm}) = (\text{DN}-2.5)/\ (414.4\ \text{DN/Watt/sq.m-micron}).$$

where DN is the amplitude reading from the DISR dataset.

This relationship is dependent on the probe spin rate, solar zenith angle and temperature. It is correct at 4 rpm spin, 50 degrees solar zenith angle, and 295.185 ºK but must be corrected for variations in these parameters, as described in the following sections.

Correction for solar zenith angle (SZA)...

The following plot shows the variation in response vs. elevation angle (90-SZA),

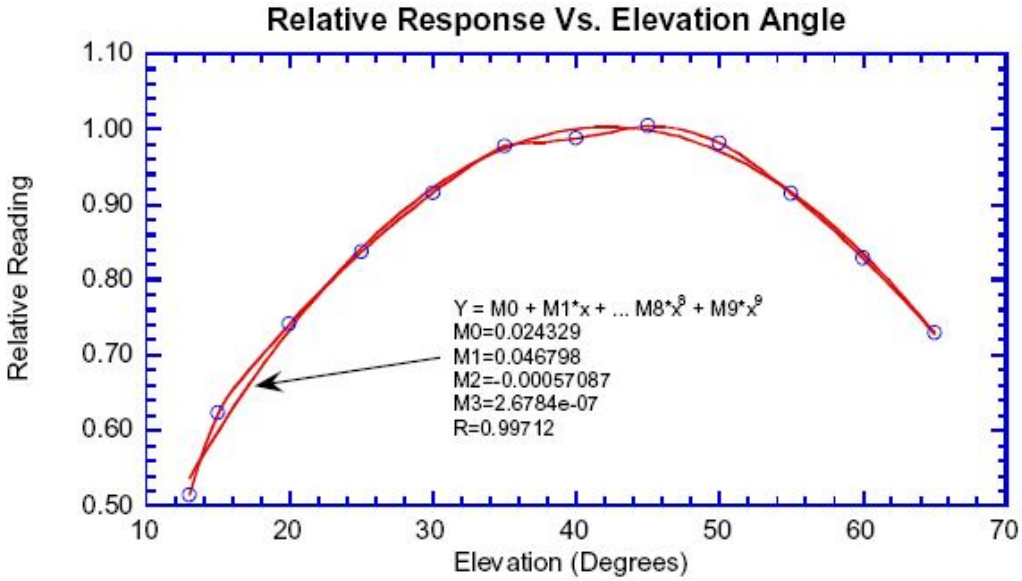

Figure 5.5-4 – Sun sensor variation with elevation angle. Data, cubic spline, and 3rd order polynomial fit (with coefficients) are shown.

From this fit comes the SZA correction equation:

$$DN'(40\ degeees) = DN'(elevation) / (0.024329+0.046798*el-5.7087x10^{-4}*el^2+2.6784x10^{-7}*el^3).$$

or

$$Re = 0.024329 +0.046798 *el -5.7087x10-4 *el^2 +2.6784x10-7 *el^3$$

where:

DN' is the unbiased data number, (DN - 2.5), and
el is the elevation angle (90º - SZA).

The equation models the variation by better than 2%.

The solar zenith angle was 40 degrees at the beginning of the descent; decreasing to 33.8° by impact continuing to about 32 degrees at loss of signal as described in Appendix 14.

Correction for spin rate...

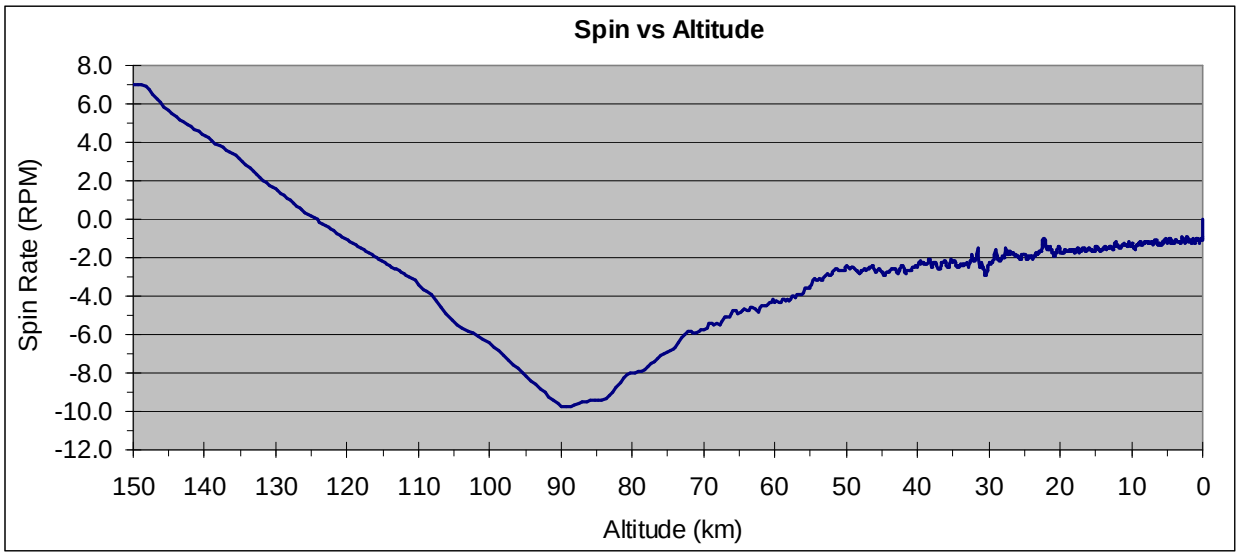

Figure 5.5-5: Huygens probe spin rate vs. altitude. Note the reversal in spin direction around 125 km altitude.

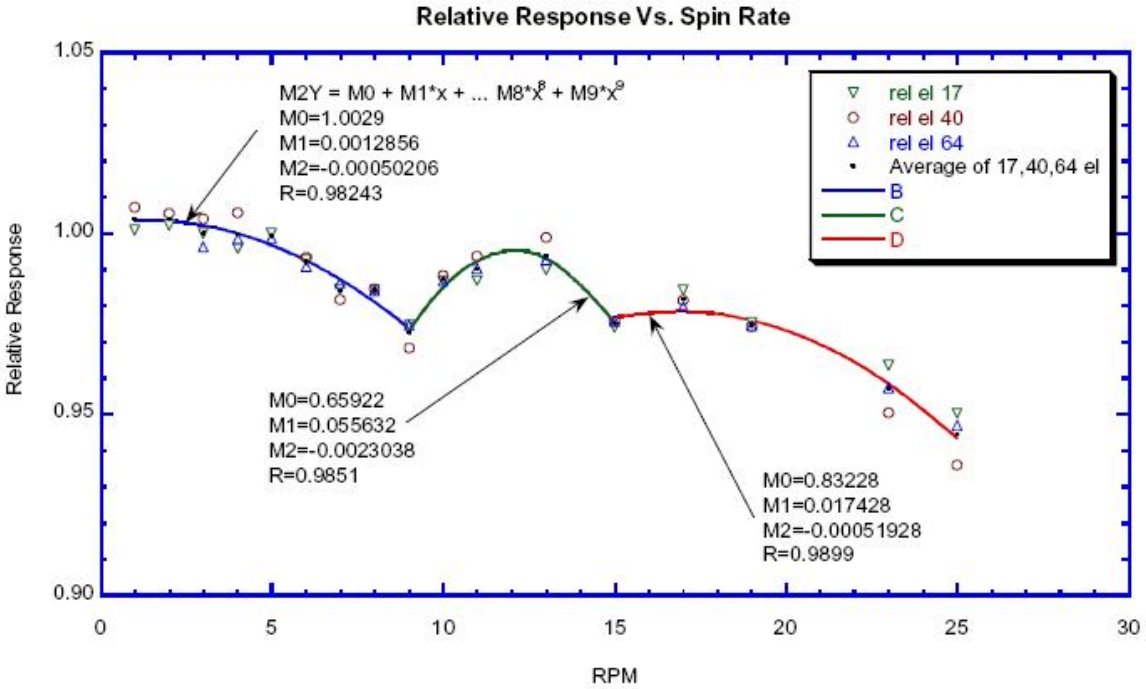

Figure 5.5-6 – This plot shows the Sun sensor variation with probe spin rate. The symbols show the calibration data at three different Sun elevations, and the average. The Sun sensor spin rate variation has different characters over 3 spin regimes. The curve fits and corresponding polynomial coefficients (M0, M1 & M2) are shown.

Therefore there are 3 spin correction equations...

for rpm < 9, $R= 1.0029 + 0.0012856 *rpm - 0.00050206 *rpm^2$,
for 9 < rpm < 15, $R=0.65922 + 0.055632 *rpm - 0.0023038 *rpm^2$,
for rpm > 15, $R=0.83228 + 0.017428 *rpm - 0.00051928 *rpm^2$.

where R is relative response, to be divided into the unbiased response:

DN'(4 rpm) = DN'(spin) / R

Correction for temperature difference...

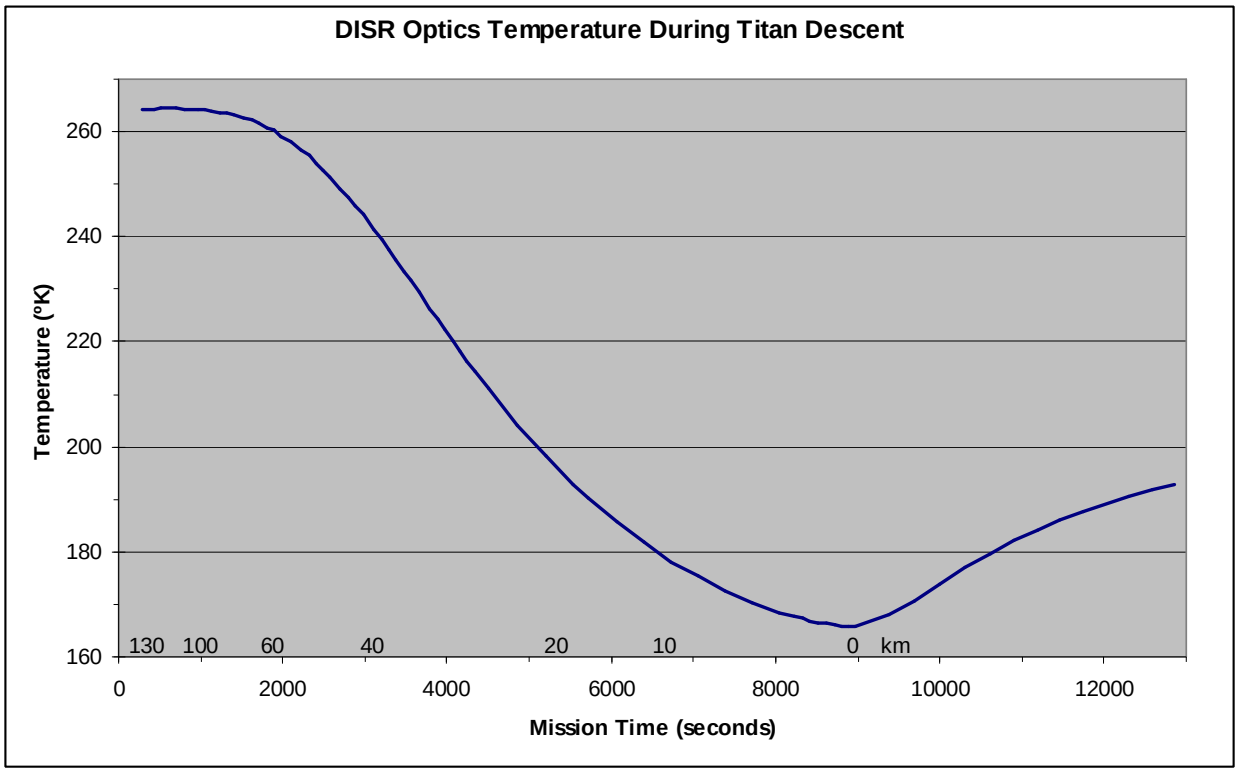

Figure 5.5-7: DISR optics temperature during Titan descent vs. mission time with altitudes noted. The probe began to warm after touchdown.

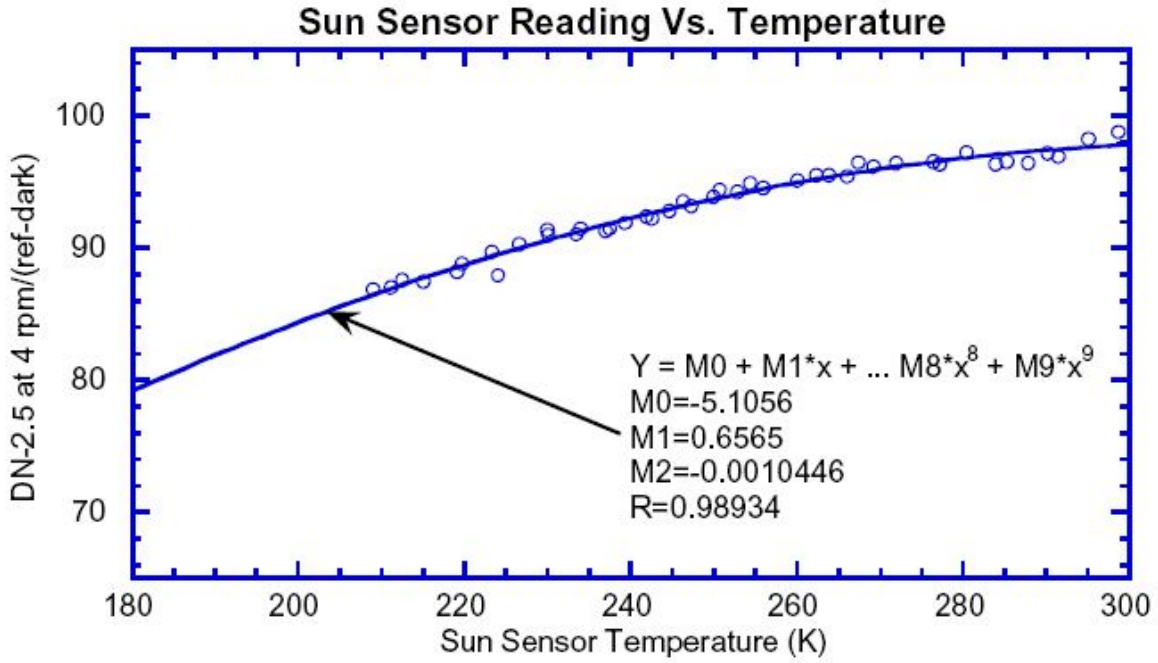

Figure 5.5-8: For a constant source intensity, the Sun sensor's responses varies as shown. The circles are the calibration data, and the blue line is the curve-fit indicated by the polynomial equation with coefficients M0 thru M2.

To correct a measurement at any temperature (T) to the calibrated (Optics) temperature of 295.185 requires the scaling factor described in the Sun sensor calibration document in the section named "Variation of Responsivity with Temperature" (Reference 9, section 6):

$$(\text{DN-2.5}) \text{ at } 295.185 \text{ K} = (\text{DN-2.5 at T}) / [-0.05228 + 0.006722*\text{T} - 1.0696\text{x}10^{-5}*\text{T}^2]$$

or

Rt = -0.05228 + 0.006722*T –1.0696x10-5*T^2

Thus, the procedure for converting the data numbers from the Sun sensor to the flux in the direct solar beam is to remove the bias of 2.5 DN then correct the result to 4 rpm, 50º SZA & 295.185ºK by dividing by R, Re & Rt. The result is then divided by the Sun sensor absolute responsivity of 414.4 DN/(Watt/sq.m-micron) to give the absolute flux in the solar beam in Watts/sq.m-micron.

$$Flux(943nm) = \frac{(DN - 2.5)}{414.4 * R * R_e * R_t}$$ in Watts/(sqm micron)

Diffuse Flux...

As Huygens descends through Titan's thick atmosphere, the direct solar flux observed by the DISR Sun sensor is increasingly contaminated by diffuse, scattered light. At 943 nm the diffuse flux is negligible at 400 km altitude, but increases to almost 1% of the signal near Titan's surface as seen in the plot below.

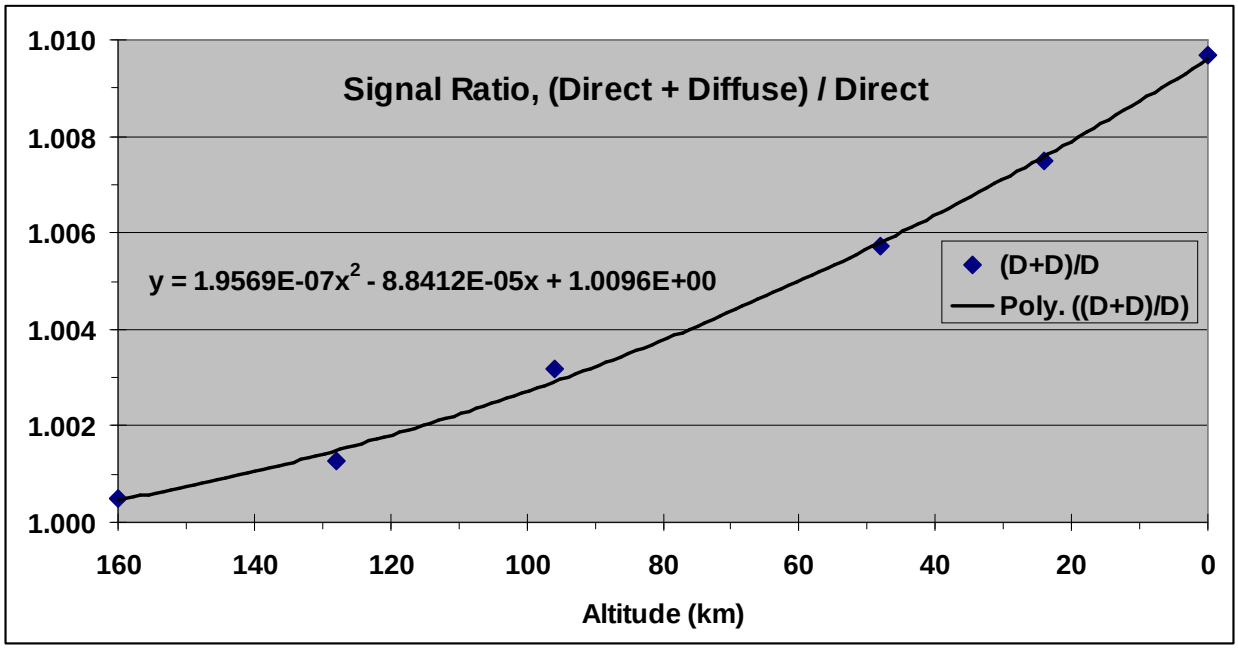

Figure 5.5-9: Ratio of Direct plus Diffuse flux seen by the DISR Sun Sensor to the direct solar beam at 934 nm, as a function of altitude. The diffuse flux is essentially 0 (ratio = 1) at 400 km, but increased to about 1% of the signal near Titan's surface. (Ref 9, Sun Sensor Cal. Report, table 10)

To compensate for diffuse flux contamination we introduce a correction factor Rh, which is a function of altitude as:

$$Fs = Fm / Rh$$

where:

Fs is the direct solar flux,
Fm is the flux measured by the DISR Sun sensor, and
Rh is the correction factor, which is a function of altitude (h) thusly:

$$\mathbf{R_h = 1.9569E\text{-}07h^2 - 8.8412E\text{-}05h + 1.0096E+00}$$

Flux Calculation Example...

Of the 4 components (scattered flux, probe spin, temperature & solar zenith angle) that modify the Sun sensor's flux measurement, the apparent solar zenith angle is the least well known.

1) The scattered flux is measured to around 1% by the DISR spectrometers.

2) The probe spin is well measured by the Sun sensor's period, variation in the link AGC, intensity variations in the optical instruments, and features in the images (ref Karkoschka), although short term variations are possible. Our azimuth function is smoothed to the scale of half a rotation, and fits quite well, however instantaneous measurements may be several degrees in error, resulting in significant rate variations. However even a factor of two error in spin rate results in only a few percent error in measured flux by the Sun sensor.

3) The temperatures are well measured by the DISR and probe sensors (albeit with some lag and gradients).

4) But lacking a good probe dynamics model, the 6 degree of freedom (DOF) motion of the probe is not so well known. So although the SZA is well known, the instantaneous angle between the Sun vector and the probes spin axis could be in error by several degrees as described below.

The Sun's apparent elevation in the sky has 3 components:

1) The solar zenith angle (90º-elevation) history at the probes position vs. time:

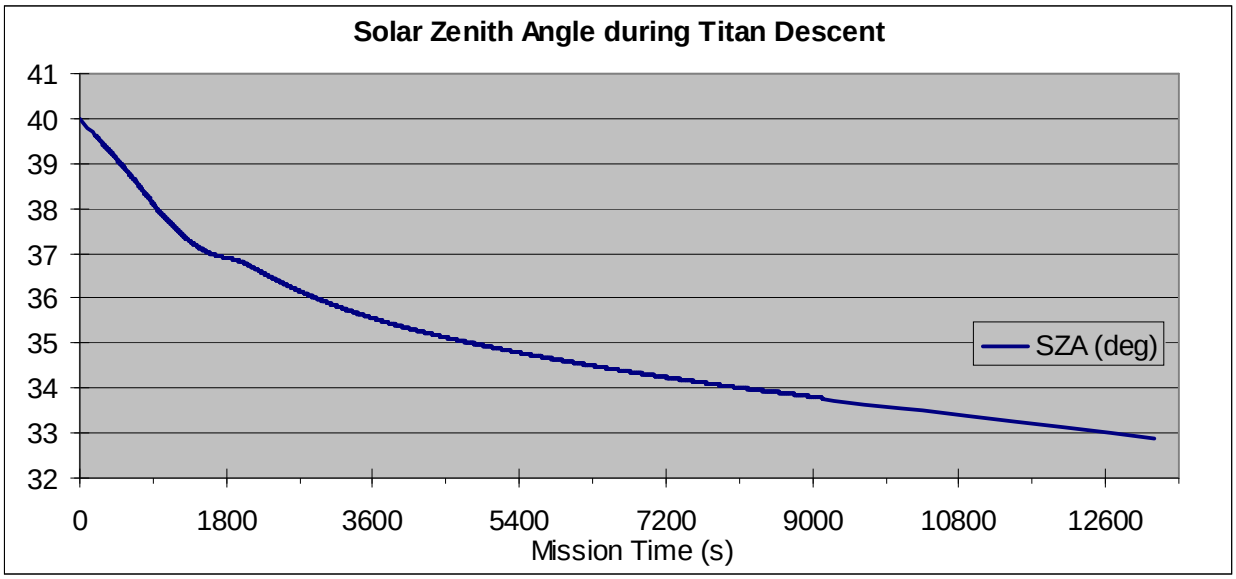

Figure 5.5-11: Solar Zenith Angle (SZA) relative to the Huygens probe's position during the Titan encounter.

2) The East-West tip of the probe's spin axis during the Titan descent caused by wind and pendulous motion (~0.1 Hz) below the parachute, and

3) A higher frequency (~1 Hz) swaying motion caused by movement relative to the parachute swivel (Ref 5, Karkoschka).

Figure 5.5-12 – Parachute stability

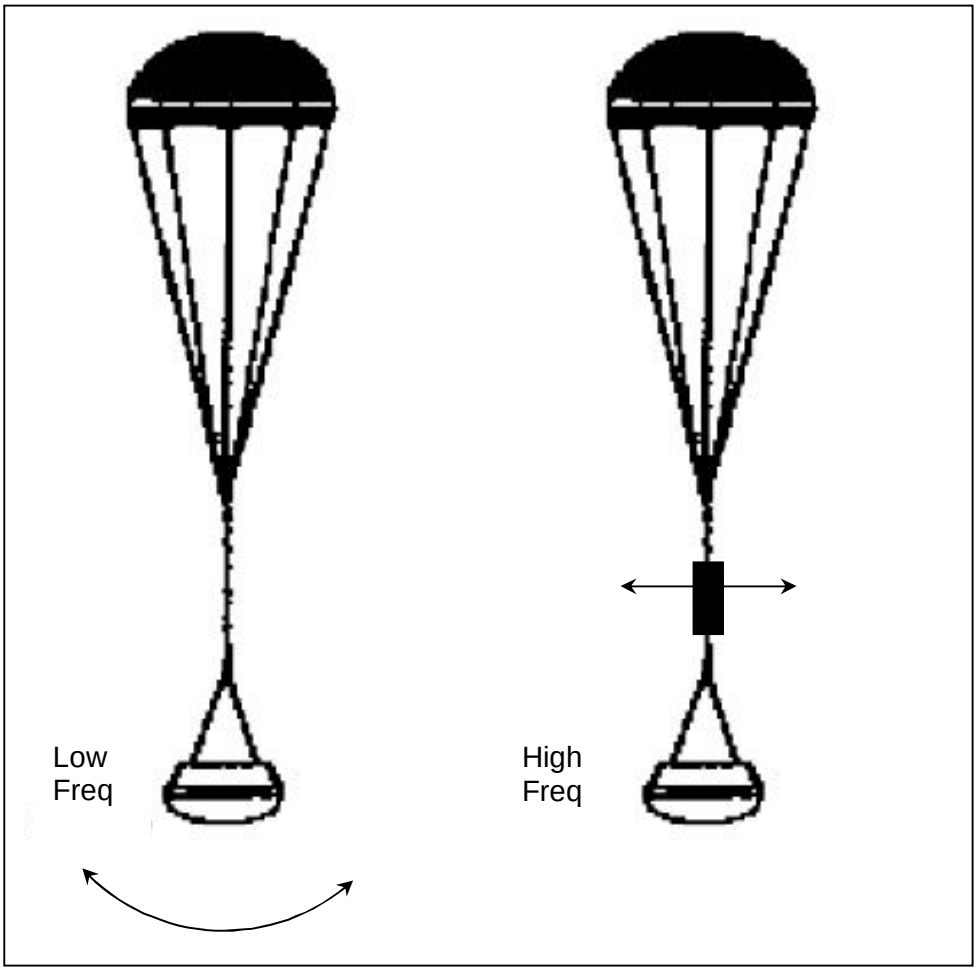

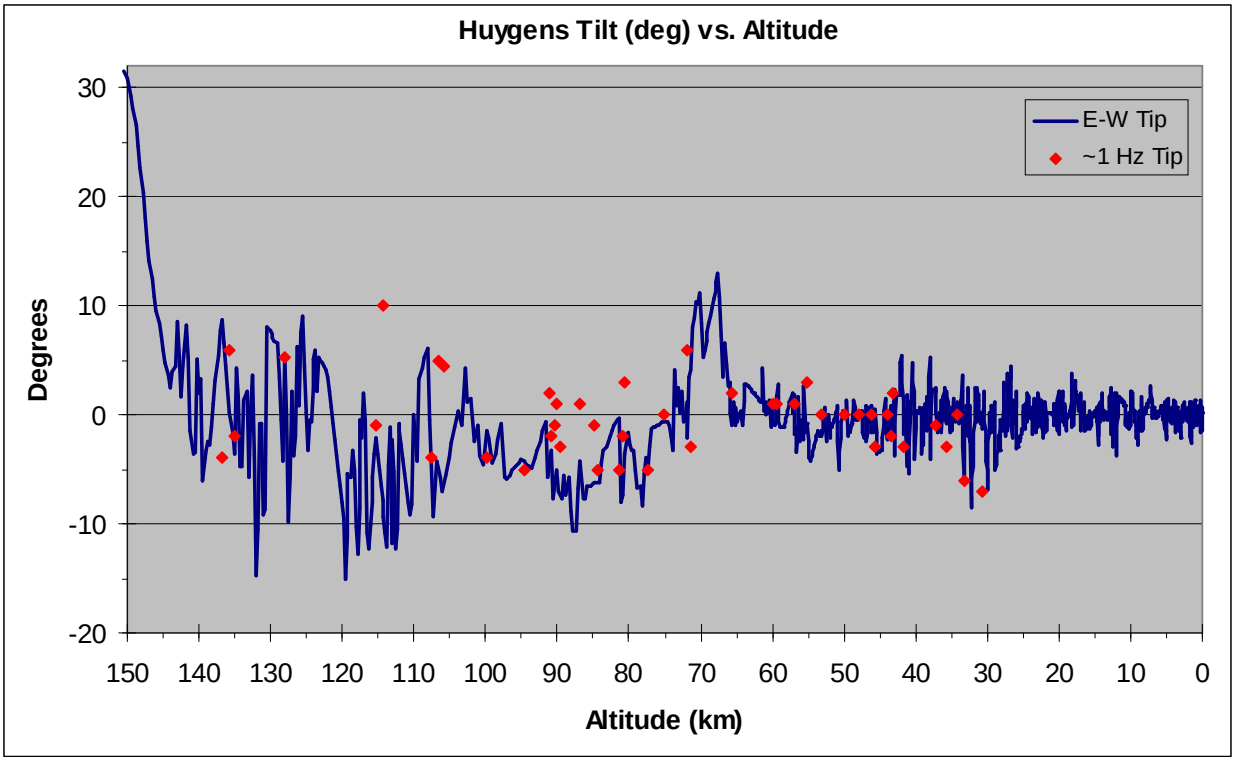

Figure 5.5-13: Two components of probe tilt motion during the Titan descent. The blue line is the low frequency (~0.1 Hz) pendulous motion of the probe - parachute system. The red dots represent the implied tip from the higher frequency (~1 Hz) swinging motion of the probe due to the parachute swivel movement.

The summary of the DISR Sun sensor data presented in Appendix 28 was calculated using:

$$Flux(943nm) = \frac{(DN - 2.5)}{414.4 * R * R_e * R_t * R_h}$$ in Watts/(sqm micron)

To obtain the apparent Sun elevation the East-West tip component toward the Sun was added to 90-SZA for each observation. The unknown high frequency tip was adjusted within the limits of ±10º to contain out-of-family measurements, resulting in the red dots shown in the figure above, and included in Appendix 28 as "Tip toward Sun".

The result is presented in the figure below, fit with two exponentials (F1 & F2), one for the upper atmosphere, and one for the lower. The results are also in Appendix 28 as "Flux @ 943 nm".

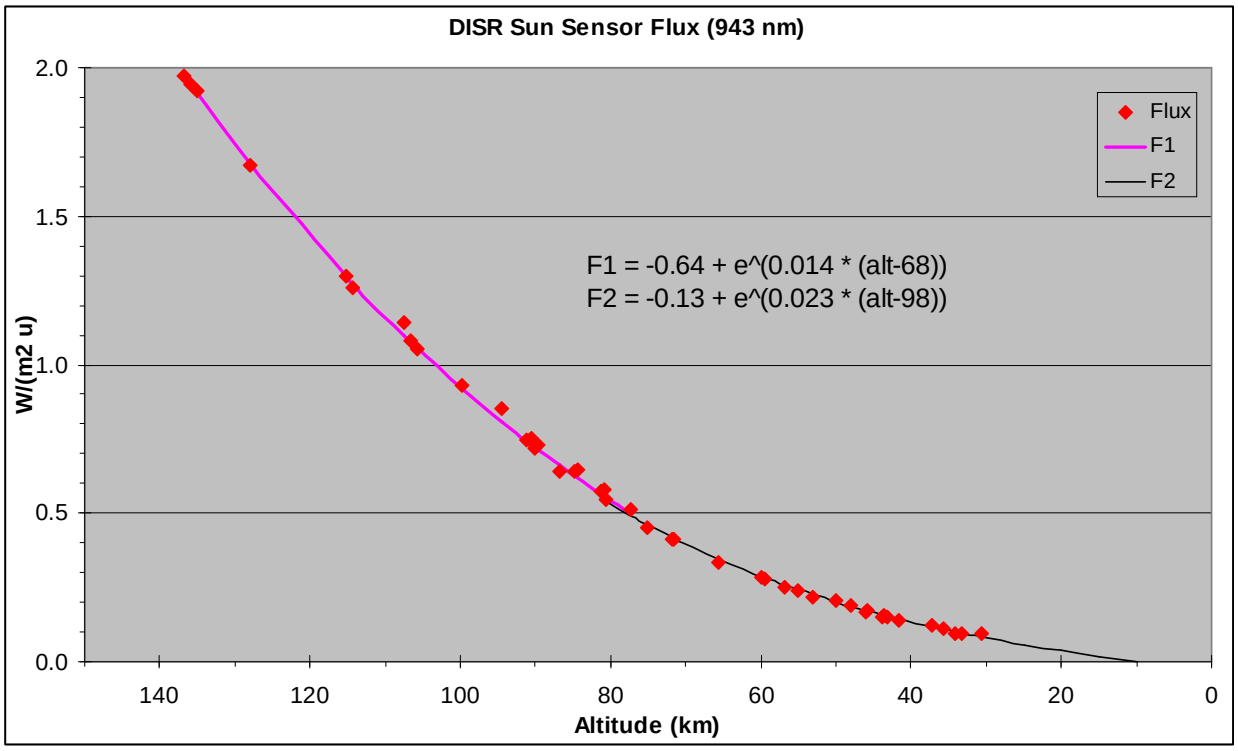

Figure 5.5-14: Downward flux at 943 nm as measured by the DISR Sun Sensor.

These results do not take into account the degradation in absolute responsivity of the Sun sensor during cruise. See section, "Sun Sensor Performance" (7.1) of the "Engineering Appendix Companion Document" for details.

5.6 Violet Photometer Measurements

Detailed descriptions of the Violet systems operation are presented in the calibration document in the data archive (Ref 4), SP-1177 (Ref 1a), and in section 2.3 (Violet Photometer) of the PSS aerosol paper (Ref 2).

There are two violet photometers in the DISR sensor head, the Upward Looking Violet (ULV) and Downward Looking Violet (DLV). Both violet spectrometers have baffles which limit their fields of view (FOV) of roughly ½ a hemisphere (π steradians), and consist of a one element filtered silicon photodetector providing a single value representing the integral of the violet flux over the spectrum of 350 to 480 nm.

Photometer calibration was carried out in 3 steps:
1) The relative spectral response (Rel_{spec}) of the system was determined using an integrating sphere stimulated with monochromatic light scanned across the photometer's pass band.
2) The systems Absolute Responsivity (Resp) was determined using the same integrating sphere and a broad-band white source, traceable to the National Bureau of Standards (NBS).
3) Variations in the systems response across its field of view (Relative Spatial Response, Rel1) was determined using a collimated light source and a precision azimuth/altitude tilting device.

Steps 1 and 2 above were repeated for detector temperatures from about 300º K down to 200º K, the expected temperature range during the Titan descent. Polynomial fits of the systems response with temperature determine the coefficients for equations 5.6.1, 5.6.2, & 5.6.4 as detailed in the calibration report (Ref 4). Since the shape band pass filter is not a perfect rectangle, variations in Rel_{spec} are defined for an energy equivalent idealized filter with wavelength cutoffs λ_1 & λ_2 with temperature dependence as indicated in equations 5.6.2 & 5.6.4.

The equation relating the instruments response to a spectral radiance < I > is given in the flux determination calibration report:
DOCUMENT/DISR_CALIBRATION_DOCUMENTS/VIOLET_PHOTOMETERS/VIOLET_PHOTOMETER_CAL_DOC
(equation 1) as:

$$DN - DNdark = \mathrm{Resp}_{peak} \int \left[\iint I(\lambda, \vartheta, \varphi) \mathrm{Rel}_{spec}(\lambda) d\lambda \right] \mathrm{Rel}_1(\vartheta, \varphi) d\Omega \qquad \text{(eq. 5.6.0)}$$

Where:
DN is the data number observed,
DN_{dark} is the data number due to the electrical bias when the instrument is in the dark,
Rel1 is the relative spatial response function when the observations were collected,
$Resp_{peak}$ is the peak absolute responsivity (at the maximum of the spectral and spatial relative response functions) of the instrument,
Rel_{spec} is the relative spectral response at each wavelength (λ)
I is the average diffuse spectral radiance over zenith angle and azimuth angle.
φ and ϑ are the Sun azimuth and elevation

Units:
The integrals of Rel1 and Rel_{spec} are dimensionless, and normalized to unity at their peaks.
$Resp_{peak}$ has units of DN/(watts/(m^2*micron*sr)) or DN*m^2*micron*sr/watt
λ is in microns, resulting in:
< **I** > having units of watts/(m^2*micron*sr)

Inverting equation 5.6.0 for determining spectral radiance, **I** from the DISR data, considering the isotropic nature of the calibration source, and defining a constant, equivalent energy, spectral shape results in equation 5.6.1 for the average spectral radiance over the DISR's field of view:

$$< \mathbf{I} > = [DN - DN_{dark}] / [Resp_{peak} * \int Rel_{spec}\, d\lambda * \int Rel1\, d\Omega] \qquad \text{(eq. 5.6.1)}$$

Determining the radiance variation as a function of wavelength within the spectral window, and the variation with azimuth and solar zenith angle requires some assumptions about the absorptivity and scattering of light by the atmosphere, as they are not measured directly by the DISR violet system. See the calibration report (Ref 4) for more details. For this example it is assumed that the spectral shape can be well represented by a quadratic across the photometers band; and an equivalent rectangular spectral profile is used as described in the Violet Flux Determination calibration document in the archive (Ref 4). We believe this to be a very good approximation.

This example also uses an isotropic radiance profile, however adaptation to a non-isotropic case is discussed in section 5.6.3.

Consequently, for this example: $\int Rel1\ d\Omega = 1.0$

5.6.1 Upward Looking Violet (ULV) Photometer Example

Laboratory calibration characterization of the ULV photometer (as seen in the calibration report, Ref 4, & detailed below) yields the following polynomial coefficients relating the temperature dependence of the terms required to complete equation 5.6.1:

Table 5.6.1-1

DISR ULV Calibration Coefficients					
	Rel1	**$Resp_{peak}$**	**Rel_{spec}**	**λ1**	**λ2**
Coef.	**1**	**2**	**3**	**4**	**5**
A	1.0	918.9	0.8089	354.2	478.45
B		1.8446	0.000111	-0.0095199	-0.0072
C		-0.0030642			
Ref.		p 59, fig 33	p 42, eq 25	p 42, fig 22	p 42, fig 22

For the form: $R = A + B*T_v + C*T_v^2$ Where T_v is the violet detector temperature, and dλ= λ2-λ1 (in nanometers).

Thus for the ULV Equation 5.6.1 becomes:

$$< I > = [(DN-DN_{dark})] / [A_1*(A_2+B_2*T_v+C_2*T_v^2)*(A_3+B_3*T_v)*((A_5+B_5*T_v)-(A_4+B_4*T_v))] \quad \text{(eq. 5.6.2)}$$

Where the coefficients are shown in table 5.6.1-1 and the detector temperature, T_v is available in the corresponding label file, and of course DN is available from the ULV data file.

The value for DN_{dark} is not as well established. It is a function of the Violet detector temperature, and the DISR electronics temperature. For large values of DN (>>50) variations in DN_{dark} are insignificant, however for measurements deep in Titan's atmosphere the variations in DN_{dark} must be addressed. For comparison of these dark offset values the data is scaled to the typical laboratory temperature values of 295ºK detector temperature, and 302ºK electronics temperature.

$$DN_{corr} = DN + (A_1 + B_1 * T_v) * (295 - T_v) + A_2 * (T_e - 302) \quad \text{(eq. 5.6.3)}$$

Where
DN is the measured data number,
T_v is the violet detector temperature in ºK,
T_e is the DISR electronics temperature (EA_BOX_T11 in Housekeeping datasets) in ºK,
DN_{corr} is the corrected data number, and the coefficients are from this table:

Table 5.6.1-2

Temp. Extrapolation Coef's		
	T_v	T_e
Coef	1	2
A	-0.05156	0.0203
B	2.4858E-04	

During the trip from Earth to Saturn all detector systems were stimulated at approximately 6-month intervals using the on-board calibration lamp system. During some of these in-flight checkouts substantial variation were noted in the ULV dark measurements. Below is an example from in-flight check 14 (F14), taken in July of 2004.

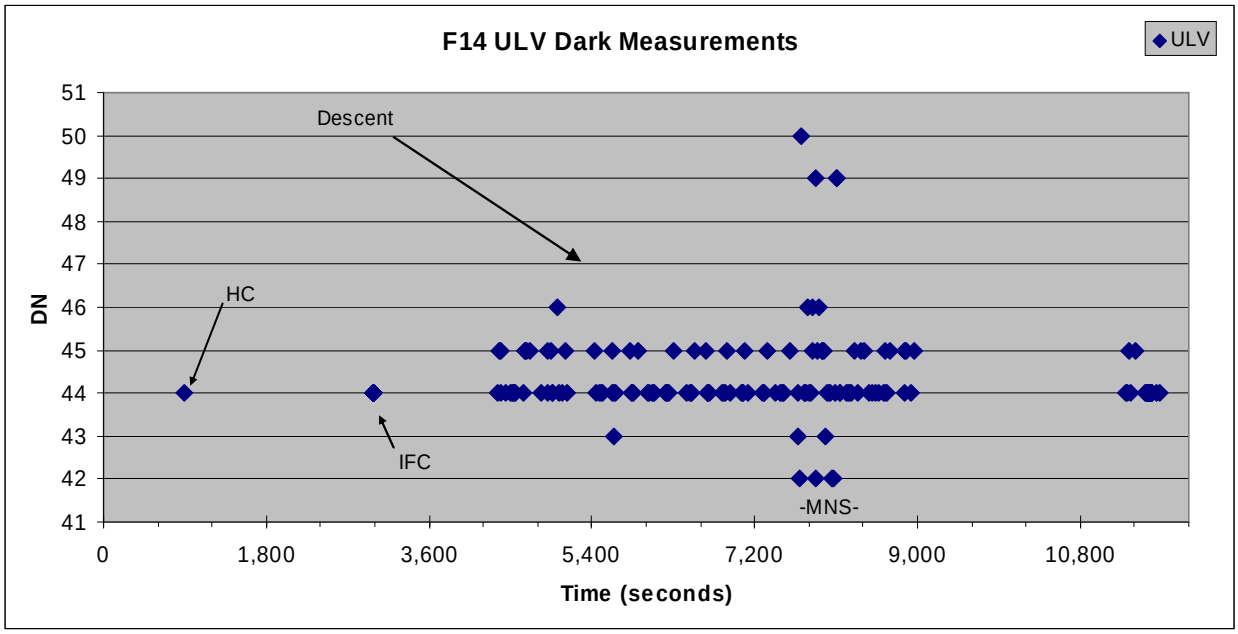

Figure 5.6-1: ULV dark measurements taken during the 14th In-flight test. HC indicates Heath Check routine exposures, IFC indicates In-Flight Calibration sequence exposures and the rest are simulated descent mode measurements. MNS indicates when the Medium Near Surface Cycles executed, which correlates to the most noisy violet measurements.

This test consisted of Health Check (HC) & In-Flight Calibration (IFC) sequences, followed by a portion of a simulated descent. The darks taken during the HC & IFC sequences were consistent (44 DN). For the simulated descent portion of the test, which is most similar to the Titan encounter, the majority of the readings are between 44 and 45 DN with a deviation of a fraction of a DN. However there were significant outliers (as high as 5 DN) especially during the Medium Near Surface (MNS) cycle which pushed the 1 sigma variation to ~1DN.

The situation was improved during the final in-flight checkout (F16) which occurred about 2 months before encounter (see below).

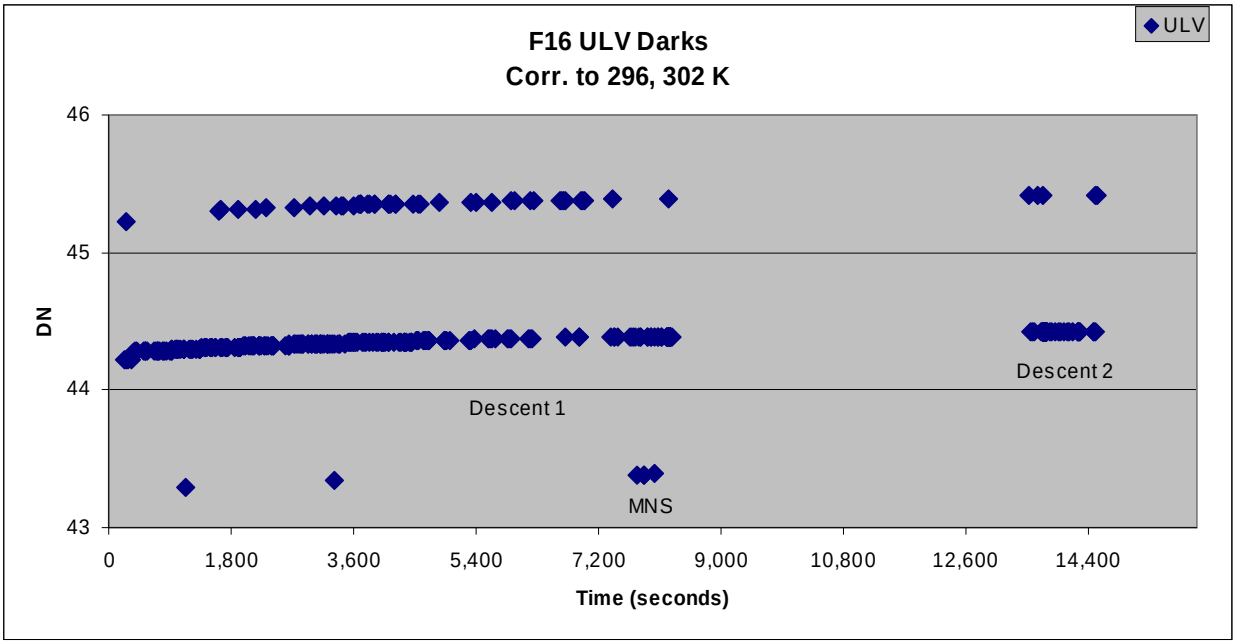

Figure 5.6-2: ULV photometer measurements taken during the last In-flight test sequence in November of 2004. A complete descent simulation was completed, then later in the test (at ~13,000 seconds) the instrument was re-commanded into descent mode to collect additional data (at zero altitude).

Again there were a number of outliers, particularly associated with the MNS cycle, but none were greater than 1 DN. The standard deviation for this set was only 0.37 DN.

A systematic change in the ULV bias was also observed from lab calibration to encounter as can be seen in this historical plot (below) of all tests taken with the instrument mated to the Huygens probe.

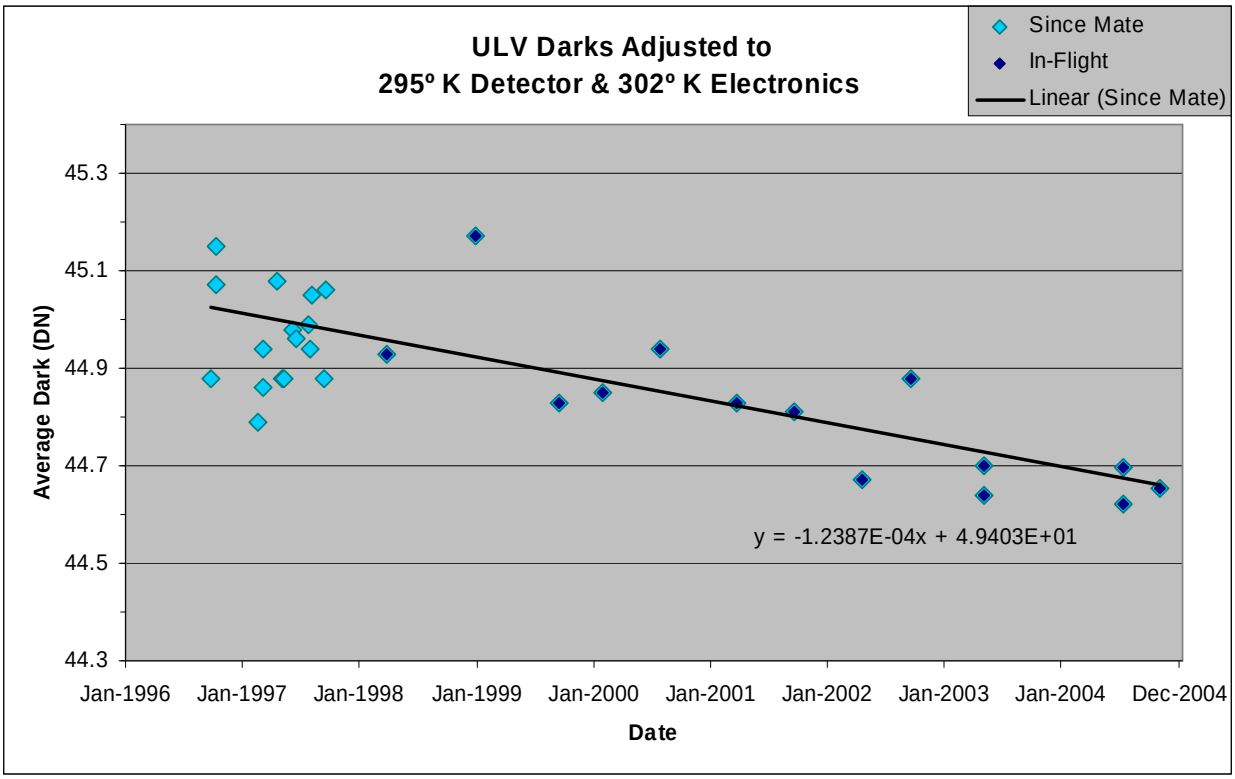

Figure 5.6-3: History of ULV photometer data from the installation of DISR into the Huygens probe until Titan encounter. Each point represents the average reading during a particular test sequence.

Extrapolating this data to the Titan encounter epoch (14 Jan 2005) yields an anticipated ULV dark current offset of 44.65 DN with a standard deviation of 0.18 DN (at T_v = 295ºK & Te=302ºK).

Using this information for the ULV dark offset in equation 5.6.2 allows us to plot the Titan Descent data as seen below.

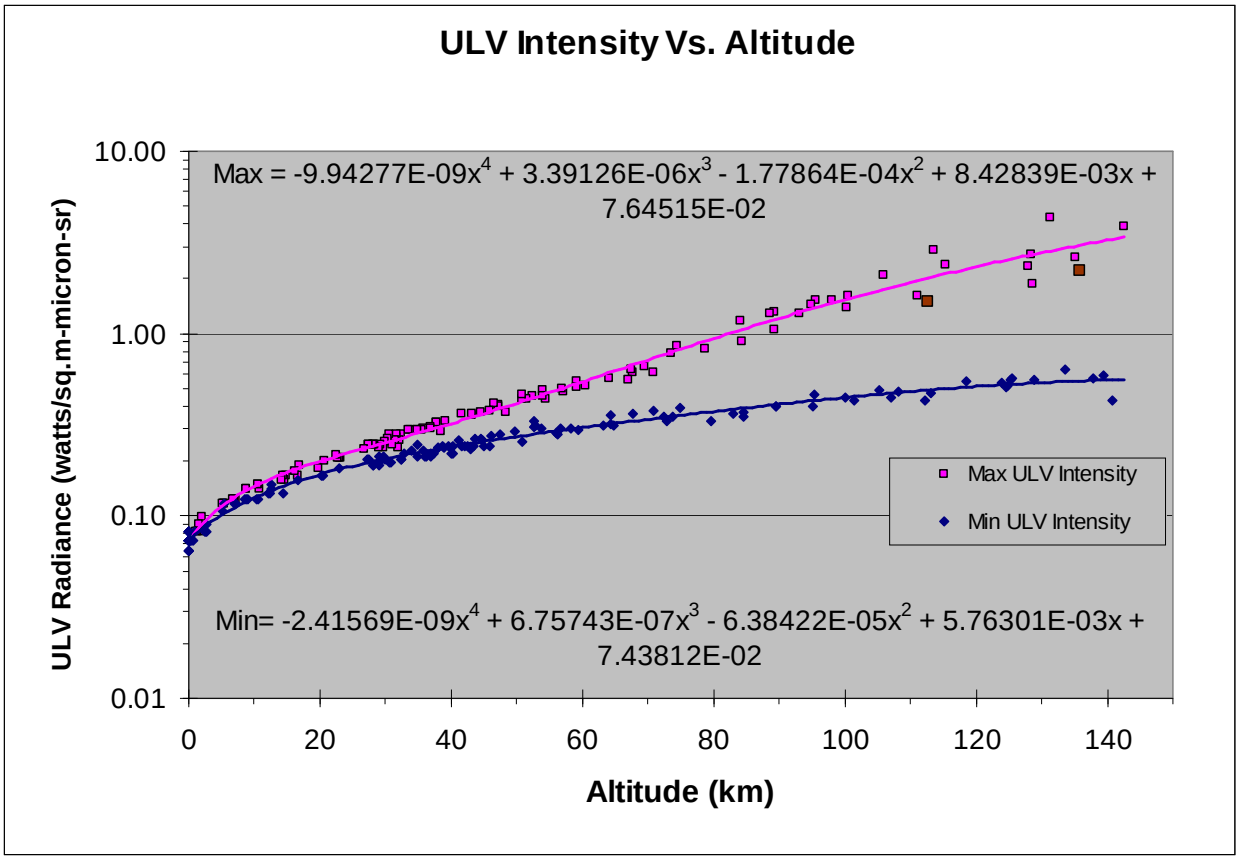

Figure 5.6-4: The hemispherical average upward looking radiance measured during the Titan descent by the violet photometer (350 to 470 nm) as a function of altitude. Red observations include Sun in the field of view.

As one might expect there are two populations of ULV data, one with the Sun in the field of view, and one without. These populations converge at around 2 km altitude as the direct solar beam becomes small in comparison to the diffuse sky flux. Erich Karkoschka has calculated that in this wavelength band the Sun in Titan's daytime sky delivers about the same relative energy to the surface as the half moon delivers to the earth during the day. That is, although the Sun would be visible, it would not deliver significant direct illumination.

As a further example of reducing the ULV data let us consider a pair datasets near 79 km altitude, one with the Sun in the field of view, and one without. The following information is available from the DISR archive datasets:

Table 5.6.1-3

ULV Data near 79 km, from PDS Archive						
File	M_Time	Altitude	Azimuth	EW_Tilt	Tv	DN
	(sec)	(km)	(deg)	(deg)	(deg K)	
VIOLET_0080_002342_1905	1422.19	79.61	152.77	-3.16	255.1	85
VIOLET_0081_002401_4356	1441.44	78.70	319.94	-8.02	245.9	146

In Table 5.6.1-3, 'File' is of course, the DISR archive file name. As encoded in the file name, these are the 80th and 81st violet measurements taken during the descent. M_time is the

mission time relative to T0 (the parachute deployment and DDB time reset epoch). Azimuth is the position of the probe +Z axis (i.e. DISR sensor head) in degrees counter-clockwise from above (i.e. spin vector coincident with probe +X axis using right hand rule) relative to the Sun at the start of the measurement. EW_Tilt is the angle between the probes +X (spin) axis and Zenith in the east-west direction (east positive). T_v is the violet detector temperature. DN is the 12 bit digital data number corresponding to the violet detector measurement (4096 max).

Next we will update the altitude, azimuth and tilt parameters. Interpolating in the June 2011 DTWG altitude table (echoed in Appendix 11) yields 79.62 km and 78.70 km for epoch's 1422.19 seconds and 1441.44 seconds respectively, so these header values are correct and do not have to be updated; however, this is not always the case, as can be seen in the altitude comparison presented in Appendix 7.

The azimuth information can be updated using Karkoschka's table presented in Appendix 5 (& Ref 5). This produces rotations of 74.9876 and 77.42826 East of North (or Naz = 355.5º & 154.2º). Obtaining the Sun positions from Appendix 14 (Saz = 113.61º & 113.6184º) allows us to calculate Huygens azimuth relative to the Sun at our two data points as AZ= Naz-Saz = 207.64º & 40.37º, somewhat different than the header entries.

Appendix 4 contains the east-west tilt information from 2007. Interpolating in this table results in tilts of -3.12º & -6.75º for our measurement epochs.

Our ULV data with updated parameters is presented in the following table.

Table 5.6.1-4

ULV Data near 79 km, updated						
File	M_Time	Altitude	Azimuth	EW_Tilt	Tv	DN
	(sec)	(km)	(deg)	(deg)	(deg K)	
VIOLET_0080_002342_1905	1422.19	79.62	207.64	-3.12	255.1	85
VIOLET_0081_002401_4356	1441.44	78.70	40.37	-6.75	245.9	146

To calculate the measured intensity we still need the DISR electronics temperature for determination of the correct dark offset. Interpolating to the measurement epochs in the table in Appendix 15 yields an electronics temperature of 292.1ºK for both measurements (Quantization error in the DISR temperature measurements is about 0.1K). Recalling that the extrapolated dark offset is 44.65 DN at T_v=295 & T_e=302 we determine the offset at the observation conditions using equation 5.6.3:

$$DN_{corr} = DN + (A_1 + B_1 * T_v) * (295 - T_v) + A_2 * (T_e - 302) \qquad \text{(eq. 5.6.3)}$$

$$DN_{corr} = 44.65 + (-0.05156 + 2.4858E\text{-}04 * 255.1) * (295 - 255.1) + 0.0203 * (292.1 - 302)$$

Which results in dark offsets of:

Table 5.6.1-5

File	M_Time	Dark Offset
	(sec)	(DN)
VIOLET_0080_002342_1905	1422.19	44.92
VIOLET_0081_002401_4356	1441.44	44.92

We are now ready to calculate the radiance for our two measurements using equation 5.6.1:

$$< I > = [(DN-DN_{dark})] / [A_1*(A_2+B_2*T_v+C_2*T_v^2)*(A_3+B_3*T_v)*((A_5+B_5*T_v)-(A_4+B_4*T_v))] \quad \text{(eq. 5.6.4)}$$

For VIOLET_0080_002342_1905:

$$< I_{80} > = [(85 - 44.92)] \ / \ [1.0*(918.9 + 1.8446 * 255.1 - 0.0030642 * 255.1^2) * (0.8089 + 0.0001112 *255.1) * ((478.35 - 0.00726 * 255.1) - (354.1 - 0.0095 * 255.1))]$$

$$< I_{80} > = 0.0003222 \text{ watts/(m}^2\text{-nanometer-sr)} = 0.322 \text{ watts/(m}^2\text{-micron-sr)}$$

and for VIOLET_0081_002401_4356:

$$< I_{81} > = 0.0008158 \text{ watts/(m}^2\text{-nanometer-sr)} = 0.816 \text{ watts/(m}^2\text{-micron-sr)}$$

We cannot accurately correct for tip-tilt (i.e. misalignment between probe spin axis and zenith) since the zenith angle dependence of the radiation field is not measured directly. To do this properly requires development of a radiative heat transfer model. However we can apply a first order adjustment which likely over corrects the flux by assuming a sinusoidal variation.

$$I_{corr}=I_{meas}*(1+\sin(tilt_1)*\cos(E_{az}))*(1+\sin(tilt_2)*\cos(90+E_{az})) \quad \text{(eq. 5.6.5)}$$

where:

I_{meas}	is the measured radiance,
I_{corr}	is the corrected radiance,
$tilt_1$	is the tilt in the E-W direction in degrees, E positive as in Appendix 4,
$tilt_2$	is the tilt in the N-S direction in degrees, S positive, and
E_{az}	is the observation azimuth relative to East in degrees.

Eaz is calculated from our table information as E_{az}=AZ+(SAZ-90), where AZ is the azimuth of the observation from our table and SAZ is the position of the Sun relative to north obtained from Appendix 14 (~113º to 115º).

Since we have no information about the north-south tilt we will assume that it is zero. In reality it is probably similar in magnitude to the east-west tilt, but until a detailed probe dynamics model is completed we do not have this information.

Applying this tilt correction to our measurement results in:

Eaz = 207.64 + (113.61-90) = 231.25º

$$< I_{80} > = 0.3222 * (1+\sin(-3.12º)*\cos(231.25º))*(1+\sin(0)*\cos(90+231.25º))$$
$$= 0.3332 \text{ watts/(m}^2\text{-micron-sr)}$$

and

$$< I_{81} > = 0.7738 \text{ watts/(m}^2\text{-micron-sr)} \quad \text{(vs. 0.816 before tilt adjustment)}$$

These results agree well with the trend line established in Figure 5.6-4.

So at 79 km altitude the diffuse upward looking (downward directed) radiance averaged over roughly one hemisphere and averaged across the photometer's spectral range (350 to 470 nm) is:

$I_{diffuse} = I_{80} = 0.336$ watts/(m^2-micron-sr),

and the direct solar beam contribution to the average downward radiance is:

$I_{direct} = I_{81} - I_{80} = 0.388$ watts/(m^2-micron-sr).

5.6.2 Downward Looking Violet (DLV) Photometer Example

We will now consider a similar set of data for the DLV. In anticipation of calculating the net flux (down-up) we will choose the two DLV measurement from the same data cycle (14). From Appendix 16 we find that there are 2 DLV measurements in cycle 12, sequence numbers 77 & 78, and we fetch the following data from the DISR archive (in hpdisr_0001/DATA/VIOLET/VIOLET_00XX):

Table 5.6.2-1

DLV Data near 79 km, from PDS Archive						
File	M_Time	Altitude	Azimuth	EW_Tilt	Tv	DN
	(sec)	(km)	(deg)	(deg)	(deg K)	
VIOLET_0077_002330_2148	1410.215	80.19	5.18	-1.80	255.4	255
VIOLET_0078_002333_7809	1413.781	80.01	194.41	-2.63	255.3	214

Updating this data as we did in section 5.6.1 for the ULV we end up with the values listed below (also see Appendix 16):

Table 5.6.2-2

DLV Data near 79 km, updated						
File	M_Time	Altitude	Azimuth	EW_Tilt	Tv	DN
	(sec)	(km)	(deg)	(deg)	(deg K)	
VIOLET_0077_002330_2148	1410.215	80.19	355.35	-1.7	255.4	255
VIOLET_0078_002333_7809	1413.781	80.02	166.11	-2.3	255.3	214

From the Violet calibration document (hpdisr_0001/DOCUMENT/DISR_CALIBRATION_DOCUMENTS/VIOLET_PHOTOMETERS/VIOLET_PHOTOMETER_CAL_DOC) we obtain the coefficients for the Peak Responsivity (Pg 59, Fig 33), Relative Spectral Response (Pg 42, Eq 26), and λ1 & λ2 (Pg 42, Fig 22) as shown in the following table:

Table 5.6.2-3

DISR DLV Calibration Coefficients					
	Rel1	**$Resp_{peak}$**	**Rel_{spec}**	**λ1**	**λ2**
Coef.	**1**	**2**	**3**	**4**	**5**
A	1.0	7202.4	0.8182	353.97	478.26
B		18.671	0.000116	-0.0094799	-0.0073198
C		-0.027489			

For the form: $R = A + B*T_v + C*T_v^2$ Where T_v is the violet detector temperature, and $d\lambda = \lambda2-\lambda1$ (in nanometers).

Since we are using the Peak Responsivity instead of the Measured Responsivity, Rel1 is 1.0 as explained in the section named "Absolute Responsivity as a function of temperature" (V) of the calibration document.

Determination of the dark offset values (DN_{dark}) is discussed in section, "Dark data values during descent" (VII-A) of the calibration document (Ref 4). This offset is semi-randomly bimodal, but is also a function of the descent cycle in which the data was taken. The best way to determine the offset is to iteratively trend the data using all of the possible offsets and acquire a best fit. This was done by the DISR team and a table of resulting offsets for each of the Titan descent DLV measurements is presented in Appendix 17. Below is an excerpt for our two observations...

Table 5.6.2-4

Seq #	Cyc. #	Cycle Type	Time (sec.)	DN	Bias	Lamps
77	14	Image	1410.22	255	43	0000
78	14	Image	1413.78	214	31	0000

We are now ready to calculate the radiance for our two measurements using equation 5.6.4:

$$< I > = [(DN-DN_{dark})] / [A_1*(A_2+B_2*T_v+C_2*T_v^2)*(A_3+B_3*T_v)*((A_5+B_5*T_v)-(A_4+B_4*T_v))] \quad \text{(eq. 5.6.4)}$$

For VIOLET_0077_002330_2148:

$$< I_{77} > = [(255 - 43)] / [1.0*(7202.4 + 18.671 * 255.4 -0.027489 * 255.4^2) * (0.8182 + 0.000116 *255.4) * ((478.26 - 0.0073198 * 255.4)-(353.97 - 0.0094799 * 255.4))]$$

$< I_{77} >$ = 0.0001968 watts/(m^2-nanometer-sr) = 0.197 watts/(m^2-micron-sr)

and for VIOLET_0078_002333_7809:

$< I_{78} >$ = 0.0001699 watts/(m^2-nanometer-sr) = 0.170 watts/(m^2-micron-sr)

We will now correct for the east-west tilt as before:

$$I_{corr}=I_{meas}*(1+\sin(tilt_1)*\cos(E_{az}))*(1+\sin(tilt_2)*\cos(90+E_{az})) \quad \text{(eq. 5.6.5)}$$

where E_{az}=AZ+(SAZ-90), E_{az} = 18.95 for seq. # 77 and 189.71 for seq. # 78, and the corrected radiances become:

$< I_{77c} >$ = 0.0001913 watts/(m^2-nanometer-sr) = 0.191 watts/(m^2-micron-sr)

$< I_{78c} >$ = 0.0001766 watts/(m^2-nanometer-sr) = 0.177 watts/(m^2-micron-sr)

So even looking downward the radiance is brighter in the Sun's direction.

As promised we will now calculate the net flux in our violet band, near 79 km altitude, in Titan's atmosphere using these observations. From equation 50 of the calibration document the upward streaming flux is given by:

$F_{up} = \pi * I_{ave}$, where I_{ave} is the azimuthally averaged down-looking radiance, and likewise for the downward streaming flux:

$F_{down} = \pi * I_{ave}$, where I_{ave} is the azimuthally averaged up-looking radiance.

To do this properly of course requires a radiative heat transfer model to calculate the azimuthal dependence, however since our observations represent the average over half a hemisphere and are nearly 180º apart their average is a good representation of the hemispherical average. There will be some error of course since our upward observation of the direct beam does not have the Sun squarely in the center of the FOV.

Fup = π * Average(0.191,0.177) = 0.1840 Watts/(m^2-micron),

Fdown = π * Average(0..3333,0.7738) = 0.5535 Watts/(m^2-micron), and

The net flux, Fnet = Fdown - Fup = 0.3696 Watts/(m^2-micron)

Since this is the average flux we can multiply by our detector bandwidth to determine the Total Irradiance:

$$E = I * d\lambda = 0.3696 * (0.48-0.35) = 0.0480 \text{ Watts/m}^2$$

which becomes the measured energy absorbed in our layer at 79 km altitude.

Trending the data with altitude minimizes errors due to noise, probe motion and bias uncertainty. The figure below shows a polynomial curve fit to the Net DLV data (measured DN minus chosen bias). The equation thus becomes our expression for the average downward looking violet measurement at each altitude (ignoring the azimuthal variations).

Evaluating this equation at the average of our example observations (80.11 km) gives an average value of 196.9 DN, vs. our measured value of 197.5 DN (0.3% different).

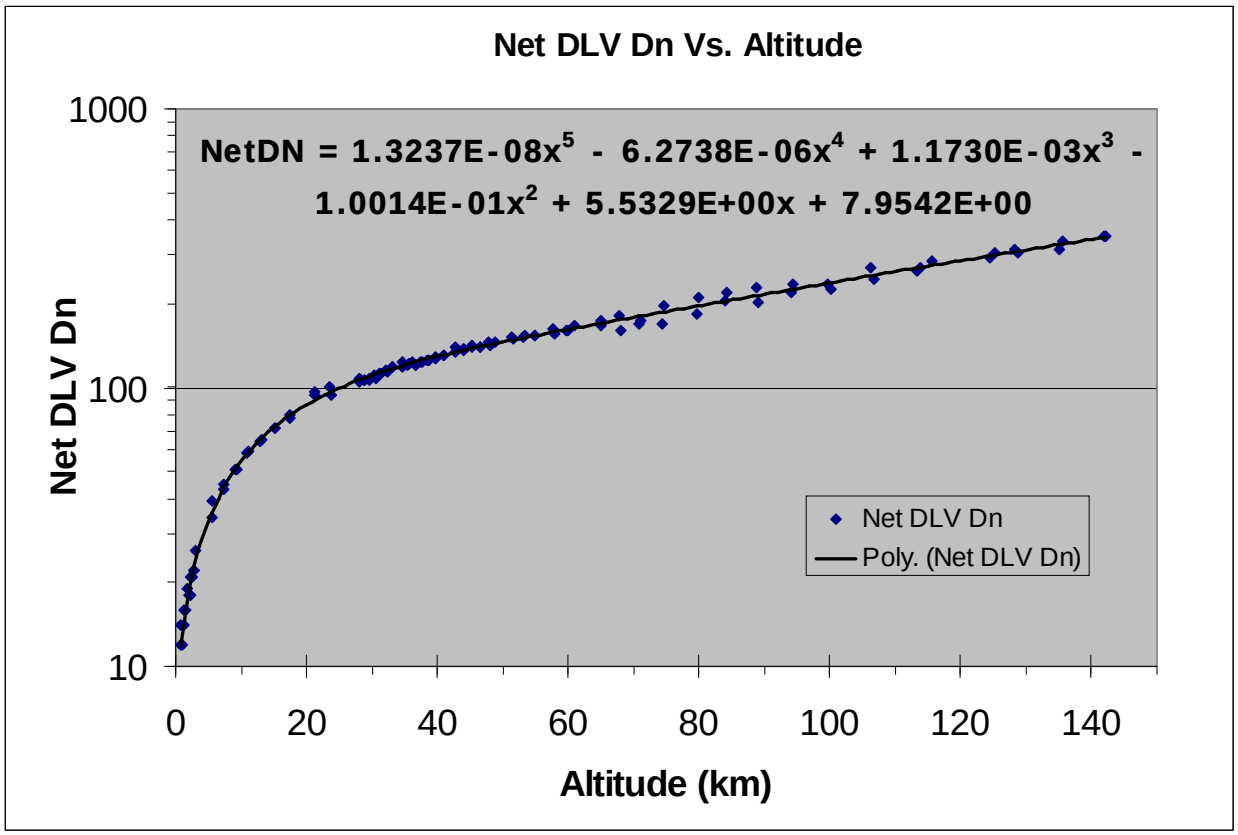

Figure 5.6-5 - Measured data number (DN) minus the derived dark DLV offset vs. altitude.

Similarly we can trend the downward looking radiance as a function of altitude (figure below). The blue trendline represents the average radiance at each altitude. The grey lines show the extent assuming that the azimuthal variation is ±7% of the average value i.e.:

$I = I_{ave} + 0.07 * I_{ave} * \text{Cos(Azimuth)}$

where: I is the radiance, I_{ave} is the azimuthally averaged radiance, and 'Azimuth' is the azimuth of the observation relative to the Sun.

One could get better agreement by varying this value with altitude.

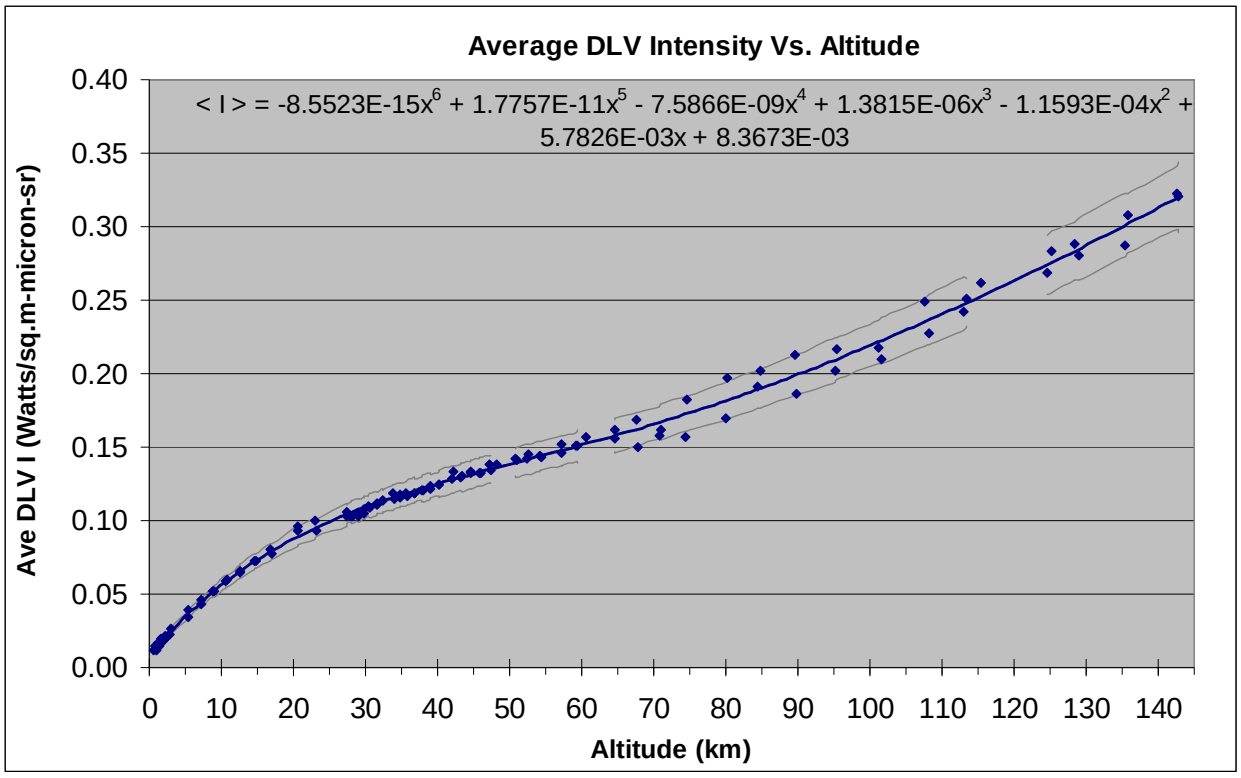

Figure 5.6-6: Downward looking spectral radiance as a function of altitude with expected azimuthal variation.

Correspondingly we can plot the upward streaming flux as a function of altitude from the DLV data (below).

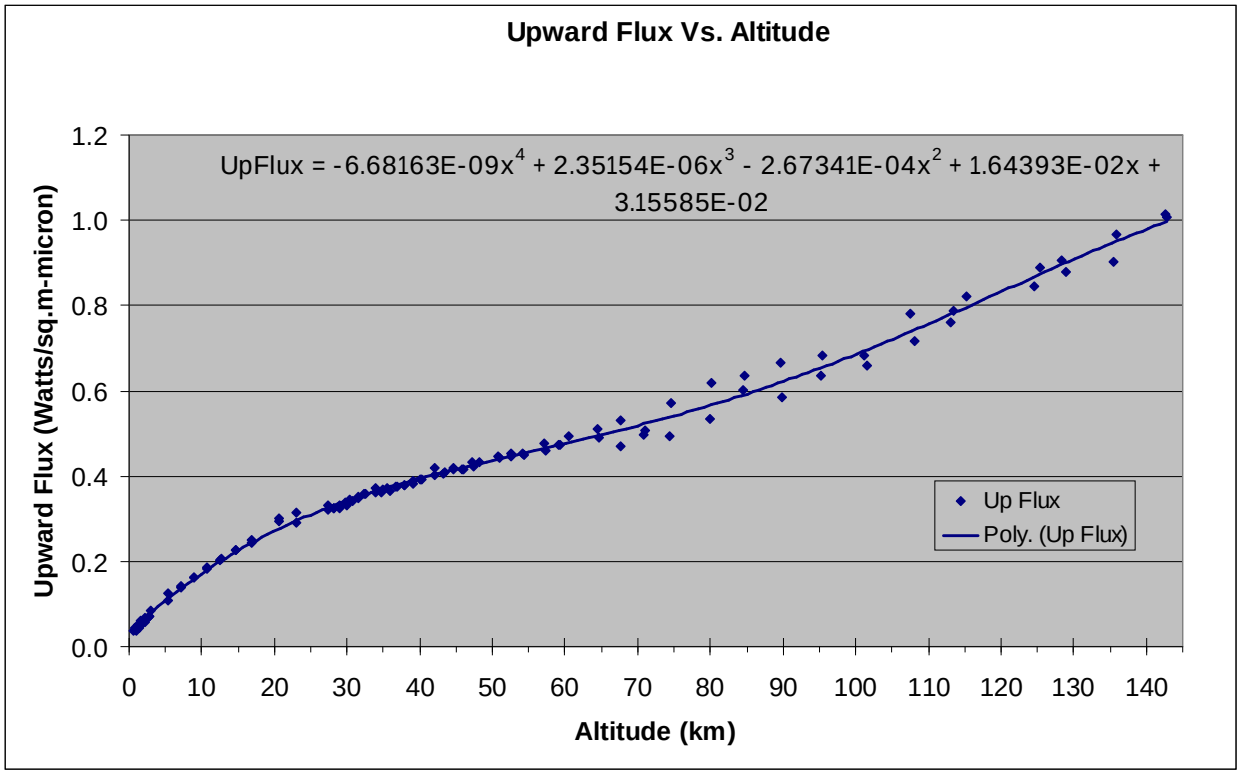

Figure 5.6-7: Upward streaming spectral flux as a function of altitude as measured by the DISR Downward Looking Violet Photometer (~350 to 480 nm).

Similarly we calculate the downward streaming flux from the average of the sunward and anti-sunward ULV data presented in Figure 5.6-4. Evaluating the downward flux equation at the surface (x=0) we find the flux at the Huygens Landing site is 0.226 W/(m^2 * micron), or 0.03 W/m^2 across our UV band (compared to ~100 W/m^2 on the Earth), and the net flux as the difference of the two.

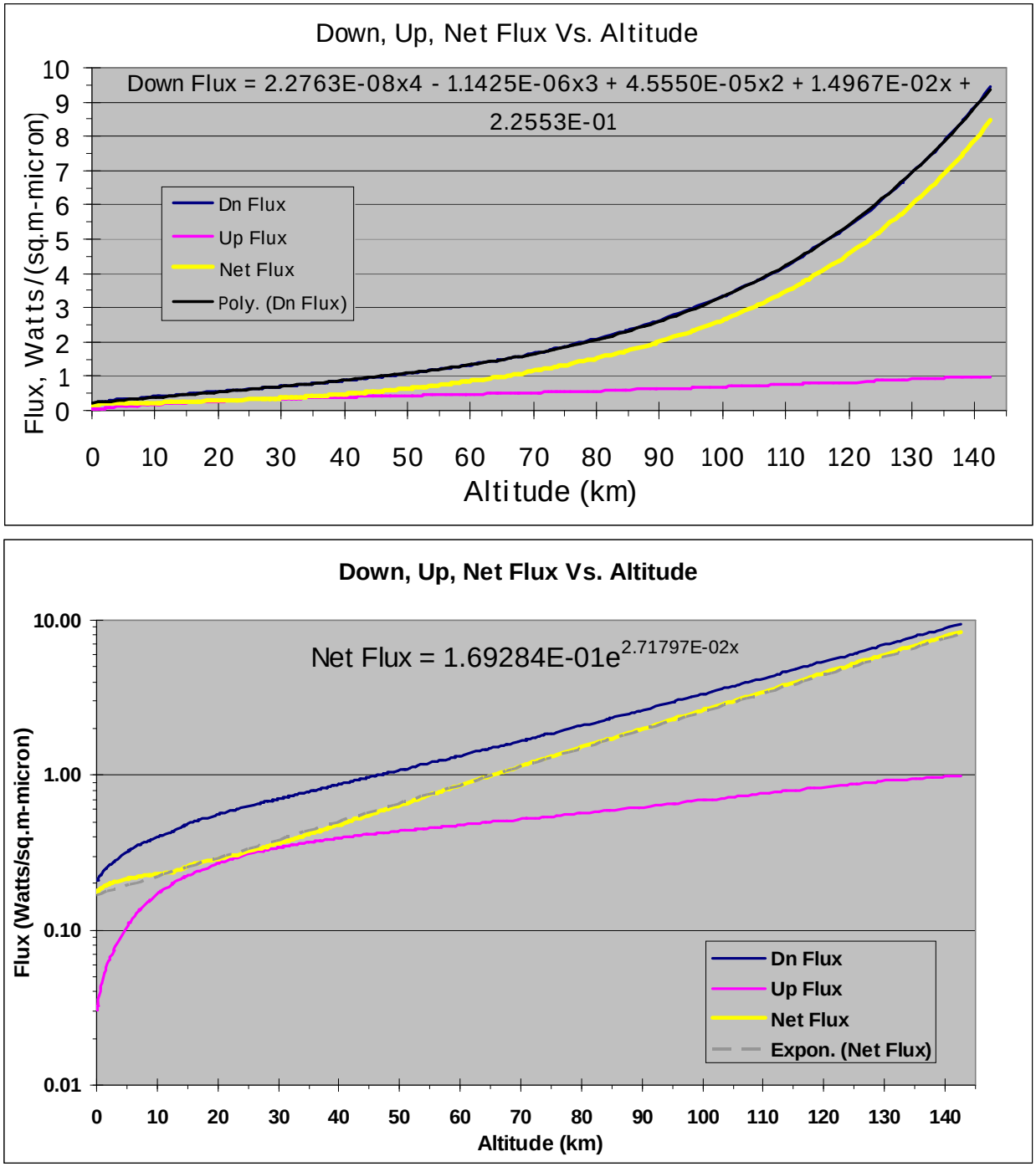

Figure 5.6-8: Violet Flux (~350 to 480 nm) in Titan's atmosphere as measured in January 2005 by the DISR instrument aboard the Huygens probe.

5.6.3 Other Violet Photometer Considerations

Relative Spatial Response...

We have discussed how to calculate the average response over the photometers field of view, however the user may wish to explore the shape of the radiation field. There is no unique answer to this quest, however it is possible to determine if a proposed radiation profile is consistent with the DISR data. To do this one would need the Relative Spatial Response Function (Rel1) of the instrument which is described in section IV, "Relative Spatial Response" of the Violet Photometer Calibration Document (Ref 4).

Any radiation field who's product with the Rel1 (figures 24 & 25 of Reference 4) integrates to 1 is consistent with the isotropic case used to develop the DISR calibration. Some simplistic examples are all of the radiation occurring at the peak of Rel1, or a radiance of 2 times the average distributed evenly over the area between the 0.45 and 0.55 contours in figures 24 or 25. One can always adopt a candidate radiation field by normalizing the integral of its product with Rel1 to unity:

$$[\int \mathbf{I} * \mathrm{Rel1}\ d\Omega\ ] / E_{ave} = 1$$

where:

$\mathbf{I}$ is the Irradiance per unit solid angle at each point in the FOV.

Rel1 is the Relative Spatial Response Function from Ref 4

E_{ave} is the average Irradiance over the field of view

The upward looking violet photometer (ULVP) is obscured by a shadow bar in its FOV. This allows the measurement of the sky's diffuse intensity both toward and away from the Sun. Since the instrument was calibrated with an isotropic radiation field, this does not effect the results in the isotropic case. However, it does have implications if one wishes to model a non-isotropic sky. The location of the shadow bar, and parachute baffle is apparent in the Rel1 (Figure 24 of Reference 4). To facilitate analytic removal of the shadow bar the following fit to the 95% attenuation contour is presented. Azimuths here are in degrees to the left (CCW from above) relative to the DISR's (& Probes) +Z axis. Attenuation occurs between the horizontal lines (i.e. near 0 azimuth)

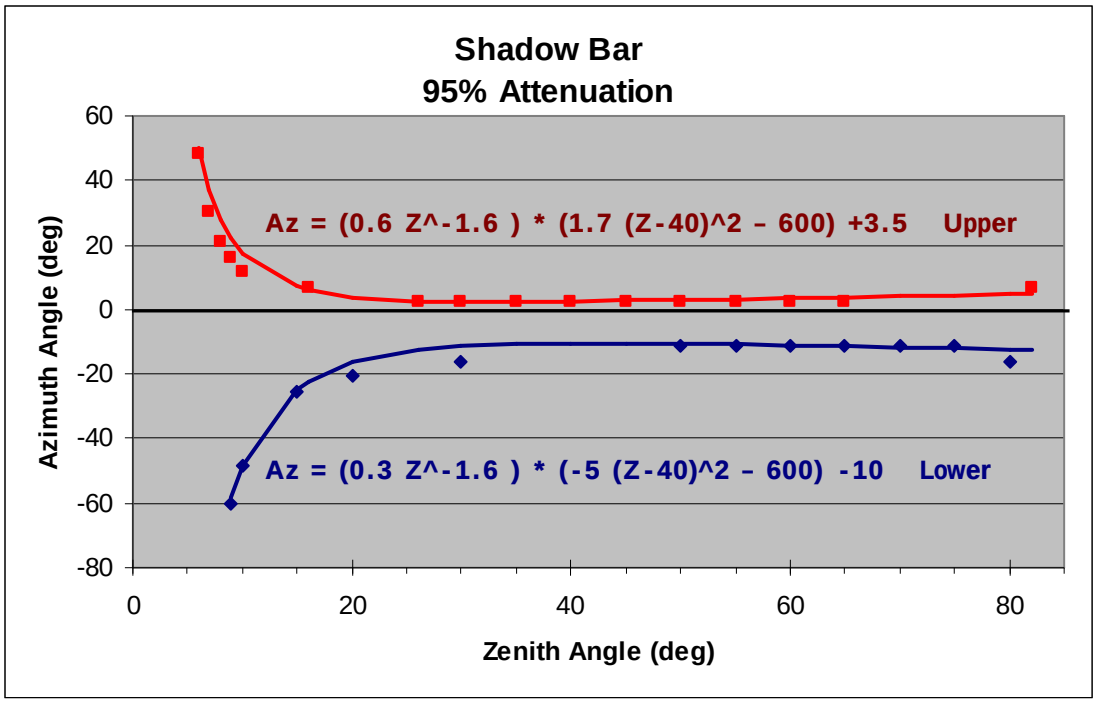

Figure 5.6-9: Attenuation of the ULV signal by the DISR shadow bar.

$Az = (0.6\ Z^{-1.6}) * (1.7\ (Z-40)^2 - 600) + 3.5$ Upper - for zenith angles from 6 to 82 deg.
$Az = (0.3\ Z^{-1.6}) * (-5\ (Z-40)^2 - 600) - 10$ Lower - for zenith angles from 9 to 80 deg.

Although the ULV photometer is physically baffled 5 degrees from the probe from horizon to horizon (5º zenith, from -90º to +90º azimuth), in actuality fiber optic geometry of the ULV photometer significantly attenuates radiation to about 8 degrees zenith angle from -90º to 0º Azimuth.

A word about azimuths, and the Relative Spatial Response plots:

The probe rotated clockwise as viewed from above for most of the descent, which is opposite what was expected. The convention used in the calibration document assigns azimuth angles increasing counter-clockwise when viewed from above, which would result in the Sun progressing in decreasing azimuth angle through the field of view with time. This was true at the beginning of the descent; however after about 550 seconds (i.e. below about 124 km) the probe began to rotate clockwise (from above) and so the Sun's progress was opposite that shown in figures 24 & 25 of the Violet Photometer calibration report.

In Reference 5 (also Appendix 5), Karkoschka defines the azimuth relative in full rotations relative to north, which is consistent with figures 24 & 25 at all altitudes (i.e. a measurement taken at 0.1 rev (36 degrees) azimuth would have the Sun on the right side of the plot, and an observation at 0.9 rev (-36 or 324 degrees) would have the Sun on the left). Thus these two figures present the instruments response from the view of an inverted DISR, such that up is down, and down is up, left is right & right is left (i.e. the plot is rotated 180º in the plane of the paper). A rotated version of Figure 24 is presented in the ULVS portion of this Guide with annotation.

Earth to Saturn Cruise Effects...

We have already discussed the progression of the Violet Photometer dark current during the Cassini cruise from Earth to Saturn. There has also been noticed an attenuation of the absolute responsivity of both the ULV and DLV. The responsivity decline appears to have begun when the Radio Isotope Heater Units (RHUs) were installed at Kennedy Space Center.

It is not known for certain what caused the responsivity reduction. It is proposed that it may be due to darkening of the Schott radiation hardened glass used in the fiber optics. Leftover specimens have turned a darkened yellowish brown color over time, even in Earth atmospheric environment.. The ratio of the attenuation between the two violet systems is roughly consistent with the length of the fiber optic bundles that transmit the light from the optics to the detectors. It may also be attributable to radiation or vacuum exposure of the detectors or electronics.

The overall reduction in responsivity is 19.2% for the ULV and 11.5% for the DLV from the laboratory calibration values (see plots below). The spectral shape in the UV is unknown, but there is likely greater attenuation toward the blue end. At a minimum the data user would be well advised to include a correction factor for the Absolute Responsivity:

$$Resp_{corr} = Resp * Q$$

where

$Resp_{corr}$ is the corrected Absolute Responsivity
Resp is the lab measured Absolute Responsivity (at the peak of the spectrum), and
Q is 0.8851 for the DLV and 0.8079 for the ULV.

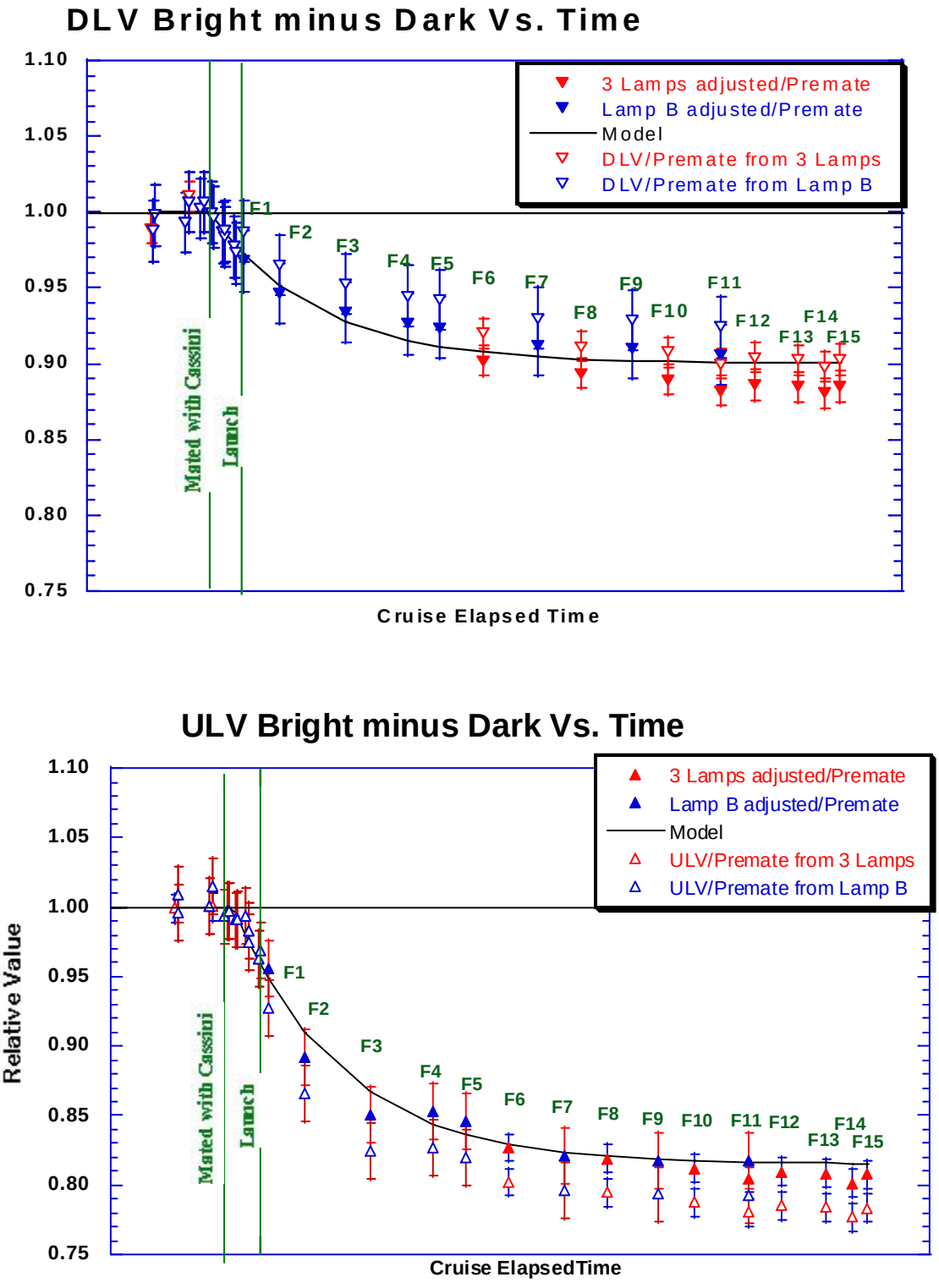

Figure 5.6-11- Violet Photometer responsivity history during Cassini cruise phase

5.7 CCD Covered Column Dark Data

It is the nature of Charge Coupled Devices (CCDs) to accumulate signal even in total darkness. This Dark Current generation rate is a strong function of temperature. DISR's IR spectrometers are equipped with a mechanical shutter which allows automatic removal of dark current from every measurement, by subtracting a like exposure with the shutter closed. However, the DISR's CCD instruments do not have a mechanical shutter, so the dark current portion of the signal must be calculated and removed by post processing. The CCD's covered columns (Dark datasets) and null pixels (in data headers) can be used for this.

The CCD layout is described in section 5.8 and shown in Figure 5.8-5.

The dark current is comprised of 4 components; the Image Zone Dark Current (R_I), which accumulates during the exposure; the Memory Zone Dark Current (R_M) which accumulates while the image is waiting under the covered section of the CCD to be read-out, the Serial Register Dark Current (R_S), which occurs as the row is being clocked-out, and an electronics offset (*O*) of about 8.9 DN:

$$DN = O + R_s + R_M \Delta t_M + R_I \Delta t_I \,, \qquad \text{(Equation 5.7-1)}$$

where:

DN is dark current contribution to the observed signal,

O is the electronics offset (about 8.9 DN during calibration),

R_s, R_M, and R_I are the dark current generation rates in the serial register, memory zone, and image zone, respectively, and,

Δt_M and Δt_I are the residence times in the memory zone and image zone, respectively.

R_s, R_M, and R_I are functions of detector temperature.

Details of how to determine the CCD dark current is presented in the "Dark Current Estimation" document in the Archive, (Reference 7), however an overview, with some update is presented in this section.

The dark current for every CCD pixel was measured during the lab calibration, and related to the dark current generation rate of the extra columns of pixels along the edge of the Image section (which are returned as "Dark" datasets by the instrument). In order to make this calculation accurately the contribution of the Serial Register must be removed. The value of O+Rs is related to the value of the 'null pixels' which exist in serial register, whose values are returned in the header of each dataset.

The amplitude of the dark current rate is strongly a function of temperature (particularly above 220ºK). It is also a function of radiation exposure, and increased consistently during the cruise from Earth to Titan. To adjust for changes during cruise, special, per pixel, measurements were made during the in-flight tests, and the relationship to the value measured by the Dark Datasets was updated using the 16th In-Flight test performed on 23rd November 2004 (52 days before Titan encounter). These relationships are presented in the "Dark Current Estimation" document in the Archive (Reference 7). The F16 data are summarized in Appendix 26. The examples below describe how this information can be used. In general the image zone and memory zone dark current rates are determined at one temperature (~262K) using the special F16

measurements, and the Titan descent Dark datasets are used to determine the temperature dependence.

Saturation of the CCD instruments by the Surface Science Lamp light obstructs determination of the dark current after landing, however the temperatures are low enough during this period of operation that the dark current can be neglected for datasets collected on Titan's surface (except the 8.9 DN electronics offset of course).

It is important to be aware of the difference in CCD readout modes when calculating dark current. There are two modes, Full Readout & Spectral Readout. As suggested by the name, Full Readout mode is used to readout the entire CCD contents. This mode is used when collecting Image datasets (SLI, MRI, HRI) and "Full" datasets (which are not collected during a descent). The covered column "Dark" datasets are also collected in Full Readout mode. The rest of the datasets are collected in the quicker, Spectral Readout mode, which reads out only the first 41 columns of the CCD. This includes ULVS, DLVS, & SA. The dark current accumulations rates are different for the two modes. It takes 2159 ms to shift the data through the CCD memory zone in Full Readout mode, and 263 ms in Spectral Readout mode (Ref 7).

The Dark Current Estimation document (Reference 7) has a good summary of the DISR CCD characteristics in its Appendix II ("CCD Architecture and Operation in Two Readout Modes").

Image Data Example...

For our first example we will find the dark current for one pixel in an HRI exposure. Let's choose dataset #21 (IMAGE_0021_000324_7662), since it was taken at the upper, warm part of the descent (259.2ºK). We will choose a pixel near the center of the 160 pixel wide by 256 pixel high array, which should have good signal, and not be effected by edge effects of fiber optic bundle. We will choose row #125, and column #80 (pixel 124, 79).

Here is a summary of information regarding our target pixel:

The signal level of this pixel is 2177 DN.
The CCD temperature is 259.2ºK.
Null Column 2 = 81 DN
Null Column 3 = 75 DN
Exposure Time = 7 ms

The first step is to determine how much of the signal is from the electronics offset and serial register (O+SR).

The equation for determining O+SR from Reference 7 is:

$$(Serial\_Register + Bias)_{FULL} = ((NullPixel2/4.0 + 0.125) + (NullPixel3/4.0 + 0.125))/2.0 \qquad \text{(Equation 5.7-2)}$$

where:

NullPixel2 is the floating point value of Null Column 2 in the measurement in question.
NullPixel3 is the floating point value of Null Column 3 in the measurement in question.

The flight software multiplies the average of the null pixels by 4, truncates the result, and sends the outcome in telemetry for every CCD measurement. These values are in the dataset header, and the label file as "null_col2:" & "null_col3:".

So:

O+SR = { (81/4.0 + 0.125) + (75/4.0 + 0.125) } / 2.0 = 19.6 DN

To minimize the effects of pixel-to-pixel variations and make it easier to calculate O+SR for spectral mode measurements (which are scaled from the full frame O+SR), we have fit a temperature dependent exponential to the Titan descent (see Appendix 24).

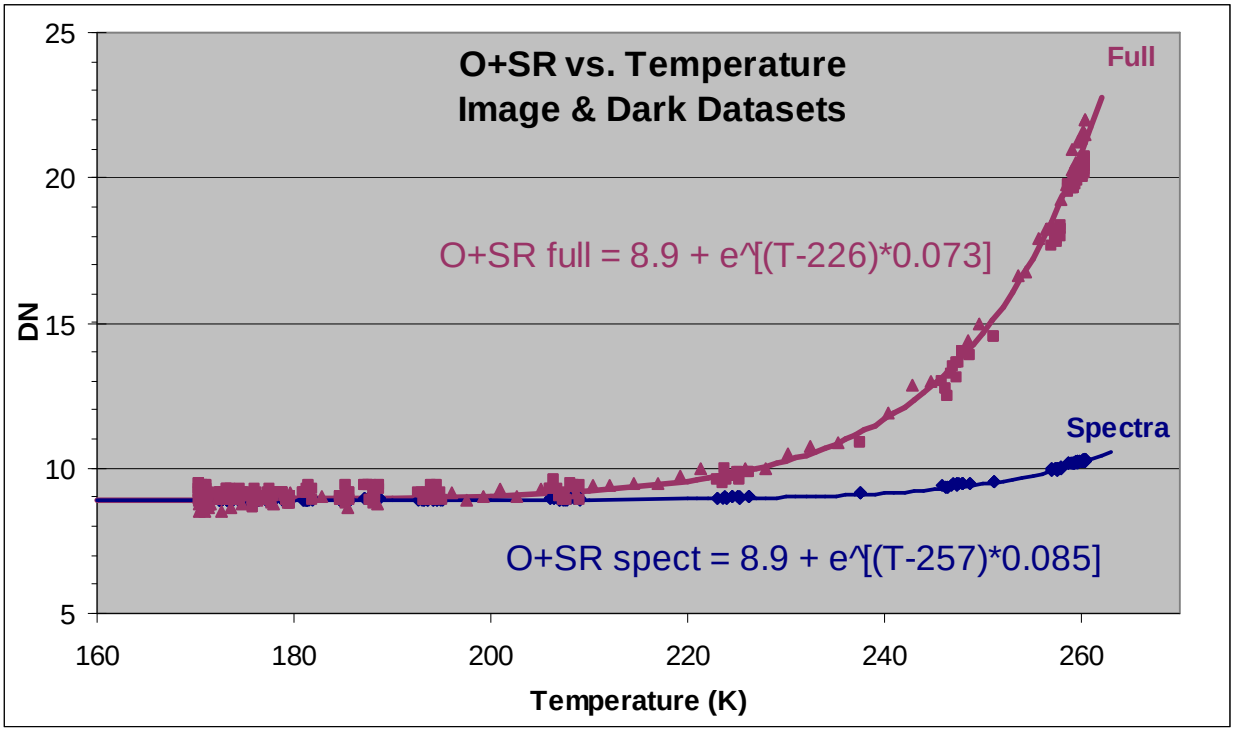

Figure 5.7-1: Electronics bias plus Serial Register dark current from full frame data (Image & Dark datasets) as measured during the Titan descent. The blue "Spectra" line is the same data scaled for the difference in serial register dwell time for the spectral mode datasets.

Thus for any full read mode dataset (i.e. Image and Darks), O+SR can be estimated by:

$$O+SR = 8.9 + e^{[(T - 226) * 0.073]} \qquad \text{(eq 5.7-2a)}$$

This relation evaluated at the CCD temperature of our observation (259.2ºK) yields:

$$O+SR = 8.9 + e^{[(259.2 - 226) * 0.073]}$$

= 20.2 DN, which is 0.6 DN higher than the null pixels suggest.

Tables in the Dark Current Estimation document (Reference 7) provide proportionality constants which relate the dark current signal in each pixel of each CCD instrument to the average of the Dark datasets. The per-pixel dark current (i.e. Equation 6 from Reference 7) then becomes:

$$DN_f = O+SR + t*f_1*D + m_f*f_2*D \qquad \text{(eq. 5.7-3)}$$

where:

DN_f is the dark current signal for the given pixel,
O+SR is the offset plus serial register component calculated above,
t is the exposure time
f_1 it the proportionality constant from the tables of Reference 7
D is the per-pixel average dark signal in the Dark dataset with O+RS removed.
m_f is the memory zone residence time in seconds = (row + 1) * 0.0084, and
f_2 is the memory zone proportionality constant from the tables.

Again, to allow determination of dark current for any Titan Descent dataset, the per-pixel average value of the Dark datasets, D has been calculated and fit by the following temperature dependent exponential (see Figure 5.7-2). As noted from the F16 data, D is nearly identical for the image and memory zones of the DISR CCD.

$$D = e^{\mathbf{[\,(T - 228) * 0.107]}} \qquad \text{(eq 5.7-4)}$$

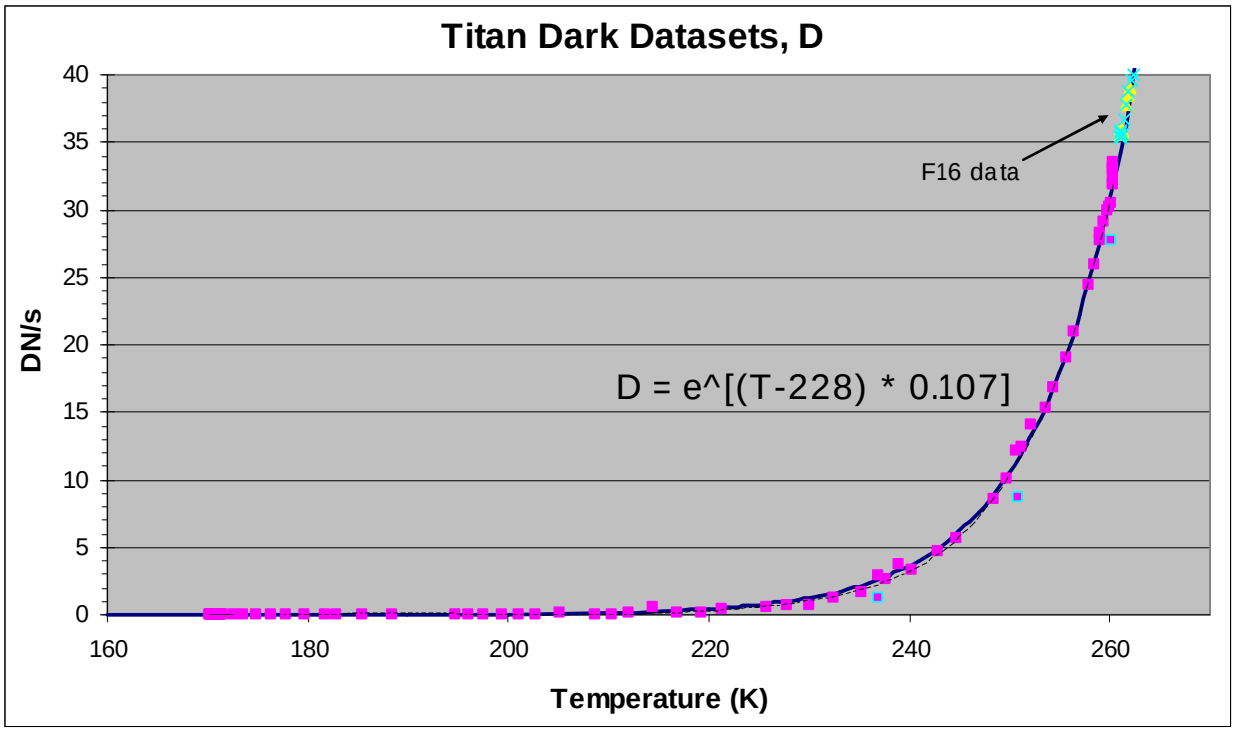

Figure 5.7-2: Average dark current rate, D (image and memory zone) for the DISR CCD as determined using the Dark datasets during the Titan descent by temperature.

At the temperature of our observation D becomes:

$$D = e^{\mathbf{[\,(259.2 - 228) * 0.107]}} = 28.17 \text{ DN/second}$$

Collecting the rest of our needed elements for equation 5.7-3:

O+SR = 20.2 DN, from above
t = 7 / 1000 seconds, from dataset header
m = (row + 1) * 0.0084 = (124 + 1) * 0.0084 = 1.05 seconds (Ref 7, eq 8)
f1 = 0.18639, from Reference 7, table VIa for pixel 124, 79
f2 = 0.77338, from Reference 7, table VIIa, pg 250, for pixel 124,79

$DN_f = O+SR + t*f_1*D + m_f*f_2*D$

$= 20.2 + .007 * 0.18639 * 28.17 + 1.05 * 0.77338 * 28.17$

$= 20.2 + 0.037 + 22.88 = 43.1$ DN

Thus, 43 DN of the 2177 DN signal for this observation for this pixel is dark current, the remaining 2030 DN is a combination of photonic signal, shutter effect and bleed thru. Shutter effect is discussed in section 5.8 below.

However before moving on to a spectral mode example; a few words about f2.

Because the dwell time in the memory zone is short for many pixels (those in the bottom row exit almost immediately), f2 is often not well defined. Figure 5.7.3 shows the values of f1 (blue) and f2 (red) for the 8 columns (0-7) of the ULVS. It can be seen that f2 for the lowest rows are unstable; and quantization continues to effect f2 for at least the lowest 150 rows. However, these effects aside, the f2 pixel to pixel variations are considerably less than those of f1. This being the case, it is recommended that one use the average value of f2 determined from rows above #150 (i.e. rows #150 to #200 for the ULVS). A summary of these 'alternate' f2 values is presented in table 5.7-1 below. Use of the value from this table for our HRI example above reduces the calculated dark current by 0.8 DN.

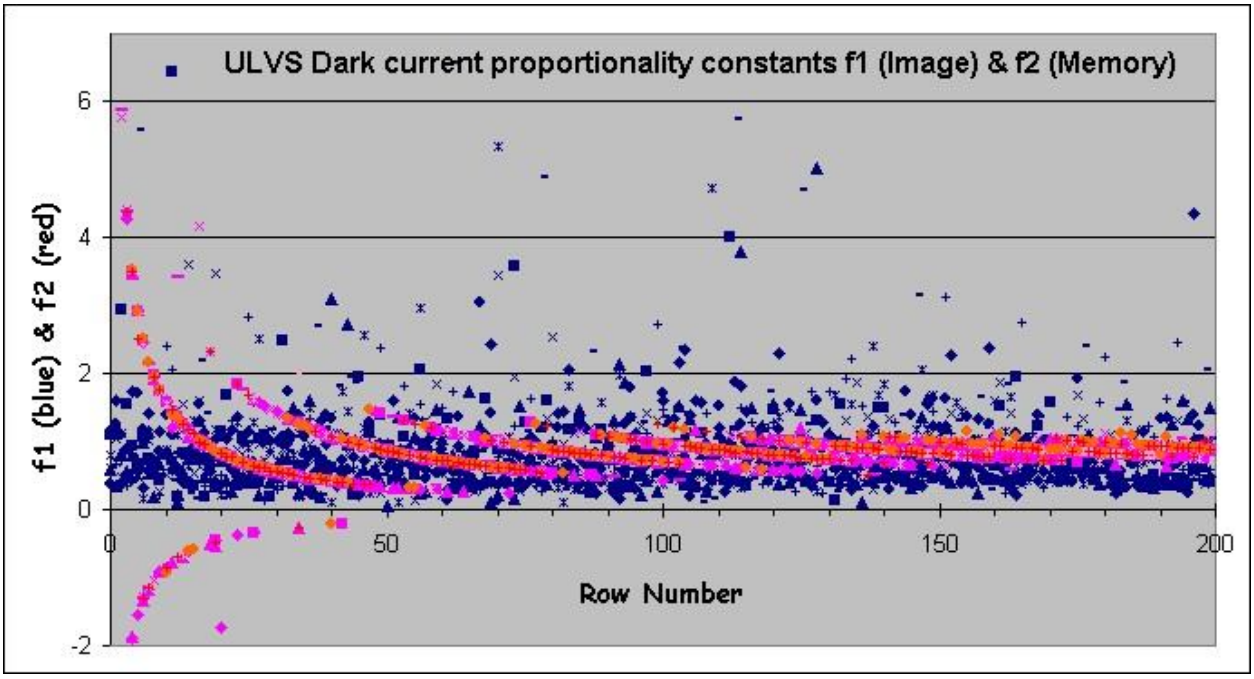

Figure 5.7-3: Dark current proportionality constants, f1 & f2 plotted vs. row number for the eight columns of the ULVS from the calibration document (Reference 7, table *IIIa*).

Table 5.7-1 Alternate (averaged) values for f2

CCD sub-instrument	Alternate value for f2
Downward Looking Visible Spectrometer	0.905
Upward Looking Visible Spectrometer	0.883
Solar Aureole 1, Blue Horizontal (0-5)	0.912
Solar Aureole 2, Blue Vertical (6-11)	0.927
Solar Aureole 3, Red Vertical (12-17)	0.919
Solar Aureole 4, Red Horizontal (18-23)	0.943
High Resolution Imager	0.872
Medium Resolution Imager	0.887
Side Looking Imager	0.893

Spectral Read Mode Example...

For this example I will choose one entry from one of the Visible Spectrometer datasets. Let us choose Visible Spectrometer dataset #67 (VISIBLE_0067_001356_0708), which is a Downward Looking Visible Spectrometer (DLVS) observation from 115 km altitude, with a CCD temperature of 260.3ºK (header information), and an exposure time of 644 ms from the label file. This dataset is summed from 20 to 10 columns width (i.e. x 2). We will choose table entry 132,0 which corresponds to the sum of pixels 132,0 & 132,1 (654 nm).

The data value from the data file is 2655 DN.

The term O+Rs in equation 5.7-1 is calculated by scaling the dwell time in the serial register from the full readout mode case:

$$(Serial\_Register + Bias)_{SPECTRA} = ((Serial\_Register + Bias_{FULL} - 8.9) * 0.992/8.384) + 8.9$$

where:

0.992/8.384 is the ratio of the pixel lifetime within the serial register in the Spectra readout mode to that in the Full readout mode.

8.9 DN is the best estimate of the electronic bias. The estimate is made from prelaunch calibration data at temperatures so cold that the serial register dark current is negligible.

Using equation 5.7-2a, the full readout O+Rs @ 260.3º K is: $8.9 + e^{[(260.3 - 226) * 0.073]} =$ 21.13 DN, and correspondingly:

(O+Rs)spectra = [(21.13 - 8.9) * 0.992/8.384)] + 8.9 = 10.35 DN

Collecting the rest of the terms for the spectral mode version of equation 5.7-3:

$DN_s = (O+SR)_S + t*f_1*D + m_s*f_2*D$ (eq. 5.7-3)

t = 0.644 seconds, from the label file,
f1 = average of 1.17633 & 0.33874 (i.e. 0.758) from Reference 7, table *Ia,*
$D = e^{[(260.3 - 228) * 0.107]}$ = 31.69 DN/s, from equation 5.7-4,
m_S = (row+1) * 0.000992 = 0.13 seconds, from Reference 7, equation 9, and
f2 = 0.905 from table 5.7-1 above.

DN_s = 10.35 + 0.644*0.758*31.69 + 0.13*0.905*31.69 = 10.35 + 15.47 + 3.73
= 29.55 DN

So 30 of the 2655 DN observed is from dark current.

New, Improved...

Lyn Doose has developed an alternate method of determining CCD dark current which is described in Appendix 35. This method also uses the F16 data to determine the image and memory zone dark current, and the Dark datasets acquired during the descent to establish the temperature dependence, but it maintains the row dependence rather than relying on only the average dark current.

5.8 DISR Images & SLI Strips

The DISR camera consists of three imagers oriented vertically (see Figure 2.2). All three take pictures in the probes +Z direction (in azimuth), cf. Figure 2.3, with the Side Looking Imager (SLI) viewing from 6º above the horizon to nearly 45° below the horizon (by 25.6º wide), the Medium Resolution Imager (MRI or DLI2) picks up at 44º degrees below the horizon (1 degree overlap), and extends down to ~16° from Nadir (21.1º wide). The High Resolution Imager (HRI or DLI1) overlaps significantly with the MRI, covering angles from 6.4º to 21.6º above Nadir but is only 9.6º wide. The three imagers are exposed simultaneously yielding a combined image that covers from 6º above the horizon to about 6º above nadir, and is mostly about 25° wide.

Figure 5.8-1 shows a joining of the three DISR imagers (known as a triplet) which were taken when the probe was resting on Titan's surface. The left triplet displays the raw images, photometrically hand stretched to reveal feature details, and sized to provide approximately matching angular coverage in the overlap regions. The triplet on the right (juxtaposed with a similarly scaled image taken on our moon) is colorized using the visible spectrometer information, and properly photometrically and spatially adjusted by Erich Karkoschka. This image is also available in the EXTRAS/POSTERS area of the DISR archive.

Each DISR imager has its own lens system, as described in the calibration document (Ref 6). Light is conducted, via fiber optic bundles, from each lens system to separate regions on the upper half (known as the image zone) of a shared CCD device. The exposure is controlled by timing the charge transfer from the image zone to the lower, covered half of the CCD (the memory zone). The images are then clocked out by row serially and read with a 12 bit Analog to Digital (A/D) converter.

The DISR pictures were not meant to be observed individually. The pictures are relatively small, around 40 kilo-pixels each, and not optimally exposed. The images are designed to be stitched together into 360° panoramas as described later (see Figure 5.8-4).

Due to the thick atmosphere the images are have low contrast. Figure 5.8-2 presents a popular Medium Resolution Imager (MRI) image (Sequence # 553) showing the effects of photometric contrast enhancement. The features are barely discernable in the raw, un-stretched image. Even an automatic stretch from the lowest to highest pixel value does not produce a suitable image (due to the black pixel in the upper right corner), an aggressive stretch (750 to 1100 DN) is needed to bring out the images details, however this removes some of the photometric information.

Still the individual images do have sufficient resolution to allow about a factor of 2 size increase to examine specific features if properly photometrically stretched. Figure 5.8-3 shows this same MRI expanded using two popular resizing routines, bi-linear extrapolation (IDL REBIN) and cubic convolution (IDL CONGRID). Notice that in some regions of the image the 16 bit square compression blocks, and their associated artifacts, become apparent at this size. The speckled pot marks are the result of imperfectly compensated fiber optics variations, as described later in this section. The type of expansion algorithm has negligible effect.

Figure 5.8-1 - Triplet of surface images: raw (left) and properly exposed & scaled (right).

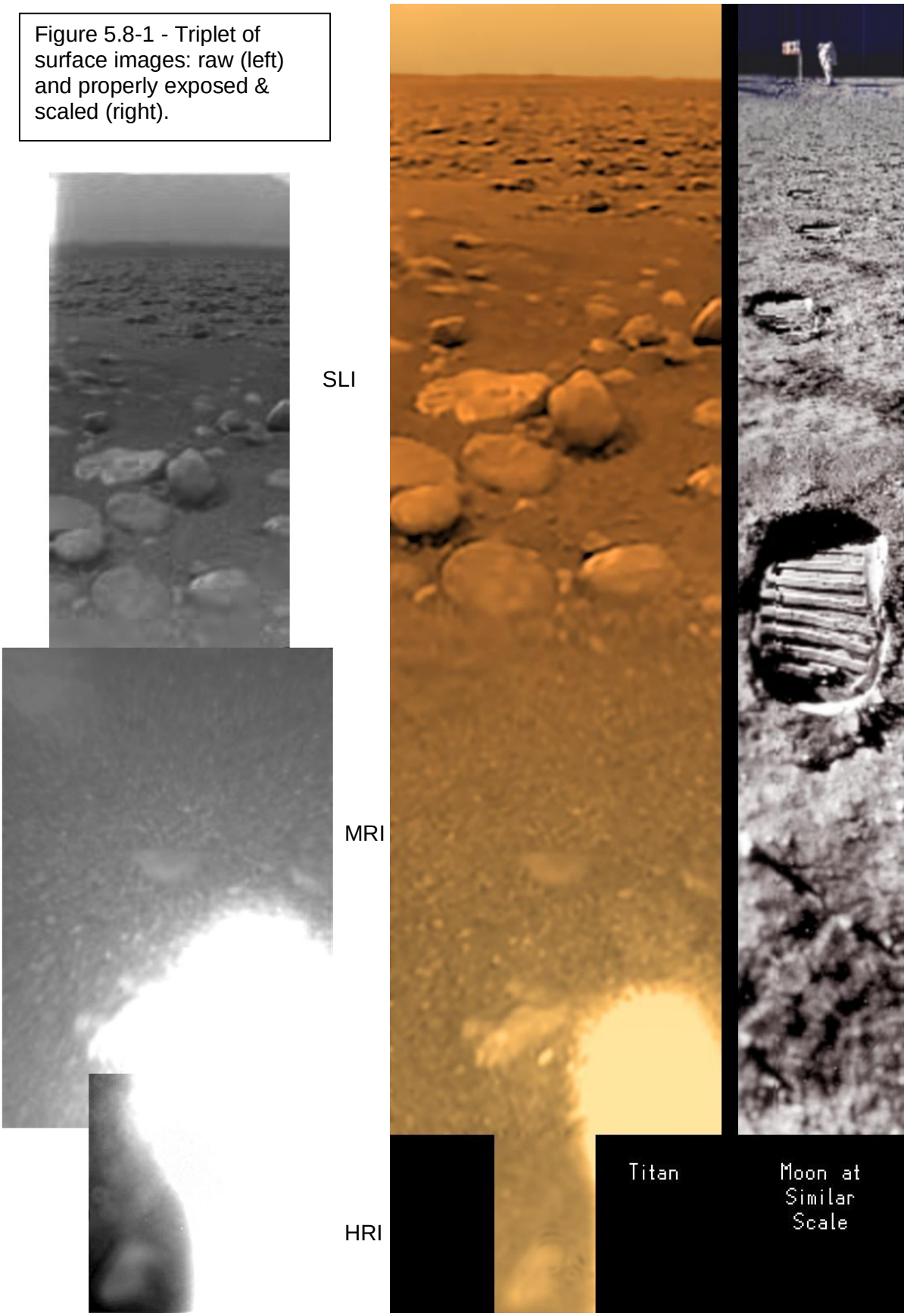

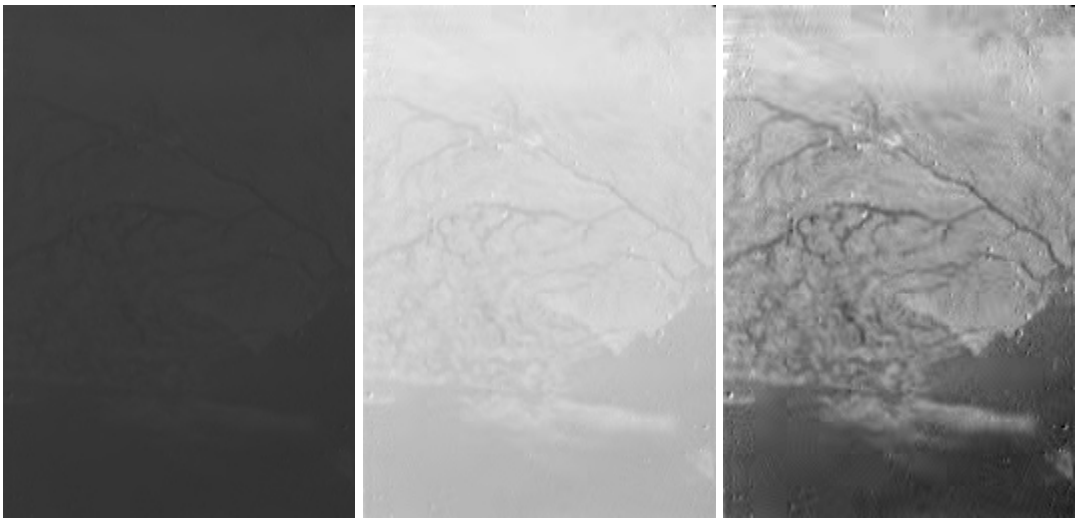

Figure 5.8-2 - Raw DISR MRI image 553 with no photometric stretch (left), stretched from minimum DN to maximum DN (middle) and stretched by hand to 37% contrast (right).

Minimum Pixel = 16 DN
Average = 939.3 DN
Maximum Pixel = 1164 DN
Standard Deviation = 64 DN
Exposure Time = 28 ms

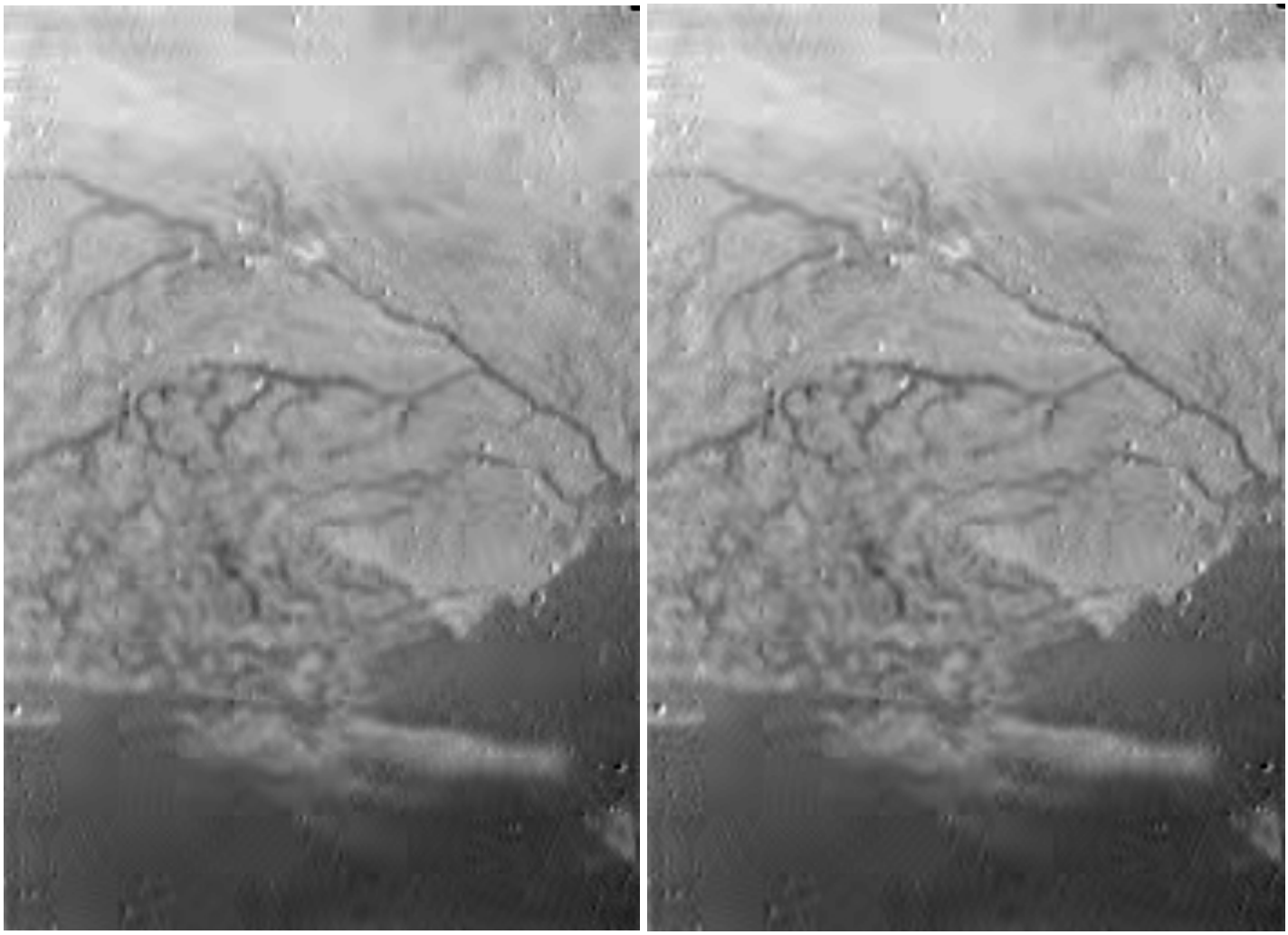

Figure 5.8-3 - Image 553 expanded using a bi-linear extrapolation (IDL REBIN) and on the right a cubic convolution algorithm (IDL CONGRID).

There are several sets of the DISR images in the PDS Archive in different formats. In the DATA/IMAGE section the images exist in two formats:

1) A table format which reports the data number (from 0 to 4095) corresponding to the light received for each individual pixel (in the TABLE_FORMAT directory), and

2) In an Image format (in the IMAGE_FORMAT directory) which is designed to work with the NASA View Image Display Software (http://pds.nasa.gov/tools/nasa-view.shtml), a tool that can be used to view the images as well as photometrically stretch and convert them to Jpeg or GIF formats.

These images are simply reconstructed by the pre-existing ground support equipment software to about 256 brightness levels (see "Image Decompression & Reconstruction", below). An improved set are to be added to the archive in 2013.

The EXTRAS/PROCESSED_IMAGES directory contains the same images with 3 separate levels of processing:

1) The "UNSMOOTHED_IMAGES" have been flat-field corrected to remove photometric distortions, temperature induced signals (dark current) have been removed, data clocking effects (shutter effect) have been compensated, bad pixels were replaced, and the images were photometrically stretched.

2) The "E_IMAGES" have been further processed to remove compressor induced artifacts, adjust for the pixels' point spread function, and adjust for negative & saturated pixels.

3) The "G_IMAGES" are further processed to adjust for geometric distortions and intensity calibrated into I/F.

The 'Unsmoothed Images' are a good representation of the scene with the instrument effects removed. The 'E' & 'G' images have been altered in an non-unique way such that low contrast features may have been eliminated or produced. These images should not be used for study of low contrast areas.

These images are in both PGM & TIFF formats. Further details of the images in the EXTRAS directory are presented in the text file:

EXTRAS/PROCESSED_IMAGES/IMAGE_PROCESSING_STEPS.TXT

The systematic design was to collect images at predesignated azimuths as the probe rotated below the parachute during the Titan descent, such that the images overlap in both azimuth and ground track. After the mission, the individual images can be assembled into mosaics of Titan's surface using any desired projection scheme. An example using flight spare images taken from the rooftop of the Kuiper Lunar and Planetary Building on the University of Arizona campus is shown in Figure 5.8-4 as a conformal conic projection. The boundries of some of the individual images are discernable.

A set of 12 evenly spaced triplets (36 images) is taken at each desingated altitude above Titan's surface (in the Image and High Near Surface cycles). Eight Image cycles (above 26 km), and nine HNS (between 23 km & 3 km altitude) cycles were executed during the Titan descent, for a total of 612 panoramic descent images, plus 24, non-azimuth controlled triplets (taken below 3 km), 27 calibration exposures, 8 half HRI images (very near the surface), and 3 Flat Field exposures, for a total of 722 images over the ~2.5 hour period. A summary of the cycles is presented in Appendix 6. Assembled mosics of Titan's surface are available in the archive in the EXTRAS/MOSAICS EXTRAS/POSTERS directories. Also, a simulated descent containing the images is presented in the EXTRAS/MOVIES directory. Due to the communication link and Sun-sensor problems described in section 3, images from variaous altitudes needed to be used to fill in gaps at each descent level.

Figure 5.8-4 - A mosiac of 30 DISR images taken from the roof of the Kuiper building (~13 m high), in conformal conic projection showing the U of A mall area.

Details of the individual imager's performance (field of view, point spread function, etc) are available in the document, "Calibration Report for the Imagers of the Descent Imager/Spectral Radiometer Instrument aboard the Huygens Probe of the Cassini Mission", located in the DISR archive under DOCUMENT/DISR_CALIBRATION_DOCUMENTS/IMAGERS (Reference 6) The derived imager pointing orientations during the Titan descent are described in Appendix 3.

The DISR cameras are far from perfect, so significant post-mission manipulation of the data is necessary to produce accurate images or do meaningful photometry. There is a significant amount of barrel distortion in the SLI, significant coma in the MRI, flat field variations, high dark current pixels, fiber-optic imperfections, bleed thru between imagers & radiation induced effects to account for. Also, although the images are captured with 12 bits of depth, they were transmitted as 8 bit words, limiting their contrast.

In order to compensate for the limitations imposed by data bandwidth, low light, and space environment, a considerable amount of on-board image processing was performed. Exposure times were adjusted based on the results of previous image exposures at similar azimuth, and additionally limited to reduce smear to less than 1.5 pixels in the center of the HRI (as derived from the probe spin rate). Flat field adjustments, and bad pixel replacements (adjacent) were made using on-board maps. The 12 bit images were reduced to 8 bits of depth using a pseudo-square root transformation via a look up table which maintains better than 100 to 1 signal to noise (S/N) ratios for pixels that exceed that threshold, and slightly reduced S/N (~7.6%) for noisier pixels. The images are compressed using an on-board hardware compressor which usually results in non-lossless compression

The list below summarizes the steps in converting a scene from a gleam in the camera's eye to a calibrated image. Details of these steps is presented in the following paragraphs.

1) The on-board software creates an image command containing the exposure time & processing options based on the observation schedule, buffer space, prior exposures & probe spin rate. The same exposure is used for all 3 imagers.
2) When the probe has rotated to the desired azimuth the CCD wells are drained and the exposure begins.
3) At the end of the desired exposure time the acquired images are shifted from the image zone down into the covered memory zone of the CCD. All 3 images (SLI, MRI, & HRI) are acquired simultaneously.
4) Each pixel's charge is read out row-by-row using a serial register at the bottom of the CCD into a 12 bit A/D converter (although the imaging devices are inverted, so the top of the image is read out first).
5) Known variations in the per-pixel Responsivity are compensated using the flat-field table.
6) Known bad pixels are eliminated by replacing their values with good adjacent pixels.
7) The images are converted from 12 bits to 8 bits using the on-board square root table described above.
8) The images are compressed by the data compression hardware.
9) The image is transmitted to the Earth via the first available telemetry channel.
10) Once the images arrive on the earth there are some options as to how they are processed. The most basic re-construction software used by the Ground Support Equipment (GSE) which processes DISR packets, decompressed the images and uses the square rooter lookup table described above to convert the 8 bit transmitted images back into 12 bit images. These are the images which reside in the DATA area of the DISR archive.
11) The two other sets of DISR images located in the EXTRAS directory of the Archive have been further processed to eliminate compressor induced artifacts, adjust for the imagers point spread functions, negative & saturated pixels, and normalize intensity (to I/F).
12) In addition to the photometric corrections described in step 11, geometric corrections are also necessary to obtain a fully calibrated image.

The detailed steps used to generate the "E" and "G" images is located in the text file:
EXTRAS/PROCESSED_IMAGES/IMAGE_PROCESSING_STEPS.TXT

Image commanding...

The flight software autonomously commands image collection. The algorithm's goal is to collect properly exposed (i.e. to approximately half of the 4095 DN available) images evenly spaced in azimuth, and staggered by ½ an image from those collected at the previous altitude. This is done by setting the exposure time of the first set (i.e. first Image Cycle) to a default value (7 ms), then adjusting the exposure time for each subsequent image taken at that azimuth to optimize the exposure (i.e. each of the 24 azimuths are optimized independently).

During the calibration cycles three sets of image exposures are taken; one set at 7 ms with the calibration lamps on, one at 7 ms with the lamps off, and a third set with 0 ms exposure time (& lamps off). This allows for determination of the dark current and responsivity changes. Near 50 km altitude one long exposure (35 ms) was taken to smear the scene and allow for flat fielding of imperfections in the imaging systems, (however only one of the flat images (the SLI) was transmitted, and most of it was saturated). Once the probe drops below 3 km, the software

abandons azimuth timing and takes images based only on the telemetry buffer level. Below 300 m only half frame HRI images are collected. After landing the instrument went back to taking image triplets.

CCD chip layout & clocking...

The figure below shows the location of the various DISR instrument which share the CCD chip.

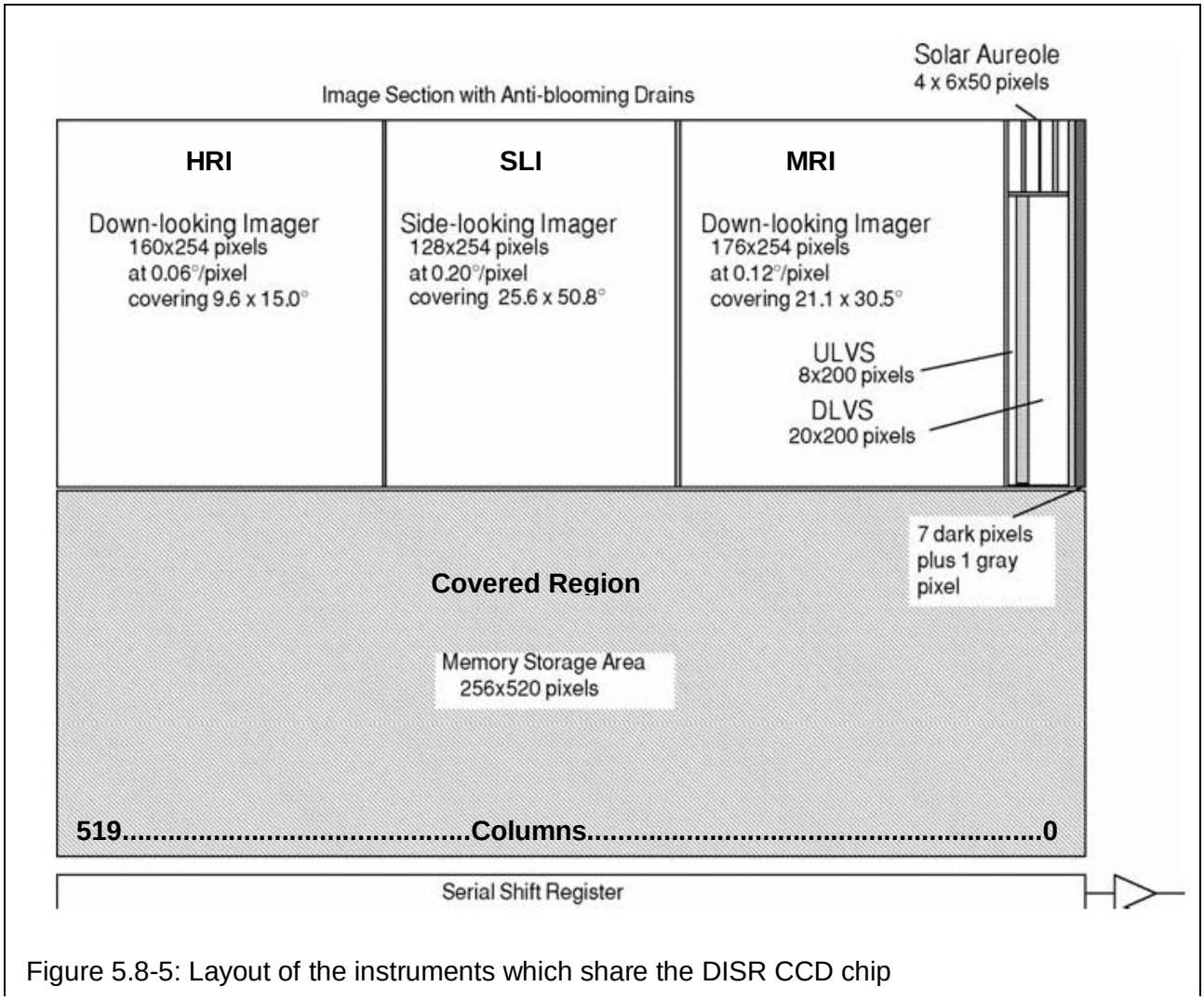

Figure 5.8-5: Layout of the instruments which share the DISR CCD chip

The CCD contains 512×520 pixels, but one half of the surface is covered by an opaque, aluminum mask. The images are formed in three subsections of the CCD, and it is then rapidly shifted (~0.51 ms transfer time) under the opaque mask. Each row of the image is deposited into a serial register, and a 12-bit analog-to-digital converter digitizes the amount of charge in each pixel in that register. The result is stored in computer memory.

The HRI uses an area of 160 columns by 254 rows on the CCD. The first and last of the 256 rows are not used, because they contain corrupted pixels. This is true for all three imagers. The MRI uses an area of 176 columns by 254 rows. The SLI uses an area of 128 columns by 254 rows.

The images are inverted. The top of the scene gets imaged to the edge of the covered region, the bottom of the scene to the top of the chip, the left and right sides of the scene map to the left and right sides of each imager, respectively. For each imager, the pixel(0,0) point is at the upper right corner of the scene. The view presented in the figure above is from the outside (or fiber optics) side of the chip. Thus, it is a mirror image compared to DISR's viewing direction (toward the outside of the probe).

The CCD is an image transfer type. Anti-blooming gates inhibit the spread of excess charge over the chip when overexposure occurs. The pixels are 23 μm squares.

Shutter effect ...

As the images are clocked downward to the covered memory storage section they pick up additional charge, both from the illuminated pixels that they traverse and dark current from all pixels they traverse. So a pixel at the top of the CCD will have additional signal that is not related to its exposure. To compensate for this it is necessary to deduct signal proportional to the dark current plus illumination signal. The time needed to shift the image to the memory section is about 0.5 ms. Shifting out the contents of the memory zone of the CCD takes about 2.2 seconds in full frame mode. The spectrometer and solar aureole data, taken in spectral read mode, take about 263 ms to drain from the memory zone.

As a simple example consider a 7 ms flat image where all the HRI pixels are at 2000 DN at the end of the exposure time. We will assume a temperature where the dark current rate is 1 DN/second for every pixel.

A pixel at the top of the HRI (which is the bottom of the scene) accumulates 2000 DN during the exposure. It acquires additional signal while clocking to the memory section of:

$$\text{Shutter signal} = n\_pix * (Ave\_DN / exp\_time) * (0.5 \text{ ms} / 253 \text{ pixels})$$

$$\text{Shutter signal} = 253 \text{ pixels} * (2000 \text{ DN} / 7 \text{ ms}) * (0.5 \text{ ms} / 253 \text{ pixels}) = 143 \text{ DN}$$

A pixel mid way down (i.e. 127th) the HRI acquires an additional:

$$\text{Shutter signal} = 126 \text{ pixels} * (2000 \text{ DN} / 7 \text{ ms}) * (0.5 \text{ ms} / 253 \text{ pixels}) = 71 \text{ DN}$$

The pixel at the top of the HRI will gain an additional dark current signal of:

$$\text{Dark Signal} = 253 \text{ rows} * (2.2 \text{ seconds} / 253 \text{ rows}) * (1 \text{ DN} / \text{second}) = 2.2 \text{ DN}$$

While the pixel at row 127 will gain essentially half that. So the resulting telemetered image will have a slope from 2000 DN at the bottom of the HRI, and 2145 DN at the top.

Dark Current ...

In actuality the dark current is comprised of 4 components, and like the shutter effect is row dependent. Details of how to determine the CCD dark current is presented in section 5.7.

Bad Pixel Replacement...

Known bad pixels are replaced with a copy of a row adjacent neighbor to avoid spending compression coefficients on unreal features, which can cause severe checker-boarding of the image. Bad pixels are typically hypersensitive (hot) pixels or those poorly illuminated by the fiber optic bundle. The majority of replaced pixels are around the perimeter of the image. Tables of replaced pixels are presented in section 5.2, "Bad Pixel Maps" of the Imager Calibration Document (Ref 6).

Flat Fielding...

A perfectly uniformly illuminated DISR imager does not produce a perfectly uniform data product. In order to compensate for spatial variations in the responsivity of the optics/CCD system a flat-fielding software algorithm was incorporated. This algorithm corrects each individual imager pixel by dividing its reported signal by a correction factor:

$$DN_{corr} = \frac{DN_{original}}{correction\_factor}.$$

Files containing these correction factors for each pixel are available, and will be placed in the archive in the future. The flat field pattern is included in the Absolute Responsivity (AR) files for the instrument, and so do not need to be applied separately when determining radiance. The AR files are located in the archive under:
/DOCUMENT/DISR_CALIBRATION_DOCUMENTS/IMAGERS/ABSOLUTE_RESPONSIVITY

The correction factors are calculated from entries in an 8 bit "Flat Field Lookup Table" for each imager (SLI, MRI, HRI).

correction_factor = (1 / 253) * Table_Entry_Value + 0.1921

The figure below shows the response pattern resulting from a uniform illumination for each DISR imager. The images are highly stretched, exaggerating the blemishes. The boundaries of the fiber optic strands create about a 3% drop in responsivity (i.e. the chicken wire pattern). Beyond that there are variations due to CCD pixel responsivity variations, and optical alignment.

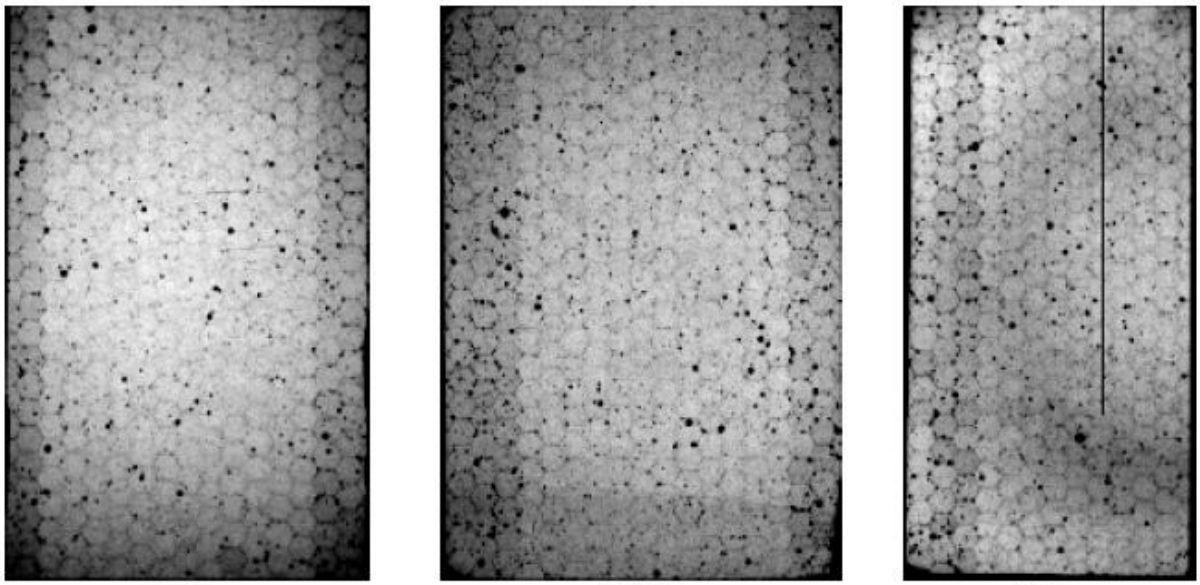

Figure 5.8-6: Response of DISR imagers to a uniform (flat) illumination. The 'chicken wire' pattern is due to the seams between individual fiber optic strands. In these views the imperfections are exaggerated; the actual deviation is about ± 8% from the mean. The black areas around the edges and strip down the SLI are non-responsive, 'bad' pixels, which are replaced.

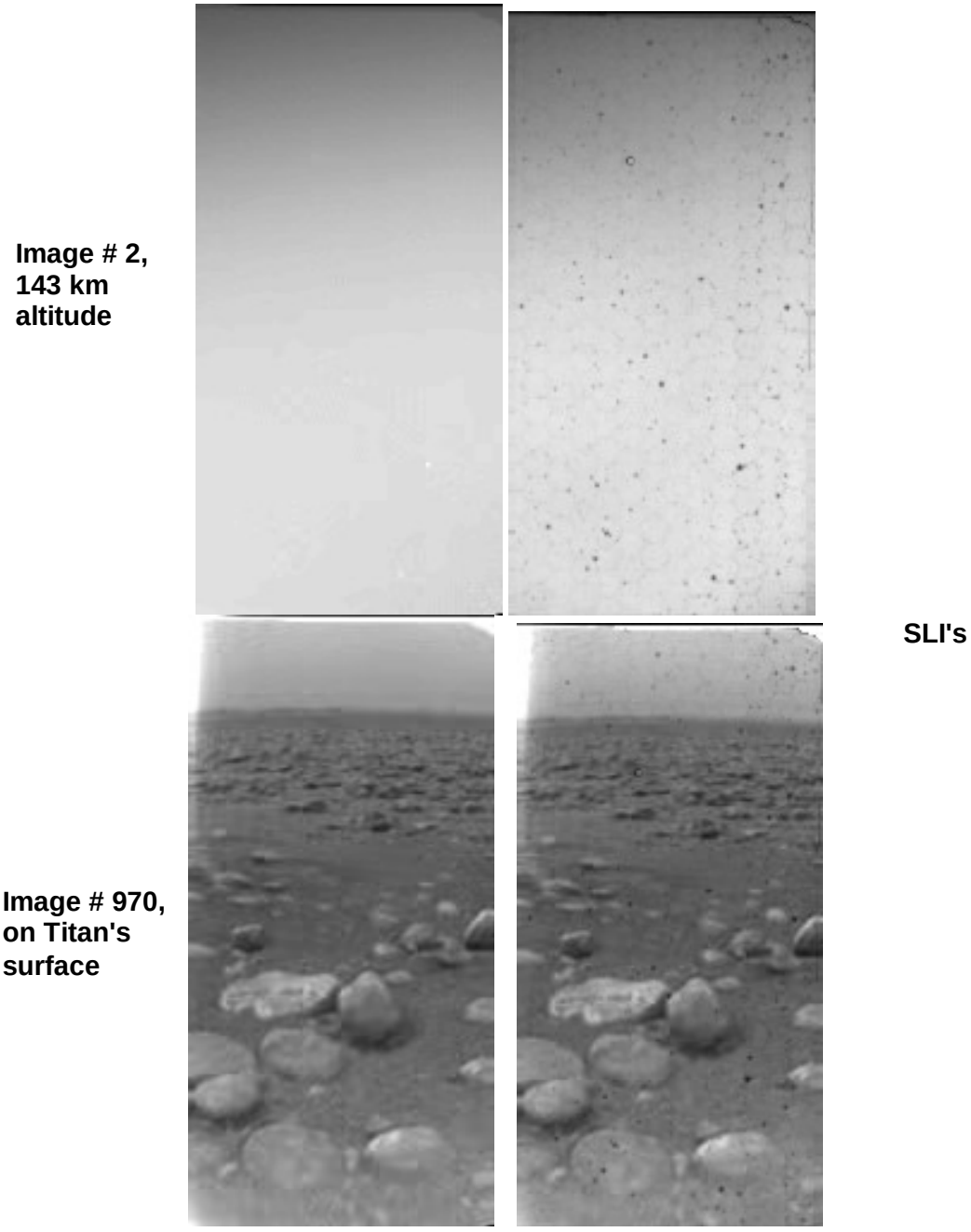

Figure 5.8-7: Comparison of DISR Titan images with the flat-fields incorporated (left), and with them removed (right) at two descent altitudes. Notice the 'chicken wire' pattern caused by the fiber optic bundles, as well as inclusions are visible in the images with no flat fields.

The flat fields were developed at ~245ºK, and are relatively temperature independent. However, some mild blemishes are introduced by the flat fields at the coldest temperatures. See the Image Calibration document (Reference 6) for details.

A more significant effect is movement of the fiber optic bundle during launch, SOI, entry and descent. Since the bulk of the responsivity changes are due to variations in the fiber optics, application of the on-board flat fields after movement of the fibers introduces imperfections in the scene rather than removing them. Erich Karkoschka has characterized these environmentally induced changes using exposures from the top of the descent, which views a relatively uniform appearing atmosphere. His flat-fields will hopefully be incorporated into the archive in 2013.

Data Compression...

The DISR images are hardware compressed using a discrete cosine transform (DCT) algorithm similar to JPEG compression (a flight qualified JPEG compressor was not available at the instrument development time). The main differences from the JPEG scheme is that DISR works on 16 x 16 pixel blocks (instead of 8 x 8), has fixed quantization value (rather than a table), and discards some low-valued coefficients. One advantage of the DISR compressor is that it incorporates sync markers into each block to allow partial image reconstruction in the event of telemetry dropout. Also, the DCS software compensates on-the-fly for hot and cold pixels as described in section 5.5.1, "DCS automatic bad pixel replacement" of the calibration document, Reference 6.

At the compression ratios used, the DCT image compression is lossy. Detailed discussion of the compression effects is presented in section 5.6, "Imaging system performance" and section 6, "Improved Processing of Compressed DISR Images" of the calibration document, reference 6. Compression ratios for the descent images range from 3.6 to 16.6 with respect to 8 bit/pixel images, and are listed in Appendix 20.

The data compressor operates on 8 bit images. A lookup table, similar to a square root translation, is used to convert the 12 bit images to 8 bits (and simultaneously accentuate darker features) prior to compression (see Appendix 25). The images are all flat-fielded, have bad-pixel replaced and are 'square rooted' to remove as many artifacts as possible before being compressed.

As discussed in section 6 (Improved Processing of Compressed DISR Images) of the Image Calibration Document (Reference 6), there are characteristics of the DISR images that make them less than optimal for compression and reconstruction including CCD noise, imprecise dark current knowledge and flat field temperature variations. To help compensate for some of these difficulties improved processing steps were devised by Erich Karkoschka. There are two basic levels of images available in the DISR archive, those reconstructed using the original reconstruction software (which are in the DATA & BROWSE directories), and those with the "Improved Processing" steps outlined in section 6 of Reference 6 which are in the EXTRAS/PROCESSED_IMAGES directory of the archive.

Section 6 (Improved Processing of Compressed DISR Images) of the calibration document (Ref 6) also provides more detail as to the workings of the DISR data compressor.

Image Data Transmission...

The DISR image data dominates the instruments telemetry allocation. Early on in the program it was recognized that redundantly transmitting the images would significantly limit the total amount of science data that could be obtained by the instrument. Therefore it was decided that the images would not be sent redundantly, on both telemetry channels, but that they would be split between channels in hopes of getting additional coverage and stereography. Sadly the loss of one telemetry channel during the descent caused the loss of half the DISR images. However it was still possible to get complete surface coverage, as evidenced by the movies and posters which can be found in the EXTRAS and HIGHER_LEVEL_DATA directories of the DISR archive. Although, many of the image triplets (SLI, MRI, HRI) are incomplete.

Image Decompression & Reconstruction...

Because the image compression is not lossless there is some element of freedom in how they are reconstructed. This is discussed in some detail in section 6 (Improved Processing of Compressed DISR Images) of the calibration document (Ref 6). The variations occur primarily at the 16 x 16 pixel block boundaries and in relatively low contrast features within the blocks. Besides the two levels of images already contained in the archive (and described above), another higher level set with slightly improved photometric accuracy should be available in the near future.

Since the 8 bit to 12 bit conversion is not a one to one mapping, some freedom is also available in reconstructing the 12 bit images from the 8 bit transmitted images. The table in Appendix 25 gives the available low, high and midpoint 12 bit values corresponding to each 8 bit transmitted value for one image. Also, since the square root tables have no overlap some freedom is available near quantization boundaries to compensate for variations from CCD noise, flat field temperature variations, dark current uncertainty, etc.

One deficiency with the images currently residing in the Archive is that the decompression software used did not treat the threshold and rounding of the data as accurately as possible (that is, the Discrete Cosine Coefficients, DCTs). Since the contrast in the majority of the images is quite small, these inaccuracies translate into significant photometric variations in the images. These inaccuracies have been compensated for in the E & G images, residing in the EXTRAs directory of the Archive, but the 'raw' images residing in the DATA directory have not been corrected.

The noise in the 12-bit images is mostly photon noise, which is SQRT(DN/30) for DN = 0 to 4095 since the analog-to-digital converter gives 1 DN for every 30 electrons measured. There are about 700 distinguishable signal levels using the 1-sigma photon noise as the step size from one level to the next. Since 8-bit data can distinguish only 256 levels, a factor of three is lost in the standard 12-to-8 bit conversion. The standard conversion has three distinguishable levels for each 8-bit data number. Roughly, 8-bit-DN = 4 SQRT(12-bit-DN), which is why this conversion is sometimes called the square-rooter.

The damage of the 12-to-8 bit conversion described above is only valid for features of the size of 1 pixel. For features larger than 1 pixel it is worse since the photon noise decreases as more pixels are averaged, but the digitization noise remains the same if intensity levels are similar. Even worse, photon noise is easily recognized and interpreted as such, but digitization noise creates features that run parallel to isophotes and that can easily be confused with real features.

Thus, images using the standard 12-to-8 bit conversion scheme are of low quality and their interpretation is compromised by difficulties of distinguishing real from artificial features.

In order to significantly improve the 12-to-8 bit conversion, an adaptive scheme was used for most images. The software determined a low and a high 12-bit DN using the image histogram in such a way that most of the recorded data numbers fall between both values. Then, the density of 8-bit DNs was increased by up to a factor of about 10 between the low and high DN, which means that the density of 8-bit DNs below the low DN and above the high DN had to be decreased since there are only 256 8-bit DNs available. The decrease of density was never more than a factor of 2. This means that the density of 8-bit DNs jumped by up to a factor of about 20 at both transition points. It also jumped somewhat within each of the three regions.

The low and high DN determined by the software was transmitted, and we know exactly how the software created the adaptive scheme for each set of two numbers. Thus, the 12-to-8 bit conversion scheme is known for each image, and the scheme for each image will be added to the archive. Using each scheme, the compressed 8-bit images can be converted back into 12-bit images. The compressed 8-bit images do not have integer data numbers since they are the result of a DCT transform. Thus, for each adaptive scheme, one can define a continuous function that maps the 8-bit fractional DNs into 12-bit fractional DNs.

During the descent, the MRI and HRI images had generally very narrow histograms, which meant that the adaptive scheme adopted had large improvements in the density of data numbers. Thus, the 12-to-8 bit conversion was almost lossless, and the noise in these images is essentially the photon noise of the CCD. On the other hand, the SLI images had wide histograms, due to the bright sky above the horizon and the dark surface looking halfway down, so that the adaptive scheme could not improve much above the standard scheme. About half of the SLI images during the descent used the standard scheme, while the remaining ones used the adaptive scheme with only slight improvements relative to the standard scheme. Thus, most of the noise in the SLI images is digitization noise in the 12-to-8 bit conversion, not photon noise of the CCD.

One important aspect of the adaptive scheme is that it decreases the 8-bit amplitude of features that have DNs below the low DN or above the high DN of the scheme, by up to a factor of 20 relative to features between both limits. For bad pixels such as constantly bad pixels on the CCD or cosmic ray hits, this is beneficial. Bad pixels can have contrasts close to 100 %, some 100 times larger than typical contrasts in the scene due to Titan's surface features, which are typically around 1 %. Since the compression algorithm transmits most DCT coefficients for the features of largest contrast, but few coefficients for the features of lowest contrast, the compression algorithm will create a compressed image that gives very accurate detail on bad pixels but has little data left for real features. Since the adaptive scheme reduces the amplitude of bad pixels by large factors, the compression works much better and will focus mostly on real features.

The adaptive scheme also had a negative effect on a few MRI and HRI images taken at low altitude. Ideally, the software should have determined the high DN just above the DNs of real features but well below the DNs of bad pixels. However, for these few MRI and HRI images, the software set the high DN a little lower than ideal. This means that the brightest features had DNs above this limit and thus have error bars an order of magnitude larger than error bars for the remaining part of the scene. This fact is important in interpreting these images. For example, in raw images some bright ridges have very bright spots that may seem like snow-covered peaks. However, the DNs for these bright spots are above the high DN of the adaptive

scheme. The error bars for the DNs of the bright areas is so large that they may have the same brightness as the ridges elsewhere, or they may be even much brighter. Correct interpretation of raw images requires knowledge of the low and high DN of the adaptive scheme.

Photometric Calibration...

The details of the photometric calibration done on the DISR are presented in section 4.2.1 ("Image Absolute Responsivity Reductions") of the Image Calibration Document (Reference 6). In this section we will present an example of how to determine the Radiance and Irradiance for an image pixel.

From Reference 6 (equation 1) the count rate (r) of an imager pixel in DN/s is:

$$r = A\int I(\lambda)RSR(\lambda)d\lambda$$

where:

A is the absolute responsivity in (DN/s)/[W/(m2-sr)],
I(λ) is the spectral radiance of the source seen by the imager in W/(m2-u-sr),
RSR(λ) is the relative spectral response of the imager pixel (dimensionless), and
λ is the wavelength in microns.

The Radiance (R) in W/(m2-sr) is then:

$$R = \int I(\lambda)\, RSR(\lambda)\, d\lambda = r / A$$

And the Irradiance, E is:

$$E = \int R(\Omega)\, d\Omega$$

where:

Ω is the solid angle of the field of view of the pixel of interest.

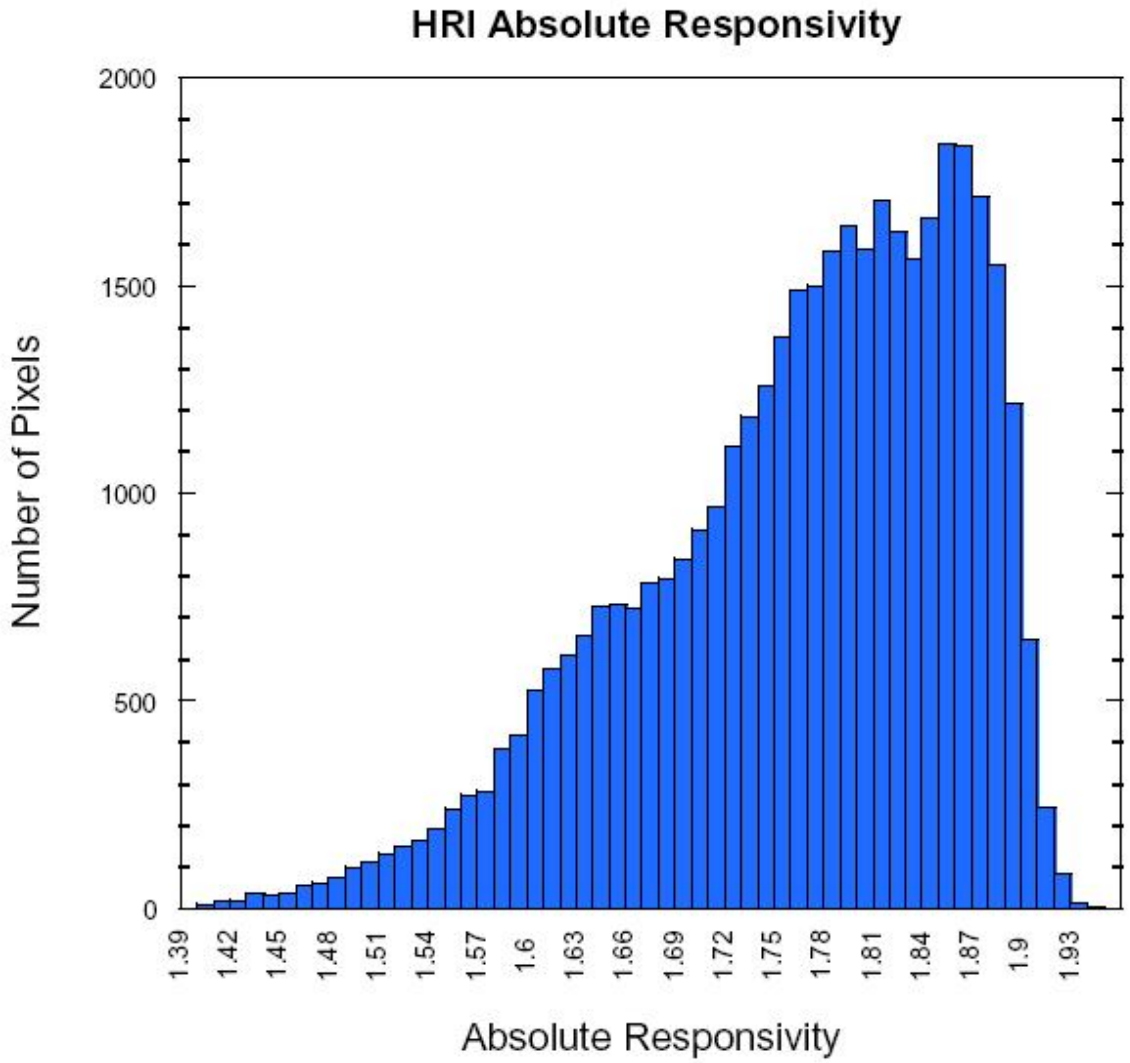

Figure 5.8-8: Absolute Responsivity Histogram for the HRI. The average is 1.74 x 10^6 (DN/s) / (W/sqm-str). The shape is similar for the MRI and SLI distributions.

HRI pixel example...

Using the same HRI pixel chosen as the image dark current example in section 5.7 above, we again summarize the data from the DISR archive:

Type: HRI exposure.
Dataset: #21 (Filename: IMAGE_0021_000324_7662)
Pixel: Row #125, & column #80, HRI(124, 79), near the center of the 160 wide by 256 high HRI
The signal level of this pixel is 2177 DN.
The CCD temperature is 259.2ºK.
Null Column 2 = 81 DN
Null Column 3 = 75 DN
Exposure Time = 7 ms

To determine the signal rate, 'r' we must first remove non-source contributors. Bleed through from the other CCD instruments can be neglected for imager data (but not for spectrometer or solar aureole data). This observation was taken with the Surface Science Lamp off, so there is no contribution from the SSL. Dark current for this pixel, during this observation, has been calculated to be 43.1 DN, as shown in section 5.7. The other significant contributor is shutter effect, which is described above.

To calculate the shutter effect for this pixel, during this observation we must average the data generation rates for all the pixel positions that this measurement must pass through (i.e. all pixels below the pixel of interest, HRI(0:124,80)).

The average signal in HRI (0:123,79) = 2125.75 DN for the 7 ms exposure.

Shutter signal = n_pix * (Ave_DN / exp_time) * (0.5 ms / 253 pixels)

Shutter signal = 125 * (2125.75 / 7 ms) * (0.5 ms / 253)
= 75.0 DN

So, the net signal for this pixel, for this observation is the observed minus dark current minus shutter effect:

DN = 2177 - 43.1 - 75.0 = 2058.9 DN, and the signal rate becomes:

r = DN / exp_time = 2055.1 / 0.007 = 294,129 DN/second

From the Absolute Responsivity (AR) table for the HRI (DLI1) at 259.71ºK (nearest this observation) we obtain A:

A = 1,842,400 (DN/s) / [watts/(m^2 sr)]

The AR tables are located in the DISR Archive under:
/DOCUMENT/DISR_CALIBRATION_DOCUMENTS/IMAGERS/ABSOLUTE_RESPONSIVITY

We are fortunate to have an AR table near our temperature of interest. However it is possible to interpolate between tables using the relations given in section 4.2.2 (Image Absolute Responsivity Reduction Results) of the calibration document (Reference 6), shown below for the HRI:

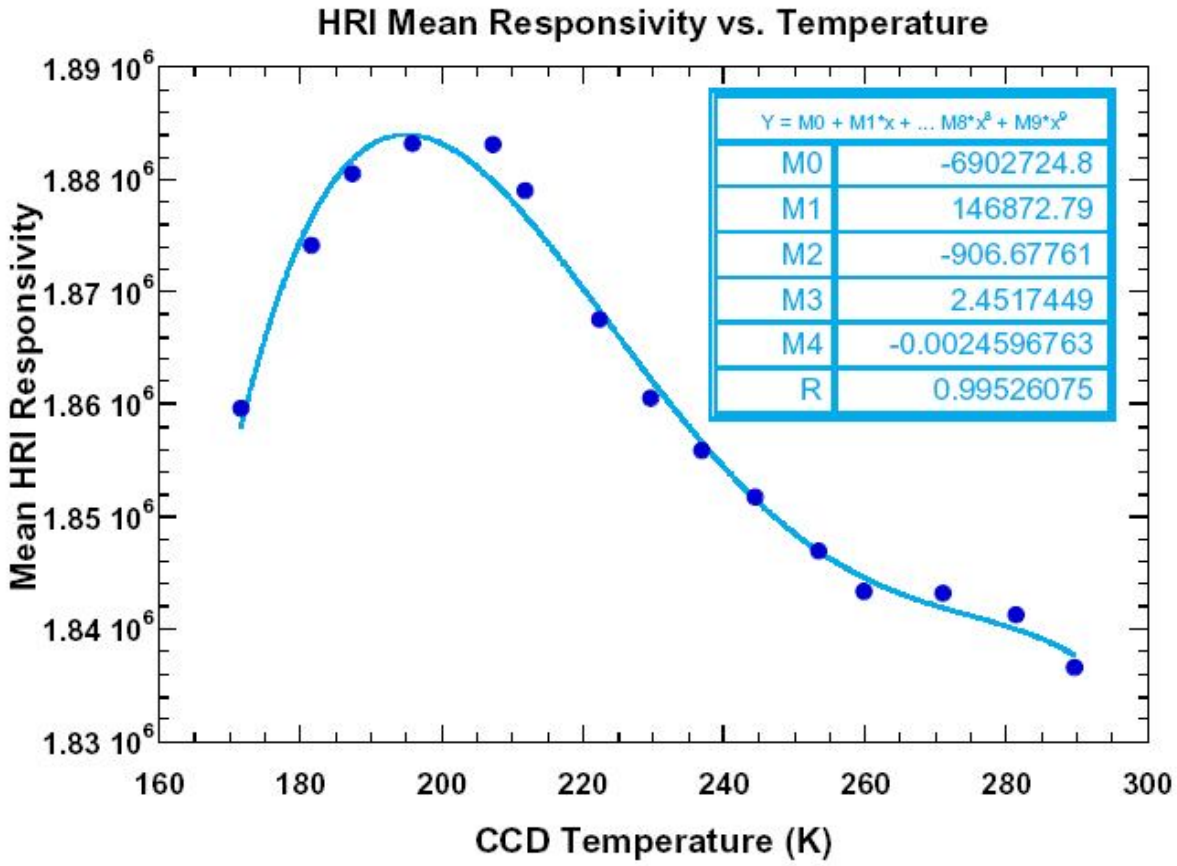

Figure 5.8-9: Temperature model of the absolute responsivity for all good HRI pixels. Dots are the measurements, and the curve is a fourth-order polynomial fit.

$$A = M0 + M1*T + M2*T^2 + M3*T^3 + M4*T^4 ,$$

where the M's are from the table in the plot, T is the CCD temperature of the observation, and A is the Absolute Responsivity in (DN/s) / [W/(sqm sr)]. And so...

$$dA/dT = M1 + 2M2T + 3M3*T^2 + 4M4*T^3 ,$$ for our observation at 259.2ºK..

dA/dT = -324 (DN/s) / [W/(sqm sr)] per deg Kelvin.

Corrected: A = 1,842,400 + (259.2-259.71) * (-324) = 1,842,565 (DN/s) / [watts/(m^2 sr)]

For completeness we include the AR temperature sensitivity plots for the other two imagers below:

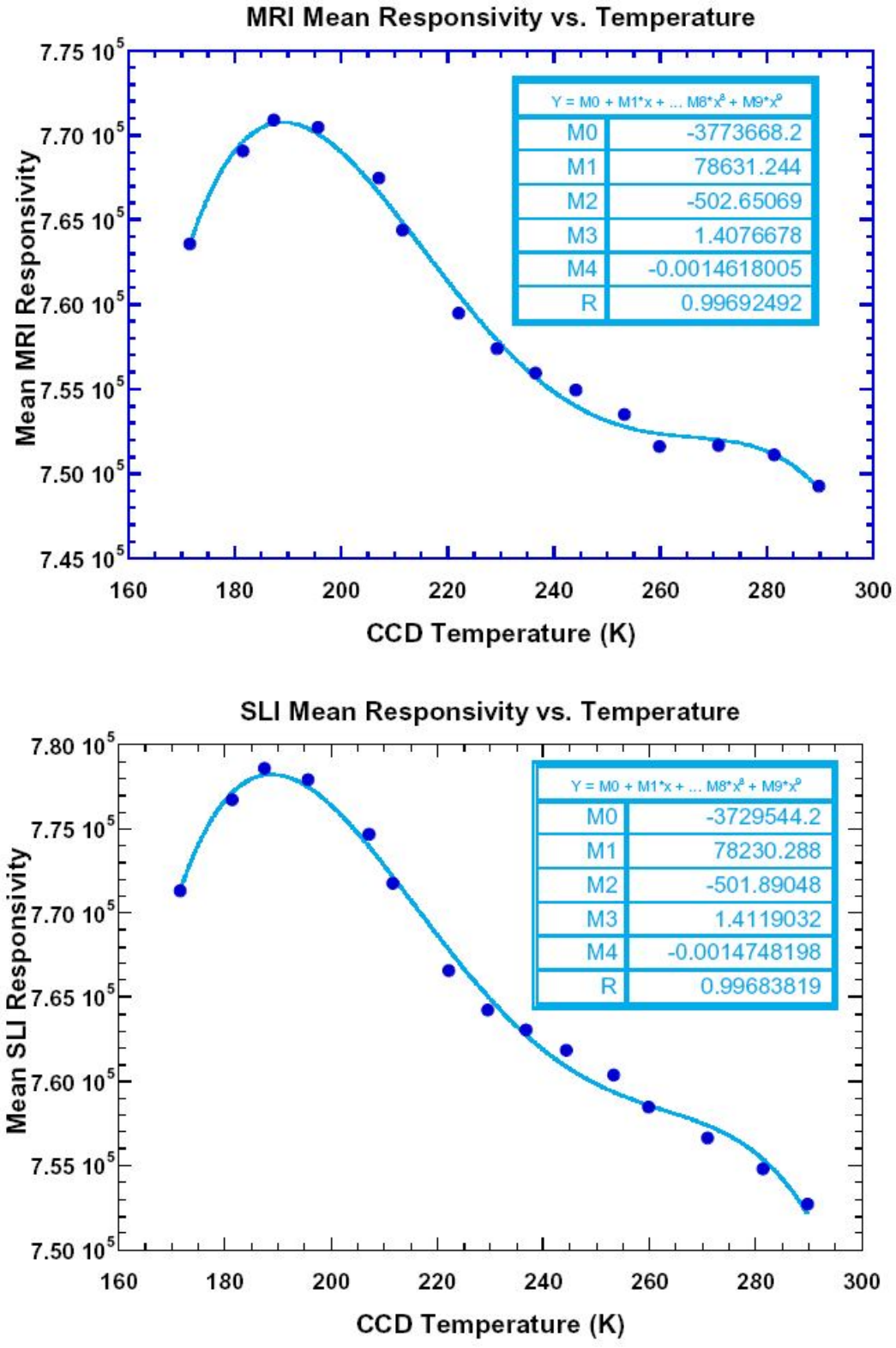

Figure 5.8-11: Temperature model of the absolute responsivity for all good MRI & SLI pixels. Dots are the measurements, and the curve is a fourth-order polynomial fit.

Completing our calculation of the radiance experienced by our example HRI pixel...

$$R = \int I(\lambda)\, RSR(\lambda)\, d\lambda = r / A = 294{,}129 / 1{,}842{,}565 = 0.160 \text{ watts}/(m^2 \text{ sr})$$

Because the DISR imagers are panchromatic, but not imaging spectrometers, it is not possible to exactly determine the spectrum at each pixel. However because we have coordinated downward looking spectrometer observations throughout the descent we can tell something about the albedo variations across the scene. We know that Titan's albedo is dominated by absorption from methane and aerosols, giving its reflectance a distinctive spectral shape. Titan's albedo is also affected by the absorption of its surface, especially for observations at low altitudes, and at wavelengths outside the methane bands toward the near IR. By using DLVS observations in concert with the DISR imager observations it should be possible to constrain the brightness, and possibly even something of the character of Titan's surface.

Below is a plot showing the relative spectral response of the images overlaid with the normalized downward looking flux from the visible spectrometer. The relative amplitude of the peaks at 940 nm, 830 nm & 740 nm (and even some bluer wavelengths) are characteristic of dark and light patches seen in the DISR images.

Relative Spectral Response (RSR)...

The Relative Spectral Response (RSR) is a function of temperature, generally shifting up in wavelength as temperature increases, as can be seen in the figure below.

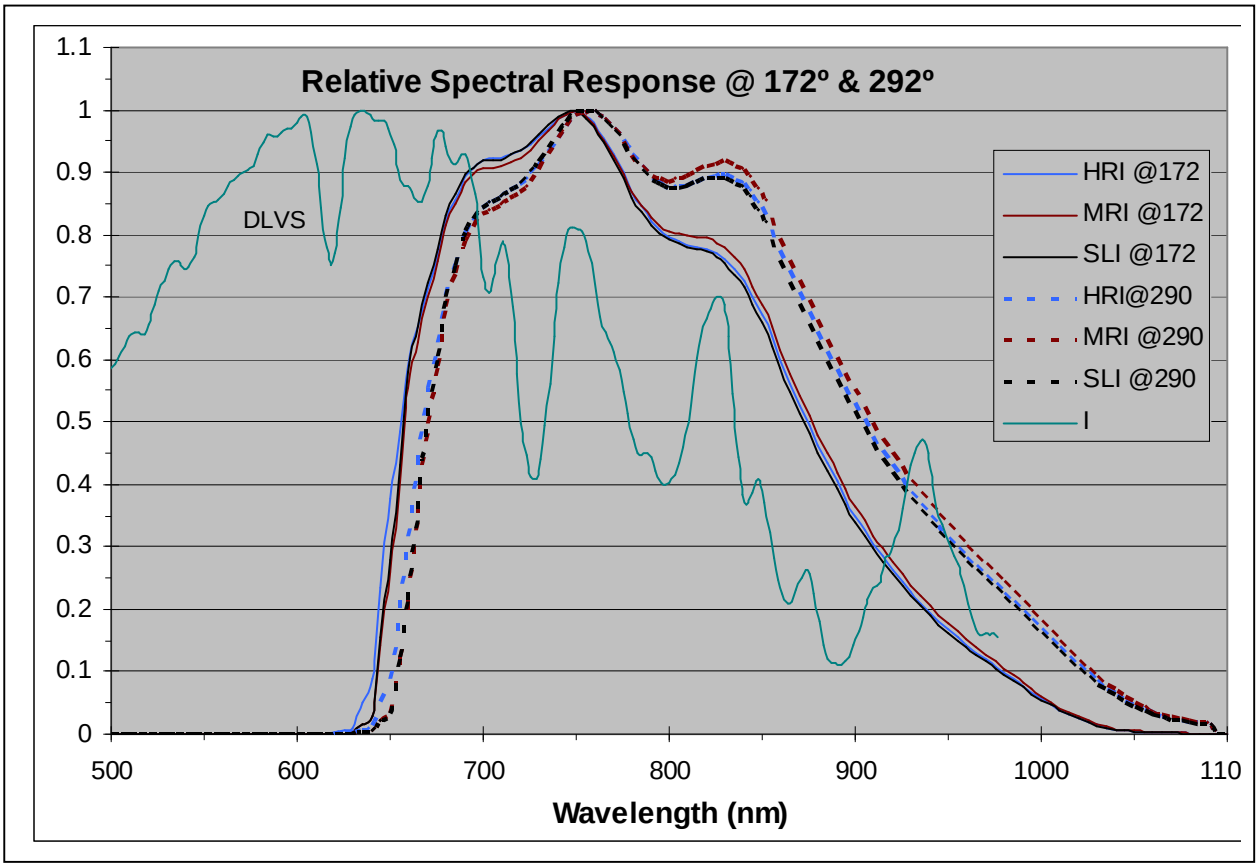

Figure 5.8-12: Pixel average, Relative Spectral Response curves for the 3 DISR imagers at the temperature extremes. The green line is the downward looking intensity at 143 km altitude from the DLVS, normalized to 1.0 at its peak (i.e. divided by 1.555). The dotted lines are the imagers' response at 290°K, and solid lines their response at 172°K (also normalized to 1 at their peak).

There are generally 3 ways to determine the relative spectral response curve for each imager at the temperature of interest.

The most straight-forward way is to interpolate between the RSR tables closest to the temperature of interest. A linear interpolation yields a result that is generally better than 0.5% accurate, however ignores the pixel-to-pixel variations.

A slightly more accurate method is to use the method described in section 4.1.2.2 ("Development of the model at all Temperatures") of the Imager Calibration Document (Reference 6). That method takes advantage of the relative consistency of the RSR between pixels and purports a temperature dependence curve based on a quadratic extrapolation from the RSR curve at 239ºK (which is provide in Appendix 27) as described by the equation and quadratic coefficients shown below. This method also ignores pixel-to-pixel variations.

$$RSR(\lambda,T) = RSR(\lambda,T_0)\left(a + b \cdot T + c \cdot T^2\right)$$

where:

RSR(λ,To) is the Relative Spectral Response Curve at 239ºK (Appendix 27),
a, b & c are the coefficients from the table below, and
T is the CCD temperature of the image observation.

RSR temperature dependence coefficients for quadratic extrapolation from 239ºK (To).

a	b	c
0.769592	5.84289E-04	1.548489E-06

The most accurate way to determine the RSR for an image observation is to use the method outlined in section 4.1.2.3 ("Use of the model (or how to get the RSR for any pixel)") of Reference 6, which preserves the pixel-to-pixel variations. An example of this method is presented in section 4.1.2.4 of Reference 6.

Imager Geometry and Irradiance...

In order to complete the calculation of the Irradiance seen by our sample HRI pixel, we must determine the pixels field of view. The relatively rectangular pixel arrangements of the individual imagers map to a rather non-rectangular fields of view as projected on an azimuth - nadir angle grid as shown in the following figure.

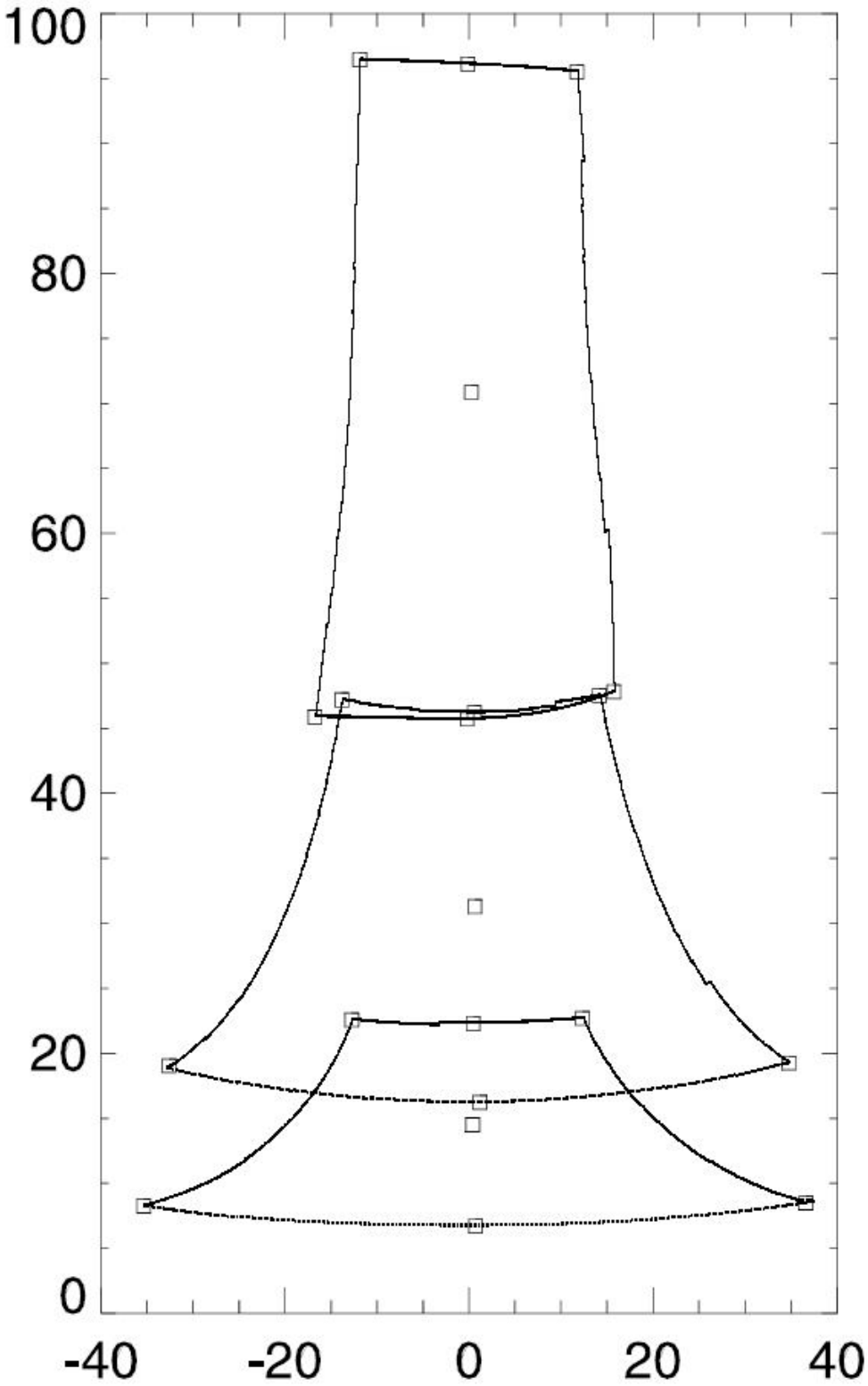

Figure 5.8-13 – Outline of the DISR 3 Field of View in Azimuth (from +Z) and Nadir angle. Corners and centers are indicated by squares.

In general, distortions should be removed from the images before determining the pointing geometry. Section 2.1 through 2.3 of Imager Cal document (Ref 6) describes this procedure ("DISR Image Distortion and Geometry Calibrations").

The imagers' pointing geometry are discussed in section 2.4 ("Geometry Calibration") of the calibration document (Reference 6). The equations presented presume that have been processed by the sharpening software described in section 3 ("Deconvolution of DISR Images") of Reference 6, however using the following row and column conversion equations we can map the DISR archive data into arrays that can be used directly in the equations provided in section 2.4 of Reference 6:

c = 2 * Co, and
r = 2 * (Ro -1)

where,

Co is the column number (starting with column 1) of the pixel of interest,
Ro is the row number (starting with row 1) of the pixel of interest, and
c & r are the column and row numbers corresponding to those of the sharpened images.

Note that there are approximately twice as many rows and columns in the sharpened images and that the top and bottom rows are typically not used because they contain many bad pixels.

The azimuth for a given pixel is described as:

$$\phi = \arctan\left[\frac{\tan\alpha}{\sin\theta o - \tan\beta\cos\theta o}\right]$$, and the nadir angle is given by:

$$N = -\arctan\left[\frac{\sqrt{\tan^2\alpha + (\sin\theta o - \tan\beta\cos\theta o)^2}}{\cos\theta o + \tan\beta\sin\theta o}\right]$$

where α and β are the dihedral angles associated with the pixel columns and rows and θo is the central zenith angle. Here the azimuth angle is defined as degrees clock-wise (CW) from above (to the DISR's right), opposite the header convention. The angles α and β are given by:

$$\alpha = m\left(c - \frac{(n_c + 1)}{2}\right)$$

$$\beta = m\left(r - \frac{(n_r + 1)}{2}\right)$$

where m is the pixel size, n_c and n_r are the number of columns and rows in each image given in the table below and c & r are our converted column and row number described above.

Image Geometry Parameters	MRI	SLI	HRI
m – Size of sharpened pixel (o)	0.06	0.1	0.0308
θo – Nominal Zenith Angle of Central Pixel (o)	148.5	109.4	166
n_c – Number of Columns (sharpened)	353	257	321
n_r – Number of Rows (sharpened)	509	509	509

To determine the field of view of our sample pixel we will average the pixel-to-pixel center spacing of the adjacent pixels:

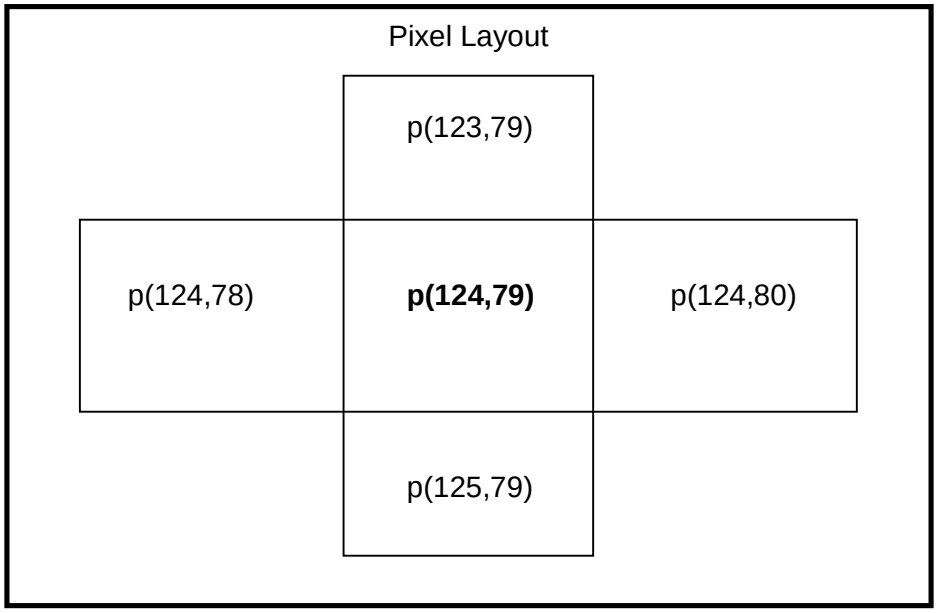

Figure 5.8-14

Coordinates of pixels surrounding target pixel (deg)

Pixel Coordinates			
Row	Column	Azimuth	Nadir
79	123	-0.39	13.66
79	124	-0.39	13.72
79	125	-0.39	13.78
78	124	-0.65	13.72
79	124	-0.39	13.72
80	124	-0.13	13.72

Distances from surrounding pixels to target pixel

Center to Center Distances			
Direction	From	To	Degs
Column	P(123,79)	P(124,79)	0.062
Column	P(124,79)	P(125,79)	0.062
Row	P(124,78)	P(124,79)	0.260
Row	P(124,79)	P(124,80)	0.260

So assuming a roughly rectangular field of view the size of our pixel is:

Pixel FOV = 0.062 x 0.260 = 0.0160 sq degs = 4.874 $x10^{-6}$ sr.

And the measured up flowing Irradiance contribution measured by this pixel is:

$E = \int R(\Omega)\, d\Omega$ = 0.159 watts/(m^2 sr) * 4.874 $x10^{-6}$ sr = 0.777 $x10^{-6}$ W/m^2

Calculating I/F for an imager pixel...

Using the information we have developed for HRI pixel(124,79), we will now calculate I/F for that pixel (where I is the incident flux and F is the solar flux outside Titan's atmosphere). Our method will be to use the DLVS data from a similar altitude (142 km) as our image observation (134 km) to determine the spectral character of the light in the imager band. And, we will assume no azimuthal variation in intensity. A higher fidelity calculation could be obtained by interpolating within DLVS data for these quantities (the proverbial 'left as an exercise for the reader'). Since the pixel-to-pixel variations are small, we will interpolate in the relative spectral response (RSR) tables to temperature compensate, rather than using the H bin factors described in Reference 6.

We have calculated the spectrally integrated radiance for our pixel above as:

$$R = \int I(\lambda)\, RSR(\lambda)\, d\lambda = r / A = 293{,}586 / 1{,}842{,}565 = 0.159 \text{ watts}/(m^2 \text{ sr})$$

We use the DLVS spectrum from the archive in file: DATA/DERIVED_DATA_PRODUCTS/DLVS/DLVS_DDP, and extend it into the near IR using the DLIS data from: DATA/DERIVED_DATA_PRODUCTS/DLIS/DLIS_AV_DDP. The relative spectral response curves are available for CCD temperatures of 253.98ºK and 259.71ºK. We linearly interpolate to 259.2ºK. The plot below shows the downward looking spectral irradiance curves (DLVS & DLIS) in blue, and the relative spectral relative spectral response (RSR) plots at the 3 temperatures in black. Note there is not a great deal of temperature dependence over this range.

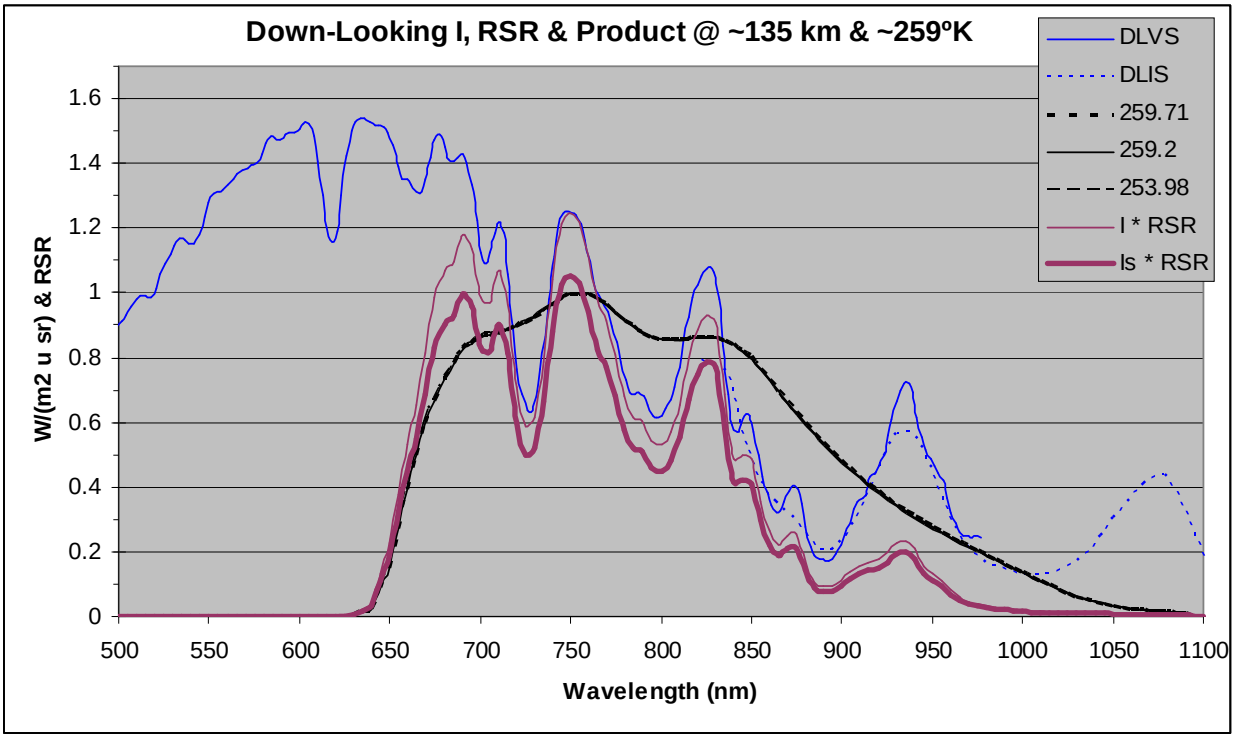

Figure 5.8-15: Over-plots of the downward looking spectral radiance (in W/(m2 u sr)) as measured by the DISR DLVS and DLIS, in blue; The HRI average Relative Spectral Response

(RSR) at 3 temperatures in black; their product (I * RSR) in red, and their product scaled to match the overall measured radiance (0.159 W/m2 u sr) of HRI pixel(124,79), as the heavy red line (Is * RSR).

The radiance calculated using the DISR spectrometer spectral radiance (I) over the RSR of the HRI yields:

$$R = \int I(\lambda)\, RSR(\lambda)\, d\lambda = 0.188 \text{ watts}/(m^2 \text{ sr})$$

$$F = F0 / (\pi * 9.053^2)$$

I/F is calculated for our target pixel by integrating the product of the spectral radiance determined by the downward looking spectrometers (blue lines) and the relative spectral response of the imager (black lines), over the imager pass-band. The resulting spectral radiance (thin red line) is then scaled by the ratio of the result to the HRI measured radiance (0.159 / 0.188), resulting in the heavy red line, which is then divided by the solar radiance (determined by dividing the spectrum in Appendix A (F0) by Pi times the distance from the Sun to Titan squared).

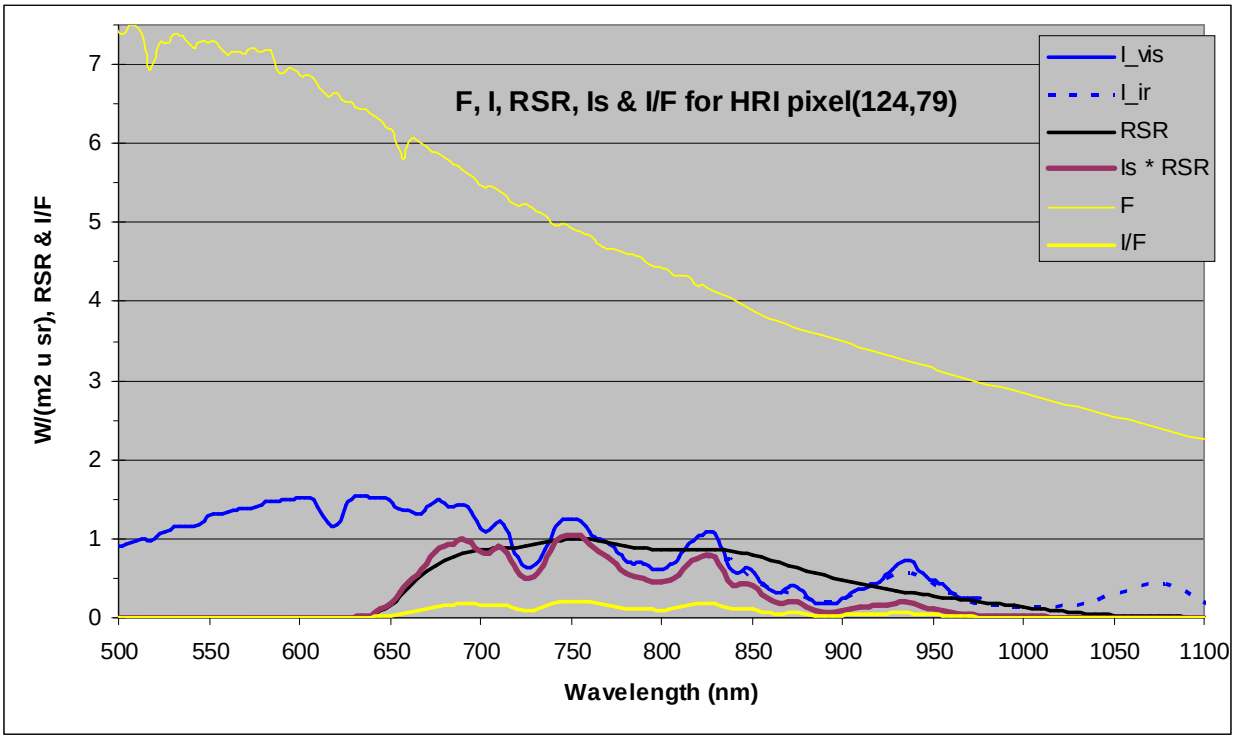

Figure 5.8-16: Plots of Solar spectral radiance at Titan, (F); downward looking radiance spectrum as measured by DISR spectrometers (I) from 142 km altitude; Relative Spectral Response function of HRI pixel(124,79); spectral radiance as measured by this pixel (Is * RSR); and resulting I/F for this pixel.

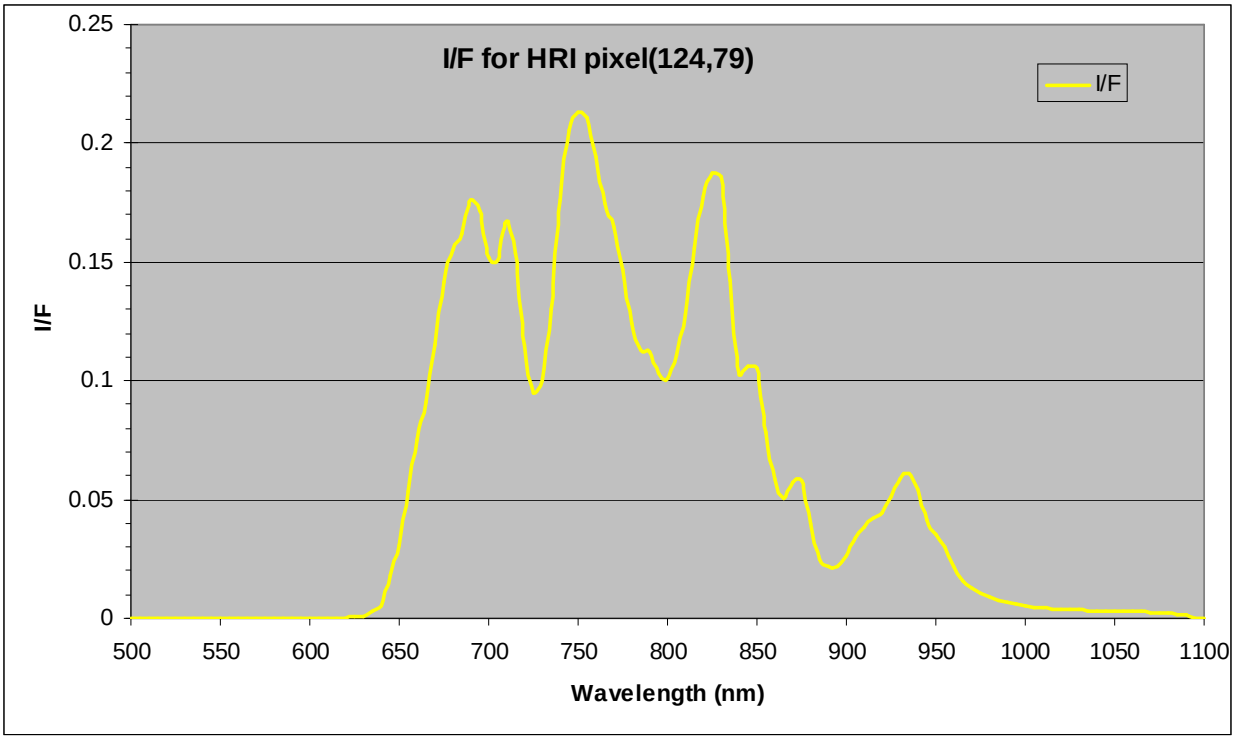

Figure 5.8-17: Expanded view of I/F for HRI pixel(124,79) from 134 km altitude.

Earth to Saturn Cruise Responsivity Effects...

There were very slight changes noted in the responsivity of the Imager systems during the Cruise Phase. Most of the DISR systems displayed a drop in responsivity, typically attributed to yellowing of the fiber optic glass. In the case of the Image systems it appears that the variations in glass transmittance are likely overwhelmed by movement of the fiber-optic bundles during launch. There is a distinctive shift at launch, which appears to produce a gradient pattern. This is likely due to a changed coupling between the calibration lamp and the detector (both of which are conducted via fiber optics). The change since launch has been small, generally less than 1%.

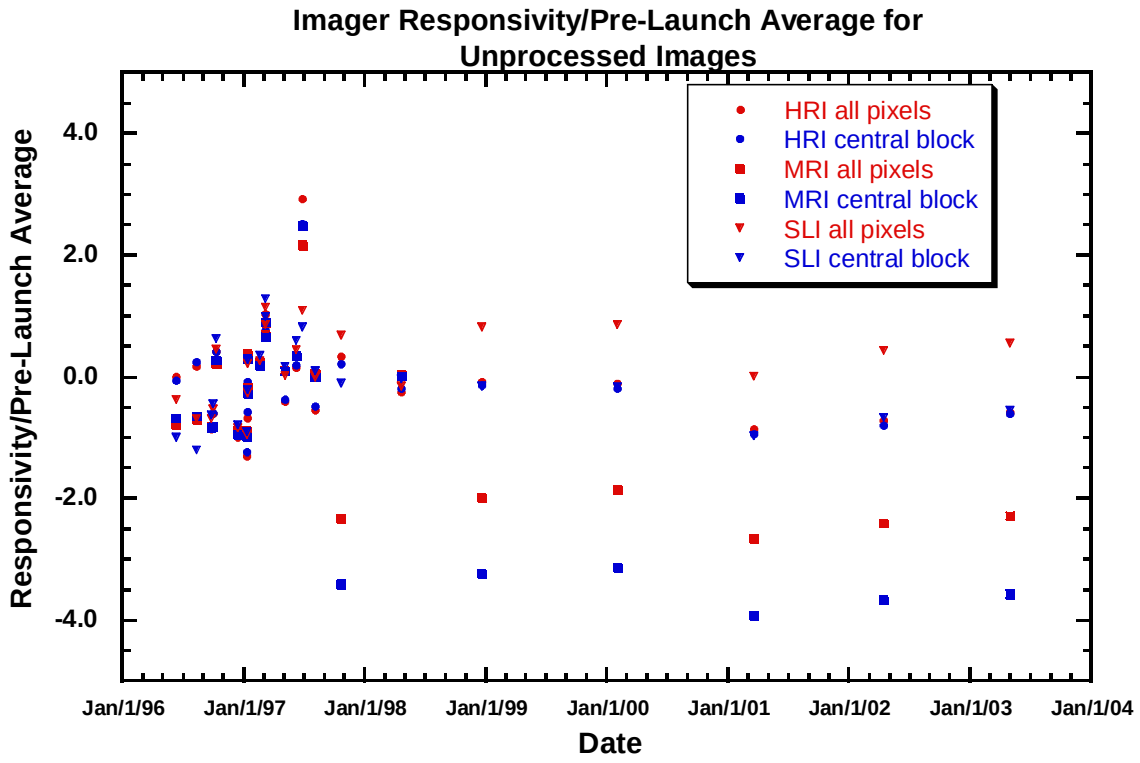

Figure 5.8-18: Imager responsivity variations during Cassini cruse. Two groups are presented for each imager: an average of all pixels and a 64 pixel square central block.

SLI strips...

During the descent 101 Side-Looking Imager strip data sets were acquired. These sets are formed from pixels in the Side-Looking Imager, but they are processed differently from other imager data. Two strips, each 13 columns wide are formed from the pixels in columns 6 - 18 and 109 - 121. For each row on the CCD the 13 columns are summed by the flight software, compressed with lossless techniques and telemetered.

The motivation for these data sets is that they retain the high signal-to-noise-ratio inherent in the image data without using much telemetry volume. The images themselves undergo square-root and compression processing, which reduces their signal-to-noise ratio in exchange for transmitting more images. The Side Looking Imager views the sky looking generally out toward the horizon. This makes the Side-Looking-Imager strips ideal for detecting atmospheric features, such as cloud layers. Generally the signal-to-noise ratio of these data sets exceeds 500 to 1.

Detailed information regarding the SLI strips is available in the archive under:
DOCUMENT/DISR_CALIBRATION_DOCUMENTS/SLI_STRIPS

Note that the strip data set numbers are not corrected for dark current or imager responsivity. Both corrections are important to make full use of the data sets. Many of the data sets are taken at high altitude when the CCD is still warm. The dark current correction can be substantial. The on-board software flat field is also not applied to the data. The data contain the hexagonal patterns introduced by the fiber optic conduit, which feed the image to the CCD.

The dark current may be removed using the standard techniques described in the Dark Data Sets section (5.7). The responsivity may then be applied to remove the effect of the conduit. The result should be photometrically accurate measurements of intensity along strips of the Titan sky from 101 altitudes.

The absolute responsivity is defined as $A = \frac{r}{\int I(\lambda) RSR(\lambda) d\lambda}$, where *r* is the count rate (data numbers/second), I is the intensity at wavelength λ, and RSR is the relative spectral response at wavelength λ. This can also be written as $\bar{I} = \frac{r}{A \int RSR(\lambda) d\lambda}$.

5.9 Solar Aureole (SA) Measurements

Observations from outside Titan's atmosphere show that it both polarizes and forward scatters light. It was therefore deduced that the atmosphere may contain particles with a small dimension (polarizing) and large dimension (forward scattering) such as may small monomers which aggregate into large open polymers. The SA camera was designed to constrain the size and distribution of these particles.

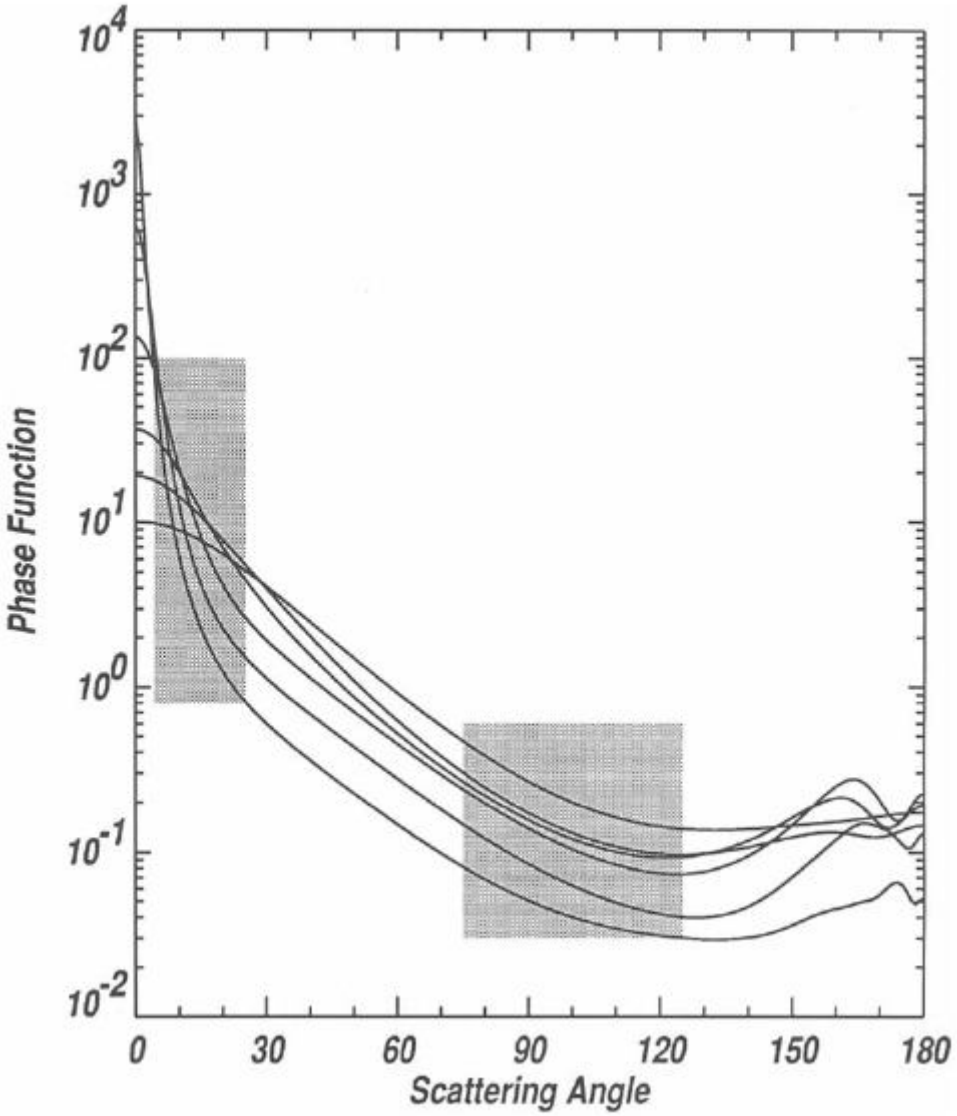

Figure 5.9-1: The SA camera is designed to sample the scattering angle ranges shown in grey. The phase function curves are for particles having 0.063 to 2 micron radii. The smallest particles have the lowest forward-scattering (0º) peak.

The Solar Aureole (SA) camera was designed to obtain Titan sky brightness contours and polarization measurements near and away from the Sun. Unfortunately due to the unexpected reversal in the spin direction of the probe, greater than expected tip-tilt dynamics and

intermittent performance of DISR's Sun sensor, the SA data products were difficult to interpret. Although the data volume was not as anticipated, after developing some understanding of the probe tip and azimuth as a function of time, the SA data proved crucial to constraining the properties of Titan's aerosols. At some altitudes a degree of uncertainty still remains lacking a complete 6 DOF probe dynamics model.

Details of the SA system is available in the DISR archive under: DOCUMENT/DISR_CALIBRATION_DOCUMENTS/SOLAR_AUREOLE (Reference 13).

The SA system is designed to collect vertical sky intensity strips, 6 degrees wide by 50 degrees in zenith at two wavelengths (500 nm & 935 nm) and with two polarizations (horizontal and vertical) totaling 4 cameras. The image scale is about one degree per pixel. A shadow bar was incorporated to block out the direct beam of the Sun. The strips were to be collected 6 degrees away from the Sun, diametrically opposed, at 174 degrees from the Sun. The slits are centered at 50 degrees zenith angle. All 4 cameras are exposed simultaneously.

The measurements through two orthogonal linear polarizers are not sufficient to uniquely determine the position angle and degree of linear polarization for light of an arbitrary state of linear polarization. Rather, we assume that the light in Titan’s atmosphere is partially linearly polarized with the position angle predicted from multiple scattering models (roughly perpendicular to the scattering plane). This is sufficient to determine both the total intensity and the degree of polarization from the measurements. We simply add the horizontal and vertical components of intensity near the Sun to obtain the total intensity as a function of azimuth relative to the Sun and zenith angle.

The following table summarizes the characteristics of the 4 SA cameras. The "Full data set columns" refers to the position of the individual cameras on the DISR CCD chip (see section 5.8). 'Blue' designates the 500 nm filters and 'red' the 935 nm filters. 'Parallel' & 'Perpendicular' refer to the orientation relative to the shadow bar.

SA data set columns	0:5	6:11	12:17	18:23
Full data set columns	40:45	31:36	23:28	14:19
Filter	Blue	Blue	Red	Red
Polarization	Horizontal	Vertical	Vertical	Horizontal
Designation sometimes used	Blue Perpendicular	Blue Parallel	Red Parallel	Red Perpendicular

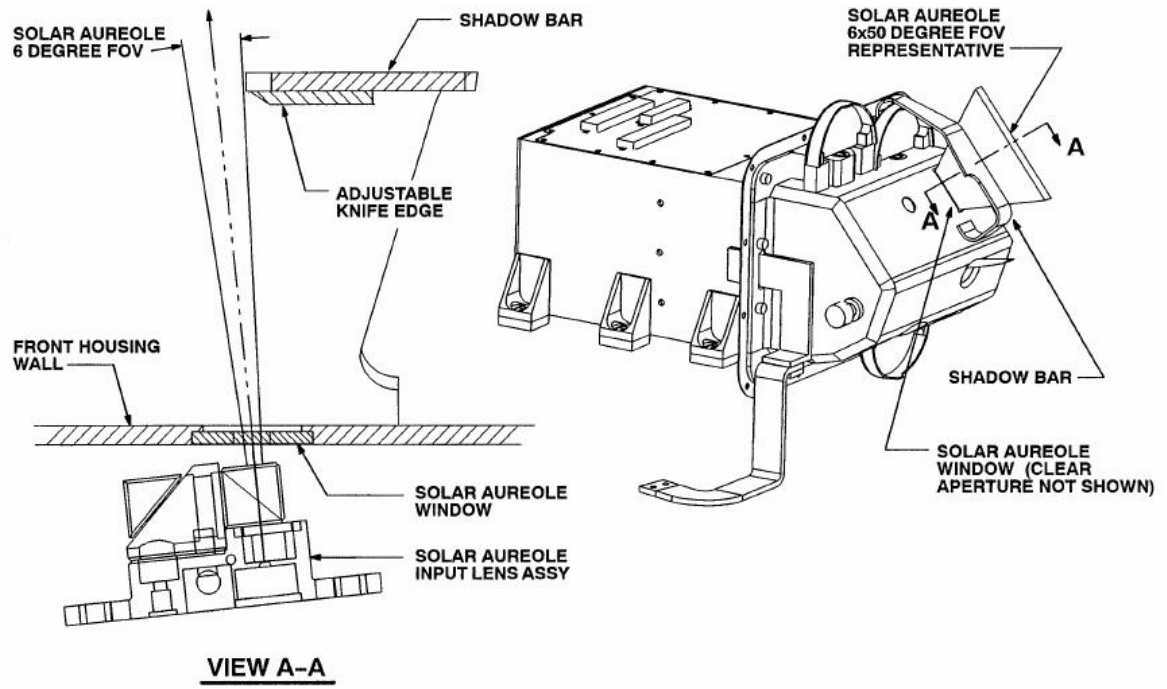

Figure 5.9-2: Layout and Field of View of the DISR SA cameras.

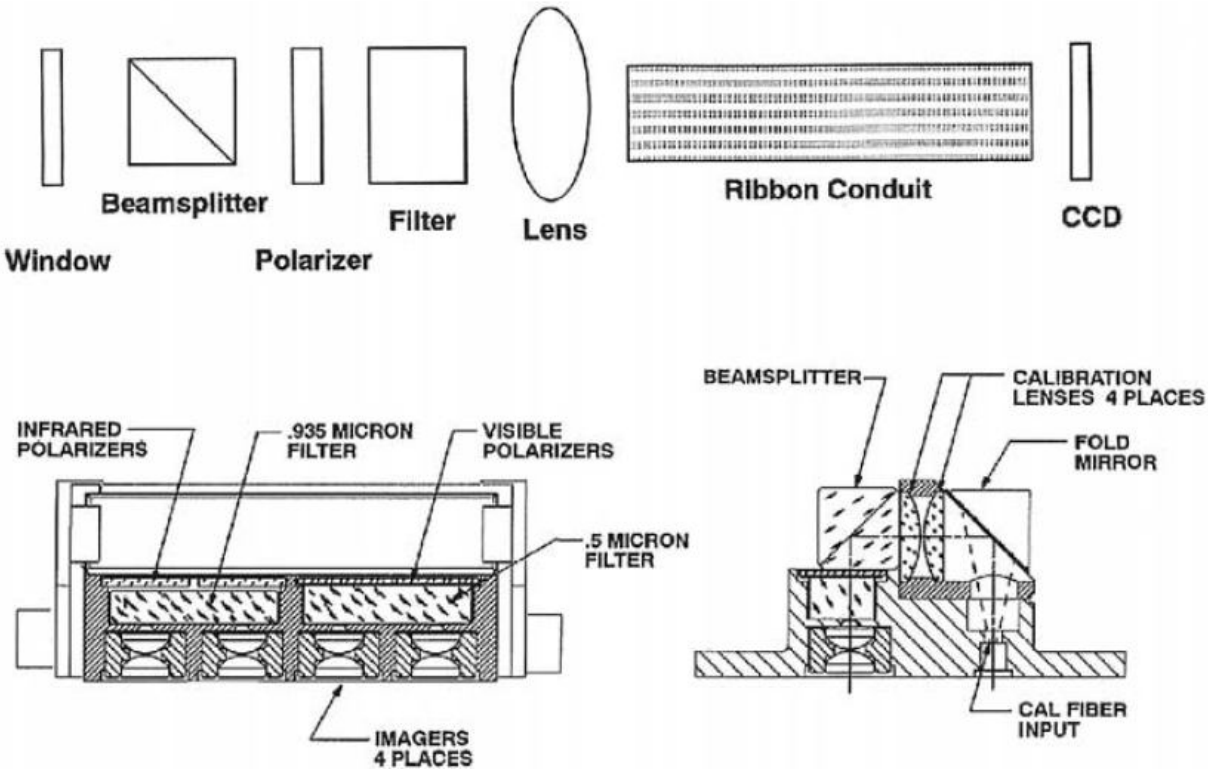

Figure 5.9-3: Schematic layout of the components of the SA system. The beam-splitter is used to introduce light into the cameras from the in-flight calibration lamps.

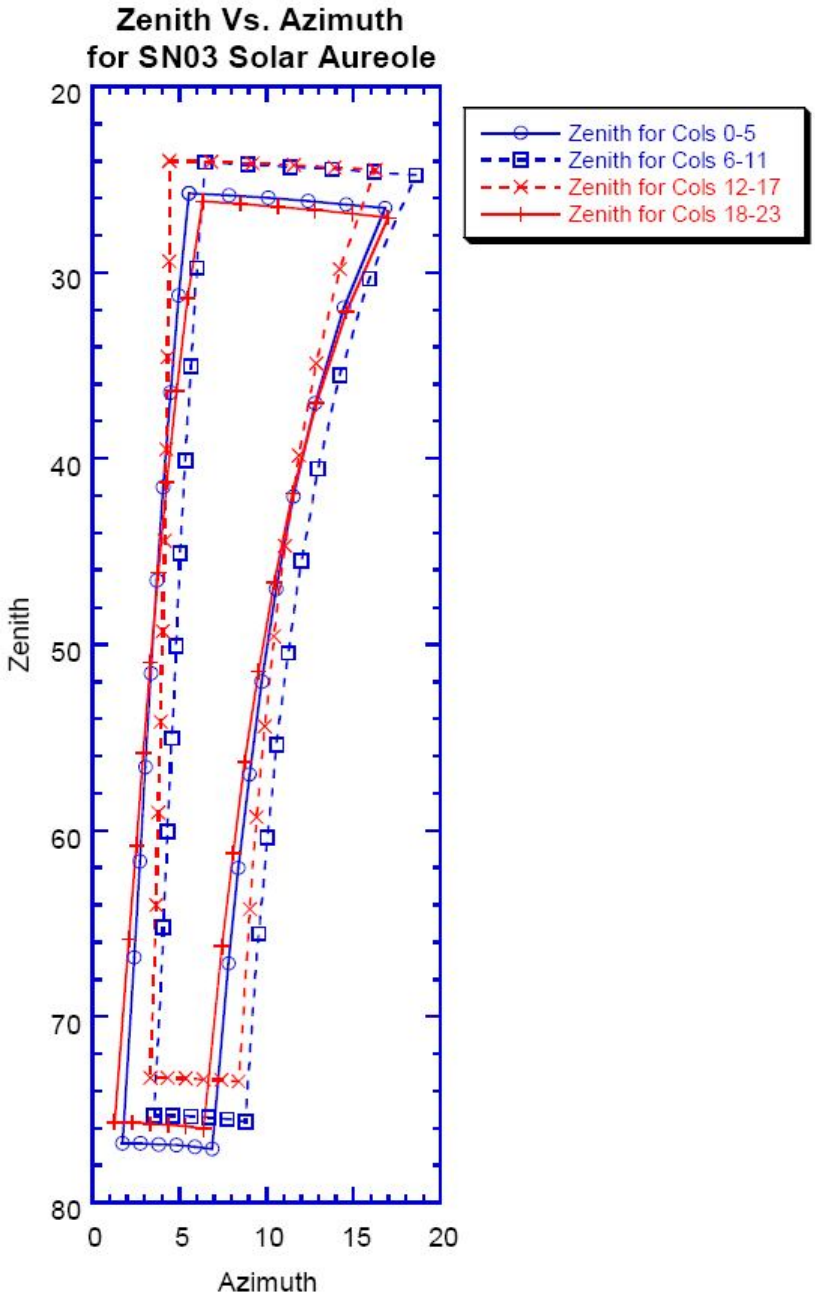

Figure 5.9-4: Location of the SA camera FOVs with respect to probe azimuth and zenith angle.

The Azimuth and Zenith angles corresponding to each Solar Aureole Camera pixel is presented in Appendix 33.

Solar Aureole Datasets...

The Solar Aureole (SA) datasets are located in the DISR PDS archive under: DATA/SOLAR.

There are two types of data in the archive: summed and un-summed. The summed data consists of 5 columns, one as the 'row' index, and the other 4 as column sums of the Blue-Horizontal, Blue-Vertical, Red-Vertical and Red-Horizontal channels respectively.

The un-summed data consists of 25 columns of data (by 50 rows). Column #1 is the row index. Columns #2 through #25 are the 24 columns of raw data in the same order as the summed data (BH, BV, RV, RH).

The following table provides file type discriminators for the SA archive data:

Dataset Type	RECORD_BYTES	File Size (KB)
Summed	24	2
Un-summed	174	9

A summary of the SA data collected at Titan is presented in Appendix 34.

Solar Aureole Camera Photometry...

The response of the SA camera can be expressed as:

Equation 5.9-1:

$$DN = t_i * Abs\_Resp(T) \iint I(\lambda, \theta, \phi, altitude) RSR(\lambda, T) d\lambda d\Omega + DN_{dark}(T, t_i) + Noise(T, t_i, DN_{nom})$$

where

DN is the response from the instrument in data numbers,
t_i is the integration time of the observation,
Abs_Resp is the Absolute Responsivity of the SA as a function of CCD temperature,
I is the spectral radiance,
RSR is the Relative Spectral Response of the SA channel,
λ is the wavelength,
Ω is the solid angle,
T is the CCD temperature (aka Tccd),
DNdark are the counts due to CCD dark current, and
Noise is the CCD noise in DN.

As described in section 4.2 ("Computing Solar Aureole Calibrated Intensities in Each Pixel") of the SA calibration document (Ref 13). The equation above can be re-written to calculate the spectral radiance at wavelength λ_0 (and accommodate the calibration data) as:

Equation 5.9-2:

$$I_w = (DN - DN_{dark} \pm DN_{noise}) / (t_i * AR_{mean} * AR_{pix} * \int I_s * RSR_f * RSR_{nfm} * Bump\ d\lambda)$$

where

I_w is the spectral radiance [W/(m²-u-sr)] at the wavelength of interest (λ_0),
DN is the observed data number by the SA camera in the pixel of interest,
DN_{dark} is the CCD dark current for the observation as described in section 5.7,
DN_{noise} is the variation in SA signal due to noise as described below,

t_i is the exposure time of the observation (in seconds).
AR_{mean} is the mean absolute response (a function of Tccd) in (DN/sec) / [w/(m2 u sr)],
AR_{pix} is the per-pixel modifier to the mean absolute responsivity for each SA camera,
I_s is the normalized spectral shape function, which evaluates to 1 at λ_0
RSR_f is the Relative Spectral Response of the SA channel's filter,
RSR_{nfm} is the Relative Spectral Response of the rest, the 'non-filter model',
Bump is the bump in the CCD quantum efficiency in the red SA channels, and
λ is the wavelength (in microns).
The calibration parameters are evaluated at the observation temperature, T.

I_s (aka I_shape) is the spectral shape of the spectral radiance (unitless and normalized to 1.0 by definition) at the specified altitude in the Titan atmosphere. It is determined by dividing the Titan model by the intensity at that wavelength as in equation 5.9-2. It is important to note that the computation of calibrated intensities at a specific wavelength is an iterative process. The I_shape is model dependent, so a proposed model must be introduced that creates an I_shape that then must result in correct SA intensity predictions. This I_shape must be consistent with the polarizing affects of both Titan's atmosphere and the SA instrument as noted in section 4.3 ("Combining Intensities...") of the calibration document (Reference 13). A good start is the spectral shape as determined by the upward looking spectrometers at the altitude of interest.

Noise and Uncertainties...

The SA noise is given by:

DN_{noise} = Read noise + Quantization Noise + Shot Noise = 0.57 + 0.29 + sqrt(DN*30)/30 DN

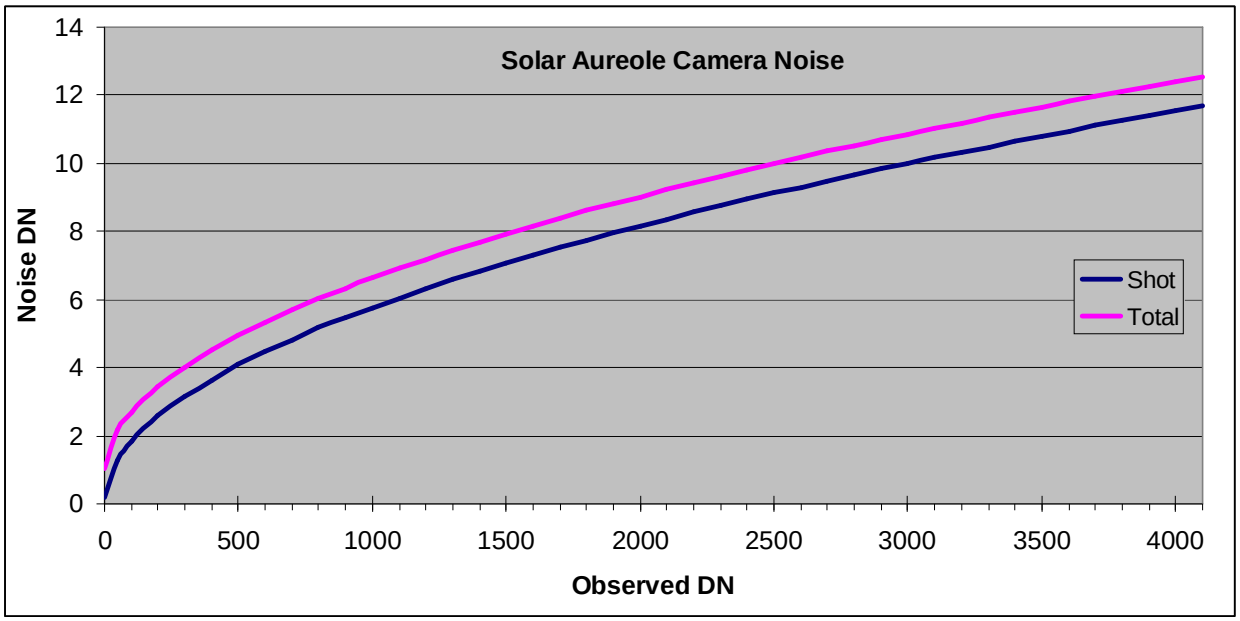

Figure 5.9.5 - Solar Aureole Camera noise as a function of observed data number.

Beyond the noise there are uncertainties due to impurity of the calibration fit. They are discussed in section 13 ("Appendices") of the calibration document (Reference 13) and summarized in the table below:

Type of Data	Relative Calibration Along:	Accuracy
Summed Blue	Column	1%
Summed Red	Column	1%
Un-summed Blue	Column 2	Within noise
Un-summed Red	Column 2	Much within noise, some within 1%, all within 2%
Un-summed Red	Column 0	Within 3%
Un-summed Blue	Row 23	Most within 1%, some within 2%
Un-summed Blue	Row 48	Most within 1%, some within 2%
Un-summed Red	Row 23	1%
Un-summed Red	Row 48	2%

There are a number of instrumental effects that complicate the SA measurements. These include changes in the optical parameters with temperature and the discovery of optical retardance in the system. Fortunately all of these effects were properly calibrated before launch. The polarization can be retrieved from the SA data, and the polarization and intensity can be successively compared to the predictions of radiative transfer models which include a 3x3 Stokes matrix. The methods are described and the data are compared to models in Tomasko, et al., Reference 12.

Absolute Responsivity...

The average absolute responsivity varies significantly with temperature for all the SA channels. The blue and red channel variations have different character as can be seen in the plot below, suggesting that the effect is coupled to the input optics, however the model was developed relative to the CCD chip temperature, which should be used in these equations. Details are in section 10 ("Absolute Response") of the calibration document (Reference 13).

The channel mean Absolute Responsivity is given by:

$$AR_{mean} = A0 + A1*T + A2*T^2 + A3*T^3 + A4*T^4 + A5*T^5 + A6*T^6 \quad \text{(eq. 5.9-3)}$$

where

T is the CCD temperature at the time of observation, and
A is from the table below:

	Blue Horizontal	Blue Vertical	Red Horizontal	Red Vertical
A0	-1.320628900000E+08	-1.043157230000E+08	-6.342293175000E+07	-4.764707846875E+07
A1	3.439118281250E+06	2.708450062500E+06	1.392982078125E+06	1.053106603516E+06
A2	-3.693190771484E+04	-2.898806738281E+04	-1.200406482697E+04	-9.126064826965E+03
A3	2.100620784760E+02	1.643101100922E+02	5.120302107930E+01	3.914550912380E+01
A4	-6.678061112761E-01	-5.205441340804E-01	-1.080477217911E-01	-8.309265802382E-02
A5	1.125490496634E-03	8.742839563638E-04	9.032962566380E-05	6.989951356218E-05
A6	-7.858712436359E-07	-6.084150783181E-07	0.000000000000E+00	0.000000000000E+00

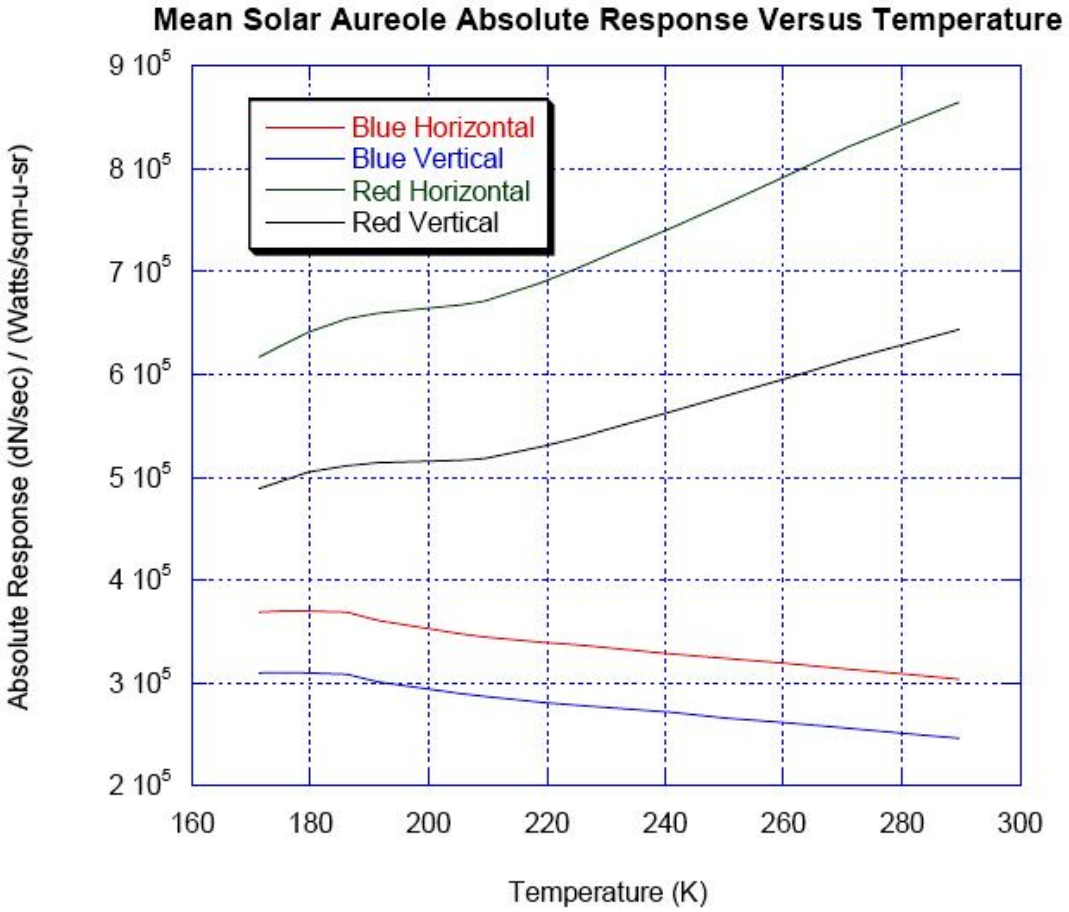

Figure 5.9-6: Mean absolute response for each SA camera vs. CCD temperature.

Each SA pixel varies from the camera mean, of course. To determine the actual Absolute Responsivity for a particular pixel it is necessary to multiply its mean value by its 'Map' value which is determined from this polynomial:

$$AR_{pix} = M0 + M1*T + M2*T^2 + M3*T^3 \qquad \text{(eq. 5.9-4)}$$

where

AR_{pix} is the per-pixel scaling factor for pixel(row, column),
T is the CCD temperature at the time of the observation, and
M is the coefficient from the tables in Appendix 32 for the row & column of interest.

Relative Spectral Response...

The plots below show the Relative Spectral Response for each of the SA channels:

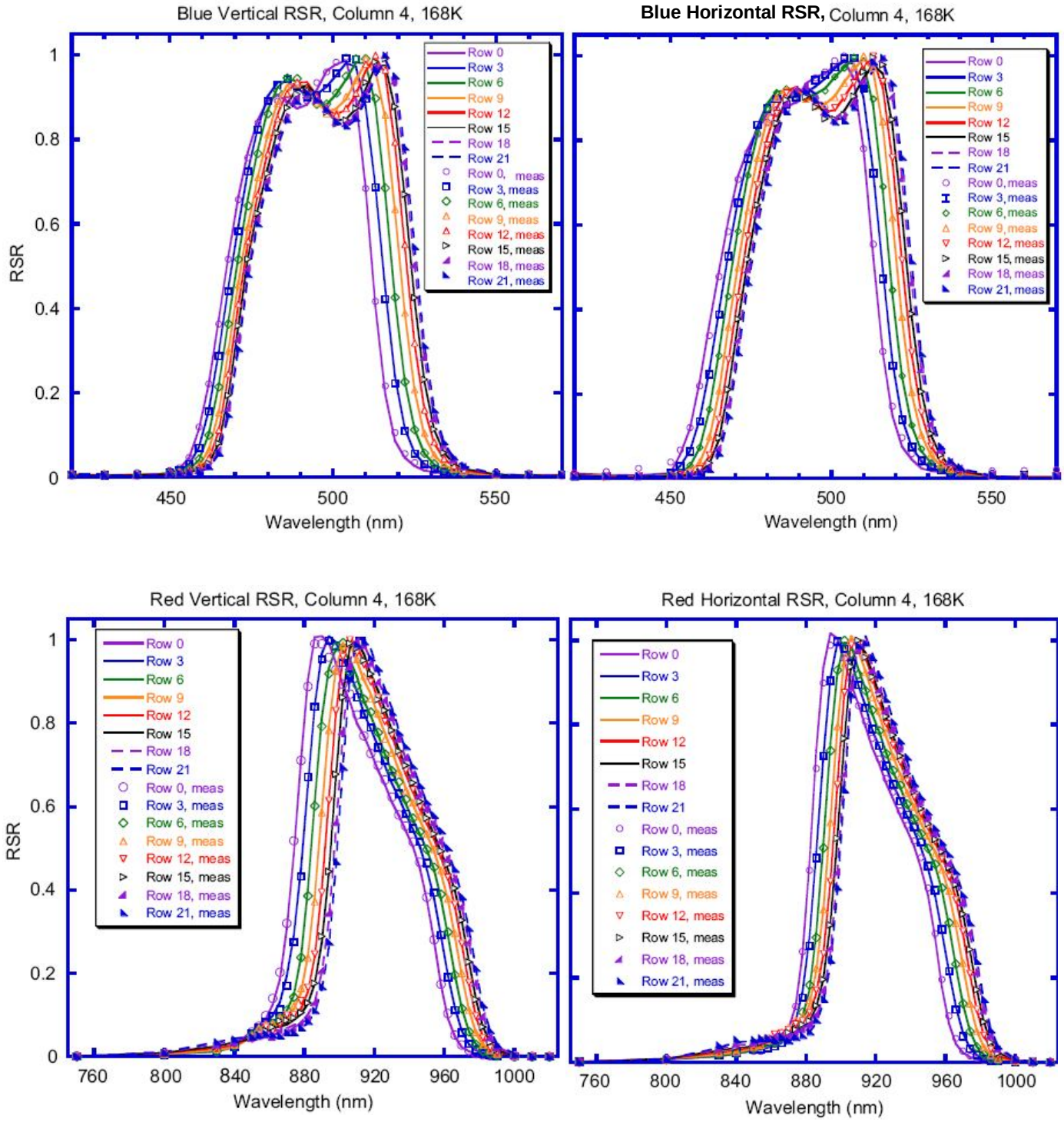

Figure 5.9-7 – Relative Spectral Response Plots for the SA channels.

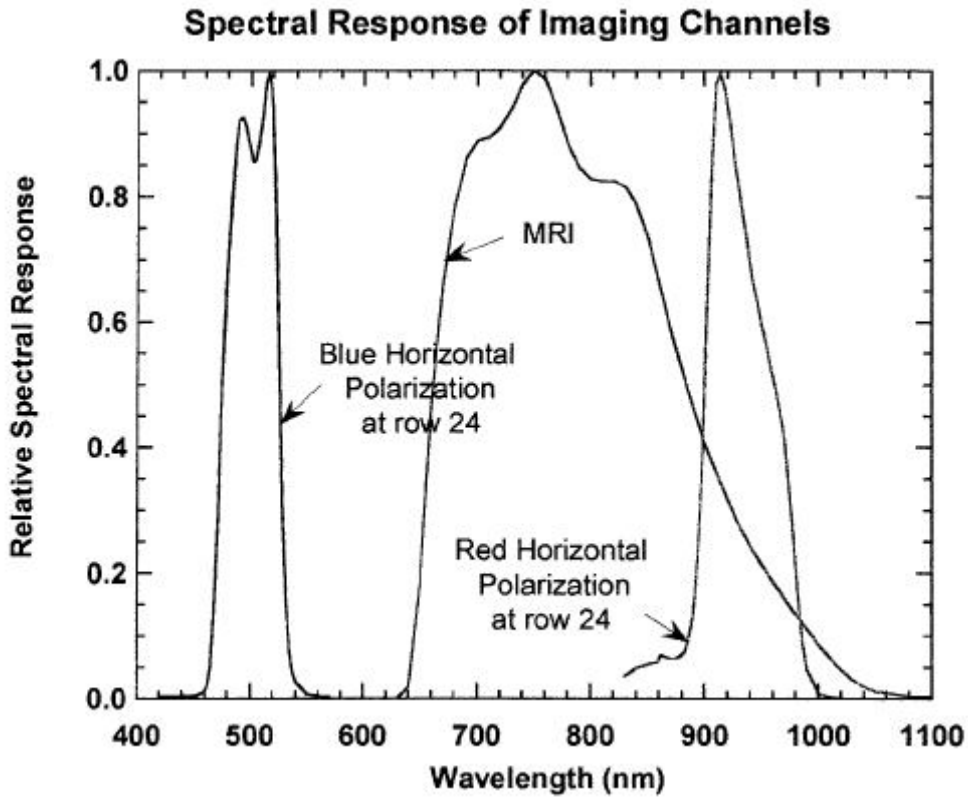

Figure 5.9-8: Comparison of the RSR for the SA cameras with that of the Medium Resolution Imager on the DISR.

As with the SA's Absolute Responsivity, the Relative Spectral Response of the cameras is the product of two terms, a filter term, and non-filter model term:

$$RSR_{SA} = RSR_f * RSR_{nfm} \qquad \text{(eq. 5.9-5)}$$

RSR_f is the Relative Spectral Response component from the narrow band-pass interference filters on each system. RSR_f is normalized to 1.0 at its peak, and is considered temperature independent (as temperature is compensated for in the nfm term). RSR_f is found by interpolating in the tables in Appendix 31 for the row and column of interest. Note that most columns within a specific channel (i.e. blue-vertical) have the same curve, with a few exceptions (Red-Vertical, column 0 and Red-Horizontal columns 0 & 1), which have their own tables in Appendix 31.

RSR_{nfm} is dependent on both SA column number and temperature (and, of course wavelength), and has the form:

$$RSR_{nfm} = (M0 + M1*\lambda + M2*\lambda^2 + M3\lambda^3) + (224.7-T)*(a + b*\lambda + c*\lambda^2 + d*\lambda^3) \quad \text{(eq. 5.9-6)}$$

where

T is the CCD temperature at the time of the observation,
λ is the wavelength of interest,
M are the map coefficients from Appendix 33 (different than the AbsResp M's!!), and
a thru d are the coefficients from the table below.

Table: SA RSR temperature coefficients.

Channel	Polar	a	b	c	d
Blue	Hor	2.05192050E+00	-1.21127860E-02	2.38543920E-05	-1.56729180E-08
Blue	Ver	2.67177940E+00	-1.59196380E-02	3.16325900E-05	-2.09609370E-08
Red	Hor	4.16278530E+00	-1.33554800E-02	1.43166060E-05	-5.12789290E-09
Red	Ver	4.66941200E-01	-1.46212600E-03	1.56549540E-06	-5.73364770E-10
Red	Hor_0	5.28510430E+00	-1.68045650E-02	1.78443640E-05	-6.32867930E-09
Red	Hor_1	4.94097690E+00	-1.58300100E-02	1.69381230E-05	-6.05314650E-09

The bump...

A known bump in the CCD quantum efficiency can be seen in the red SA RSR, so it is modeled empirically in the initial NFM as a lorentzian function with a center wavelength of 854 nm, a full-width at half maximum response of 15 nm, and a peak amplitude of 0.4, as follows:

Equation 5.9-7:

$$Bump(\lambda) = 1 + \frac{0.4}{1 + \left(2 * \frac{(854 - \lambda)}{15}\right)^2}$$

The coefficients of the initial NFM quadratic fit of the quantum efficiency roll-off for the red horizontal and vertical channels are as follows.

Table: Bump Coeff's for Red SA channels

	Horizontal	Vertical
nfm0	6.790040E+01	2.531123E+01
nfm1	-1.337283E-01	-4.310580E-02
nfm2	6.615752E-05	1.800659E-05

So the bump term becomes:

$$Bump = Bump'(\lambda) * (nfm0 + nmf1*\lambda + nmf2*\lambda^2) \quad \text{(eq. 5.9-8)}$$

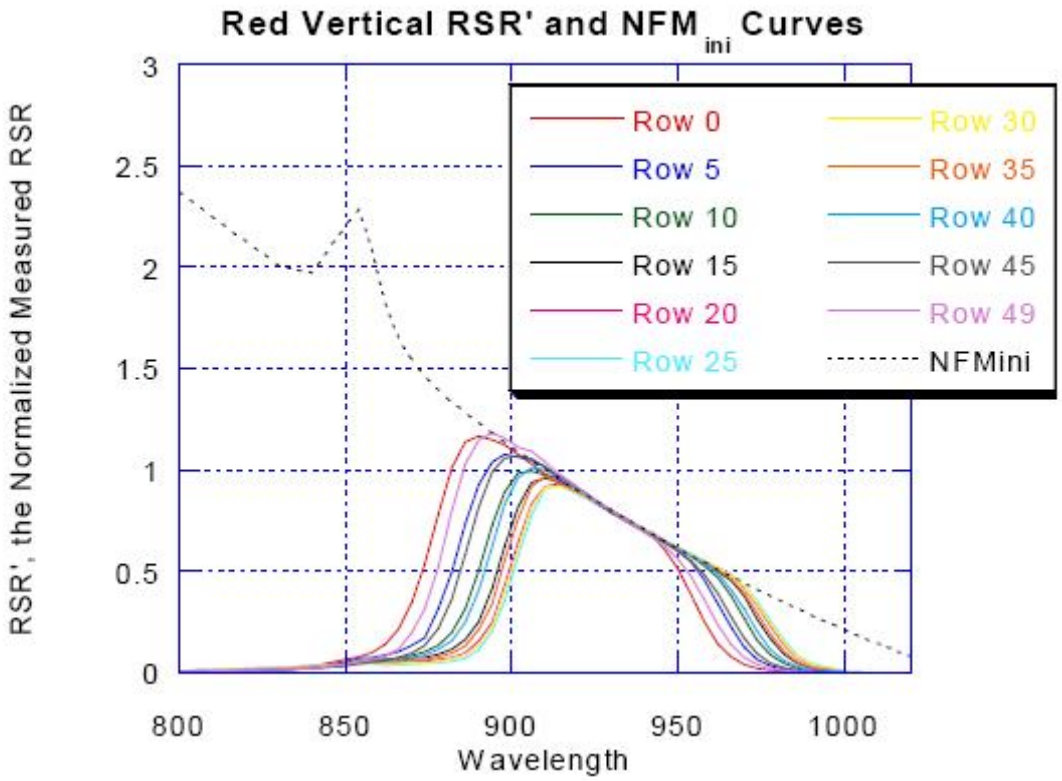

Figure 5.9-9: Red-Vertical SA channel including Bump & Non-Filter Model.

Cassini Cruise Phase Effects...

As discussed in section 5.6, many of the DISR detector systems exhibited changes in the absolute responsivity during the trip from Earth to Titan. The dark current effects are discussed in section 5.7. The observed changes in the Solar Aureole Camera system are small, and may be a combination of yellowing of the fiber optic bundles, and/or movement of the fibers during launch. The observations are presented below.

The changes in the SA system are varied, but generally less than 5%. They are likely due to a combination of movement of the fiber-optic strands that conduct light from the calibration bulbs to the detector (as seen in the imagers) and yellowing of the fiber optic glass (as seen in the violet photometers). The calibration lamp fibers are thin and flexible. Their movement would not indicate a change in the responsivity of the cameras. The situation is complicated by the fact that for many cruise exposures only one of the three calibration lamps (B) was used (to extend the life of the others). It is left to the reader to decide how to use this information, but generally the stability of absolute responsivity of the DISR CCD instruments has been better than about 1%.

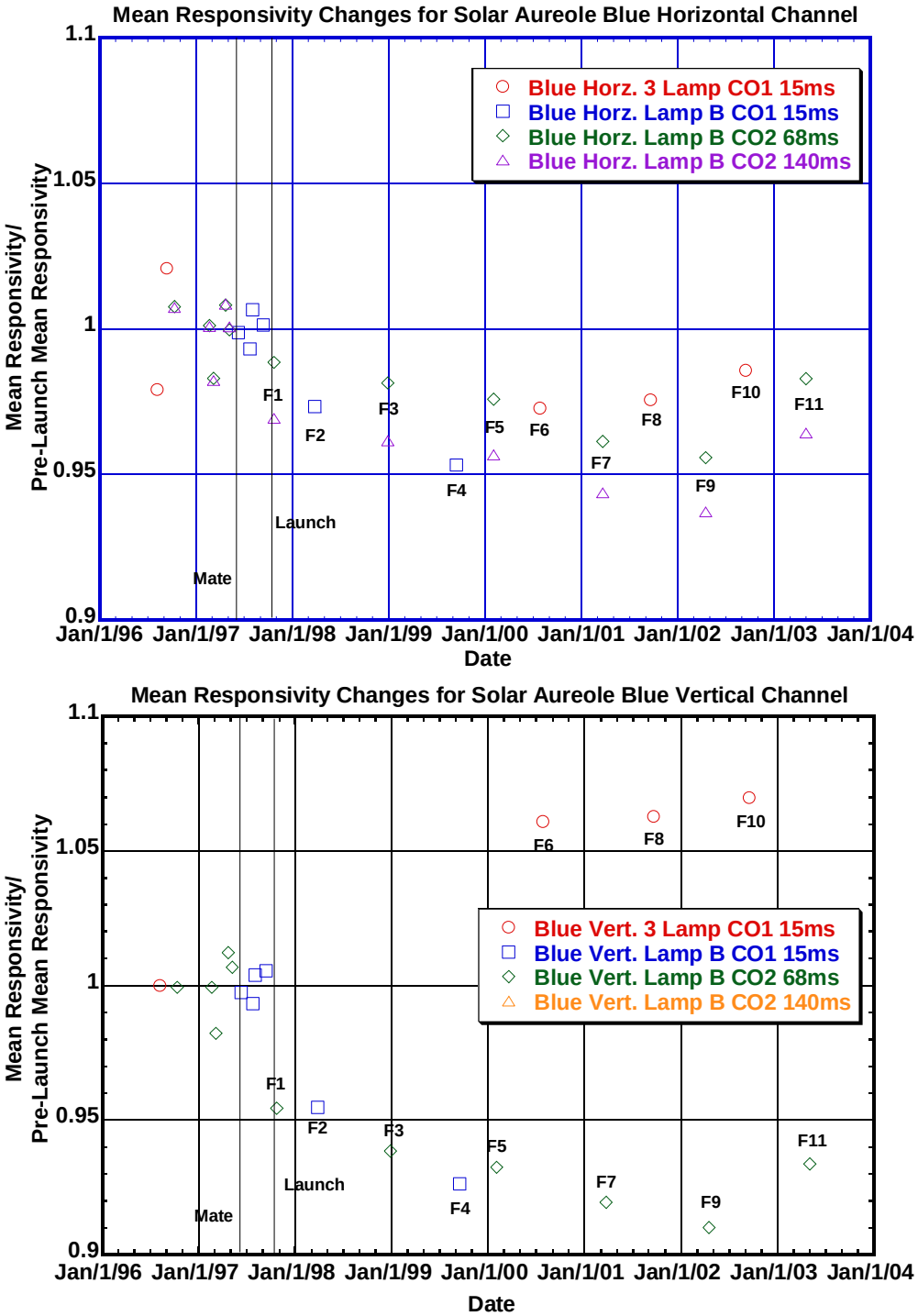

Figure 5.9-11: Absolute Responsivity history of the Blue Solar Aureole Camera channels for the cruise phase to Saturn, normalized to the pre-launch average. Horizontal on top, Vertical on bottom.

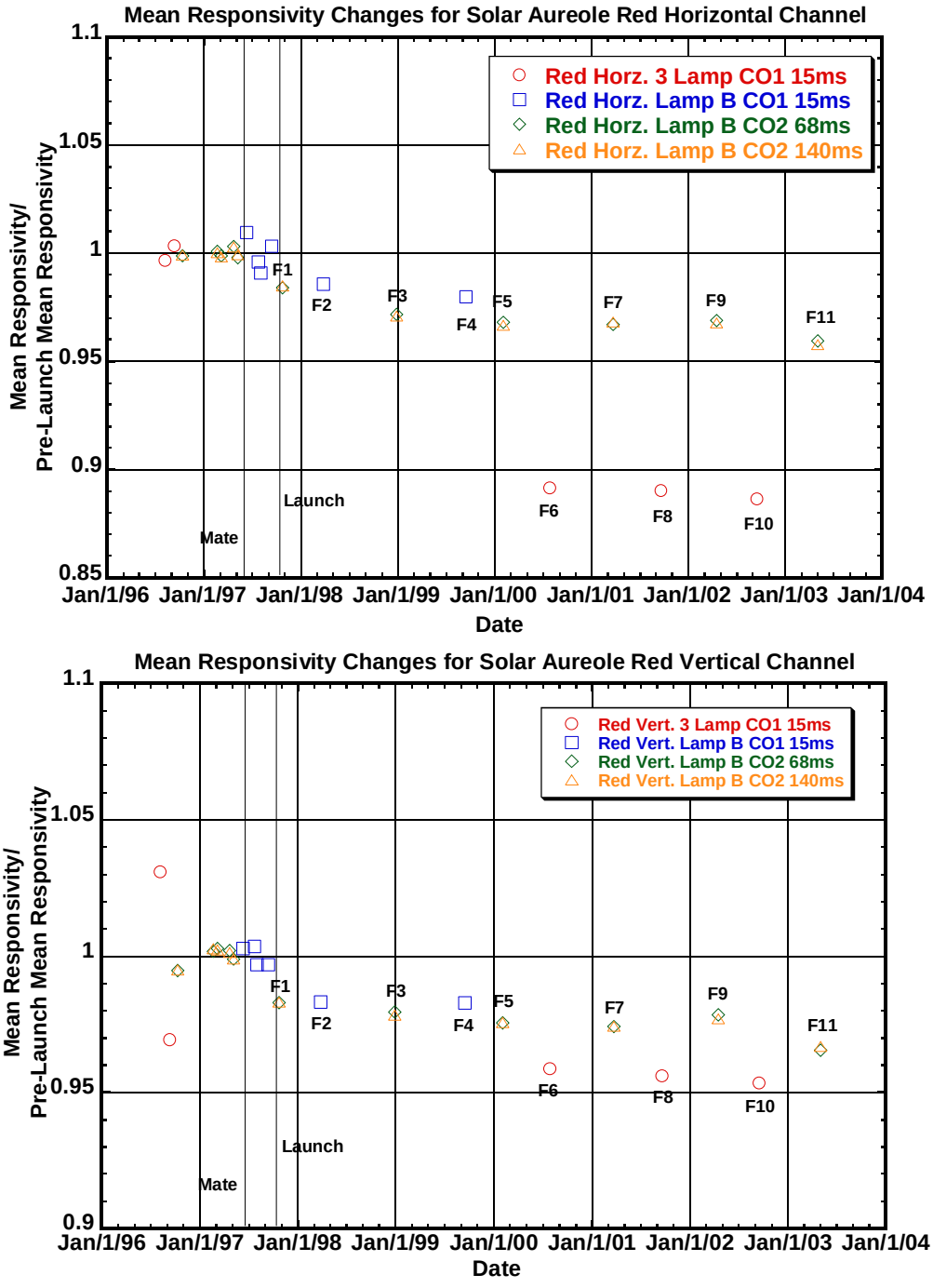

Figure 5.9-12: Absolute Responsivity history of the Red Solar Aureole Camera channels for the cruise phase to Saturn, normalized to the pre-launch average. Horizontal on top, Vertical on bottom.

5.10 Visible Wavelengths Spectra

The DISR contains two visible wavelength spectrometers (actually near IR also, from 480 to 960 nm). One spectrometer looks up and is aptly named the Upward Looking Visible Spectrometer (ULVS) and the other looks down and as you might expect is called the Downward Looking Visible Spectrometer (DLVS). The ULVS views about ½ the sky (π/2 sr) using the same window as the ULV (see section 5.6.1), and thus has the same view obscurations of the DISR shadow bar (see section 5.6.3) and baffles. To decrease noise and increase bandwidth the 8 columns are summed into two columns (i.e. 4 columns each), which are transmitted (x 200 spectral rows).

The DLVS is in essence an imaging spectrometer, with 20 pixels of linear spatial resolution oriented vertically (10º to 50º Nadir angle), and about 4 degrees wide. The FOV is asymmetric and results in the Zenith-Azimuth map shown below. The data is transmitted in one of 4 modes: 20 columns (raw), 10 columns (summed by 2's), 5 columns (x4s), or 'near-surface', which provides two special, SSL illuminated columns (summed by 2's). As with the ULVS there are 200 spectral resolution pixels.

Details of the Visible spectrometers are available in the archive under:
DOCUMENT/DISR_CALIBRATION_DOCUMENTS/VISIBLE_SPECTROMETERS
One would be well advised to also review Reference 15 (Karkoschka) for calibration updates.

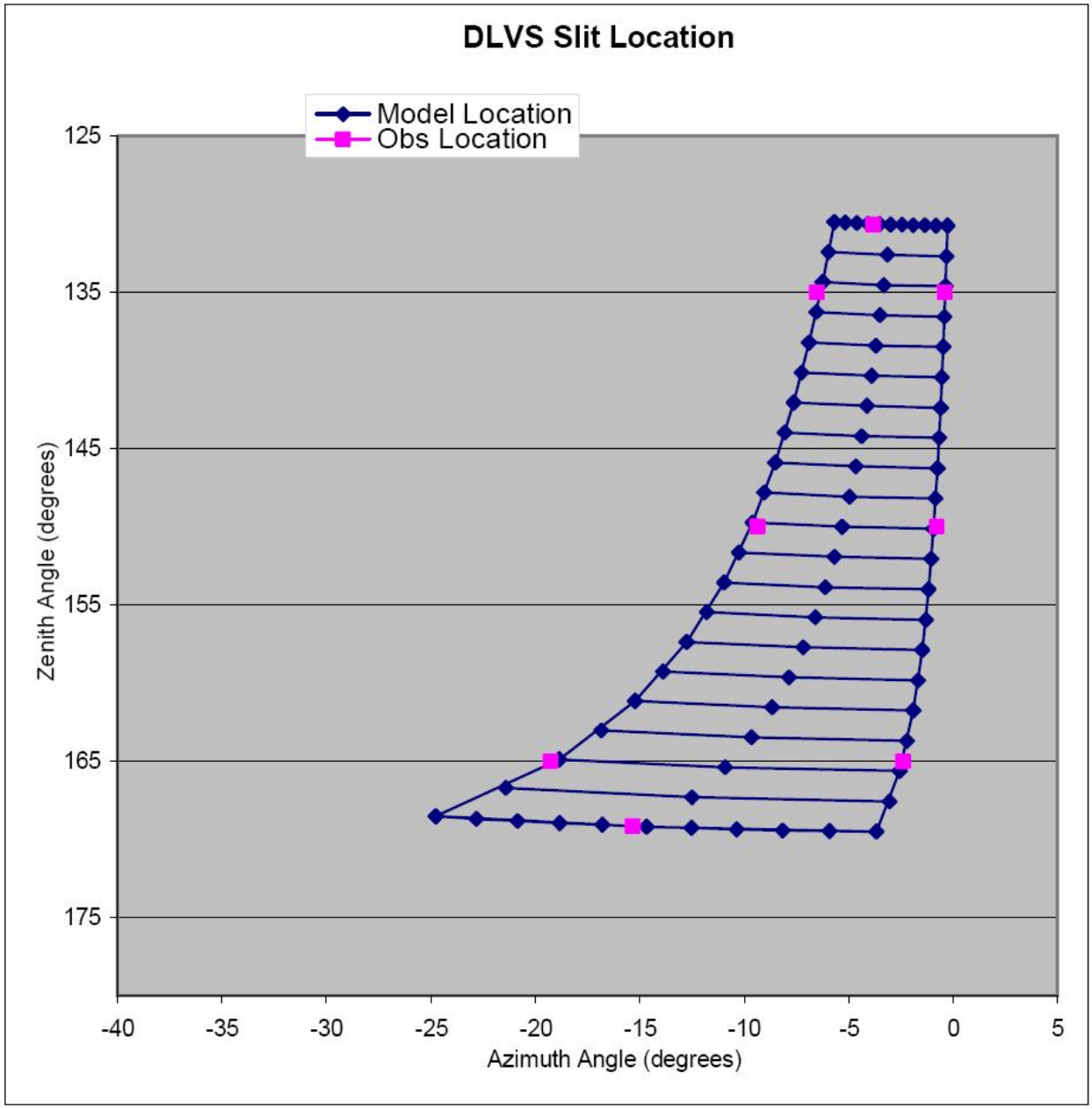

Figure 5.10-1: Fields of view for the 20 DLVS spatial pixels. Pink points are the lab calibration grid observations on which the FOV model is based. Pixel(0,0) is in the lower right corner.

Visible Spectrometer Archive Data...

The Visible Spectrometer archive data is located in directory: DATA/VISIBLE

The data is presented in tables that are n+1 columns wide by 200 rows deep, where n is the number of columns after summing. So for the ULVS data (DETECTOR_ID = "ULVS") there are 3 columns, the first is the row (or spectral pixel) number and the other two columns are the sum of CCD columns 38 to 41 (right half of the sky as viewed by the DISR), and the sum of CCD columns 42 to 45 (left half of the sky as viewed by the DISR).

For DETECTOR_ID = "DLVS" the number of columns may be 21, 11, 6 or 3, where the n columns are:

In the 20 column case - the raw observed DN for CCD columns 14 through 33.
In the 10 column case - the sum of CCD columns 14+15, 16+17, 18+19, ..., 30+31, & 32+33.
In the 5 column case - the sum of columns 14 thru 17, 18 thru 22, 23 thru 26, 27 thru 30, and 31 thru 33.
In the 2 column case - the sum of columns 18+19, and columns 20+21.

As an example we will use DLVS dataset VISIBLE_0543_013223_1446. Below is the abbreviated data in its original format, as seen in the Archive (without the header row). The first column is row index (i.e. row(n)), the next 20 columns are the spatially oriented data (in DN) with the first column being the most nadir. The rows increase from reddest (1) to bluest (200).

DLVS 20 column data (VISIBLE_0543_013223_1446.TAB)																				
	1	2	3	4	5	6	7	8	9	10	11	12	13	14	15	16	17	18	19	20
1	13	15	13	15	15	14	14	11	13	16	15	14	15	15	15	14	15	14	15	15
2	14	14	15	14	16	15	14	12	15	15	14	14	15	15	16	15	15	16	15	15
3	12	14	14	14	15	13	15	11	15	15	15	15	14	14	15	17	14	15	15	14
≡	≡	≡	≡	≡	≡	≡	≡	≡	≡	≡	≡	≡	≡	≡	≡	≡	≡	≡	≡	≡	≡
198	186	191	189	194	199	200	201	210	206	215	221	219	218	226	223	224	231	222	208	190
199	160	172	174	177	184	181	183	187	196	199	198	195	205	204	204	208	209	205	200	178
200	142	152	153	159	160	161	159	168	168	173	176	174	178	180	184	182	184	182	172	153

The table below is the same data, as if it were collected in 10 column mode (with each 2 columns summed together, 1+2, 3+4, etc).

DLVS 10 column data (column summed by 2's)										
	1	2	3	4	5	6	7	8	9	10
1	28	28	29	25	29	29	30	29	29	30
2	28	29	31	26	30	28	30	31	31	30
3	26	28	28	26	30	30	28	32	29	29
≡	≡	≡	≡	≡	≡	≡	≡	≡	≡	≡
198	377	383	399	411	421	440	444	447	453	398
199	332	351	365	370	395	393	409	412	414	378
200	294	312	321	327	341	350	358	366	366	325

The table below is the same data as if it were collected in 5 column mode. The first column is the sum of columns 1-4 of the raw, 20 column data, etc.

DLVS 5 column data (column summed by 4's)					
	1	2	3	4	5
1	56	54	58	54	59
2	57	57	58	56	61
3	54	54	60	56	58
≡	≡	≡	≡	≡	≡
198	760	810	861	832	851
199	683	735	788	765	792
200	606	648	691	668	691

The same data collected in 'near-surface' (2 column) mode. It provides 4 rows of data where the Surface Science Lamp signal is strong, summed into two columns. Note it is the same data as columns 3 & 4 of the 10 column case, & correspond to 18-12° & 22-24° nadir angles (Ref 15).

DLVS 2 column data (2 columns summed by 2's)		
	1	2
1	29	25
2	31	26
3	28	26
≡	≡	≡
198	399	411
199	365	370
200	321	327

The same is true of the ULVS data, but it is only available in 2 column mode, with the first 4 columns summed together, and the last 4. Below is a fictitious ULVS raw dataset:

ULVS 8 column raw data (unavailable)								
	1	2	3	4	5	6	7	8
1	28	29	25	29	29	30	29	29
2	29	31	26	30	28	30	31	31
3	28	28	26	30	30	28	32	29
≡	≡	≡	≡	≡	≡	≡	≡	≡
198	383	399	411	421	440	444	447	453
199	351	365	370	395	393	409	412	414
200	312	321	327	341	350	358	366	366

And below is how the data above would be transmitted:

ULVS data (summed by 4's)		
	1	2
1	111	117
2	116	120
3	112	119
≡	≡	≡
198	1614	1784
199	1481	1628
200	1301	1440

The following table provides file type discriminators for the DISR Visible archive data:

Dataset Type	DETECTOR_ID	RECORD_BYTES	File Size (KB)
ULVS	"ULVS"	22	5
DLVS, 2 Column	"DLVS"	22	5
DLVS, 5 Column	"DLVS"	46	9
DLVS, 10 Column	"DLVS"	86	17
DLVS, 20 Column	"DLVS"	166	33

A summary of the Visible Spectrometer data is presented in Appendix 40. The following plots present the the average per-column data rate history during the Titan descent for both Downward & Upward Looking Spectrometers from Appendix 40 (in Data Number per second). The stray points at ~1000, 2000 & 2500 seconds are from the calibration cycles.

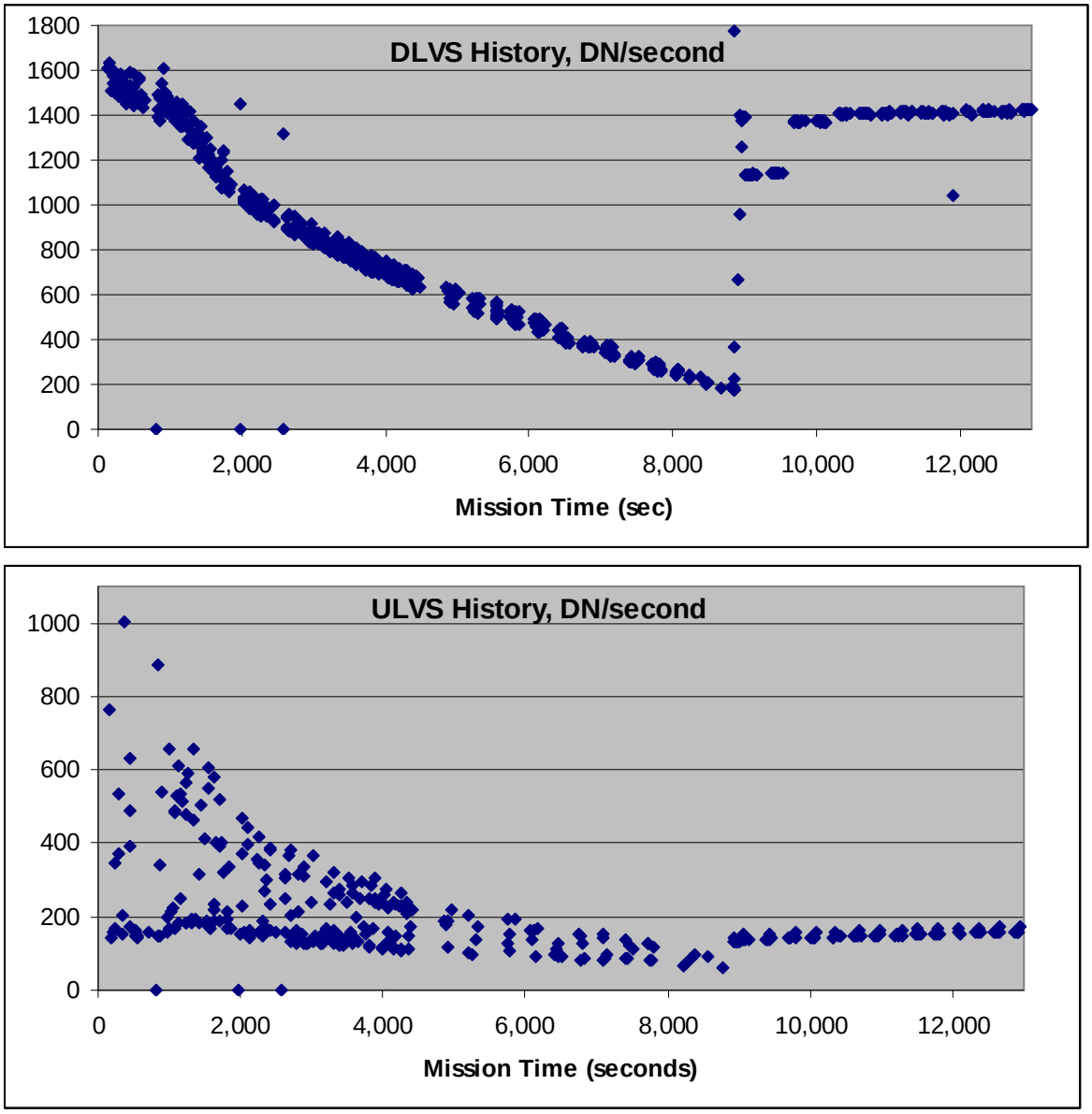

Figure 5.10-2: Downward & Upward Looking Visible Spectrometer average data from Appendix 40.

In order to use the Visible Spectrometer data from the PDS archive several pieces of information are needed:

1) The wavelengths corresponding to the pixels (which are a function of temperature).
2) The spectral resolution.
3) The absolute responsivities of each pixel.
4) The relative response over the field of view.
5) The pointing directions for the DLVS pixels.
6) Cross talk correction from the DISR Imagers
7) Fringe corrections for the ULVS measurements
8) The dark and bias signals.

Visible Spectrometers Wavelength Scale...

The wavelength corresponding to each visible spectrometer pixel is a function of optics temperature. The relations from the Visible Spectrometer Calibration Document (Reference 10) are given below with a brief example of how they are applied.

For both spectrometers the column average wavelength corresponding to a given spectral pixel (dataset row) is:

$$<WL> = a + b*pixel + c*pixel^2$$

where:

<WL> is the average wavelength in nm of the pixels in across the row.
pixel is the row number of the in the dataset, starting at 0 (0 to199).

for the DLVS the coefficients are:

$$a = 976.0126 + 0.003233571 * \text{Optics Temperature},$$

$$b = -2.310039 + 9.257741 \times 10^{-6} * \text{Optics Temperature},$$

$$c = -0.001014741 + 2.289958 \times 10^{-8} * \text{Optics Temperature}.$$

for the ULVS the coefficients are:

$$a = 966.0061 + 0.002924244 * \text{Optics Temperature},$$

$$b = -2.329799 + 5.265123 \times 10^{-6} * \text{Optics Temperature},$$

$$c = -0.001017838 + 2.616148 \times 10^{-8} * \text{Optics Temperature}.$$

There is also variation across the columns which can be calculate from:

for the DLVS:

$$\text{Wavelength (Column, Pixel, Temperature)} = \langle WL \rangle + (\text{Column}-9.5)*(0.07663108 + 3.398037\text{x}10^{-4} * \text{Pixel} + 2.081074\text{x}10^{-7}*\text{Pixel}^2)$$

and for the ULVS:

$$\text{Wavelength (Column, Pixel, Temperature)} = \langle WL \rangle + (\text{Column}-3.5)*(-0.09893011 - 6.962504\text{x}10^{-6}*\text{Pixel} - 3.571207\text{x}10^{-6}*\text{Pixel}^2)$$

where:

Wavelength is the wavelength corresponding to the pixel at (row, column) in nm,
<WL> is the column average wavelength (nm) calculated as above,
Column is the spatial pixel column number (0 to 19 for DLVS, 0 to 7 for ULVS), and
Pixel is the dataset row index (from 0 to 199).

The optics temperature profile during the Titan descent is shown in section 5.5 (and Appendix 38). A table of the DLVS column average wavelengths is presented in Appendix 29.

It should be noted that the laboratory measurements these numbers are based on occurred at around 920 mb pressure, while the observations above Titan occurred from 3 to 1470 mb, which shifts the wavelengths up to 1 nm due to the well-known change of refractive index of air with its density. A correction curve has been published by Erich Karkoschka in Reference 16:

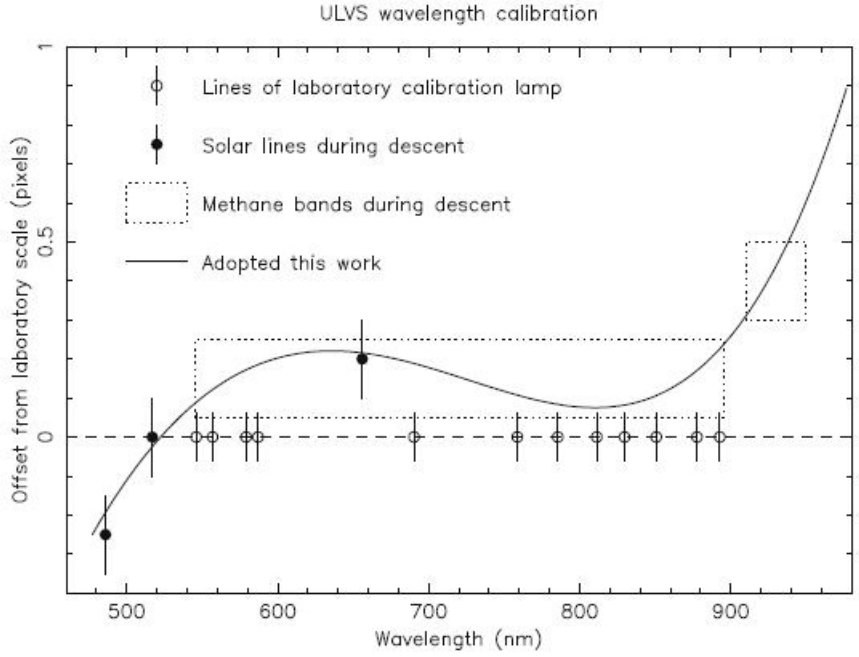

Figure 5.10-3: Offsets of the ULVS wavelength calibration to the laboratory calibration for various lines and bands, and adopted calibration from Reference 16. One pixel corresponds to ~2.6 nm. A positive offset means that the spectral pixel probes a longer wavelength than expected.

The following plot shows the variation in average wavelength scale from their values at 210ºK. The maximum variation over the Titan descent was about ±0.3 nm at the blue end of the spectrometer, and about 0.16 nm at the red end.

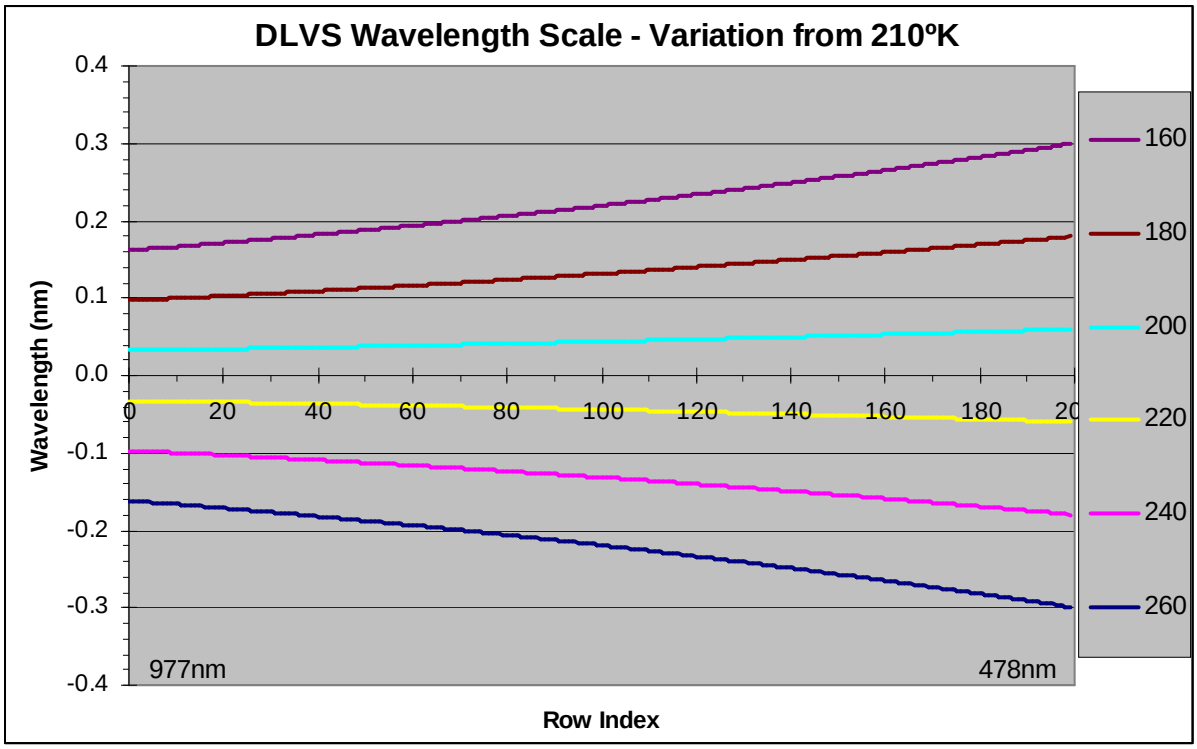

Figure 5.10-4: Variation in the DLVS column average wavelength scale from its value at 210ºK, for temperatures from 160º to 260ºK. The maximum variation of about ±0.3 nm occurs at the blue end of the scale.

The wavelength variation across the rows (in the spatial dimension) is more severe. The corresponding wavelengths vary by about 0.7 nm at the red end of the scale and by almost 1.5 nm at the blue end for our example at 210ºK, shown below. A subset of this data is presented in tabular form in Appendix 29.

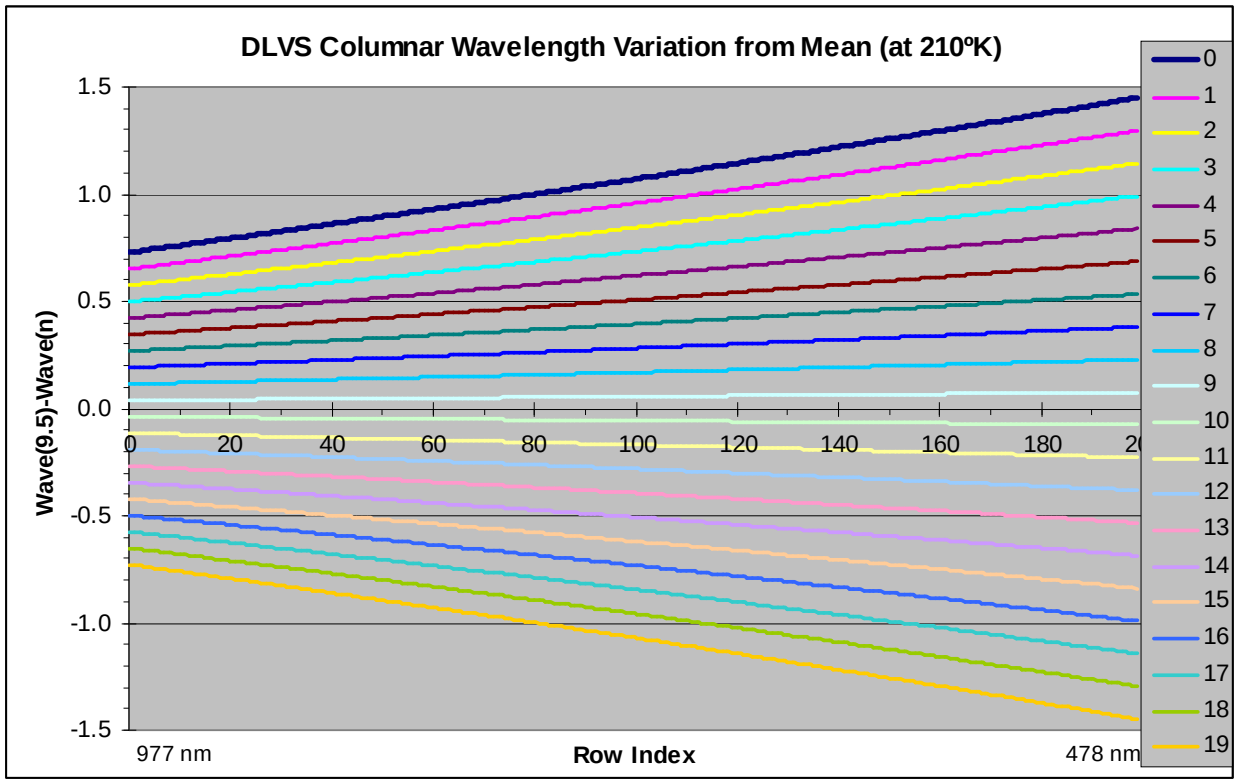

Figure 5.10-5: The variation in wavelength from the column mean for the 20 columns of the DLVS at 210ºK.

Below are the same plots of the wavelength scale variations, except for the ULVS.

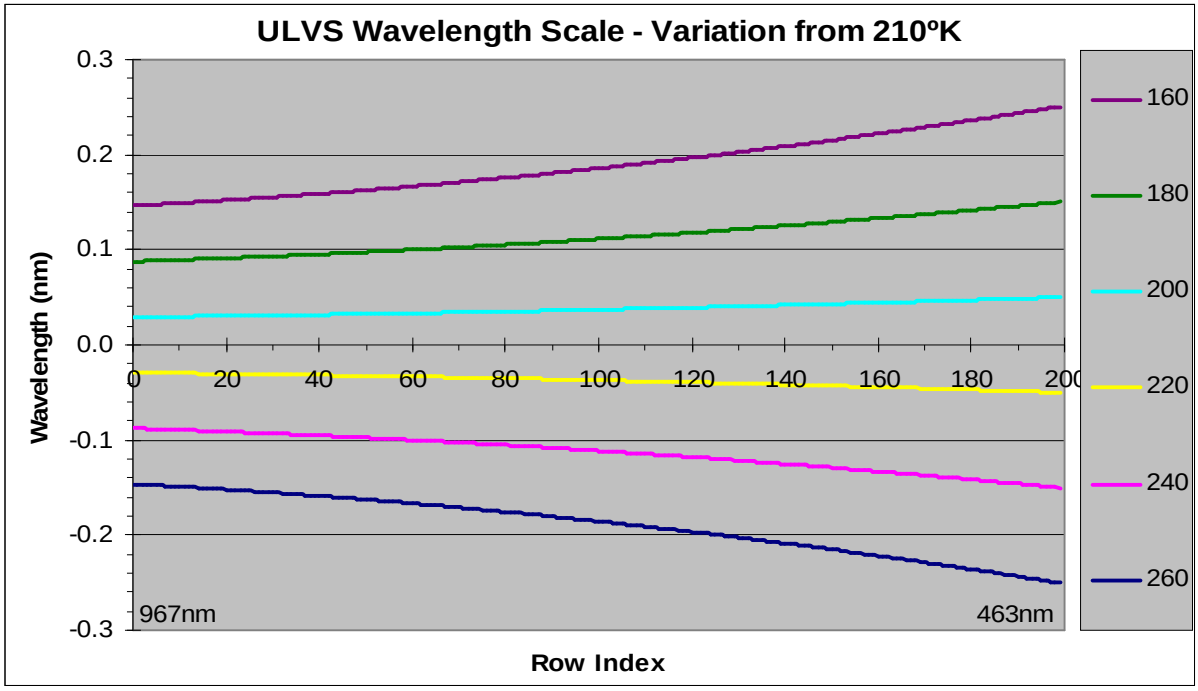

Figure 5.10-6- Variation in the ULVS column average wavelength scale from its value at 210ºK, for temperatures from 160º to 260ºK. The maximum variation of about ±0.3 nm occurs at the blue end of the scale.

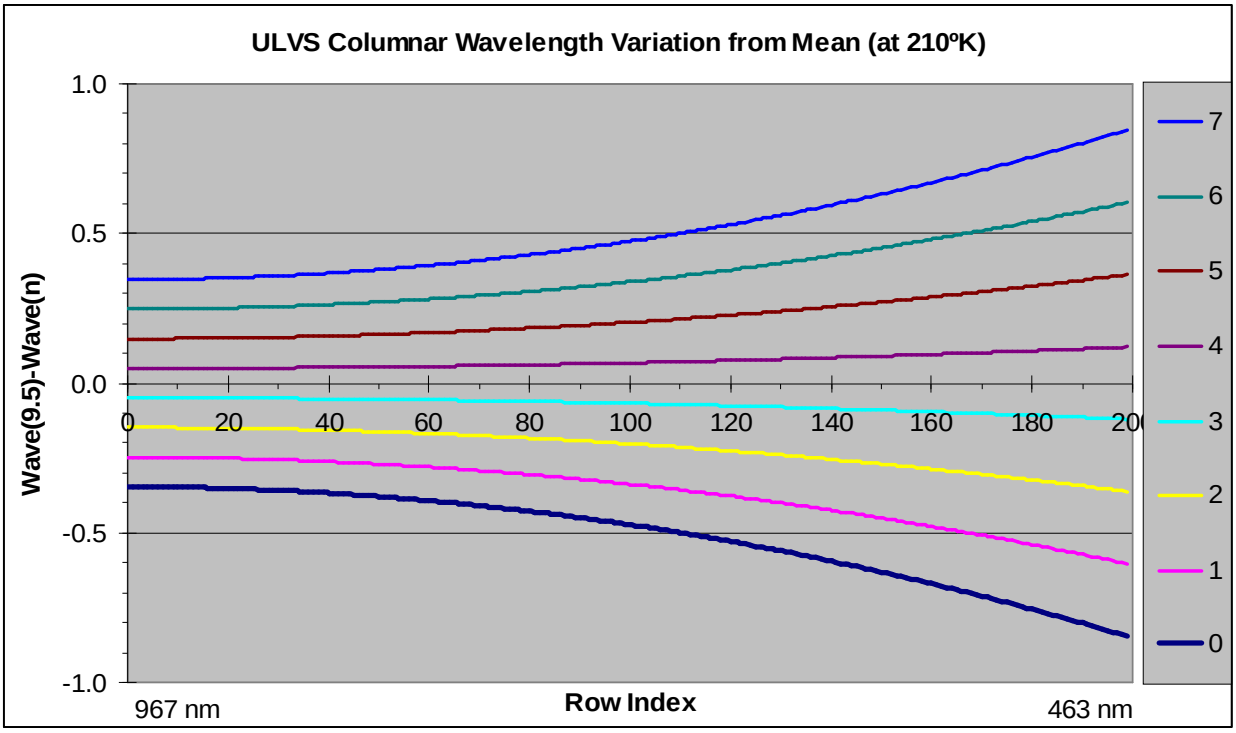

Figure 5.10-7: The variation in wavelength from the column mean for the 8 columns of the ULVS at 210ºK.

Spectral Resolution...

The spectral resolution of each Visible Spectrometer pixel is dependent on its location in the dataset (i.e. wavelength and spatial column), and temperature. The line spread function is described as a Gaussian with the full width at half maximum (FWHM) response:

For the DLVS:

$$\begin{aligned} \text{FWHMcore} = {} & (9.7249 - 0.0156\lambda + 8.0975\times10^{-6}\lambda^2) * \\ & (1.04554 - 4.7941\times10^{-3} * \text{Column}) * \\ & (1.1733 - 1.3936\times10^{-3}T + 2.79656\times10^{-6}T^2) \end{aligned}$$

where:

FWHMcore is the full width at half max of the Gaussian in nanometers,
λ is the wavelength corresponding to the pixel in nanometers,
Column is the spatial column index of the pixel (0 to 19), and
T is the DISR Optics Temperature in degrees Kelvin.

Similarly for the ULVS:

$$\begin{aligned} \text{FWHMcore (nm)} = {} & (4.8412 + 3.5474\times10^{-4}\lambda) * \\ & (1.02868 - 8.565\times10^{-3} * \text{Column} + 1.060\times10^{-4} * \text{Column}^2) * \\ & (1.5808 - 4.598\times10^{-3} * T + 9.057\times10^{-6} * T^2). \end{aligned}$$

A summary of the spectral resolution for both the DLVS and ULVS at 210ºK is presented in Appendix 30 in tabular form, and graphically below:

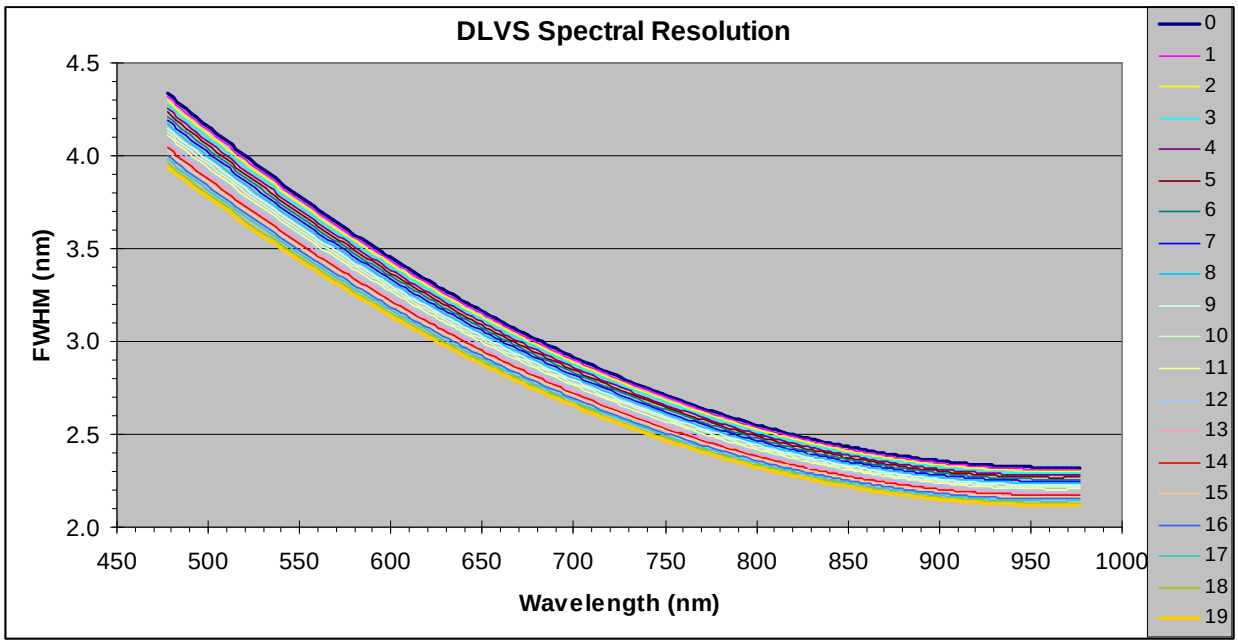

Figure 5.10-8: DLVS spectral resolution at 210ºK for all 20 columns.

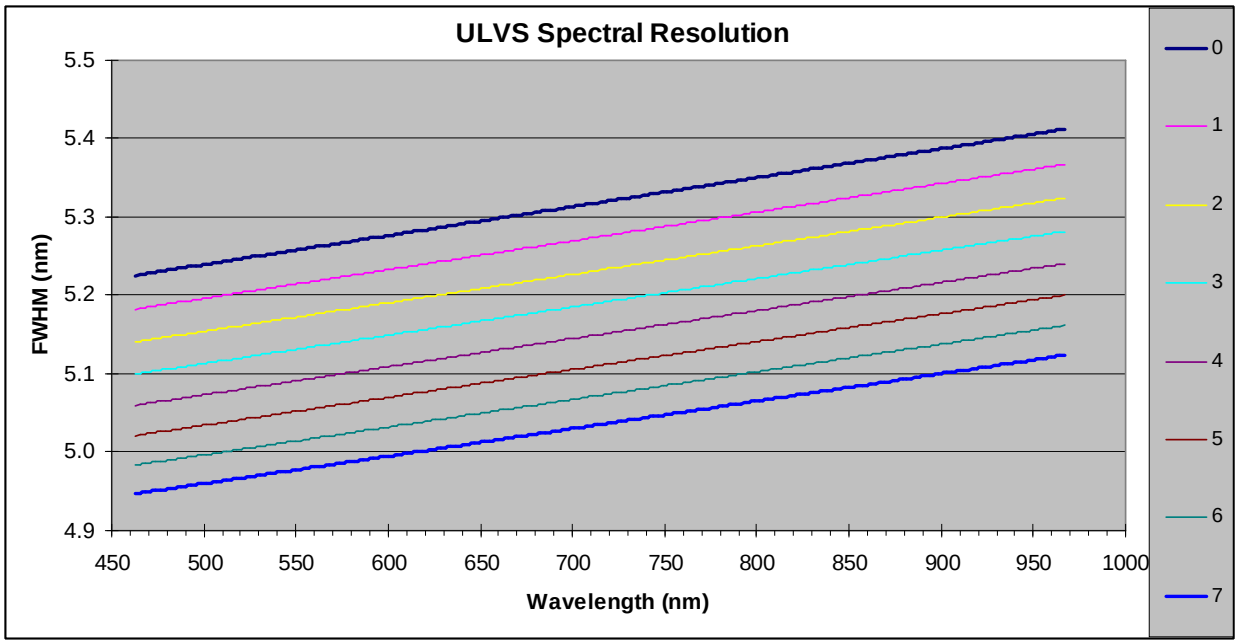

Figure 5.10-9: ULVS spectral resolution at 210ºK for all 8 columns.

Absolute Responsivity...

The absolute responsivity of the Visible Spectrometer pixel are a strong function of pixel number (spectral and spatial location) and temperature, and often vary sporadically from pixel to pixel. Tables of the absolute responsivities in (DN/second) / [Watts/(m^2-micron-steradian)] for each pixel are presented in the Visible Spectrometer Calibration Document (Reference 10).

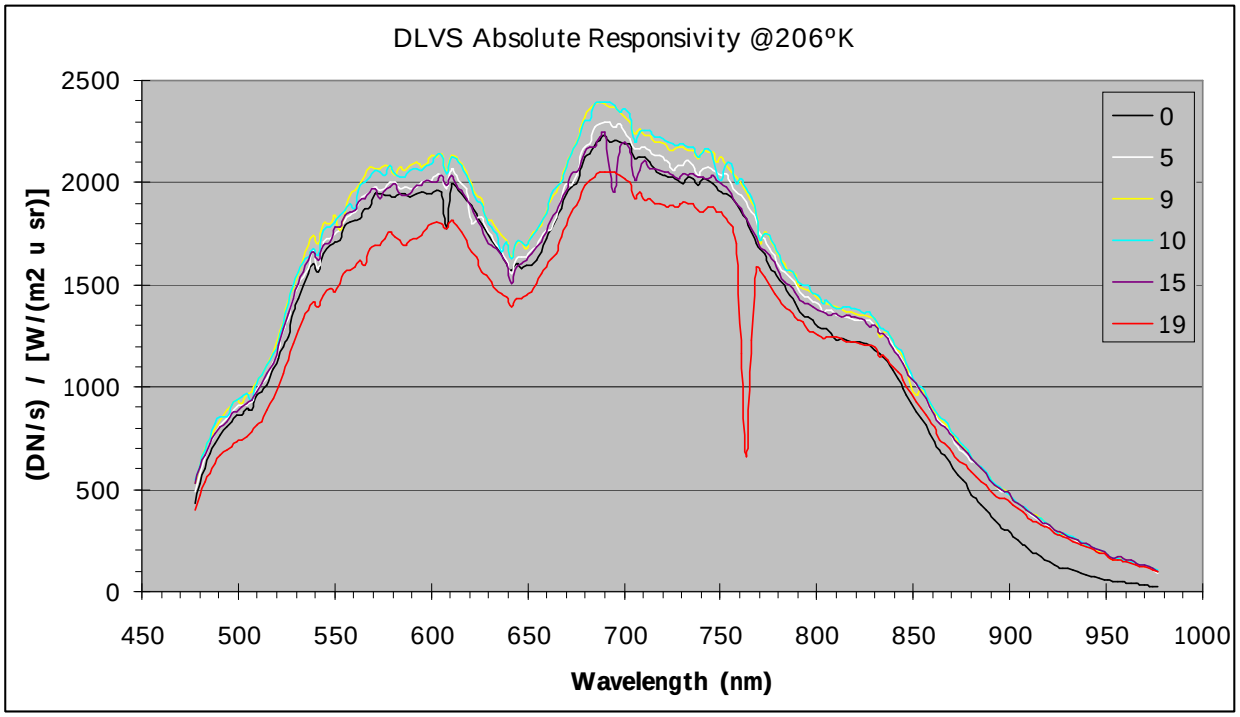

Figure 5.10-11: DLVS Absolute Responsivity vs. wavelength (row) at 205.4ºK CCD temperature (213ºK optics temperature) for selected columns (spatial pixels). From tables 7.2 of Reference 11. Note: there are significant pixel-to-pixel variations in some cases.

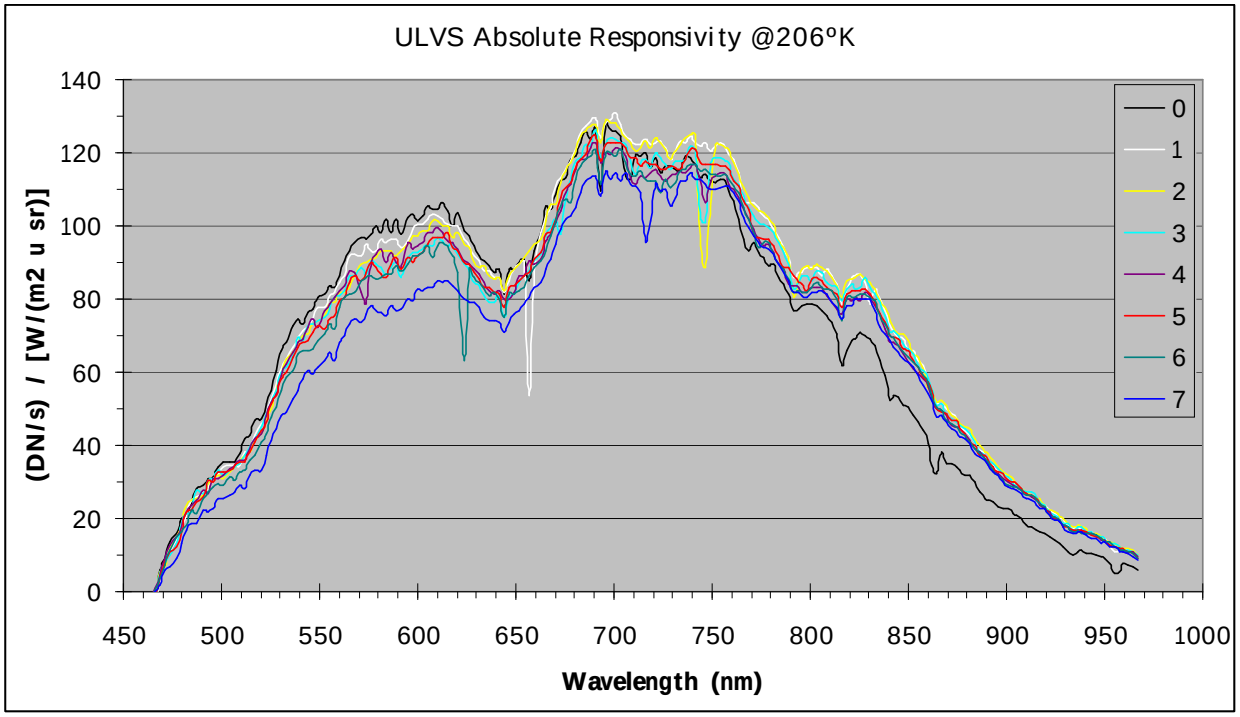

Figure 5.10-12: ULVS Absolute Responsivity vs. wavelength (row) at 205.7ºK CCD temperature (213ºK optics temperature) for all 8 columns (spatial pixels). From tables 7.1 of Reference 11. Note: there are significant pixel-to-pixel variations in some cases.

Relative Spatial Response...

DLVS:

As you will recall, the DLVS has a spectral and spatial dimension. The column dimension is spatial with the relationship:

Zenith Angle (in deg) = 2.0272 * (83.45063 - Column Number)

However there is some tilt, introducing a row effect into the spatial dimension.

$$\text{Zenith Angle(Col, Row)} = 169.174 - 2.02724*(\text{Col} - 2.431874 + 0.04087319*\text{Row} - 0.0001213306*\text{Row}^2)$$

The half amplitude azimuth boundaries for the spatial column element are represented by:

$$\text{Azimuth} = A0 + A1*\text{Zenith} + A2*\text{Zenith}^2 + A3*\text{Zenith}^3 + A4*\text{Zenith}^4 + A5*\text{Zenith}^5$$

where the coefficient for the two azimuth limits are presented in the following table:

Coef.	Azimuth 1	Azimuth 2
A0	1.3320E+04	-4.1082E+04
A1	-4.5959E+02	1.3831E+03
A2	6.3344E+00	-1.8567E+01
A3	-4.3601E-02	1.2416E-01
A4	1.4991E-04	-4.1333E-04
A5	-2.0603E-07	5.4757E-07

For a graphic representation see figure 5.10-1, plot of DLVS Zenith vs. Azimuth.

It should be noted that the azimuthal edge cut-off is not sharp, but more gaussianesque. Plots of the spatial shape and a more detailed description of the DLVS azimuth extent is discussed in section 4 (Geometry) of the calibration document (Ref 11).

ULVS:

The ULVS views roughly ¼ of the sky at any epoch. However the spatial response over that π/2 sr is not constant, nor even a pleasant function. Tables of the ULVS's column averaged spatial response for every azimuth (-90 to +90) and every zenith angle (0 to 90) are presented in tables 4.1 of Reference 10a. These values are normalized to 10,000 at the peak response. Those values normalized to 1 at the peak are presented graphically below.

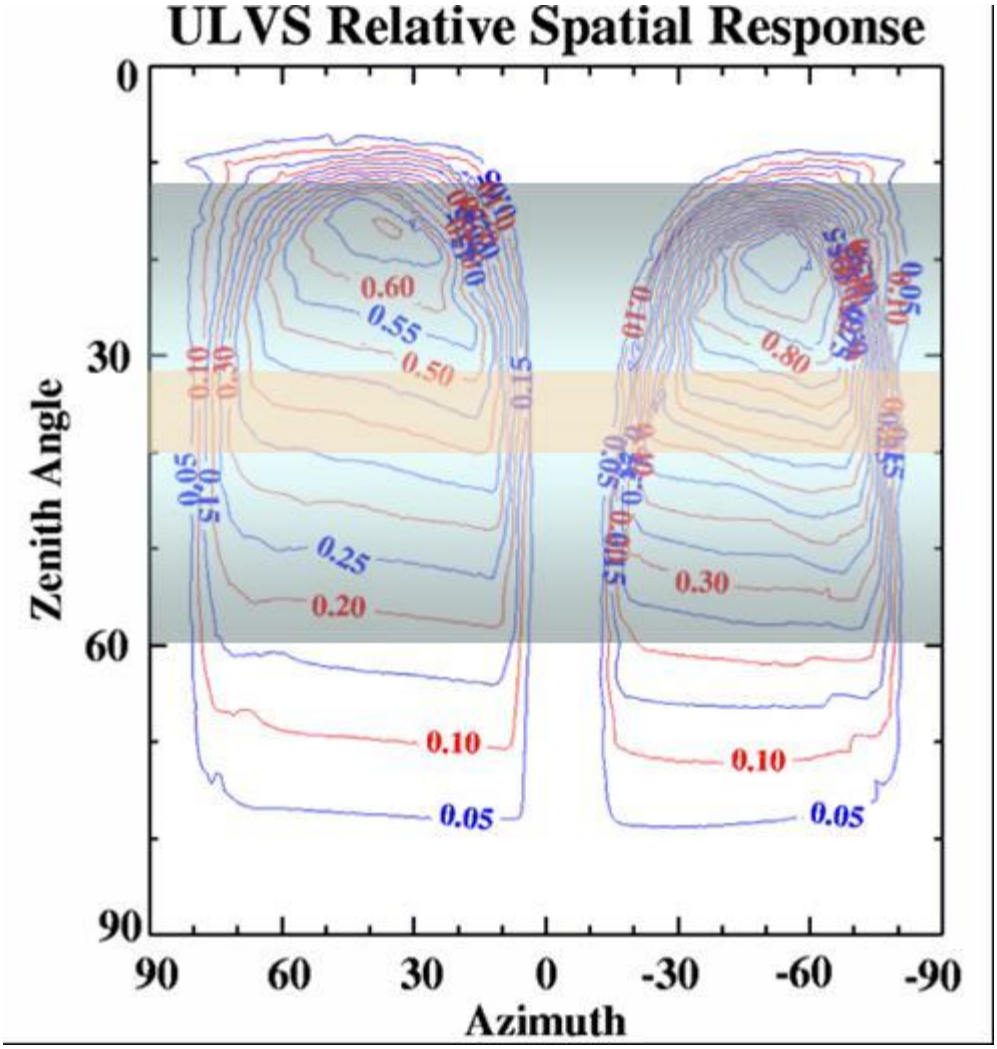

Figure 5.10-13: ULVS relative spatial response, normalized to 1.0 at the peak. The valley near the center of the response is due to the shadow-bar. The red band from 40 to 32 degrees zenith angle show the locus of potential positions for the Sun during the descent for zero probe tilt. Probe tilt can extend this region by ±20°, and cause significant obscuration by the parachute, which nominally extends 5° down from Zenith. The direction of the Sun in this diagram was from left to right at the beginning of the descent (above 124.5 km) and from right to left for the lower part of the descent. Azimuths are defined as CCW + from above.

A word about azimuths, and the Relative Spatial Response plots:

The probe rotated clockwise as viewed from above for most of the descent, which is opposite what was expected. The convention used in the calibration document assigns azimuth angles increasing counter-clockwise when viewed from above, which would result in the Sun progressing in decreasing azimuth angle through the field of view with time. This was true at the beginning of the descent; however after about 550 seconds (i.e. below about 124 km) the probe began to rotate clockwise (from above) and so the Sun's progress increased in DISR azimuth with time for the remainder of the descent.

Furthermore some analyses define the azimuth as increasing in time relative to T0, which is consistent with figure 5.10-13 at all altitudes (i.e. a measurement taken at 60 degrees azimuth

would have the Sun on the left side of the plot, and an observation at 300 degrees would have the Sun on the right). Thus this figure presents the instrument's response from the view of the DISR, i.e. when the Sun is on the right side of the plot it is on the 'purge fitting' side of the sensor head. The pink region on the plot shows the variation in SZA during the descent (without probe tip), which began around 40 degrees and ended near 32 degrees at LOS.

Cross Talk...

As a result of the Visible Spectrometers and Imagers sharing the same CCD and fiber optics bundle, having substantially different exposure times, and having no mechanical shutter, there is considerable crosstalk between them. This generally results in contamination by the instruments with the longest exposure times (ULVS & DLVS) by those with the shorter exposure times (Imagers & DLVS). When the spectrometers are reasonably exposed the imagers are overexposed by a factor near 100.

To combat this problem, two additional CCD columns (31 & 49), one on each side of the ULVS were read-out whenever a visible spectrometer measurement was taken. These make up the Visible Extra (DATA/VISIBLE_EXT) datasets. During calibration, crosstalk factors were developed, as described in section 5 ("Cross Talk into the Visible Spectrometer") of the calibration document (Reference 11) which relate the signal in the extra columns to contamination of the spectrometers.

Column 31 lies between the DLVS and the ULVS and column 49 lies between the ULVS and the MRI. Thus the contamination from the MRI into both the ULVS and DLVS is determined using column 49, and contamination from the DLVS into the ULVS is determined using column 31. Contamination of the DLVS by the ULVS is negligible.

Crosstalk factors are presented in Section 5 ("Cross Talk into the Visible Spectrometer") of the calibration document (Reference 11), and are applied on a row by row basis as:

$$dDN_U = f49 * DN_{49} + f31 * DN_{31}$$

where

dDN_U are the additional counts to be subtracted from the ULVS,
f49 & f31 are the Crosstalk factors from the tables, and
DN_{49} & DN_{31} are the counts in the extra columns.

$$dDN_D = f49 * DN_{49}$$

where

dDN_U are the additional counts to be subtracted from the ULVS,
f49 is the Crosstalk factor from the tables, and
DN_{49} is the count in extra column 49.

Separate factors are developed for the DLVS 20,10 & 5 column data, but all are applied on a per-pixel basis (i,e. un-summed). Below is a plot of the crosstalk factors for the DLVS from extra column 49 for the 5 column mode (i.e. 4 columns summed). In the worst case (the column closest to the MRI), about 6% of the number of counts in extra column 49 must be subtracted from the average counts in CCD columns 30-33 (DLVS columns 16-19).

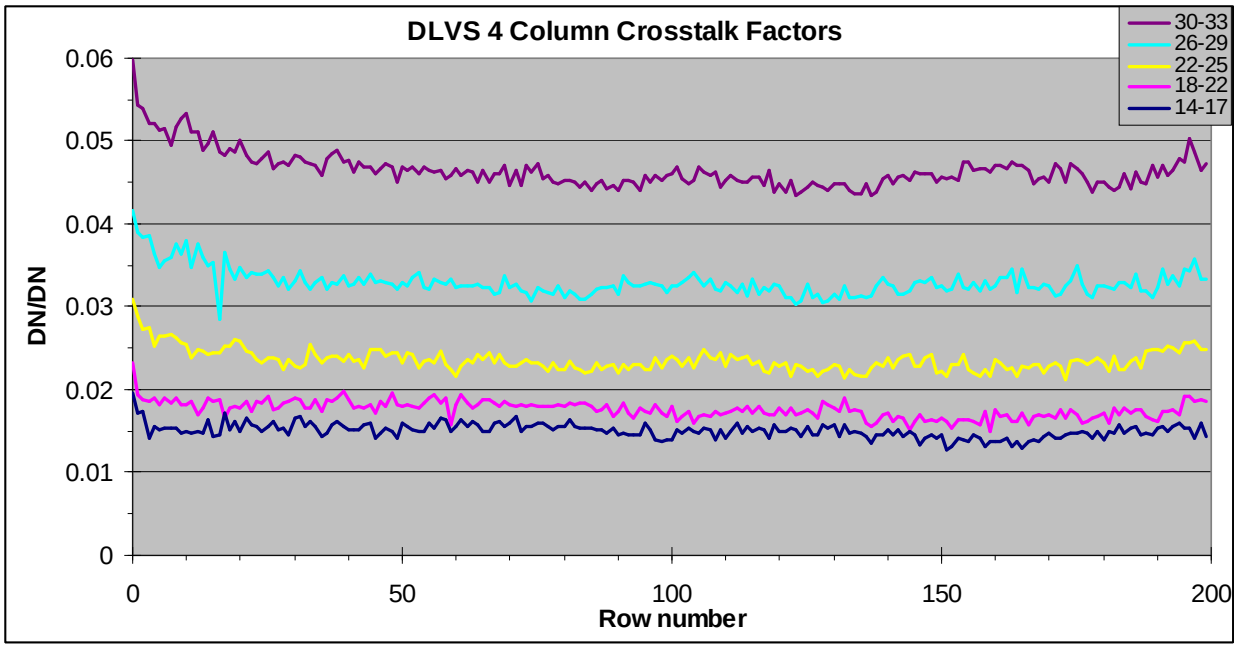

Figure 5.10-14: Crosstalk factors from CCD column 49 to the DLVS columns for the 5 column collection mode.

The crosstalk factors were measured at room temperature, about 295K. They are temperature dependent.

The variation with temperature is caused by motion of the light pattern on the CCD. It is presented below for the ULVS, and should be similar for the DLVS. Factors are defined for the blue (row 199) and red (row 0) ends of the spectrometers and for columns on each side. The factors must then be linearly interpolated to get their values for intermediate pixels. The factors are multiplied to the crosstalk factors to modify them for use at temperatures away from 295ºK.

At the red (row 0) end:

$$\text{Fred 0-3} = 0.98835 - 2.6826\text{x}10^{-3} * \text{Tccd} + 9.0812\text{x}10^{-6} * \text{Tccd}^2, \text{ and}$$
$$\text{Fred 4-7} = 1.2026 + 1.481\text{x}10^{-2} * \text{Tccd} - 2.4965\text{x}10^{-5} * \text{Tccd}^2.$$

where

Fred 0-3 and Fred 0-4 are the factors for the low (0-3) & high (0-4) columns.
Tccd is the CCD temperature at the time of the observation.

Similarly for the blue (row 200) end of the spectrometers:

$$\text{Fblue 0-3} = 28.387 - 0.34256 * \text{Tccd} + 1.4061\text{x}10^{-3} * \text{Tccd}^2 - 1.8898\text{x}10^{-6} * \text{Tccd}^3, \text{ and}$$
$$\text{Fblue 4-7} = 8.897 - 0.10456 * \text{Tccd} + 4.4691\text{x}10^{-4} * \text{Tccd}^2 - 6.1849\text{x}10^{-7} * \text{Tccd}^3.$$

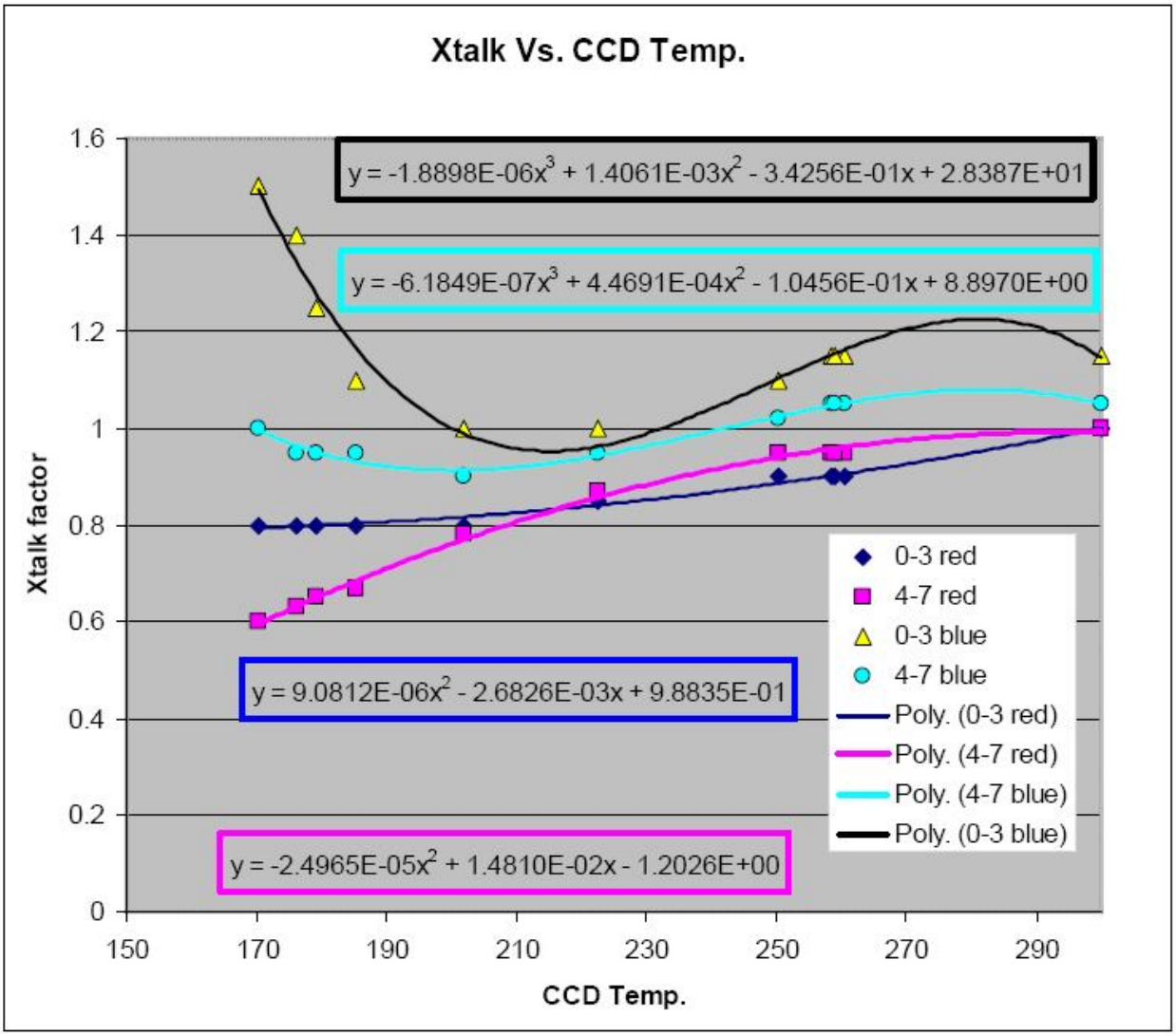

Figure 5.10-15: Temperature dependence of the cross talk factors for the red and blue ends of the spectrometers, and for the left (0-3) and right (4-7) columns.

For the DLVS the crosstalk factors have been further refined in Reference 15 (sect 3.2) as:

relative cross talk = 10.2 / (305-T) - 0.02

where T is the measured instrument temperature in Kelvin. This function decreases from unity at T=295 K (room temperature) to 0.06 at T=178 K, indicating that the cross talk is some 16 times less at the coldest temperatures. This factor is multiplied to the cross talk from the calibration report. Since the cross talk in the DLVS is small and only significant in methane bands, the improved correction decreases any uncertainty due to cross talk to insignificant levels.

ULVS Fringes...

A weak 'fringe' pattern exists on the ULVS signal (but not the DLVS). The 'fringes' present an amplitude modulation with wavelength of the ULVS responsivity as show in the plot below. The peak amplitude variation is around ±3%.

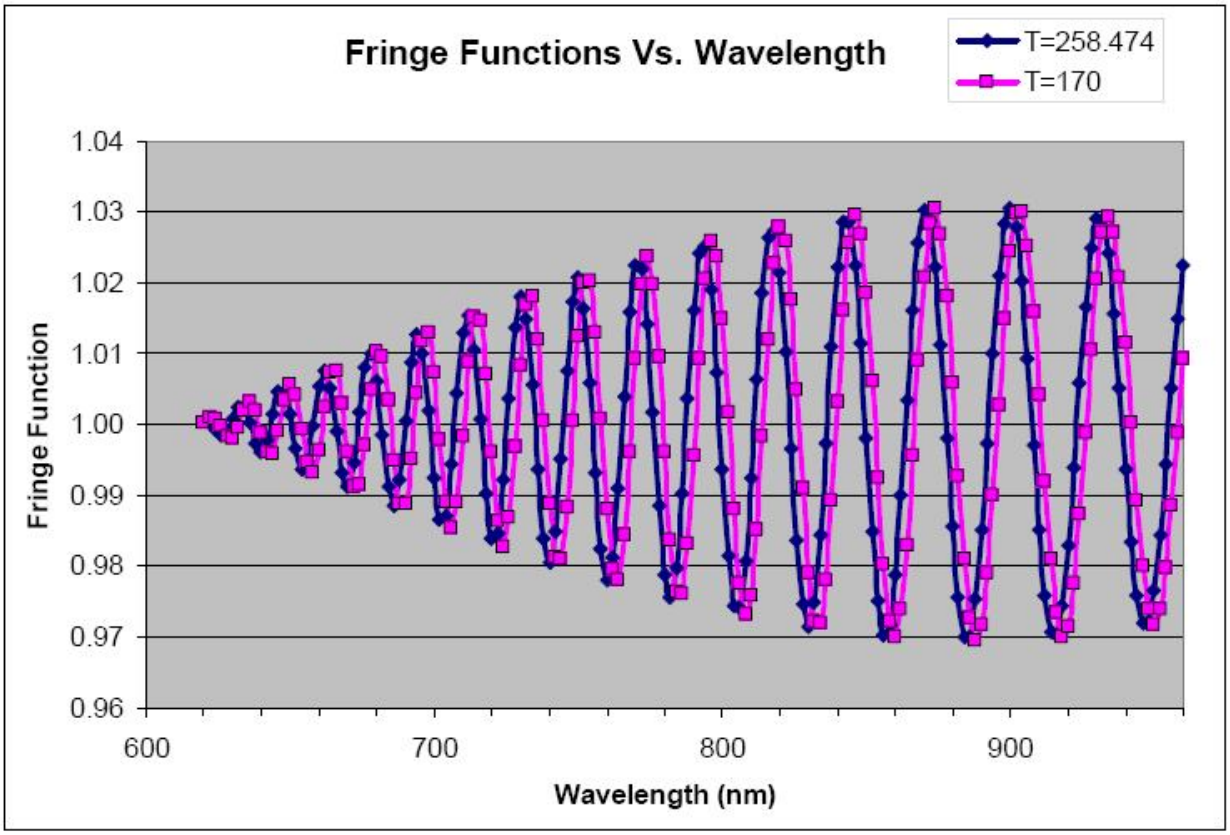

Figure 5.10-16: ULVS fringe function at two temperatures.

The fringe factor corrects the intensity measured by the ULIS:

Corrected Intensity = Measured Intensity / Ff

$Ff = 1 + (A * \cos(\omega(\lambda-\lambda_0))$

where:

Ff is the fringe factor at wavelength λ,
A is fringe amplitude given below,
ω is the fringe rate in radians per nm, given below,
λ is the wavelength of the observation in nm, and
λ_0 = 620 nm.

$\omega = 2\pi / (0.75*p + Tf + 11.0)$

where

p is the wavelength position:
$p = 0.34242 - 3.136032 \times 10^{-4} \lambda + 1.05 \times 10^{-7} \lambda^2$
Tf is the temperature factor = 0.0012 * (258.474 - Tccd)

where Tccd is the CCD temperature at the time of the observation.

$A = -6.038085 \times 10^{-4} + 1.2831 \times 10^{-6} \lambda - 7.072 \times 10^{-10} \lambda^2$

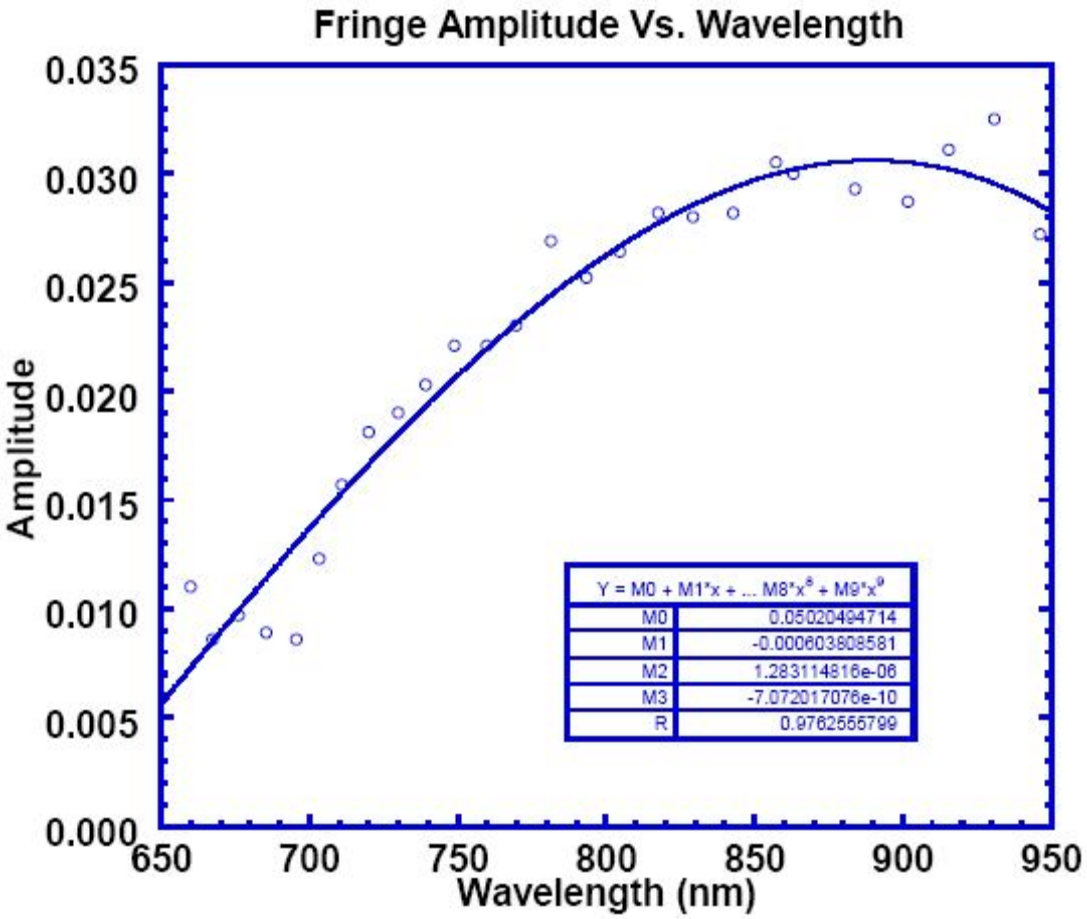

Figure 5.10-17: ULVS fringe amplitude, A as a function of wavelength. This plot shows the derivation of the amplitude function, and local variations from that function (typically a few tenths of a percent).

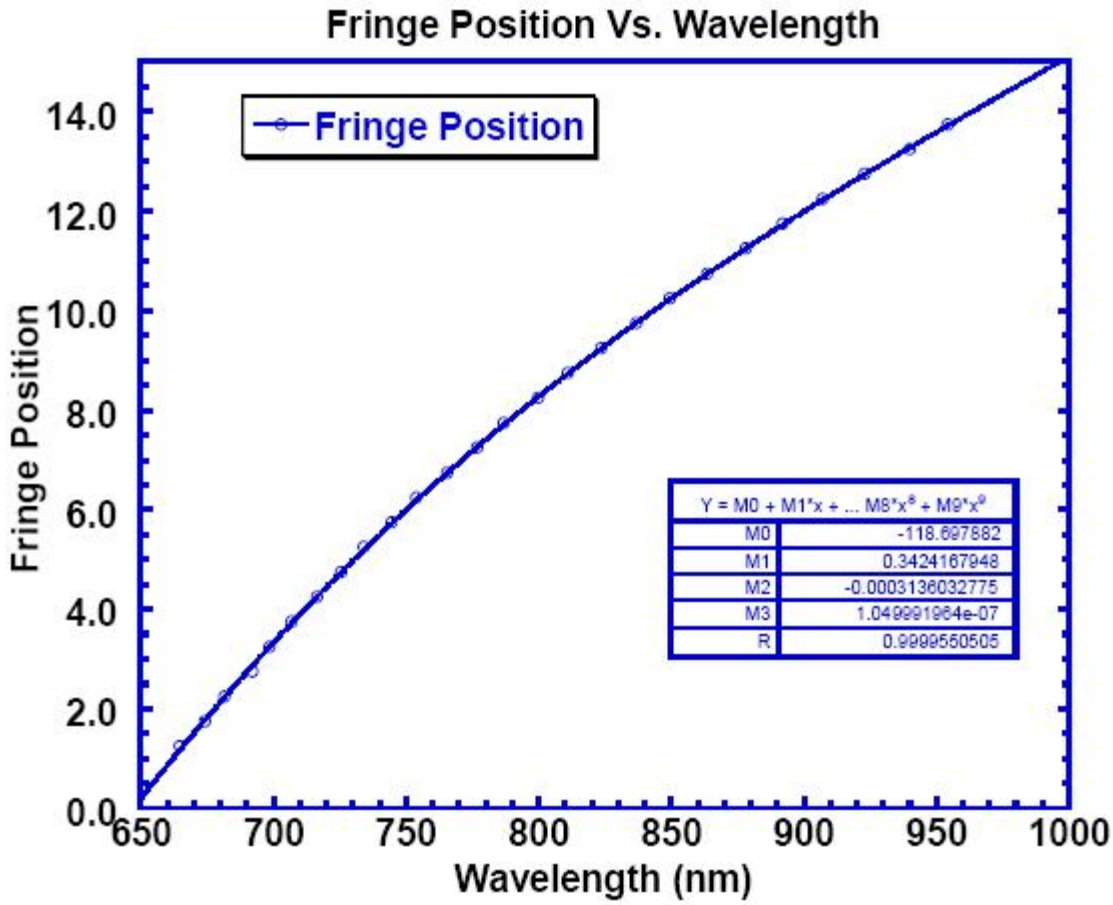

Figure 5.10-18: ULVS fringe position, p as a function of wavelength. This plot shows the derived fringe position function and local variations from that function, which are quite small (typically less than 0.1 nm).

Radiance Determination...

The spectral radiance, I, can be determined for the Visible Spectrometer measurement via the following steps:

1) The net DN/second is determined by subtracting the dark current from the measurement as described in section 5.7, and subtracting the shutter effect as described in section 5.8, then dividing by the exposure time of the measurement. For the DLVS the shutter effect is typically negligible due to the long exposure times.

2) After the net DN/sec are computed for each pixel of interest, the wavelength can be found from the wavelength calibration equations at the appropriate optics temperature as described above.

3) The DN/sec due to crosstalk can be subtracted at the appropriate CCD temperature using the tables given in section 5 ("Cross Talk into the Visible Spectrometer") of the calibration document (Reference 11), as well as the red and blue temperature dependent factors described above. The crosstalk factors are applied using the extra columns associate with the dataset from the archive (hpdisr_0001/DATA/VISIBLE_EXT). These need to be linearly interpolated to the pixel (row) of interest, and subtracted from the DN/sec.

4) The responsivity can be interpolated in the tables 7.1 & 7.2 of Reference 11 for the CCD temperature of interest, and the net DN/sec can be divided by the responsivity at the appropriate CCD temperature for the pixel of interest.

5) Finally, the fringe pattern can be evaluated, and the fringes can be divided out using the amplitude as a function of wavelength, the phase as a function of wavelength, and the phase shift as a function of optics temperature, as described above.

The result is the absolute spectral radiance in watts/sq.m-micron-sr averaged over the field of view of the visible spectrometer.

Cassini Cruise Phase Effects...

As discussed in section 5.6, many of the DISR detector systems exhibited changes in the absolute responsivity during the trip from Earth to Titan. The dark current effects are discussed in section 5.7. The observed changes in the Visible Spectrometer system are small, and may be a combination of yellowing of the fiber optic bundles, and/or movement of the fibers during launch. The observations are presented below.

The overall effect is a drop of about 3% in the ULVS and 2% in the DLVS. Since most of the reduction occurred near launch, it may be that the majority of the change is due to movement of the fiber-optic strands that conduct light from the calibration bulbs to the detector (as seen in the imagers). This would infer that only about 1% of the reduction was an actual change in the spectrometers responsivity.

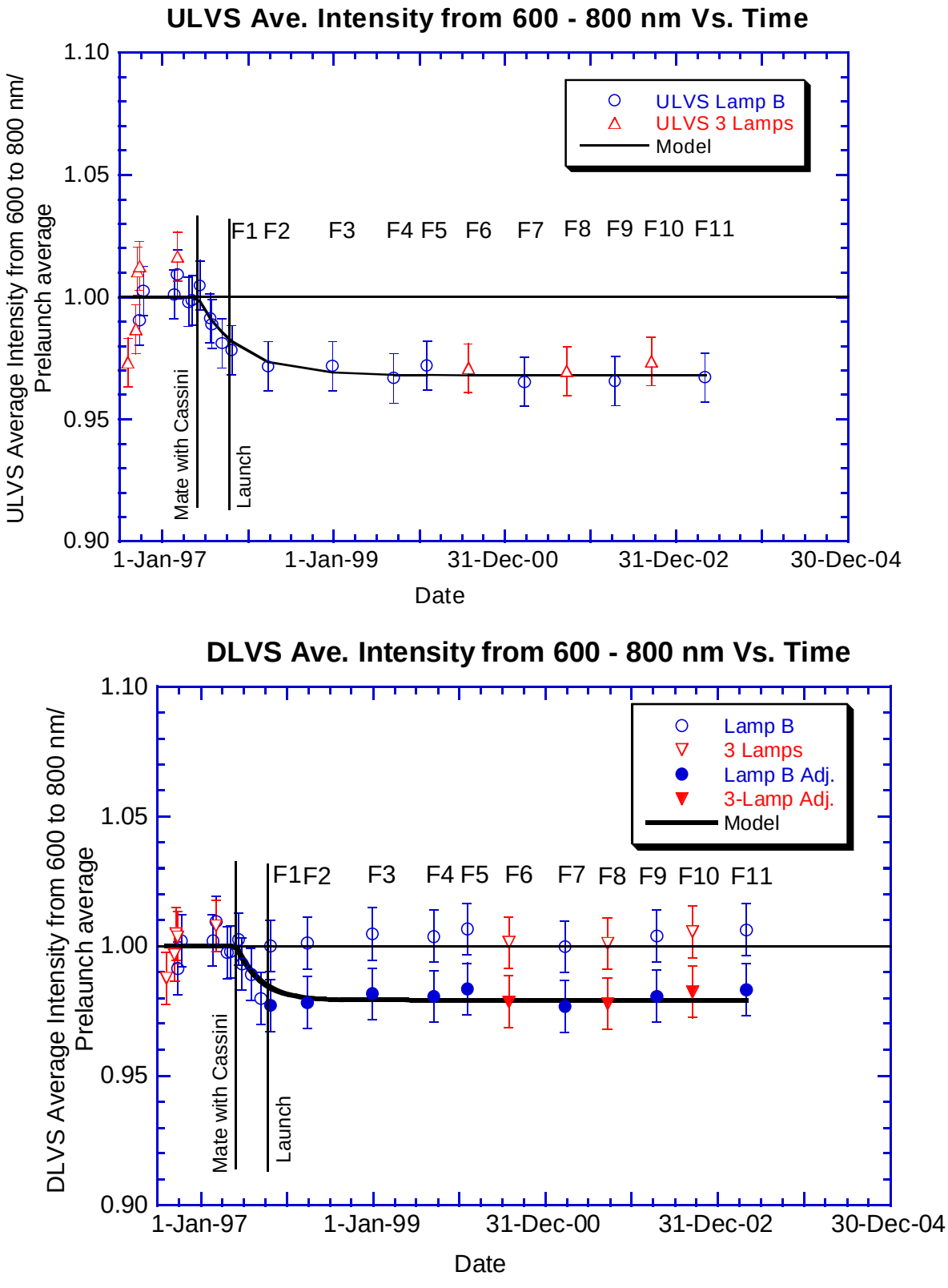

Figure 5.10-19: Normalized change in calibration lamp response for the Visible Spectrometers, Upward Looking on top, Downward Looking on bottom.

5.11 IR Wavelengths Spectra

The IR spectrometer is considerably complex. It is designed to collect exposure-balanced spectra, both upward and downward looking in discrete regions (bins) relative to the Sun. It has an active shutter to allow encompassing dark readings. The upward bins are twice as large as the downward bins, and both are clocked relative to the Sun's position in the sky. The IR calibration document in the archive, "IR_SPECTROMETER_CAL_DOC.pdf" has an informative introduction in section 1 ("General Information"), and I encourage you to read it.

The shutter osculates at something less than 5 Hertz and the spectrometer simultaneously collects upward and downward light readings while the shutter is open and places the values in the proper bins associated with the probes azimuth. The dark readings are also binned. The detector has 150 elements, of which 132 are active for spectral information. The data is digitized into 14 bits, but transmitted as a 16-bit word (i.e. max signal is 65,535 DN, but quantization is only 16,384 levels). The reading is the amount of charge needed to refill the detector well, therefore there is an inversion in the reading, and brighter measurements have lower data numbers (i.e. 0 DN is bright saturated, and 65,535 DN is complete darkness).

The measurement exposure is governed by three numbers: the "Sample Time" is the shutter open time per collection sample and is analogous to the exposure time. The "Collection Time" is the total time data is taken, and is akin to integration time. The "Shutter Time" is the total time the shutter is active per sample (several 'samples' are often taken during one measurement), and is generally about twice the Sample Time (i.e. shutter open plus shutter closed).

The IR spectra come in several modes.

Near the surface the IR exposures were obtained as quickly as possible in order to maximize the spectra of the surface. These spectra were taken in what is called 'Snapshot Mode" where the exposure times are as short as possible (to get reasonable signal to noise), and are not binned, but taken randomly in azimuth (i.e. as soon as possible). Unfortunately since only one telemetry channel was operating, many of the near surface IR spectra were lost. There are, of course several spectra taken with the probe setting on the surface, but they are all of one small area (~8 cm^2) on the surface. A summary of the IR datasets, collected and lost, appears in Appendix 13.

At higher altitudes the IR spectra are generally averaged over one probe revolution, but placed into 'bins' relative to the Sun to acquire azimuthal dependence information. The upward looking spectrometer data is place in 4 bins, and the DLIS data is placed in 8 bins.

During the calibration cycles the IR data are not averaged, but taken as quickly as possible with set exposure times.

In the Spectrophotometric cycles many separate DLIS exposures are taken as quickly as possible while maintaining a good exposure levels to optimize ground coverage.

Appendix 2 summarized the IR data transmitted during the Titan descent.

The following table summarizes the characteristics of the IR data types taken during the Titan descent:

Type of IR	LBL size (KB)	TAB size (KB)	# Data Columns	Regions	Comments
Combo, Binned - ULIS	23	28 to 31	24	4	Typical Data
Combo, Binned - DLIS	23	28 to 31	24	8	Typical Data
Combo, Calibration Cycle	15	6	4	1	Calibration Lamps on and off
Combo, Long (Cal cycle)	14	4	2	1	Long Exposure - Shutter Open only.
Combo, Near Surf.	15	6	4	1	Long Exposure - Short Collection
Combo, NS, no dark.	14	4	2	1	Only shutter open data.
DLIS Spectrophotometric	14	4	2	1	DLIS only, short collection time
Combo, on surface	23	28	24	8	Short Exposure - Long Collection

The first two rows in the table ('Binned' data) are the typical IR spectra taken during most of the descent, especially in the upper atmosphere. The second two rows are the data taken during the (nominally 4, but actually only 3) calibration cycles during the descent. The 'Combo, Near surface" data is the snapshot data taken quickly as the probe approached Titan's surface; it is interspersed with the "Combo, NS, no dark' exposures (darks skipped to speed data taking). During the two Spectrophotometric cycles, only downward looking data was taken, rapidly to get a spectral map of Titan's surface. The values in the last row are the IR datasets taken while the probe was resting on Titan's surface.

The columns of the table help delineate the type of data in the archive. ' LBL size' is the size of the label file in the PDS archive in kilobytes. 'TAB size' is the size of the associated table file in the archive. # Data Columns is the number of columns of data in the table file, and Regions tells the number of azimuthal bins (regions) that the data is broken into.

5.11.1 Binned IR Data Example

Most of the IR spectra taken during the Titan descent were binned into azimuthal regions relative to the Sun.

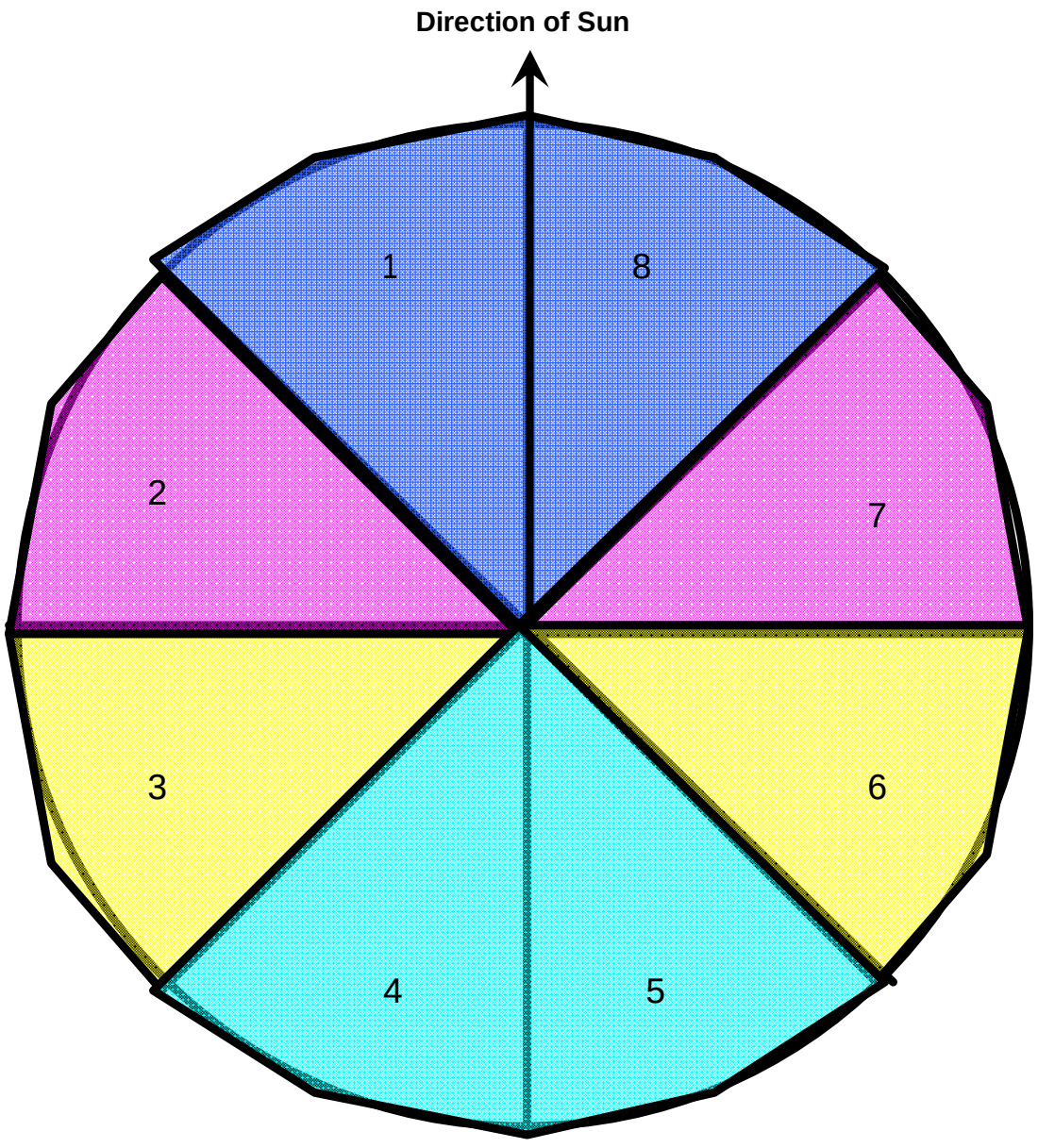

Figure 5.11-1 - Azimuthal regions for binned IR spectrometer measurements. The eight numbers identify the 8 DLIS bins, and the colored regions show the 4 ULIS bins. Note the ULIS bins are not contiguous, but symmetrical relative to the Sun vector.

We will use a dataset taken at about 30 km altitude during the Titan Descent for our example:

Filename: IR_0048_010745_4377
Mission Time: 4065.4377 seconds
Altitude: 29.60 km (label file), 29.91 km (DTWG 2011)
DLIS bins 8 (#1 through #8)
ULIS bins 4 (#11 through #14)
Cycle Info.: #45, No-Image
Temperature: 217.7 K (indicated, ~208 K actual)
Detector_ID "IR_COMBINED"
Lamp State: 0000
Columns: 24
Rows: 150

The table file (IR_0048_010745_4377.LBL) contains 4 tables. The first 150 rows are the Data Table, which contains the measured intensity in DN per sample (inverted as described above, dark 65,000 dn, bright 0 dn). Rows 152 and following contain the 'g' structure described in Appendix 36 and below.

The g structure contains information about the observation's exposure time and azimuthal distribution. It consists of 3 tables, the Regions array (g.regions), the sample Readings array (g.reading), and the Bins array (g.bins).

The Regions array defines, in azimuthal space, where the bins (regions) are relative to the Sun vector. Here is the Regions array for our sample dataset:

region (bin)	Start Az (deg*100)	End AZ (deg*100)	ULIS bin #	DLIS bin #
1	0	4500	11	1
2	4500	7000	12	2
3	9000	13500	13	3
4	13500	18000	14	4
5	18000	22500	14	5
6	22500	27000	13	6
7	29000	31500	12	7
8	31500	36000	11	8

There are eight bins, as shown in the diagram above. The first bin (#1) extends from the Sun 45 degrees CCW as viewed from above, the second from 45° to 90°, etc. The first bin is identified as DLIS bin #1 and so on to DLIS bin #8, The ULIS bins are different as they are not distributed in sequence around the circle, but rather symmetrically about the Sun vector. So the first ULIS bin is designated ULIS bin #11, and corresponds to DLIS bins 1 & 8, therefore extending from -45 degrees to +45 degrees from the Sun vector. ULIS bin #12 is two non-contiguous regions corresponding to DLIS regions 2 & 7 (the pink regions in the above figure), etc.

The next array in the file is the Reading table. It reports, in chronological order, how the data was binned and the corresponding exposure times. The left 6 columns are the Reading table for our sample dataset, and the right 3 columns are to aid explanation.

Rotation	Bin (region)	Start Time (sec * 10,000)	Collection Time (8.064 ms steps)	Shutter Time (8.064 ms steps)	Sample Time (8.064 ms steps)		Lapsed time start to start (s)	Collection Time (s)	Lapsed - collection (steps)
1	3	40654412	342	168	84		2.774	2.758	2.0
1	4	40682152	342	168	84		2.782	2.758	3.0
1	5	40709972	342	168	84		2.774	2.758	2.0
1	6	40737713	342	168	84		4.000	2.758	154.0
1	7	40777710	190	92	46		1.548	1.532	2.0
1	8	40793193	342	168	84		2.782	2.758	3.0
1	1	40821014	342	168	84		2.895	2.758	17.0
1	2	40849964	190	92	46		2.774	1.532	154.0
2	3	40877704	346	170	85		2.798	2.790	1.0
2	4	40905686	346	170	85		2.790	2.790	0.0
2	5	40933588	346	170	85		2.790	2.790	0.0
2	6	40961489	346	170	85		4.040	2.790	155.0
2	7	41001890	190	92	46		1.540	1.532	1.0
2	8	41017292	346	170	85		2.798	2.790	1.0
2	1	41045274	346	170	85		2.943	2.790	19.0
2	2	41074707	190	92	46		2.798	1.532	157.0
3	3	41102689	346	170	85		2.806	2.790	2.0
3	4	41130752	346	170	85		2.814	2.790	3.0
3	5	41158895	346	170	85		2.806	2.790	2.0
3	6	41186958	346	170	85		4.048	2.790	156.0
3	7	41227439	194	94	47		1.573	1.564	1.0
3	8	41243164	346	170	85		2.806	2.790	2.0
3	1	41271227	346	170	85		2.951	2.790	20.0
3	2	41300741	194	94	47			1.564	

The Rotation column reports the spin rotation over which the data was collected. The data is often more that one probe rotation in length. The Bin column shows which azimuth region the data is collected into. The Start Time is the mission time a the start of the collection in seconds times 10,000 (i.e. the first entry is at T0+4065.4412 seconds). The Collection Time is the total spectrometer operation time associated the entry, in 8.064 ms steps (i.e. the spectrometer operated for 342 * 8.064 = 2758 ms during the collection of bin 3 on the first rotation). The Shutter Time is the total number of steps that the shutter was open. For the first entry this was 168 * 8.064 = 1355 ms. The Sample time is the integration time between readings, which is half the sample time, i.e. two readings for each shutter open event. This is a typical data collection scheme called a 1-2-1 where the shutter is closed for one sample period (dark), open for two sample periods (bright), then closed for the final sample (dark). This was obviously done twice during the first collection event to accumulate a Collection Time of 342 steps.

The next three columns elucidate the instruments activity. The Lapsed time is the time between beginnings of data collection from one bin to the next. The next is the total spectrometer operation time during that collection, the difference is the time the instrument spent doing other things between collection events.

The final table in the file is the Bins table, which summarizes the data collected by bin (region), and related it to the Data table columns.

Bin #	0=DLIS, 1=ULIS	0=Open, 1=Closed	Total Shutter open time (sec * 10^4)	# samples	Data Table Column
1	0	0	40965	6	0
2	0	0	22417	6	1
3	0	0	40965	6	2
4	0	0	40965	6	3
5	0	0	40965	6	4
6	0	0	40965	6	5
7	0	0	22417	6	6
8	0	0	40965	6	7
1	0	1	40965	6	8
2	0	1	22417	6	9
3	0	1	40965	6	10
4	0	1	40965	6	11
5	0	1	40965	6	12
6	0	1	40965	6	13
7	0	1	22417	6	14
8	0	1	40965	6	15
11	1	0	81930	12	16
12	1	0	44835	12	17
13	1	0	81930	12	18
14	1	0	81930	12	19
11	1	1	81930	12	20
12	1	1	44835	12	21
13	1	1	81930	12	22
14	1	1	81930	12	23

The information in this table, in conjunction with the data table, can be used to determine the data rate for each bin. The exposure time in seconds per sample is determined by dividing column 3 by column 4 (i.e. 4.0965 seconds / 6 samples for bin #1). Thus the data rate is determined by:

DN/s = (data value closed - data value open) / [Bins(3,i) / Bins(4,i)]

For example, the first pixel of DLVS, bin 1 has a data value open of 52,230 DN/sample (from Data table column 0) & and a data value closed of 52,241 (from column 8), so;

Rate = (52,241 - 52,230) / (4.0965 / 6) = 16.1 DN/s

This is unusually low because this is not an active pixel (i.e. pixels 7 thru 142).

To extend our example let us consider the first 20 active pixels of bins 1, 8 and 11 to determine the net flux over this region. The data is presented in the table below:

Pixel	Row	Bin 1 - DLIS shutter open	Bin 1 - DLIS shutter closed	Bin 8 - DLIS shutter open	Bin 8 - DLIS shutter closed	Bin 11 - ULIS shutter open	Bin 11 - ULIS shutter closed	Bin 1 - DN/s	Bin 8 - DN/s	Bin 11 DN/s
7	8	48918	51264	48868	51258	55190	55738	3436.1	3500.5	802.6
8	9	35460	36932	35370	36830	55083	55898	2156.0	2138.4	1193.7
9	10	46487	47621	46446	47606	54602	55479	1660.9	1699.0	1284.5
10	11	50686	51544	50658	51538	54667	55520	1256.7	1288.9	1249.4
11	12	49814	50338	49786	50328	54459	55252	767.5	793.8	1161.5
12	13	51104	51456	51092	51449	55201	55925	515.6	522.9	1060.4
13	14	50972	51284	50956	51279	55078	55738	457.0	473.1	966.7
14	15	51266	51500	51256	51495	55155	55766	342.7	350.1	894.9
15	16	51366	51544	51361	51538	55002	55487	260.7	259.2	710.4
16	17	51122	51432	51109	51427	52724	53056	454.0	465.8	486.3
17	18	50698	51502	50672	51502	55210	55717	1177.6	1215.7	742.6
18	19	49162	51238	49109	51223	54911	55900	3040.6	3096.3	1448.6
19	20	46534	51434	46437	51424	53987	55618	7176.9	7304.3	2388.9
20	21	41214	50034	41044	50024	53271	55650	12918.3	13152.7	3484.4
21	22	38322	51044	38101	51039	52770	55772	18633.5	18949.8	4396.9
22	23	38310	51536	38080	51532	52339	55807	19371.7	19702.7	5079.5
23	24	40982	51387	40796	51382	52145	55839	15239.8	15504.9	5410.5
24	25	45200	51411	45076	51409	52394	55972	9097.0	9275.7	5240.6
25	26	48252	51362	48178	51358	52547	55746	4555.1	4657.6	4685.5
26	27	50107	51372	50070	51370	52827	55425	1852.8	1904.1	3805.2

The first thing to note is that in general pixels numbers start at zero (0 to 149), while the PDS Data table starts at 1 (1 to 150), so when using the DISR calibration equations it is necessary to make this adjustment.

Columns 3 through 8 in the above table are directly from the Data table in the PDS file (IR_0048_010745_4377.TAB). The Data Table column numbers are as identified in the Bins Array for Bins 1 & 11 (columns 0, 8, 7, 15, 16 & 20). The values for DN/s are calculated as described above, also using the information from the Bins Array.

DN/s = (data value closed - data value open) / [Bins(3,i) / Bins(4,i)]

Even though the DN rate for the ULIS is sometimes lower than that of the DLIS, its responsivity is also considerably lower so the observed brightness is higher.

Absolute Responsivity...

To calculate radiance we apply the absolute responsivity as described in section 4.1 ("Response of the DLIS") of Reference 14, the IR spectrometer calibration document in the PDS archive. The Absolute Responsivity must be interpolated (or in this case extrapolated) to the temperature of the observation. Below are graphs of the DLIS and ULIS Absolute Responsivity

[in (DN/s) per {Watts/(m^2-u-sr)}] at the lowest lab temperature (189°K) and our observation, 177°K.

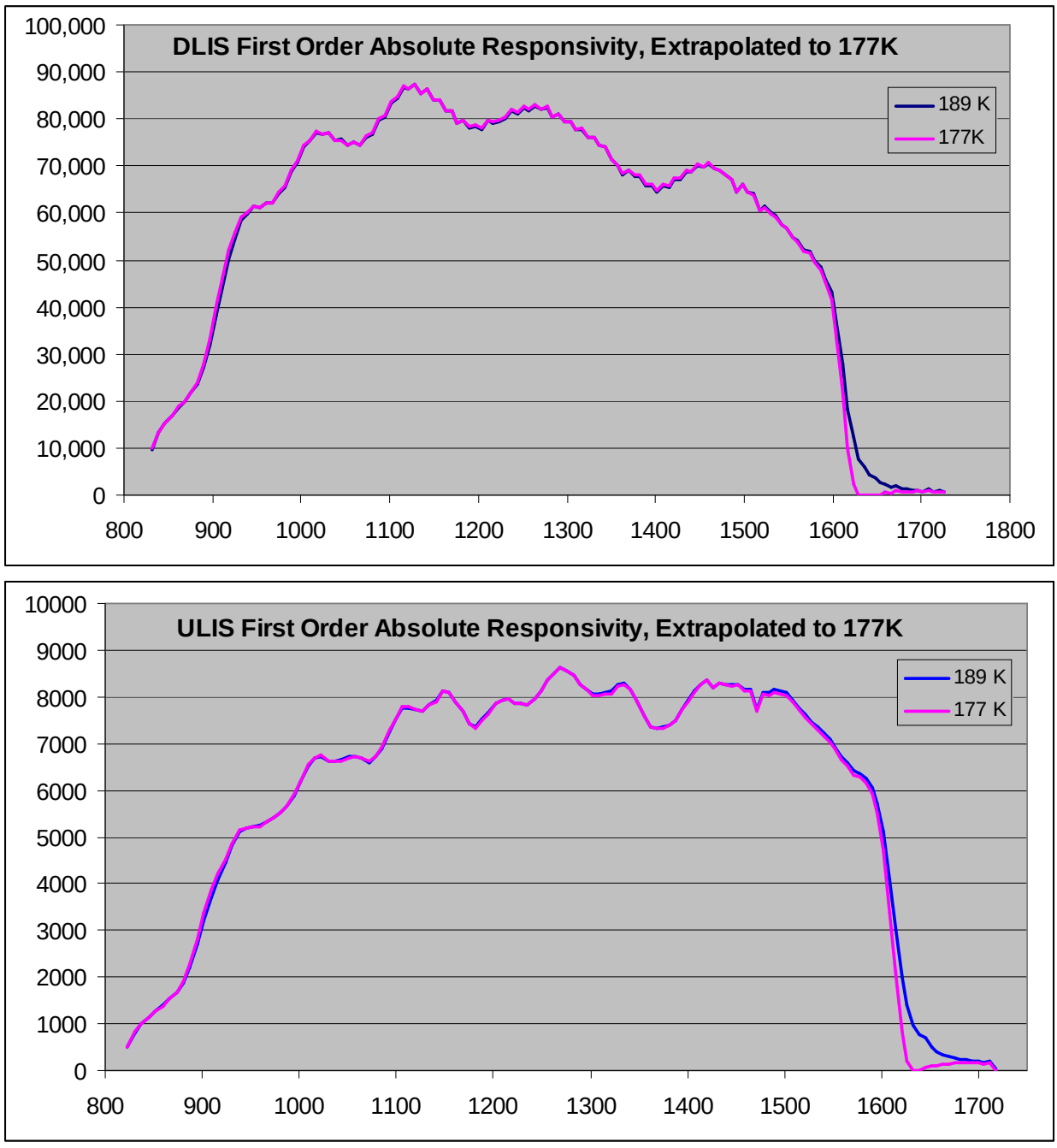

Figure 5.11-2: Absolute Responsivity for IR spectrometers in [DN/s] / [W/(m2-u-sr)] vs. Wavelength (in nm). The blue plot is the coldest measured lab data (189K), and the red line is an extrapolation to our temperature of interest.

Note that the responsivities drop considerably on each end of the wavelength scale, and it is difficult to make meaningful observations outside the range from 840 to 1600 nm. This is just the responsivity to first order light. The IR spectrometers are also responsive to second order

light from visible wavelengths. This effect becomes important for measurement above 1400 nm, and must be taken into effect using information from the DISR's visible spectrometers.

In order to apply the absolute responsivities we must know the wavelength for each pixel, which is a function of temperature as described in section 2 ("Wavelength calibration") of Reference 14 as:

$$\text{DLIS wavelength (nm)} = a + b*N + c*N^2$$

Where N is the number of the detector element (pixel) and the count begins with 0 and ends with 149. The values of a, b, and c depend on the temperature of the optics, with

$$a = 784.04 - 0.023725*T + 4.569\text{x}10\text{-}5*T^2,$$
$$b = 7.1568 + 0.0014118*T - 2.8753\text{x}10\text{-}6*T^2,$$
$$c = -0.0030065 - 1.4648\text{x}10\text{-}5*T + 3.0378\text{x}10\text{-}8*T^2$$

where T is the optics temperature.

The wavelength scale for the ULIS portion of the IR spectrometer is given by

$$\text{ULIS wavelength (nm)} = d + e*N + f*N^2$$

Where N is the detector element and the count begins with 0 and ends with 149. The values of d, e, and f depend on the temperature of the optics, with

$$d = 766.39 + 0.025199*T,$$
$$e = 7.5138 - 8.1082\text{x}10\text{-}4 * T,$$
$$f = -0.0059698 + 5.5991\text{x}10\text{-}6*T.$$

Again, T is the temperature of the optics.

In our case the optics temperature can be interpolated from the tables in Appendix 38 as 176.9°K.

An alternate (and more recent) method of determining the DLIS wavelength calibration is presented by Erich Karkoschka in Section 3.5 of Reference 15 as:

$$\text{DLIS wavelength (nm)} = 784.62 + 7.1082N - 0.001086N^2 - 0.000018N^3$$

where N is the pixel index (i.e. 0-149) ranging from 6 to 143 on the light sensitive part of the DLIS. This calibration accounts for changes in the index of refraction of the air during the Titan descent.

In order to calculate the net flux we need to adopt a common wavelength scale. Here we adopt the ULIS scale, and interpolate the DLIS data to that scale.

Wavelength (nm)	ULIS Bin 11 DN/s	Average DLIS Bins 1 & 8, DN/s	ULIS AbsResp	DLIS AbsResp	ULIS 1st Order	DLIS 1st Order	Net Flux
822.2	802.6	805.7	515.3	5338.3	1.56	0.151	1.105
829.5	1193.7	2274.0	822.7	8793.2	1.45	0.259	0.936
836.8	1284.5	2644.8	1014.4	12248.1	1.27	0.216	0.825
844.1	1249.4	1853.7	1132.2	14777.1	1.10	0.125	0.768
851.3	1161.5	1422.3	1277.4	16465.8	0.91	0.086	0.646
858.6	1060.4	959.1	1386.9	18255.3	0.76	0.053	0.559
865.8	966.7	612.8	1531.7	19622.0	0.63	0.031	0.471
873.1	894.9	484.2	1678.7	21337.8	0.53	0.023	0.401
880.3	710.4	387.8	1911.0	23249.9	0.37	0.017	0.279
887.5	486.3	289.8	2257.6	26661.1	0.22	0.011	0.161
894.7	742.6	391.8	2817.4	31586.7	0.26	0.012	0.197
901.9	1448.6	948.8	3373.7	38103.9	0.43	0.025	0.318
909.1	2388.9	2446.3	3868.1	44461.5	0.62	0.055	0.442
916.3	3484.4	5870.5	4203.4	50397.5	0.83	0.116	0.560
923.4	4396.9	11155.1	4520.0	54613.4	0.97	0.204	0.604
930.6	5079.5	16945.7	4864.6	58141.2	1.04	0.291	0.591
937.7	5410.5	19300.9	5147.6	59955.5	1.05	0.322	0.573
944.9	5240.6	16677.3	5189.9	61194.3	1.01	0.273	0.579
952.0	4685.5	11102.5	5203.3	61273.5	0.90	0.181	0.565
959.1	3805.2	6009.1	5218.8	61863.7	0.73	0.097	0.496

Table: IR spectrometer measurement at ~30 km altitude at the wavelength of the ULIS, pixels 7 thru 26, and corresponding in azimuth to ULIS bin 11. Absolute Responsivities are in [DN/s] per [W/(m2-u-sr)] and are extrapolated from the laboratory data to the observation temperature of 117° K. First order radiance in W/(m2-u-sr), and net flux over π/4 radian slice (bin 11) in W/(m2-u).

The following plots present the spectral radiance and Net Flux over the useful range of the DISR IR spectrometers for the example dataset (@30 km altitude) with the second order effects included. The radiance are the azimuthal average. The flux is presented per ULIS bin as shown.

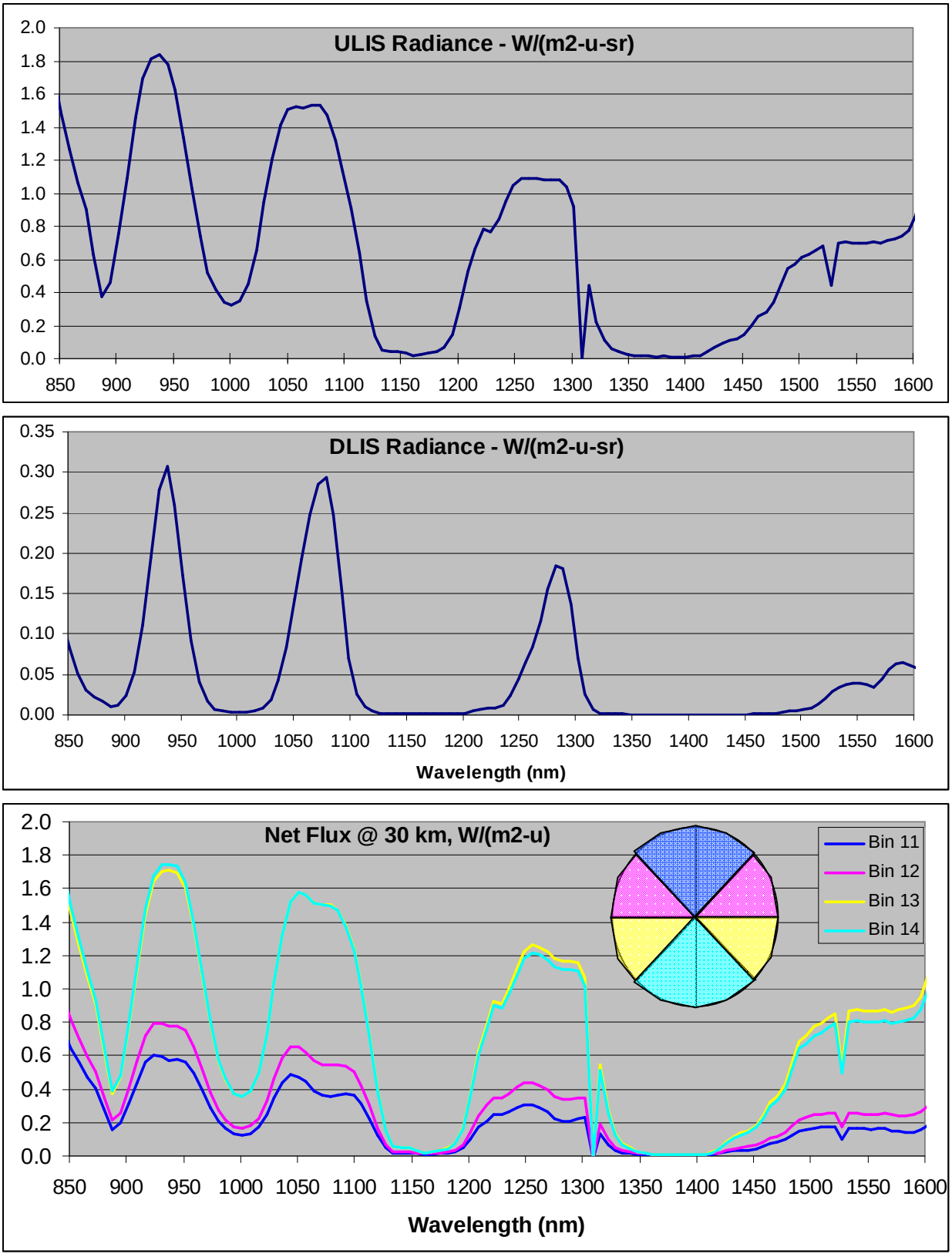

Figure 5.11-3: Up & down radiance spectra and net flux for our 30 km altitude example.

5.11.2 DLIS Near-Surface Example

The following example shows the reduction of the Downward Looking Infra-red Spectrometer (DLIS) data from 1100 meters to the surface. The spectra transmitted during this period are summarized in the following table.

Table 5.11.2 -1: Table of near-surface DLIS spectra including sequence #, epoch, altitude, cycle #, # of rows, type, lamp state, exposure time, collection time and temperature.

Archive Filename	IR	Time	Alt.	Cycle	Rows	Type	Lamp	Exp.	Collect	Temp.
	#	sec	m	#				ms	s	K
IR_0186_022334_6904	186	8614.7	1173	79	4	Comb	0000	1991.8	8.02	189.9
IR_0188_022424_4648	188	8664.5	940	81	4	Comb	0000	1991.8	8.02	189.9
IR_0190_022512_4610	190	8712.5	717	83	4	Comb	0000	1991.8	8.02	189.8
IR_0192_022602_8175	192	8762.8	485	85	4	Comb	0001	1991.8	8.02	189.7
IR_0194_022705_1821	194	8825.2	203	91	2	Comb	0001	999.9	1.02	189.6
IR_0196_022712_0214	196	8832.0	171	93	2	Comb	0001	999.9	1.02	189.6
IR_0199_022725_0398	199	8845.0	112	96	2	Comb	0001	999.9	1.02	189.6
IR_0202_022730_1726	202	8850.2	89	99	2	Comb	0001	999.9	1.02	189.6
IR_0204_022733_5947	204	8853.6	73	101	2	Comb	0001	999.9	1.02	189.5
IR_0206_022737_0187	206	8857.0	58	103	2	Comb	0001	999.9	1.02	189.5
IR_0208_022740_4448	208	8860.4	43	105	2	Comb	0001	999.9	1.02	189.5
IR_0210_022743_8699	210	8863.9	27	107	2	Comb	0001	999.9	1.02	189.5
IR_0213_022749_0091	213	8869.0	3	110	2	Comb	0001	999.9	1.02	189.5

Archive Filename is the name of the file as it exists in the archive's DATA directory (without the .TAB)
IR # is the sequence number of the IR dataset (which is also part of the archive file name),
Time is the mission time of the observation in seconds after T0
Cycle is the Descent Cycle number containing the observation
Rows is the number of rows of data in the dataset
Type is the IR observation type.
Lamp is the lamp condition, 0=off, 1=on for Cal A, B, C, & Surface Science Lamp.
Exp. is the exposure time in milliseconds
Collect is the collection time in seconds over which the observation is averaged.
Temp is the IR detector temperature in degrees Kelvin

Sadly the data taken at 3 meters and 42 meters above the surface did not have the shutter open (dark current exposures). The design was to have one dark current exposure every five measurements, however since many of the spectra near the surface were routed to the lost telemetry channel, 2 of the last 3 surviving exposures were darks.

Appendix 9 is a tabular summary of the raw data from 1173 meters through 486 meters. This data was taken in 4 column format which include columns of 1) DLIS shutter open, 2) DLIS shutter closed, 3) ULIS shutter open & 4) ULIS shutter closed data by wavelength, although only the first two columns (the DLIS data) are shown in the table for each altitude. Since photons remove charge from the device intensity increases with lower data numbers in the raw data (see figure below).

Appendix 10 presents the DLIS raw data transmitted below 250 m, which is in 2 column format where only ULIS and DLIS shutter open data is captured, except that for every 5th measurement, the shutter is inhibited (so a dark measurement is taken instead). The detector array's dark current can be determined by interpolating the shutter closed exposures in time (if

the dark current is changing significantly), or averaging shutter closed exposures that are at similar temperatures in order to reduce noise effects.

Below is a plot of the DLIS raw data taken at 1173 m above Titan's surface:

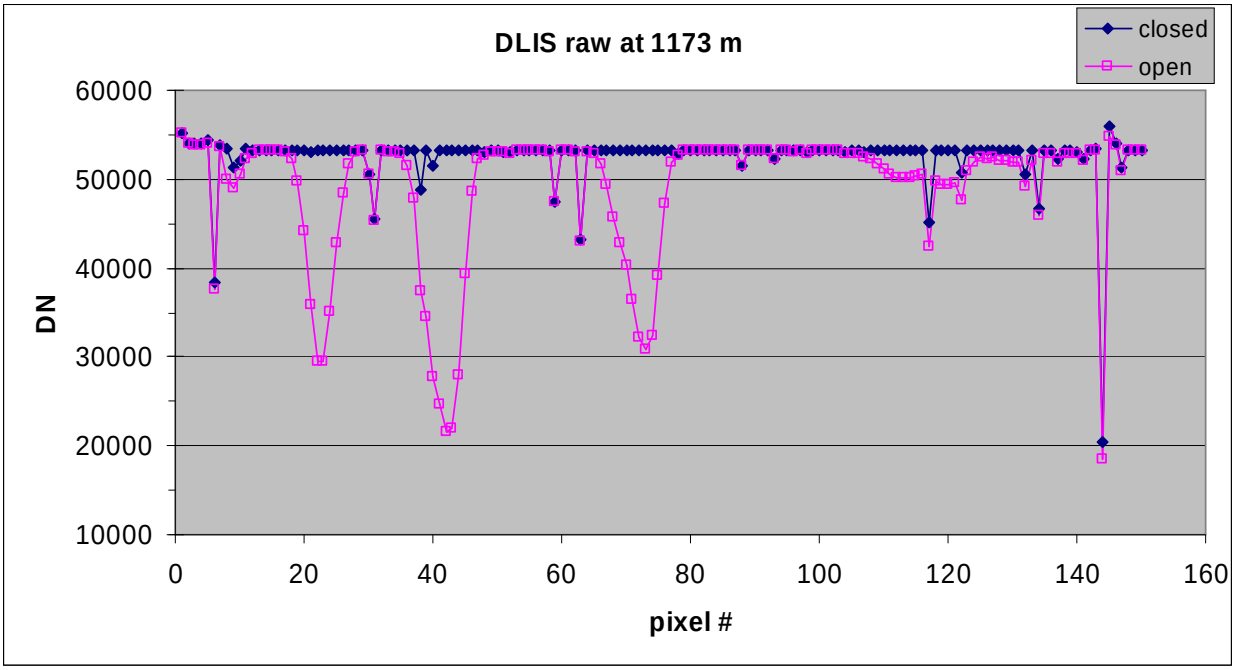

Figure 5.11-4: Raw DLIS data taken near Titan's surface

By subtracting the shutter open data from the shutter closed data, and dividing by the sample (exposure) time we obtain the measured IR signal in DN/second. This is done for the DLIS measurements below 1200 m (Appendices 9 & 10) and plotted below.

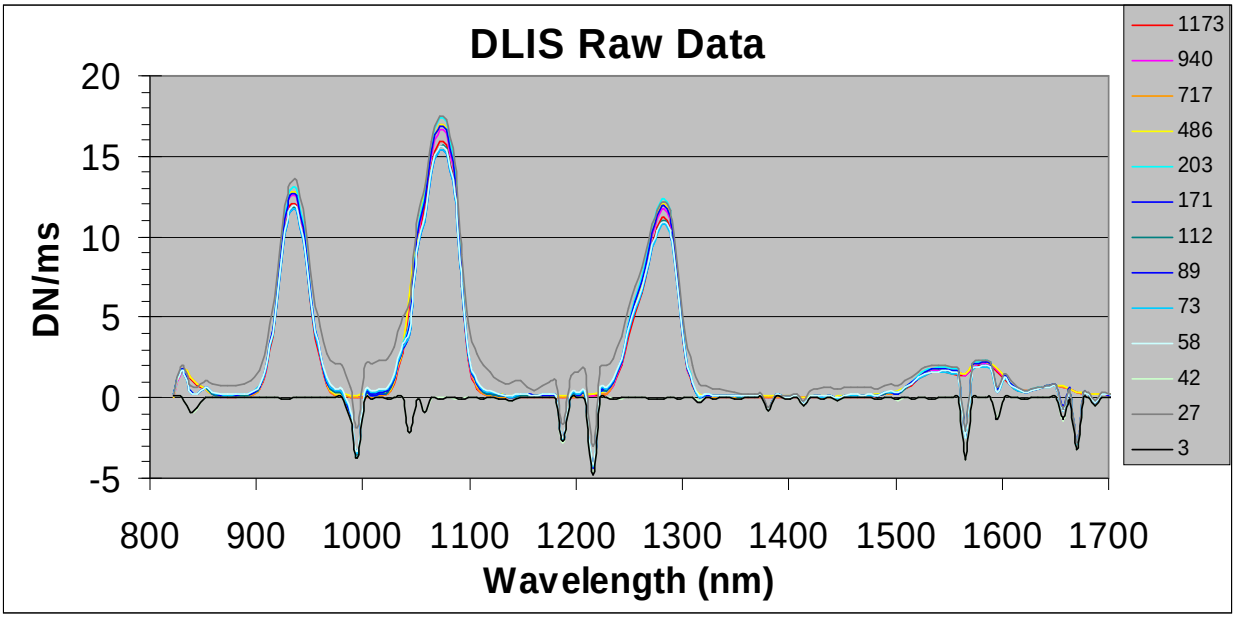

Figure 5.11-5: Raw DLIS data, dark subtracted.

Notice that in some areas the signal goes below zero, and there is considerable noise. This is due to radiation damaged pixels in the array. These can be removed by interpolation. The following plot shows the spectrum with these pixels filtered out.

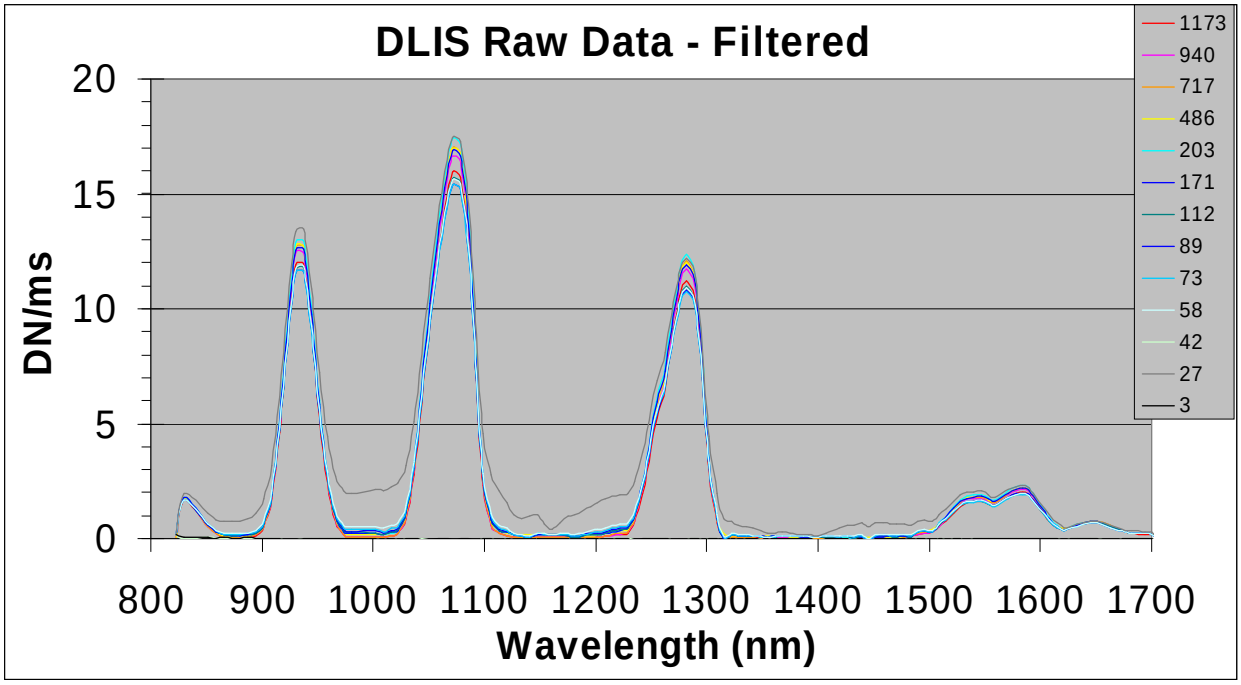

Figure 5.11-6. Raw DLIS data, dark subtracted and with the bad pixel filtered out.

Table 5.11.2 -2: listing of the bad pixels that were removed in the previous plot.

Wavelengths of 'Hot' pixels which were removed (nm).		
815	1188	1657
837	1215	1669
844	1381	1687
988	1413	1711
995	1565	1730
1044	1596	1735
1058	1602	1747

Careful examination of the preceding plot shows that the variation in spectral radiance is different within the methane windows (where the signal is strong) vs. between the methane windows (where the solar energy is absorbed by the atmosphere).

The plot below shows the variation in signal at four of the methane window wavelengths. As the probe approaches Titan's surface (from the right), the signal is fairly constant, perhaps increasing slowly, however at about 200 meters above the surface the signal decreases rapidly, down to around 50 meters, below which it begins to increase rapidly. These variations are open for speculation, but almost certainly the ratio of light from the Sun vs. Surface Science Lamp (SSL), which is on below 600 m, comes into play.

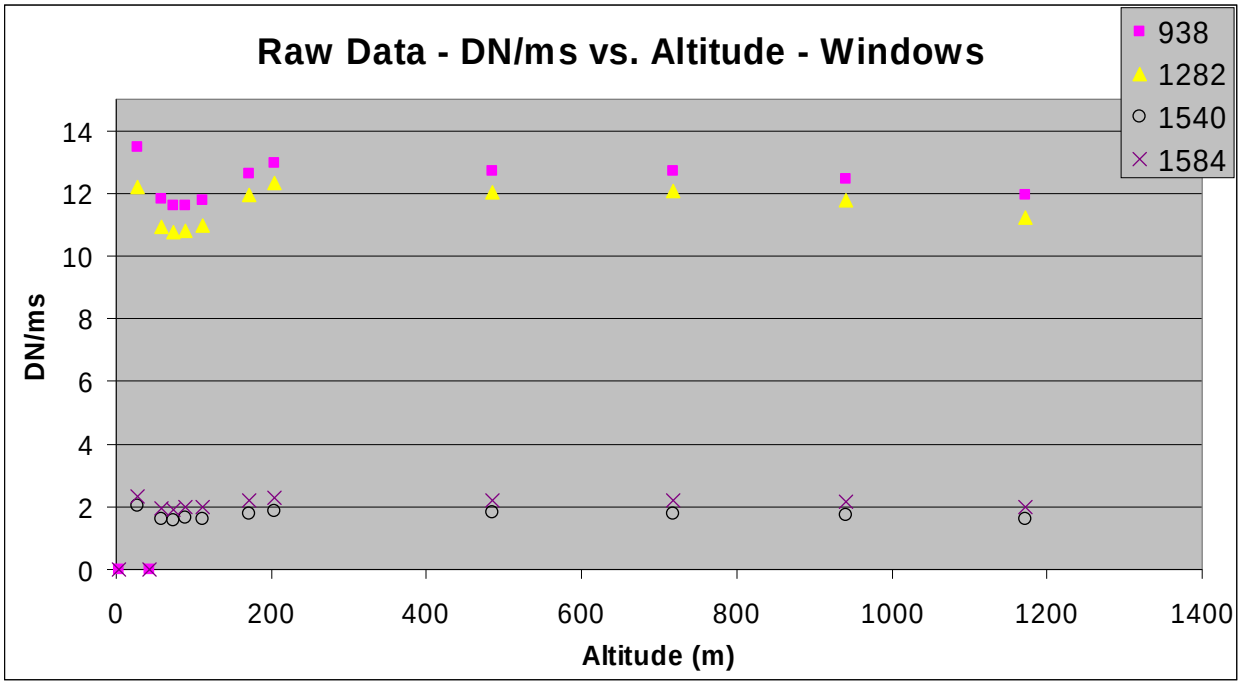

Figure 5.11-7: Raw DLIS data plotted in the methane windows vs. altitude

The situation in the methane absorption bands, where the SSL has less competition from the Sun, is somewhat different. The plot below shows the signal at 4 absorption band frequencies. As the probe descends, the surroundings are consistently dark at these wavelengths, until the SSL comes on (at 600 m). At this epoch the intensity increases and the spectrum shifts, as the increase at 1002 nm is proportional more than at the other wavelengths. The signal remains

fairly constant down to around 100 m, at which time the intensity increases and the spectrum continues to spread.

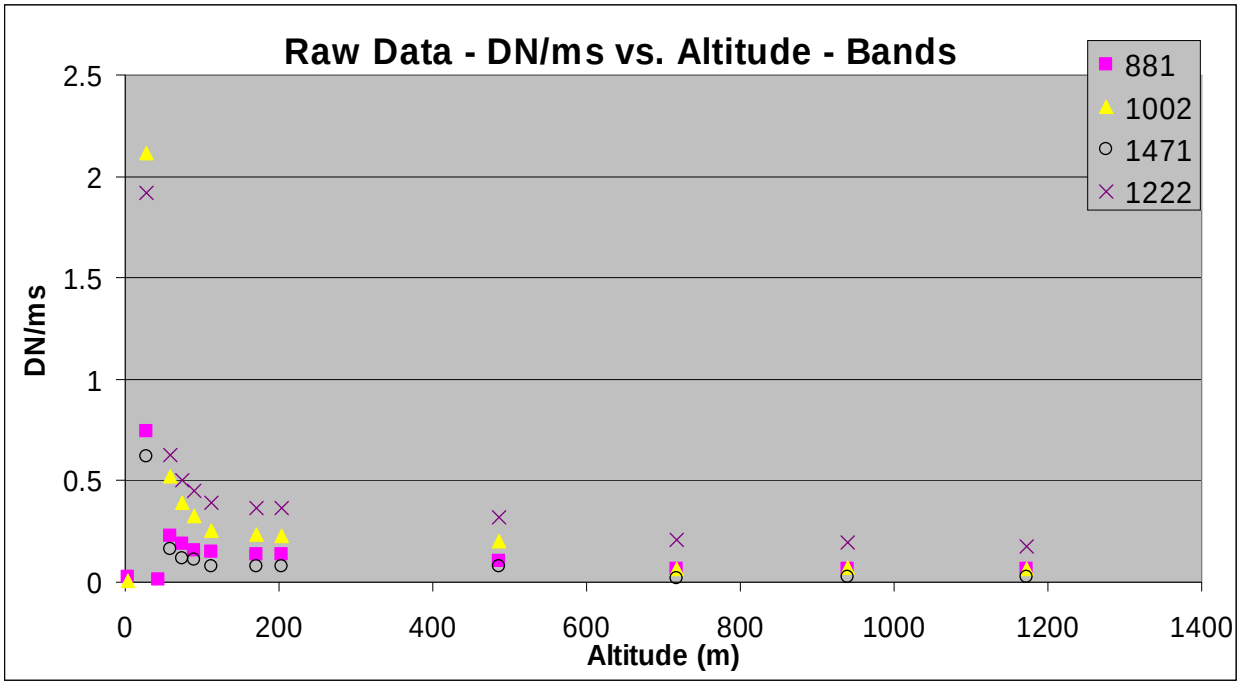

Figure 5.11-8: Raw DLIS data from the methane absorption bands plotted vs. altitude.

Caveats in working with IR spectrometer data...

There are at least two significant problems to be aware of when working with the IR spectrometer data. The first is that the spin rates and azimuthal direction were almost never what the in-flight software though it was during data-taking. Therefore, the data is not binned correctly and it is up to the user to create a model that re-apportions the data into the proper bins. This can be done by comparing the offset in azimuth between what the software predicted (i.e. pointing at the Sun at the beginning of observation for bin 1), and the actual azimuth at that epoch (from Appendix 5). And, by determining the error in spin rate from the Readings table in the data file vs. the actual spin rate calculated again from Appendix 5. Obviously not an exercise for the faint of heart. In at least one case (the data at 100.2 km) some of the bright (shutter open) data is in the dark (shutter closed) bin.

The second difficulty is that the IR system experienced difficulty with the Titan impact, and there is a significant offset introduced there. Perhaps movement of the optics or fibers. This is only a concern for analysis of the data taken on Titans surface of course.

The following plot is provided to give the reader a feeling for the scatter of the data. It is the average count rate (in DN/ms) for each bin collected during the Titan encounter. The calibration cycle, lamp-on data is removed. It shows the expected declining trend with time, but few bins with the Sun squarely in the FOV. Changes at the impact event (~8870 seconds) are apparent, but confusing. The probe is obviously not spinning during this period, but the data is not as stable as one might expect.

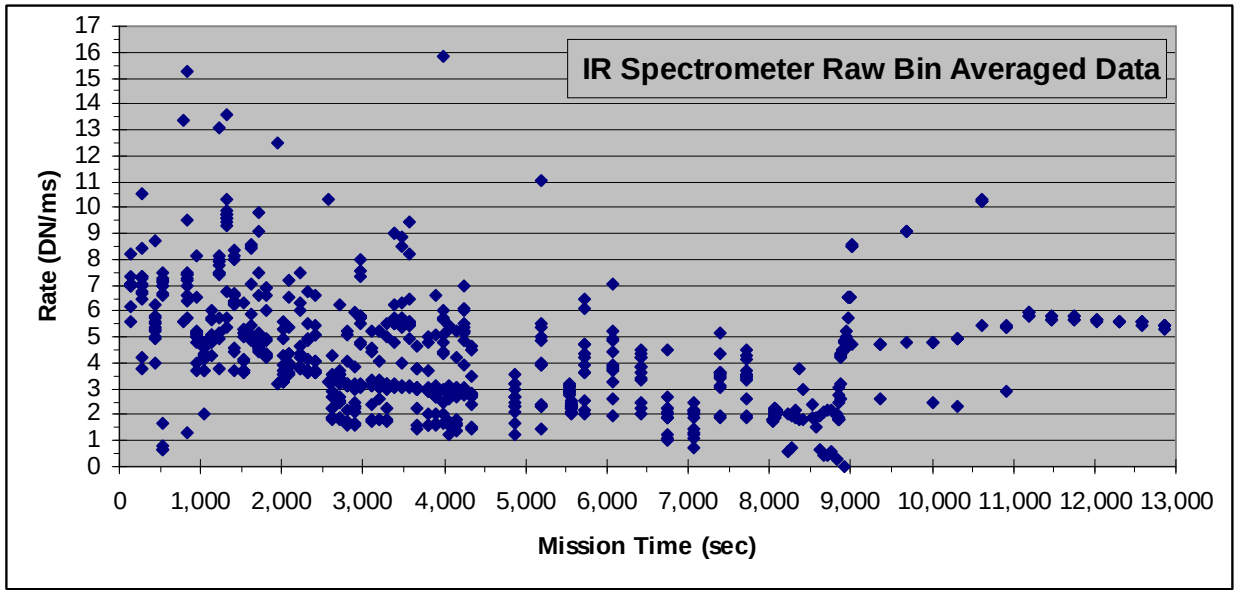

Figure 5.11-9: The average count rate for each IR spectra bin during the Titan encounter. Impact transients are apparent at ~8870 seconds. The calibration lamp-on data is well off this chart.

Cassini Cruise Phase Effects...

As discussed in section 5.6, many of the DISR detector systems exhibited changes in the absolute responsivity during the trip from Earth to Titan. The observed changes in the IR spectrometer system are small, and may be a combination of yellowing of the fiber optic bundles, and/or movement of the fibers during launch. The observations are presented below.

The changes in the IR system are small, generally less than 1%. There was some shift at launch, about 5% for the ULIS lamp B data, less for the rest. Overall the darkening of the fiber-optic bundles appears to be around 1% in the near IR from the lab calibration data.

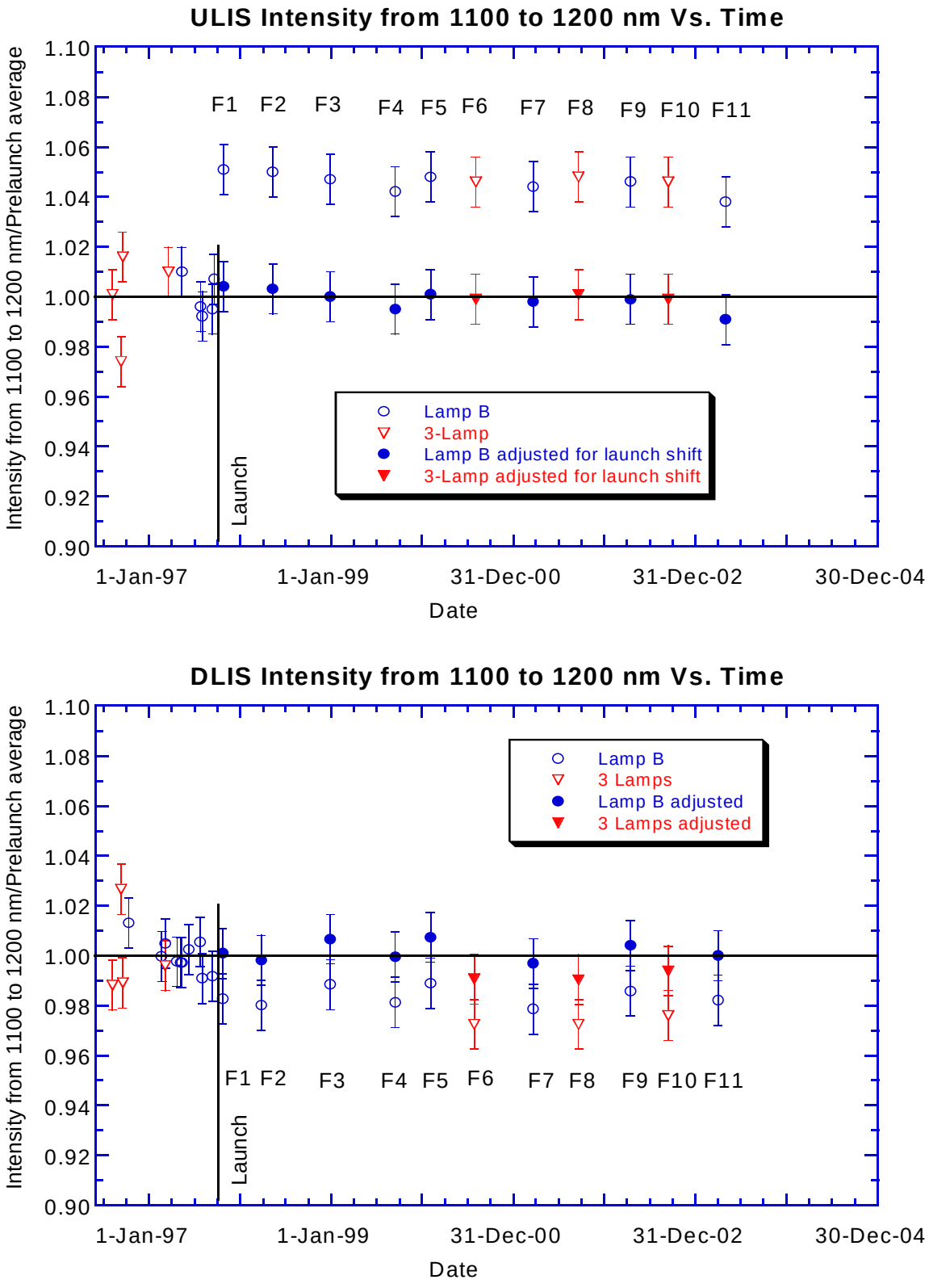

Figure 5.11-10: IR spectrometer calibration lamp response changes from lab calibration to Titan descent. ULIS on top, DLIS on bottom.

6.0 Derived Data Products (DDP)

The following Derived Data Products have been included in the archive. They represent a sample of the results of the DISR team's data analysis and reduction efforts, and provide a good reference for extended analysis. In general they show the measured spectral radiance, averaged over the instruments field of view.

DLIS/ULIS: A tabular presentation of the calculated light intensity at each wavelength of the IR spectrometers averaged over the field of view.

DLV/ULV: Two sets of tables, one presenting the Net counts measured during the descent after the detector offset is removed. The other presents the average violet light intensity over the photometer's pass band assuming a quadratic spectral shape (see Violet calibration documents for details).

DLVS/ULVS: Tables of the light intensity at each visible spectrometer wavelength, averaged over the field of view.

This figure presents the upward looking (downward streaming) spectral radiance near Titan's surface from the data in the DISR DDP archive. The IR is the average from 5.6 to 7.3 km altitude, the Visible is the ULVS average from 500 to 2300 m, and the Violet is the averaged ULV from 14 to 1400 m above the surface. The data is also presented in tabular form in Appendix 8.

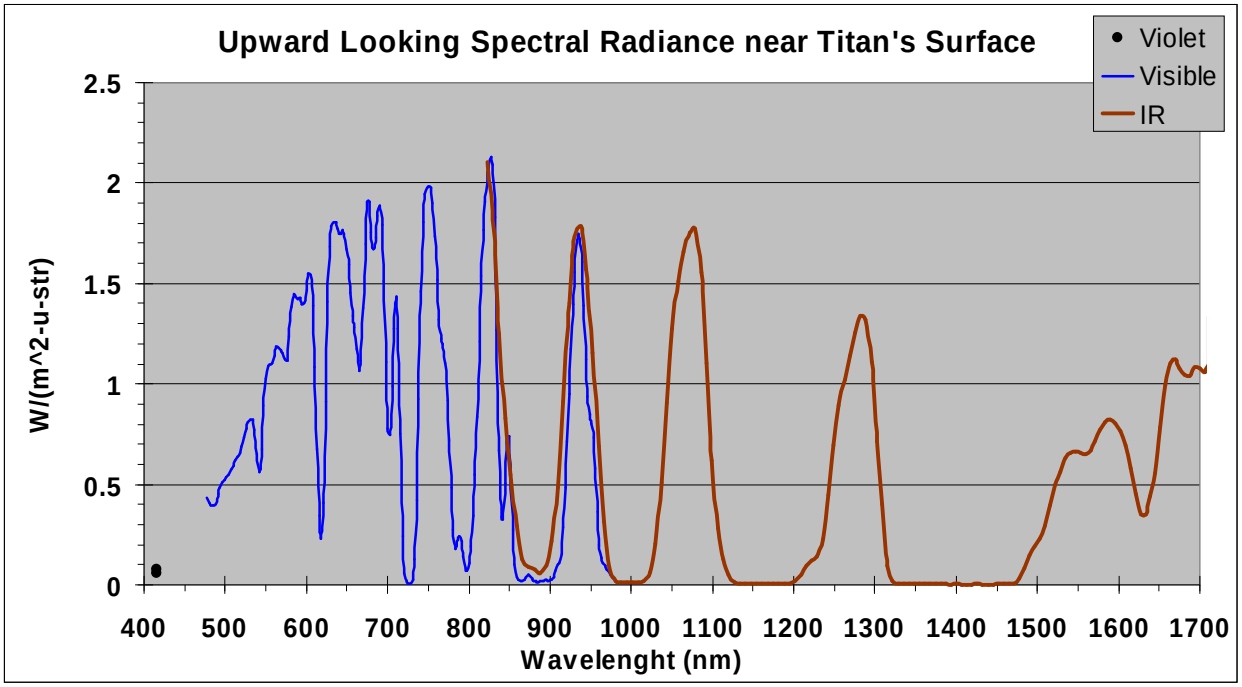

Figure 6-1: Plot of the spectral radiance near Titan's surface from all three DISR upward looking spectrometers.

7.0 Higher Level Data

In the Higher Level Data directory (DATA/HIGHER_LEVEL_DATA) are image posters in JPEG format generated as mosaics of the DISR images by Erich Karkoschka. There are 7 posters in the directory, along with the following description of each:

Description of Titan Posters
3 April 2006

Poster A - View's from the probe, in the 4 Cardinal Directions (N,S,E,W) at 5 different altitudes above Titan's surface.

Poster B - Mercator Projection of the view from the Huygens probe at 4 different altitudes.

Poster C - Nadir, Stereographic (fish-eye) view of Titan's surface from 6 different altitudes. Shows the haze layer at 20-21 Km.

Poster D - Mercator projection of Huygens probe view from 10 Km Altitude.

Poster E - Distorted fish-eye projection (in nadir direction) of the DISR images when the Huygens Probe was 5 Km above Titan's surface.

Poster F - Composite view of DISR's images taken while the Huygens Probe was setting on Titan's surface, juxtaposed with a similarly scaled picture taken on the Moon's surface. Objects near the center of the picture are roughly the size of a man's foot while objects at the horizon are a fraction of a man's height.

Poster G - When printed on letter sized paper this poster show's the size of the 'rocks' on Titan's surface in their true size.

The posters are made up of images that have been sharpened and photometrically adjusted to optimize structure visibility while minimizing the introduction of false features. The images have been colorized using the DLVS data. The variations in sharpness within the images are a result of the viewing and phase angle of the exposures and whether high resolution (HRI) coverage was available.

N.B. "Letter sized" paper is an American standard page of 8.5 inches by 11 inches.

The probe traveled Eastward during the descent, and the ultimate landing location is close to the center of the images in Poster C. The final DISR pointing direction is not well known, but is generally southward.

8.0 List of Appendices

The following table lists the Appendices that complete this document.

1 F0 - A table of values of the solar flux used in DISR data analysis.
2 IR data - A list of the IR datasets & associated attributes.
3 Image pointing - A list of the position and attitude of the probe at the image epochs.
4 E/W tilt - A table of probe east-west tilt as a function of mission time
5 Azimuth - A table of probe azimuth history.
6 Descent Cycles - A listing of the DISR descent cycles history.
7 Altitude - A comparison of DDB and DTWG 2010 altitude profiles.
8 DDP Example - Tabular data of the examples used in the Derived Data Products section.
9 DLIS Example - Tabular data of the DLIS near-surface example in section 5.11.2
10 DLIS Raw - Tabular data of the DLIS near-surface data below 200 m (sec. 5.11.2)
11 Violet Cruise Darks - Table of the violet photometer dark history during cruise.
12 IR DDP table headers - The header entries for the IR spectrometer Derived Data Prod's.
13 Lost IRs - Information on IR datasets lost due to chain B failure.
14 Sun Position - Table of Sun's azimuth, elevation & solar zenith angle during descent.
15 EA Temperature - History of the DISR Electronics temperature during Titan descent.
16 Violet Measurements - A list of the Violet measurements taken & associated attributes.
17 DLV Bias - A table of the DLV measurements with their deduced bias offset.
18 Image Thumbnails - A graphical display of the DISR images by descent cycle.
19 NASAView - Information on obtaining NASAView image viewer.
20 Image datasets - A summary of the Image datasets & associated attributes.
21 ULV Sun Location - Listing of whether the Sun was in the FOV for each ULV.
22 Violet Rel Spat - Tables of the relative spatial response for the Violet photometers.
23 Thermistors - Graphic showing the location of the DISR thermistors.
24 Dark Current Data - A summary of the CCD Dark Current datasets.
25 Square Rooter Table - 12 bit to 8 bit conversion table used for DISR images.
26 F16 Darks - Summary of the CCD dark data from the last in-flight checkout.
27 Imager RSR - Relative Spectral Response of each DISR imager at 239°K
28 Sun Sensor Data - A listing of the DISR Sun sensor data and attirbutes.
29 Visible Spectrometer Wavelength Scales - Tables of the ULVS & DLVS wavelengths.
30 Visible Spectrometer Resolutions - Tables of FWHM for ULVS & DLVS.
31 SA RSR tables - Relative Spectral Response tables for the SA channels.
32 SA AbsResp - Pixel map Absolute Responsivity 'M' coefficients for the SA camera.
33 SA RSR - Relative Spectral Response coefficients for the SA camera
34 SA Data - Listing of the Solar Aureole data & associated attributes.
35 CCD Dark Current - An Improved Method for Determining CCD Dark Current in DISR.
36 IR 'g' structure - An explanation of the IR spectrometer's g.structure tables.
37 Bibliography - The DISR publication bibliography.
38 Temperatures - A table of the DISR internal temperatures
39 Visible DDP table headers - The header entries for the Visible spectrometer DDP's.
40 Visible Spectrometer Data Summary - A summary list of the Vis. Spec. archive datasets.

9.0 References, Terms & Acronyms

1 - "The Descent Imager/Spectral Radiometer (DISR) Aboard Huygens", M. Tomasko etal., ESA_SP_1177, 1997, PDS DISR Archive DOCUMENT/DISR_SUPPORTING_DOCUMENTS/ESA_SP_1177/DISR_INSTRUMENT

2 - "A model of Titan's aerosols based on measurements made inside the atmosphere", M. Tomasko etal., Planetary and Space Science 56 (2008) 669–707

3 - "The unusual phase curve of Titan's surface observed by Huygens' Descent Imager/Spectral Radiometer", S.E. Schröder, H.U. Keller, Planetary and Space Science 57 (2009) 1963-1974

4 - "Calibration of Upward and Downward Looking Violet Photometers", M. Tomasko, M. Prout, and L. McFarlane, PDS DISR Archive, hpdisr_0001/DOCUMENT/DISR_CALIBRATION_DOCUMENTS/VIOLET_PHOTOMETERS/VIOLET_PHOTOMETER_CAL_DOC

5 - "DISR imaging and the geometry of the descent of the Huygens probe within Titan's atmosphere", Erich Karkoschka, et al., Planetary and Space Science 55 (2007) 1896-1935

6 - "Calibration Report for the Imagers of the Descent Imager/Spectral Radiometer Instrument aboard the Huygens Probe of the Cassini Mission", L. R. Doose, B. Rizk, E. Karkoschka, and E. McFarlane, PDS DISR Archive, hpdisr_0001/DOCUMENT/DISR_CALIBRATION_DOCUMENTS/IMAGERS

7 - "Dark Current Estimation for the CCD of the Descent Imager/Spectral Radiometer aboard the Huygens Probe of the Cassini Mission", L. Doose and A. Eibl, PDS DISR Archive, hpdisr_0001/DOCUMENT/DISR_CALIBRATION_DOCUMENTS/CALIBRATION_STANDARD/DARK_CURRENT

8 - "Experiment User's Manual" Diane Whiteaker, CDRL#-OP001 & SW002, MCR-93-1349 Rev: C, PDS DISR Archive, DOCUMENT/DISR_SUPPORTING_DOCUMENTS/EXPERIMENT_USERS_MANUAL, 13 Sep. 1996

9 - "Calibration of the Sun Sensor", M.G. Tomasko, PDS DISR Archive, hpdisr_0001/DOCUMENT/DISR_CALIBRATION_DOCUMENTS/SUN_SENSOR, 25 Feb. 2000.

10 - "Notes on the use of the Visible Spectrometer of the Descent Imager/Spectral Radiometer (DISR) Experiment on the Huygens Probe of Titan", PDS DISR Archive, hpdisr_0001/DOCUMENT/DISR_CALIBRATION_DOCUMENTS/VISIBLE_SPECTROMETERS, 29 June 2006

11 - "Calibration Report for the Visible Spectrometer on the Descent/Imager Spectral Radiometer (DISR) Experiment on the Huygens Probe", Martin Tomasko and Steffi Engel, PDS DISR Archive, hpdisr_0001/DOCUMENT/DISR_CALIBRATION_DOCUMENTS/VISIBLE_SPECTROMETERS

12 - "Limits on the size of aerosols from measurements of linear polarization in Titan's atmosphere", Tomasko etal., Icarus 204 (2009) 271–283, 2009

13 - "Calibration Report for the Solar Aureole Camera of the Descent Imager/Spectral Radiometer aboard the Huygens Probe of the Cassini Mission", M. G. Tomasko and L. E. Dafoe, PDS DISR Archive, hpdisr_0001/DOCUMENT/DISR_CALIBRATION_DOCUMENTS/SOLAR_AUREOLE, 27 April 2006.

14 - "Calibration Information for the Upward-Looking Infrared Spectrometer (ULIS) and Downward-Looking Infrared Spectrometer (DLIS)", PDS Archive, hpdisr_0001/DOCUMENT/DISR_CALIBRATION_DOCUMENTS/INFRARED_SPECTROMETERS/IR_SPECTROMETER_CAL_DOC, 20 February 2006.

15 - "The reflectivity spectrum and opposition effect of Titan’s surface observed by Huygens’ DISR spectrometers", Erich Karkoschka, Stefan E. Schroeder, Martin G. Tomasko & Horst Uwe Keller, Planetary and Space Science 60 (2012) 342-355

16 - "Methane absorption coefficients for the jovian planets from laboratory, Huygens, and HST data", Erich Karkoschka & Martin G. Tomasko, Icarus 205 (2010) 674-694

17 - "A soft solid surface on Titan as revealed by the Huygens Surface Science Package", John C. Zarnecki, et al, Nature 04211 (2005)

18 - "Bouncing on titan: Motion of the huygens probe in the seconds after landing", S. Schroeder, E. Karkoschka, R. Lorenz, Planetary and Space Science (2012)

19 - "DISR Engineering Data Companion Document", C. See, PDS Archive, 28 September 2012

Contributors

This document was compiled by Chuck See, UA-LPL, largely from the calibration and other documents originally generated by the DISR team.

DISR Team:

LPL ...
Martin Tomasko
Lyn Doose
Andrew Eibl
Bashar Rizk
Chuck Fellows
Erich Karkoschka
Lisa McFarlane
Mary Ann Pringle
Mike Prout
Peter Smith
Steffi Engel
Tsar

Worldwide...
Athena Coustenis
Bernard Schmitt
Bjoren Greiger
Bob West
Brent Archinal
Bruno B'ezard
Chris deBerg
Emmanuel Lellouch
Fritz Gliem
Larry Soderblom
Laura Ellen Dafoe
Mark Lemmon
Michael Kueppers
Michel Comes
Nick Thomas
Peter Rueffer
Randy Kirk
Stefan Schroder
Uve Keller
Wojciech Markiewicz

Others...
Bobby Kazeminejad
Dave Atkinson
Lyle Huber
Oliver Witasse
Ralph Lorenz
Reta Bebee
Stefan Schroder

Acronyms

AGC Automatic Gain Control
AR Absolute Responsivity
ALT-AZ Two axis (altitude & azimuth) calibration mounting system
CCD Charge Coupled Device (detector chip)
CDMU Command & Data Management Unit (on probe)
CPU Central Processing Unit
DCT Discrete Cosine Transform
DCS Data Compression System
DDB Descent Data Broadcast
DDP Derived Data Products
DISR Descent Imager and Spectral Radiometer
DLI1 Downward Looking Imager 1 (HRI)
DLI2 Downward Looking Imager 2 (MRI)
DLIS Downward Looking IR Spectrometer (DISR sub-instrument)
DLV Downward Looking Violet photometer (DISR sub-instrument)
DLVS Downward Looking Visible Spectrometer (DISR sub-instrument)
DN Data Number (fundamental digital output from the detectors)
DOF Degree of Freedom -

DTWG Descent Trajectory Working Group
EA DISR Electronics Assembly
EAICD Experimenter to Archive Interface Control Document
ESA European Space Agency
FF Flat Field
FM Flight Model
FOV Field of View
FTU Flight Test Unit
GSE Ground Support Equipment
HC Health Check (pre-programmed test routine)
HNS High Near Surface (descent cycle)
HRI High Resolution Imager, aka DLI1 (DISR sub-instrument)
I/F Ratio of Intensity (spectral radiance) to solar flux unit per sr.
IC Integrated Circuit
ICD Interface Control Document
IFC In-Flight Calibration (pre-programmed test routine)
IR Infra-Red
JPEG Joint Photographic Experts Group compression algorithm for images (aka JPG)
JPL Jet Propulsion Laboratory, Pasadena, CA
LNS Low Near Surface (descent cycle)
MNS Medium Near Surface (descent cycles)
MNS Medium Near Surface (descent cycles)
MRI Medium Resolution Imager, aka DLI2 (DISR sub-instrument)
NASA National Aeronautics and Space Administration
O+SR Offset plus Serial Register (dark current component)
PDS Planetary Data System
PSA Planetary Science Archive
RSR Relative Spectral Response
SA Solar Aureole (DISR sub-instrument)
SH DISR Sensor Head
SLI Side Looking Imager (DISR sub-instrument)
SMM Single Measurement Mode (manual exposures)
SS Sun Sensor (DISR sub-instrument)
SSL Surface Science Lamp (DISR device)
SZA Solar Zenith Angle
T0 Time Zero (parachute deployment command epoch)
TAT Time-Altitude Table
UA University of Arizona, Tucson, AZ
ULIS Upward Looking IR Spectrometer (DISR sub-instrument)
ULV Upward Looking Violet photometer (DISR sub-instrument)
ULVS Upward Looking Visible Spectrometer (DISR sub-instrument)
VLNS Very Low Near Surface (descent cycle)
WL WaveLength

Conventions

COLUMN_NUMBER 1 = Column #1 = Column 0 = Column(0) = column index 0
Pixel(0,1) = Pixel in Row(0), Column(1) = Pixel in Row #1, Column #2

Numbering of the DISR images (and SLI strips) starts at the upper right corner of the images (i.e. SLI pixel (0,0) is in the upper, right most corner of the image).

For the Archive Label files, DISR's azimuths are defined as degrees west of north (counter-clockwise as viewed from above) relative to the Sun vector's projection on Titan's surface, in keeping with the original intended rotation sense of the probe. Thus for an observation at an azimuth of 6°, the Sun is 6 degrees to the right of the probe's +Z axis (i.e. DISR sensor head) at the start of the measurement (which would put the Sun behind the shadow bar). However, many analyses and tables use the opposite direction (CW from above) so it is always necessary to verify the sense of rotation.

10.0 DISR Huygens Fun Facts

The Descent...

Titan was at 9.053 AU from the Sun at Encounter.
T0 is the time of parachute deployment, and resetting of the DDB time.
The Stabilizer Chute deployed 15 minutes after the Main chute.
The probe rotated 367 times from Main chute deployment to impact.
The probe reversed spin direction at ~124.5 km altitude.

Impact...

Huygens impact was at 8869.7535 sec after TO as measured by SSP (1.8 sec later on the Cassini clock).
The vertical rate at impact was about 4.54 m/s.
The peak acceleration at impact was about 175 m/s^2 (18 Earth g's, 130 Titan g's)
The peak acceleration at atmospheric entry was ~12.5 Earth g's
The probe sank about 15.4 cm after penetrometer impact (~13 cm after probe impact).
The probe moved for about 10 seconds after impact.
The probe was tilted North about 3 degrees when resting on Titan.
Final Loss of Signal (LOS) from the probe occurred at 13,203 sec. after T0.
The window of the Side Looking Imager (SLI) rested 48cm above the surface, which is 3 cm higher than the windows of the DLVS, DLIS, and the lamp (Ref 5).

DISR Data Facts...

DISR began taking data at ~143 km altitude.
360 Images were transmitted before impact (of 722 taken)
A total of 608 images were transmitted (of 1211 taken)
Images are taken as 12 bits, square rooted, transmitted as 8 bits, and de-sqrt'ed to 12 bits.
99 of 268 IR datasets were lost on chain A.
The ULV dark bias was found to be 44.65 DN (@ Tv=295 & Te=302) at Titan.
ULV noise is around 0.5 DN, 1 sigma
164 (110+54) Descent cycles were executed before loss of signal (LOS)
DISR azimuths are defined as degrees west of north (counter-clockwise as viewed from above) relative to the Sun vector's projection on Titan's surface.
Huygens transmitted 59978 DISR packets (7.38 MB) which uncompressed to 113 MB of data in XDR format.

Temperatures & Insolation...

The coldest recorded DISR temperature was the Violet photometer (154ºK) at impact.
All parts of the DISR Sensor Head began to warm significantly after Titan impact.
The DISR EA temperature varied by only 12.5º C (285.8ºK to 297.3ºK) during the mission.

The DISR Auxiliary (A/D) Board heater (1.3 W) was able to hold temperature at 263ºK for ~1000 seconds before being overcome.

The DISR Strap heater (1.4 W) was able to limit cooling to 172ºK from about T0+4500 sec to T0+10,900 s (when it began to warm again).

At 150 km altitude the Sun was 112.7º east of north, 115º at impact and ~115.5º at LOS.

The solar zenith angle (SZA) was 39º at 150 km, 33.8º at impact and ~32º at LOS.

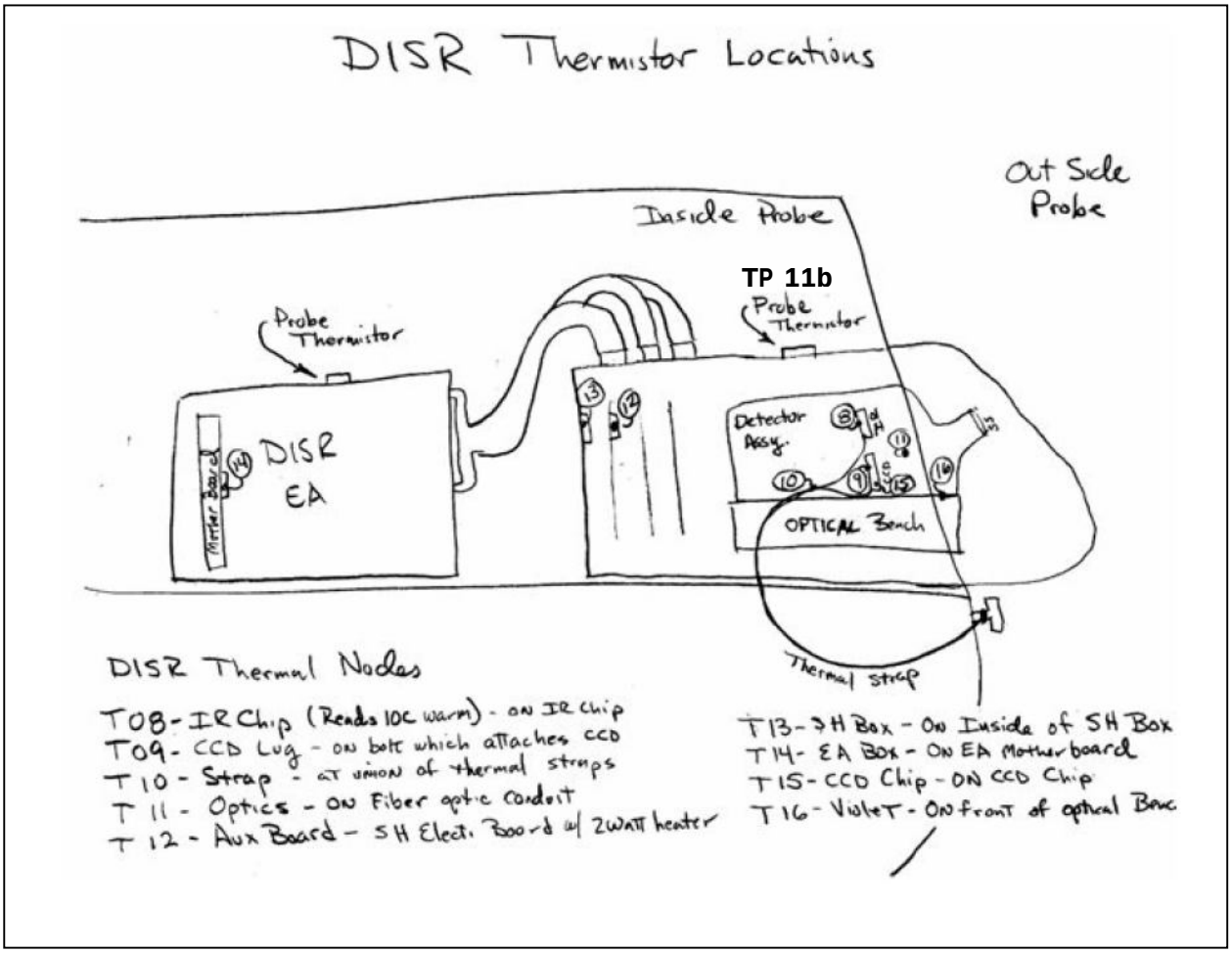

11.0 Revision History

The following table summarizes the revision history of this document.

DISR Archive Users' Guide Revision History		
Version	Date	Comments
0.0	2011.09.23	Preliminary draft, representing progress to the end of the first fiscal year of work on the Guide. It was delivered to JPL on 23rd September 2011, and was approximately 40% complete. AKA "DISR_Archive_Users_Guide2011.09.23.pdf" Included appendices 1 through 17.
0.1	2012.04.27	AKA "Draft 1.0" (i.e. "DISR Data Archive Users Guide 2012.04.27-Draft 1.0") The first comprehensive version of the Guide. Submitted to JPL on 27 April 2012. Includes appendices 1 thru 34. Submitted for team review.
0.2	2012.08.16	AKA "Draft 2.0" (i.e. "DISR Data Archive Users Guide Draft 2.0") Incorporates ITAR review and response to comments from the DISR team. Includes appendices 1 thru 39. Submitted for PDS review.
1.0	2012.09.28	First submittal of the 'completed' version of the DISR Guide; 28 September 2012. ("DISR Data Archive Users Guide 1.0 - 2012.09.27"), with appendices 1 through 40. Includes comments from Ralph Lorenz, Marty Tomasko, Lyn Doose & Erich Karkoschka.
2.0	2013.01.29	Peer Reviewed Version. Submitted to JPL on 29 January 2013. ("DISR Data Archive Users Guide 2.0 - 2013.01.28") Submitted to JPL on 29th January 2013, with appendices 1 thru 40. Includes comments from Bj"orn Grieger and Dave Heather of ESA. Significant changes to sections 3, 5.8, & 5.10, and appendices 1, 4, 5, 6, 20, 25 & 27.
3.0	2016.050.9	Current Version. Submitted to PDS on 13 May 2016. ("DISR Data Archive Users Guide 3.0 ") Addressed peer review comments. Corrected image number for figures 5.8-2 & 5.8-3.